Investigating the role of INO80 in metabolic stress response in *Saccharomyces cerevisiae*

David Shapira

A thesis submitted to Newcastle University for the degree of Doctor of Philosophy (PhD)

Biosciences Institute

Faculty of Medical Sciences

Newcastle University

December 2022

Abstract

Metabolic processes convert nutrients to energy and other useful macromolecules, enabling cell growth and proliferation. Changes to nutrient availability threaten these processes and various conserved metabolic stress response pathways have evolved to ensure survival in starvation conditions. In Eukaryotes, nitrogen starvation induces the non-selective autophagic degradation of cytoplasmic material and selective, receptor-mediated, turnover of organelles. The molecular underpinnings of non-selective autophagy are well understood, however transcriptional regulation of selective autophagy pathways is not fully elucidated.

The evolutionarily conserved ATP-dependent chromatin remodelling complex INO80 regulates the chromatin architecture of genes and promoters. INO80 has been implicated in coordinating metabolic gene regulation, but the exact mechanism is not known. How epigenetics and other chromatin-based processes regulate autophagy and coordinate the metabolic stress response remains poorly understood. We set out to characterise the role of INO80 in the metabolic stress response.

Here we report that in *Saccharomyces cerevisiae* the INO80 complex promotes selective autophagy. Using a combination of ubiquitin proteomics and cellular biology assays we show that loss of INO80 leads to defective mitophagy, ER-phagy and compromised turnover of ubiquitinated proteins. Transcriptomic analysis revealed that the INO80 complex controls the expression of the sub-telomeric COS genes which are associated with endosome-mediated protein turnover. Our functional analysis demonstrates that expression of the COS genes is required for autophagic degradation of mitochondria.

Mechanistically, our analysis reveals that INO80 promotes COS expression, ubiquitinated-protein turnover, and survival in starvation, by counteracting NAD+-dependent heterochromatic silencing by the SIR complex. We demonstrate that INO80 facilitates the acetylation of histone H3 N-terminal tails and the recruitment of the acetyl-CoA synthetase Acs2 at *COS* gene promoters.

Our results describe an epigenetic pathway which connects metabolic stress response with the regulation of transcription from sub-telomeric chromatin. They suggest that chromatin regulation of gene expression by the INO80 complex links endosomal sorting with selective autophagy and ensures viability under metabolic stress conditions.

Acknowledgements

My deepest gratitude goes to my supervisor Dr Manolis Papamichos-Chronakis, whose passion, precision and knowledge have been a constant source of inspiration. Your guidance and mentorship have been invaluable to my development as a scientist, and I am forever grateful.

I would also like to thank the members of ICAMB and the faculty of medical science for creating a supportive and collaborative research environment. A special thank you to Dr Tim Cheek for your support and understanding throughout this PhD journey. Additionally, my sincere appreciation to the examiners for taking the time to read my work.

I cannot express enough gratitude to the friends I have made over the past four years at the institute and the university. The struggles would not have been worth it without you. As noble as scientific inquiry may be, it is friendship which defines our lives and gives meaning to our pursuits. To the Friday Pub Club, my sanity owes a greater debt.

My mother Dr Marina Shapira has been a source of inspiration and encouragement my entire life. Your unconditional love and support have been my anchor and have empowered my achievements. I am also forever indebted to my grandparents Tamara and Yuri Shaginyan, who instilled in me a curiosity and love of inquiry that has defined me as a person.

My biggest thank you is reserved for my partner Madeleine Carter; without you this thesis would quite literally not exist. Your unwavering belief in me and your steadfast support have made this journey possible. Thank you.

Table of Contents

List of Figures

List of Tables

Chapter 1

Chapter 1. Introduction

1.1. Metabolism

1.1.1. Biochemistry of metabolism

All organisms must extract energy from the environment and convert it such that it can be used to sustain life. The sum of all these chemical reactions and the integrated network they form is called *metabolism*. Fundamentally, metabolism consists of a set of energy-yielding and energy demanding reactions which together enable the biochemical survival of an organism. More complex fuels are broken down by metabolic pathways into useful cellular fuels that can be used to drive energy-demanding reactions. The process of breaking down more complex molecules into simpler components is called *catabolism*.

The simple sugar glucose is the most abundant 'fuel' used by living organisms and its catabolic breakdown in the process of glycolysis forms one of the oldest and most important metabolic pathways (Berg et al., 2010; Grüning and Ralser, 2021). The breakdown of glucose leads to the generation of pyruvate and adenosine triphosphate (ATP). Nearly all energy-consuming reactions utilise the intrinsic energy of ATP to drive an otherwise energetically unfavourable reaction. In this way, the biosynthesis of complex molecules such as DNA and proteins is possible.

Metabolic pathways, while incredibly numerous and complex, share various recurring motifs across all organisms, originating from their common evolutionary heritage. One such motif is the *activated carrier*. These molecules promote otherwise energetically unfavourable reactions, modulate the activity of a protein, and can act as coenzymes within reactions (Table 1.1). ATP is an activated carrier of the phosphoryl group. ATP derives its energy generating properties through the fact that ATP hydrolysis and transfer of the phosphoryl group is a highly exergonic process.

Nicotinamide adenine dinucleotide (NAD^+) is another example of an activated carrier. NAD^+ functions in the catabolism of sugar molecules. The oxidation of molecules derived from glucose in the tricarboxylic (TCA) cycle generates electrons that are then transferred to NAD^+. Thus, NAD^+, and its reduced form NADH, act as activated carriers for electrons. Together, NAD^+/NADH are essential cofactors in the oxidation-reduction reactions during the TCA and oxidative phosphorylation (discussed below). As the reduction of NAD^+ to NADH depends on metabolic activity, the ratio of NAD^+/NADH can act as a sensor of nutrient availability (Ying, 2006; Covarrubias et al., 2021).

A further fundamental component of metabolism is Coenzyme A (CoA), an activated carrier of an acyl group. Most commonly, CoA carries an acetyl group (acetyl-CoA), and this molecule is important in the oxidation of fatty acids and the synthesis of membrane lipids (Table 1.1).

Importantly, while both NAD^+ and acetyl-CoA are involved in the core metabolic processes of the cell, both are integrated into a variety of additional enzyme reactions and specialised pathways.

1.1.2. Metabolic pathways of Saccharomyces cerevisiae

Simple sugars, such as glucose, are the most common fuel for non-phototrophic organisms, and their breakdown and subsequent metabolic consumption can define organisms and set them apart. The budding yeast *Saccharomyces cerevisiae* is a single-celled fungus, long associated with alcohol and bread production. It evolved to consume glucose molecules produced in excess in ripened fruit, and can be found in abundance, among many other places, in vineyards (Greig and Leu, 2009; Mortimer, 2000).

The glycolysis of glucose to pyruvate is an anaerobic process (without oxygen (O_2)) and generates two molecules of ATP. Under aerobic conditions, pyruvate can be further oxidised to carbon dioxide (CO_2) by the TCA cycle, leading to the production of many more ATP molecules. Alternatively, anaerobic processes can further convert the pyruvate to lactate or ethanol, but for a substantially lower yield of ATP (Figure 1.1).

Although not favoured, *S. cerevisiae* can perform aerobic respiration which involves the conversion of pyruvate to acetyl-CoA, whereupon it enters the TCA cycle. This 10-step metabolic cycle reduces the carbon source to carbon dioxide and water and in the process the electrons are 'captured' by the reduction of NAD^+ to NADH. These electrons are then used to generate a membrane potential within the mitochondria, the energy of which is used to generate many more molecules of ATP (Berg et al., 2010).

Although capable of aerobic metabolism, *S. cerevisiae* preferentially ferments pyruvate anaerobically, producing ethanol – an effective antiseptic which allows the yeast to outcompete other organisms in the same environment, despite the lower ATP produced in the process. This ability to ferment sugars into ethanol has been exploited by humans for thousands of years, and efforts in the early 20^{th} century to generate strains more adapted to brewing helped initiate the field of yeast genetics (Barnett, 2007).

S. cerevisiae (hereafter referred to interchangeably with the more general 'budding yeast') went on to be one of the most studied organisms, with a particular isolate, the S288c strain, being the first eukaryote to have its entire genome sequenced (Goffeau et al., 1996).

Interestingly, the S288c strain was isolated because of its amenability to experimental culture conditions and is typically maintained in nutrient rich conditions throughout experiments. In contrast, wild budding yeast would inevitably spend considerable time not in the presence of nutrients and thus must adapt to survive in such conditions.

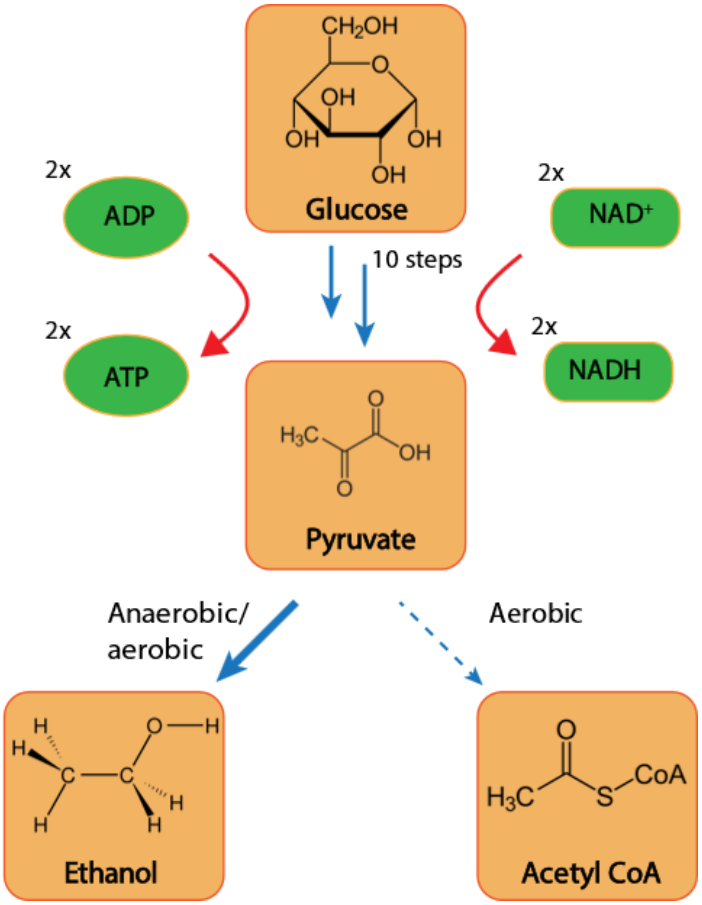

Figure 1.1. Metabolic breakdown of glucose in *Saccharomyces cerevisiae*. Glucose acts as a critical 'fuel' in budding yeast. Glucose is broken down to pyruvate through the glycolysis pathway, a series of 10 linked reactions. This generates two ATP molecules and two electrons (NADH). Budding yeast preferentially metabolises pyruvate to ethanol through anaerobic fermentation, even in the presence of oxygen. This produces ethanol and CO_2 both of which are exported out of the cell.

Activated carrier molecule	Group carried	Role
ATP	Phosphoryl	Energy currency
NADH	Electrons	Redox reactions
Coenzyme A	Acyl	Acyl-group transfer
Biotin	CO2	carboyl-group transfer
S-adenosylmethionine	Methyl	Methyl-group transfer
Nucleoside triphosphate	Nucleotides	DNA and RNA synthesis

Table 1.1. Activated carriers and their role in metabolism

1.1.3. Nutrient starvation and metabolic stress

Metabolic activity depends on the availability of 'fuel' or environmental nutrients, to generate the ATP required for lipid biosynthesis, protein production and other enzymatic activity. Nutrient starvation arises when the fuel for this process runs out, resulting in a change to the energy generating potential of a cell. To survive, the organism must effectively adapt its biochemistry to accommodate the changing availability and respond to any stresses that arise from this.

A deficiency in glucose leads to a rapid decrease in the amount of ATP available to a cell, whereas nitrogen starvation results in the inability of a cell to synthesis amino acids, and thus compromises protein production.

A state of 'starvation' begins following the complete breakdown of the final available metabolites and extends until the next time that nutrients are available (Owen and Hanson, 2013). For metazoans, such as mammals, this refers to the time between two meals.

Microorganisms such as wild budding yeast similarly spend substantial time in nutrient depleted conditions, often overlooked because many biochemical studies are performed exclusively in nutrient rich culture mediums.

For the simple reason that a state of starvation is very common, extensive pathways have evolved to ensure adaptation and survival to these conditions.

1.1.4. Cellular adaptation to starvation: growth arrest and quiescence

Nutrient rich conditions and the accompanying activity of metabolic pathways enable cells to 'grow' - accumulate mass. The process of mass accumulation requires the activity of a vast number of ribosomes, which drive all protein synthesis, and are the driving force behind cell growth. For yeast cells in nutrient rich conditions, around 60% of all transcription is dedicated to ribosomal RNA (rRNA)

production, and 50% of mRNA transcription is devoted to ribosomal proteins (RPs) (Warner, 1999). In addition to this, an extensive network of accessory proteins and noncoding RNAs is also dedicated to the processing, modification, and assembly of ribosomes (Tschochner and Hurt, 2003; Henras et al., 2008). Due to the high metabolic demand of maintaining this process, it is energetically costly and must be effectively stopped when cells encounter starvation.

Starvation induces cells to arrest growth and enter a state referred to as *quiescence*. In this state, metabolic activity is severely reduced, transcriptional pathways are redirected away from ribosome biogenesis, and yeast cell arrest in the G_1 phase of the cell cycle, entering theas the G_0 phase (Miles et al., 2021). Quiescent *S. cerevisiae* are generally characterised by increased stress tolerance, higher cell density, and longevity. Importantly, cells remain metabolically and transcriptionally active; however, their metabolic programare severely altered (Roche et al., 2017).

As cells use up all available nutrients and enter a starved state, they are left with an abundance of ribosomes and other proteins no longer required. To liberate the constituent molecules, in particular amino acids, cells upregulate the catabolic process that allows them to effectively 'recycle' amino acids and other metabolites.

Accompanying the increased catabolic processes is the upregulation of pathways for amino acid biosynthesis, cell wall integrity, resistance to heat shock, and resistance to oxidative stress (Pakos-Zebrucka et al., 2016; Wullschleger et al., 2006). The limitation or starvation of various nutrients, for example nitrogen, carbon (glucose), or phosphate (ATP), all lead to similar physiological changes (increased cell wall integrity, increased resistance to heat and osmotic stress) and transcriptional changes (downregulation of ribosome biogenesis and upregulation of catabolic processes) (Klosinska et al., 2011).

Metabolically, changes vary more significantly depending on the specific nutrient that is absent. Both nitrogen and glucose starvation lead to low intracellular levels of amino acids but high levels of nucleotide, while the opposite case was found in phosphate starvation. (Boer et al., 2010; Klosinska et al., 2011).

Furthermore, nutrient starvation can induce *S. cerevisiae* to undergo gametogenesis, more commonly referred to as sporulation which is an alternative 'developmental' pathway to quiescence. In this process, diploid yeast that are respiration competent can undergo two consecutive cycles of chromosome segregation to produce haploid daughters. The resulting haploid spores are more resistant to environmental stress and can therefore remain dormant until more favourable conditions arise (van Werven and Amon, 2011). Importantly, the master regulator of budding yeast sporulation, Ime1

(Kassir et al., 1988, p. 1; Dirick et al., 1998, p. 1), is transcriptionally silenced by the presence of glucose or nitrogen and so both typically must be depleted before this cellular pathway is induced (Matsuura et al., 1997; Smith et al., 1998).

1.1.5. TORC1 Signalling

The mechanistic target of rapamycin (mTOR) is a conserved serine/threonine protein kinase that is central for cell growth by coordinating the sensing and the downstream cellular response. In *S. cerevisiae,* two Tor genes are present, *TOR1* and *TOR2,* and serve overlapping roles within two related but distinct protein complexes, the TOR complexes 1 and 2 (TORC1 and TORC2) which likely exist as dimers (Wullschleger et al., 2006). These regulate a diverse set of cellular processes such as ribosome biogenesis, mRNA translation, metabolism, apoptosis, and autophagy (discussed below) (Figure 1.2A). Both are conserved throughout eukaryotic evolution due to the fundamental role they play in integrating environmental signals with cellular response (Loewith and Hall, 2011; Wullschleger et al., 2006).

Budding yeast TORC1 is made up of Kog1, Lst8, Tco89, and one of either Tor1 or Tor2 (Figure 1.2A). The presence of nutrients promotes its kinase activity, and the 'active' form of the complex induces cell cycle progression, promotes general mRNA translation, and activates the transcription of growth-promoting genes such as ribosomes. Constitutive activation of mTOR signalling is a hallmark of various cancers in humans (Pópulo et al., 2012; Sato et al., 2010).

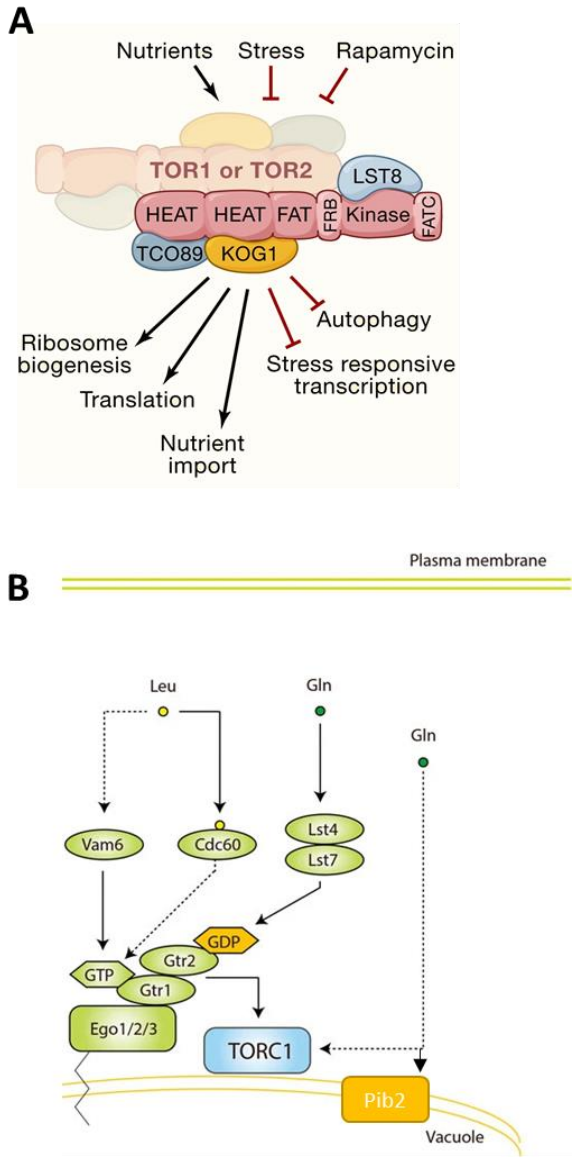

Figure 1.2. TORC1 subunit organisation and mechanisms of nutrient sensing. (A) TORC1 complex is shown as a dimer. Included are the complex subunits (TCO89, Kog1, and LST8) and the structural domains found in TOR proteins (HEAT, FAT, FRB, FATC and Kinase). TORC1 integrates nutrient and stress signalling and controls the accumulation of mass. Black arrows highlight signals that stimulate TORC1 and responses which TORC1 activity promotes. Red bars depict factors inhibiting TORC1 and the pathways which active TORC1 signalling inhibits. (modified from Wulllschleger et al. 2006). (B) TORC1 is located at the surface of the vacuole in yeast. Amino acids are sensed by Vam6 and Cdc60 which promote GTP loading of Gtr1. In its activated form the Gtr1-GTP and Gtr2-GDP heterodimer, which is anchored at the vacuole through the EGO complex, activate TORC1. Glutamine is sensed through the Lst4-Lst7 complex which also promotes the activated Gtr-Gtr2 heterodimer. Glutamine is also sensed independently of Gtr1-Gtr2 through the vacuolar membrane protein Pib2. (Modified from Shimobavashi et al. 2016).

The depletion of various nutrients and metabolites including nitrogen, glucose, and amino acids is sensed by the TORC1 complex, and leads to the inhibition of its activity (Figure 1.2B) (Düvel et al., 2010). TORC1 inhibition directly leads to growth arrest, suppression of ribosome biogenesis, downregulation of mRNA translation, and upregulation of catabolic pathways (Beck and Hall, 1999; Hinnebusch, 2005; Rohde and Cardenas, 2003; Wullschleger et al., 2006). The drug Rapamycin is also a potent inhibitor of TORC1 activity.

Downstream effectors of TORC1 signalling are extensive. Among them, Sch9 is significant as in its TORC1-phosphrylated form it controls ribosome biogenesis and translation initiation (Urban et al., 2007). The phosphatase Tap42-2A, another effector, is kept inactive by TORC1 kinase activity and the protein only becomes activated following TORC1 inhibition in nutrient deplete conditions. Tap42-2A mediates the transcriptional regulation of nitrogen metabolism, the TCA cycle, and stress response genes (Shamji et al., 2000; Düvel et al., 2003).

Transcription of stress response genes is further controlled by TORC1 through regulation of the cellular localisation of transcription factors which control their expression. The transcription factor Gln3 controls the expression of genes associated with nitrogen limitation, while the transcriptional activators Msn2/4 control carbon-source regulated gene expression. Both are excluded from the nuclease by the kinase activity of TORC1. Following the sensing of nutrient depletion, the inhibition of TORC1 leads to the localization of Gln3 and Msn2/4 to the nucleus and the activation various nutrient metabolism pathways (Beck and Hall, 1999; Hardwick et al., 1999).

Budding yeast sporulation is also regulated by Tor signalling which controls the intracellular localisation of the Ime1 transcription factor (Colomina et al., 2003). TORC1 inhibition leads to Ime1 localisation to the nucleus while the presence of glutamine leads to Ime1 being sequestered in the cytoplasm (Colomina et al., 2003).

1.1.6. Nutrient sensing by TORC1

In both yeast and humans, active TORC1 (mTORC1 in humans) is enriched on the membrane surface of the lytic compartment. In yeast, this is the vacuole, and in higher eukaryotes these are the lysosomes. These membrane-bound organelles contain an abundance of degradative enzymes and maintain an acidic pH relative to the cell cytoplasm. Multiple catabolic pathways converge on the vacuole/lysosomes as the destination for protein cargoes that require degradation.

The function of various GTPases, guanosine triphosphate (GTP) hydrolysing enzymes which convert GTP to GDP, provides the molecular basis for amino acid sensing by TORC1 (Kim et al., 2008; Sancak et al., 2008). The Gtr1 and Gtr2 GTPases (orthologs of the mammalian RagA/B and RagC/D) are components of the vacuole membrane-localised EGO protein complex and activate TORC1 by interacting with it in an amino acid dependent manner (Binda et al., 2009). The presence of amino acids promotes the GTP loading of Gtr1 while Gtr2 is GDP bound, and the proteins form a heterodimer that activates TORC1 signalling (Figure 1.2B). The GTP-loaded state of Gtr1 is essential for its interaction with TORC1, and this interaction is disrupted by nutrient starvation (Shimobayashi and Hall, 2016).

Recently, glucose starvation was found to induce TORC1 to reversibly oligomerize into a hollow helical superstructure called TOROID, in a Gtr1 dependent manner. This process has only been observed in *S. cerevisiae* so far, and it is unclear whether it is evolutionarily conserved (Prouteau et al., 2017).

Nitrogen is essential for nucleotide and amino acid synthesis, and glutamine is considered the preferred nitrogen source for budding yeast, although ammonia, glutamate, and α-ketoglutarate can also maintain growth (Cooper, 1982).

In mammals, glutamine sensing is mediated by glutaminolysis (double deamination) of glutamine to α-ketoglutarate and is mediated by Rag GTPases (Durán et al., 2012). In yeast, glutamine availability is sensed by the Lst4-Lst7 complex, which is an upstream regulator of Gtr1-Gtr2 (Péli-Gulli et al., 2015). Glutamine was also found to activate TORC1 signalling independently of Gtr1/2 GTPases. Instead, this mechanism was found to be mediated by the vacuolar membrane-associated phosphatidylinositol 3-phosphate binding protein Pib2 (Kim and Cunningham, 2015; Tanigawa and Maeda, 2017), highlighting its role as regulator of TORC1 signalling (Figure 1.2B).

Together, these pathways enable the TORC1 complex to respond to changes in the amino acid and nitrogen state of the cell and coordinate the vast number of cellular pathways in response to the availability of these molecules.

1.2. Protein Catabolism

1.2.1. Pathways controlling protein turnover

The combined set of all proteins within a cell is called the cell *proteome*. The proteome of yeast cells prior to starvation is poorly adapted to ensure survival during subsequent nutrient deprivation. Following TORC1 inhibition, genetic changes work in concert with catabolic processes to break down

and deplete no longer required cellular components. This has the effect of enabling the production of new survival-directed proteins (Harper and Bennett, 2016).

Catabolic pathways can be divided between the site of protein turnover. The vacuole/lysosome is the final destination of protein turnover mediated by autophagy and endosomal sorting through the multivesicular bodies (MVB) pathway (Boya et al., 2013; Gruenberg and Stenmark, 2004).

The proteosome is the endpoint for protein targets of the ubiquitin-proteasome system (UPS). The 26S proteasome is a multisubunit protein complex and is the primary protease of eukaryotic cells (Bard et al., 2018). The post-translation ubiquitin modification targets proteins to the proteasome, where the proteins are sequentially unfolded and proteolytically cleaved.

In addition to the respective final site of protein turnover, the different catabolic pathways differ in their targets. The UPS targets the majority of short-lived, often regulatory, proteins. Autophagy targets long-lived proteins, protein aggregates, and cellular organelles. Endosomal sorting specifically targets proteins from the outer cell membrane (Lilienbaum, 2013).

Of these pathways, autophagy plays the most significant and best studied part in the cellular response to starvation. However, endosomal sorting through the MVB and, to a lesser extent, protein turnover by the UPS also participate in the cellular response to starvation (Martin Müller et al., 2015; Willis et al., 2020).

1.2.2. Autophagy

Macroautophagy (hereafter autophagy) is a fundamental catabolic process that mediates much of the protein turnover which occurs following nutrient starvation. From the Greek *self* (auto) *devouring* (-phagos), autophagy targets superfluous or damaged cellular constituents for degradation in the vacuole/lysosome. By catabolising cellular components, autophagy releases the macromolecules that make up the cargo, primarily amino acids and lipids, and enable their reuse by the cell (Onodera and Ohsumi, 2005; Yang and Klionsky, 2007).

The process of autophagy is characterised by the engulfment of material targeted for degradation by a double-membrane vesicle called the *autophagosome*. This process can be both non-selective and selective. The autophagosome is then transported to the lytic compartment into which it fuses and releases its cargo.

Non-selective autophagy (sometimes referred to as ‘bulk’ autophagy) captures non-specific cytoplasmic volume, while selective (or receptor-mediated) autophagy can target organelles, including mitochondria (mitophagy), the endoplasmic reticulum (ER-phagy), as well as protein aggregates (aggrephagy) and ribosomes (ribophagy) (Farré and Subramani, 2016; Gatica et al., 2018).

In mammals, autophagy is also of critical importance throughout development and in immune response, tumour suppression, and aging (Allen and Baehrecke, 2020; Gozuacik and Kimchi, 2004; Levine et al., 2011; Rubinsztein et al., 2011).

Autophagy is controlled by a group of approximately 20 essential autophagy-related genes (ATGs) in yeast, many of which are conserved throughout eukaryotic evolution (Bernard et al., 2015; Nakatogawa et al., 2009).

Mechanistically, TORC1 mediated hyperphosphorylation of the Atg13 protein suppresses autophagy under nutrient rich conditions. Upon inhibition of TORC1, Atg13 dephosphorylation allows the formation of the Atg13-Atg1 kinase complex, which can then activate the autophagy pathway through its phosphorylation of various effectors (Kamada et al., 2010; Scott et al., 2000). This initial step is followed by the recruitment of additional autophagy components, including Atg9-containing vesicles, to the site of initiation where they initiate the process of membrane expansion around the target (Sawa-Makarska et al., 2020, p.). At this stage, the expanding membrane is called the *phagophore*. The expansion of the phagophore is mediated by various autophagy components, including Atg8-phosphatidylethanolamine (PE) (Atg8-PE), which becomes incorporated into the expanding phagophore. The phagophore completes its engulfment of the cargo by surrounding it, at which stage it is called an *autophagosome*. Following maturation, the autophagosome is delivered to the vacuole/lysosome where the two membranes fuse in an Atg8-dependent manner. Following fusion, the cargo is released into the lumen of the vacuole and hydrolytic processes degrade the macromolecules and allow the constituent parts to be recycled (Figure 1.3) (Farré and Subramani, 2016; Jin and Klionsky, 2013).

Atg8 (LC3 in mammals) is a small ubiquitin-like protein that is essential for both phagophore expansion and autophagosome maturation. Furthermore, Atg8 acts as a receptor adaptor in selective autophagy.

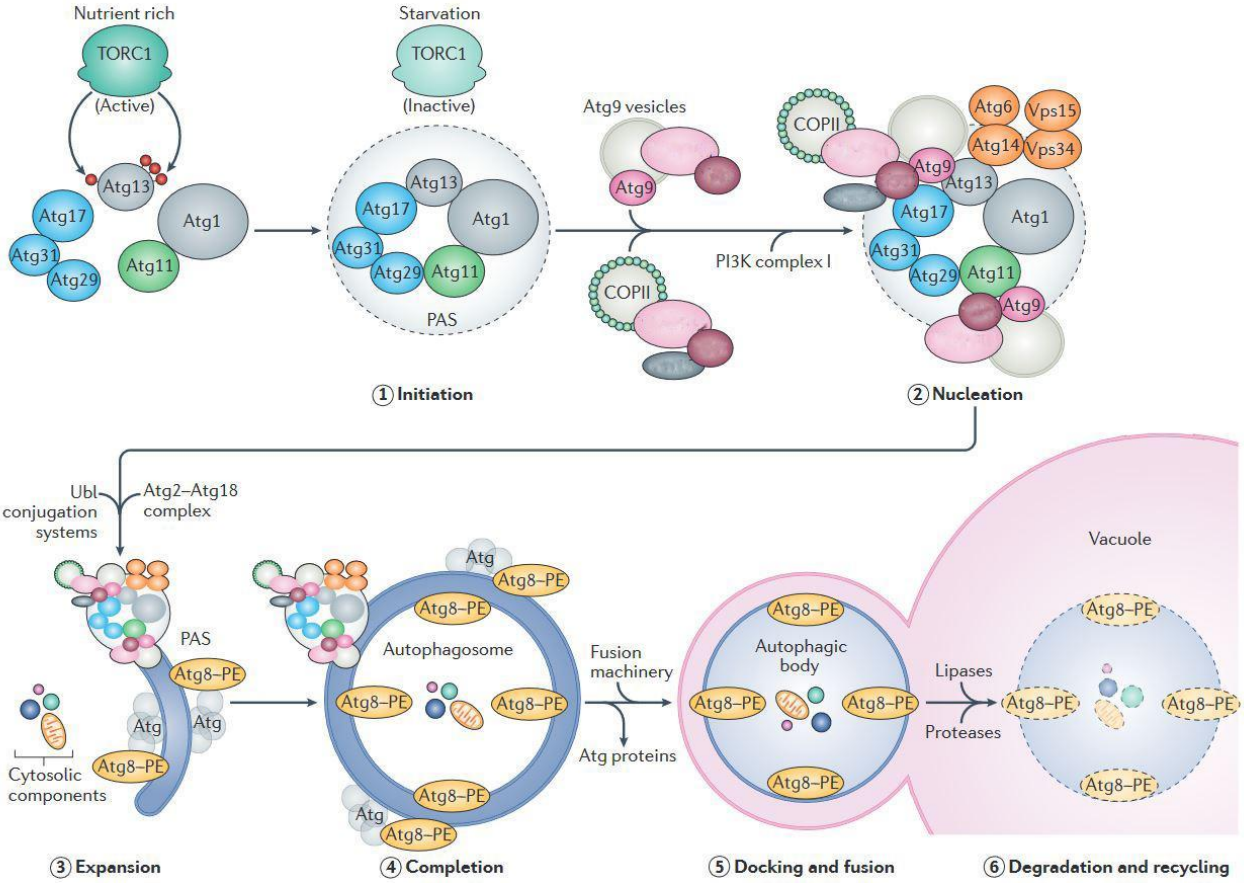

Figure 1.3. Molecular mechanism of *S. cerevisiae* autophagy and selective autophagy. The hyperphosphorylation of Atg13 by TORC1, in nutrient-rich conditions, inhibits autophagy. The inhibition of TORC1 by either starvation or rapamycin treatment, leads to the hypophosphorylation of Atg13 and its subsequent interaction with Atg1 and Atg17. This initiates the recruitment of cytosolic components of the core autophagic machinery to the phagophore assembly site (PAS). The PAS is established by the scaffold components Atg11 and Atg17, together with the Atg17–Atg29–Atg31 subcomplex, and other factors including COPII coated vesicles. Progression of the autophagy pathway involves the activity of phosphoinositide 3-kinase (PI3K) complex I, and the recruitment of additional factors such as the Atg2–Atg18 complex and the ubiquitin-like (Ubl) conjugation systems, Atg8–PE and Atg5–Atg12–Atg16. This results in the formation of a double-membrane vesicle, the autophagosome, which encloses the cargo destined for autophagic degradation. The autophagosome is then transported to vacuole (lysosomes in animals). The outer autophagosomal membrane docks and fuses with that of the vacuole to release the autophagic body into the vacuolar lumen, where hydrolases degrade and recycle the macromolecular components for cellular use. (modified from (Farre and Subramani 2016)

1.2.3. Receptor-mediated selective autophagy

Autophagy is not limited to the response and many selective autophagy pathways play a critical role in maintaining homeostasis with nutrient starvation. Although the targets of selective autophagy can

be diverse, all pathways share a common set of mechanisms. Fundamentally, all cargos have an associated selective autophagy receptor (SAR), which enables the recognition of the cargo and the targeting of the autophagy pathway to it. Examples in *S. cerevisiae* include Atg36, which is the SAR for selective autophagy of peroxisomes (Pexophagy) (Motley et al., 2012), Cue5 (TOLLIP in mammals) targets ubiquitylated proteins and aggregates (Lu et al., 2014), Atg32, which is the receptor for mitophagy (Kanki et al., 2009; Okamoto et al., 2009) and Atg39/40, which are SARs for ER-phagy (Mochida et al., 2015).

Interactions between core autophagy machinery and SARs-bound cargoes leads to autophagosome formation specifically around a given target.

Atg8-PE is critical to cargo recognition, and all SARs contain Atg8 family-interacting motifs (AIMs) through which they interact directly with Atg8-PE (Farré et al., 2013; Noda et al., 2008). Additionally, the scaffold proteins Atg11 and Atg17 also physically interact with SARs and recruit the autophagy machinery creating the nucleation site for membrane expansion and cargo engulfment in the autophagosome (Kabeya et al., 2005).

1.2.3.1. Mitophagy

Regulation of mitochondrial homeostasis is crucial as mitochondria are involved in a variety of metabolic pathways and damaged mitochondria can lead to the generation of dangerous amounts of reactive oxygen species (ROS) (Kurihara et al., 2012). Maintenance of mitochondria is energetically costly to cells, and the turnover of superfluous or damaged mitochondria by mitophagy is therefore an important quality control mechanism (Stotland and Gottlieb, 2015).

S. cerevisiae preferentially performs anaerobic fermentation in the presence of glucose, which does not require mitochondrial activity. However, in the presence of nonfermentable carbon sources such as glycerol or lactate, mitochondrial oxidative phosphorylation is induced. Increased mitochondrial activity when growing in the presence of non-fermentable carbon sources leads to the accumulation of damaged mitochondria over time, and these require clearance by mitophagy (Turcotte et al., 2009; Kanki et al., 2015).

In yeast, mitochondria are targeted for autophagic degradation by the Atg32 protein, which is present in outer mitochondrial membrane. Mitophagy is mediated by the interaction between Atg32 and Atg11 and occurs only following the phosphorylation of Atg32 (Kanki et al., 2009; Okamoto et al., 2009). Additionally, Atg32 also interacts with Atg8 via its AIM domain, which promotes the expansion of

the phagophore membrane around the mitochondria; however, this interaction is not essential for mitophagy. The kinases CK2 and Hog1 have both been suggested to regulate the phosphorylation; however, the mechanism controlling either activity is unclear (Aoki et al., 2011; Kanki et al., 2013). Although Atg32 phosphorylation is a critical step in mitophagy regulation, the exact mechanism that controls this remains poorly understood (Gatica et al., 2018).

Intact mitochondria are too large to fit inside autophagosomes, and therefore mitochondrial fission is thought to play a significant role in facilitating mitophagy (Kanki et al., 2015). Dnm1 and Fis1 both mediate mitochondrial fission in yeast, and their activity is essential for mitophagy (Abeliovich et al., 2013; Mao et al., 2013). Another potential regulatory mechanism for mitophagy is mediated by the physical interactions of mitochondrial and ER membranes. Mitochondria and ER membranes are connected via the ER-mitochondria encounter structure (ERMES), and proteins of this complex were found to be essential for mitophagy (Böckler and Westermann, 2014). It has been suggested that ERMES promotes mitochondrial fission, however, the exact mechanisms and how it is incorporated into the mitophagy pathway are not well established.

In mammals, mitophagy is important throughout development and is involved in controlling cell differentiation. In line with the more complicated cell biology of higher eukaryotes, the mechanism regulating mammalian mitophagy is more mechanistically complex than in yeast (Ashrafi and Schwarz, 2013). Interestingly, polyubiquitin chains on the mitochondrial membrane play a significant role in targeting the organelle for autophagic degradation (Harper et al., 2018), however ubiquitin has not been found to regulate yeast mitophagy. A screen in yeast did identify a deubiquitinase complex, Ups3-Bre5, to be recruited to mitochondria and inhibit mitophagy, suggesting that ubiquitin is involved in yeast mitophagy (Matthias Müller et al., 2015). However, the substrate for Ups-Bre5 deubiquitination is not known.

1.2.3.2. ER-phagy

A significant portion of all protein synthesis occurs in ribosomes bound to the ER membrane, and the ER is the site of all cell surface, vacuolar, and secretory protein synthesis. Different external and internal stimuli, such as high glucose (Chen et al., 2018) and ROS (Dandekar et al., 2015) can disrupt ER activity and lead to the accumulation of unfolded proteins in the ER. ER stress is induced when mis-folded proteins accumulate within the ER, leading to activation of the unfolded protein response (UPR) and ER-associated degradation (ERAD). In addition to these pathways, ER stress induces

selective autophagic degradation of the ER that regulates the size of the ER, counteracting the expansion caused by UPR (Bernales et al., 2006; Yorimitsu et al., 2006).

The selective degradation of the ER is mediated by the SARs Atg39 and Atg40 which are ER membrane proteins with interaction motifs for both Atg11 and Atg17 (Mochida et al., 2015). Silencing of the mammalian Atg40 homologue RETREG1 led to ER expansion, while overexpression of RETREG1 induced ER fragmentation, both results highlighting the role of ER phagy in controlling ER size (Khaminets et al., 2015).

However, in both mammals and yeast, the mechanism controlling ER-phagy induction, and the molecular dynamics co-ordinating ER stress and ER-phagy are poorly understood.

1.2.3.3. Aggrephagy

Protein aggregates and misfolded proteins must be cleared from the cell as they are dangerous to the normal functioning of a cell. In humans, several neurodegenerative disorders are linked to the accumulation of protein aggregates (Ross and Poirier, 2004).

Protein aggregates and misfolded proteins are marked by mono- and polyubiquitin modification targeting them for degradation either by UPS or by selective aggrephagy. The hierarchy of these two pathways and the decision between which pathway to use remains unclear, although the size of the aggregates is likely a major factor (Verhoef et al., 2002; Korolchuk et al., 2010).

Nitrogen starvation leads to a rapid clearance of ubiquitinated protein from the cell in an autophagy dependent manner. Work on this process identified many of these ubiquitin conjugates to be aggregating proteins (Lu et al., 2014).

In yeast, the clearance of protein aggregates, in particular proteins containing aggregation-prone polyQ (polyglutamine), is mediated by the Cue5 SAR (Lu et al., 2014). Cue5 directly recognises ubiquitin and contains an AIM which allows it to target ubiquitinated protein conjugates to Atg8 and lead to autophagic degradation of the aggregates in the vacuole.

Evidence suggests that increasingly large protein aggregates promote Cue5 oligomerization, which then preferentially leads to autophagy activation over UPS (Lu et al., 2017).

Interestingly, this is the only example of ubiquitin-mediated autophagy in yeast. Whether Cue5 can target non-aggregating, ubiquitin marked proteins, for autophagic degradation is not known.

1.2.4. Ubiquitin mediated endosomal sorting

The turnover of outer membrane integrated proteins, such as those forming ion channels and other cell surface receptors, is predominantly mediated through the endosomal protein sorting pathway. Targets for turnover are ubiquitinated and subsequently endocytosed into the cell and trafficked to the vacuole (lysosome in animals) for degradation. Essential to this pathway are Multivesicular bodies (MVBs), which are membrane enclosed structures containing intraluminal vesicles (ILVs). Sorting of cargo into ILVs by the MVB pathway is an essential step prior to vacuolar/lysosomal degradation (Piper and Katzmann, 2007).

Mechanistically, a group of protein complexes called the Endosomal sorting complex required for transport (ESCRTs) carry out the several stages of ubiquitinated-cargo recognition, vesicle budding and trafficking to the MVB pathway. For this reason the entire pathway is also referred to as the ESCRT pathway (Henne et al., 2011). The ESCRT pathway is involved in cell signalling and regulating membrane composition during normal growth but becomes further induced following nutrient starvation. Budding yeast cells which reach the plateau phase of growth upregulated endosomal sorting via the MVB pathway as nutrients become limiting (Babst and Odorizzi, 2013). The turnover of no longer required nutrient transporters and receptors provides the cell with additional amino acids during the initial stages of nutrient stress and this has been shown to complement the autophagy pathway (Müller et al., 2015). Evolutionarily conserved connections between the autophagy pathway and MVB sorting pathway are numerous and suggest that protein sorting to the vacuole/lysosomes links these two processes (Hatakeyama and De Virgilio, 2019; Lee et al., 2007; Raiborg and Stenmark, 2009; Rusten et al., 2008, 2007). Several human diseases, including cancer, neurodengerative conditions, Huntington's and Parkinson's are associated with dysfunction in the ESCRT pathway (Saksena and Emr, 2009). The interplay between ESCRT pathway and selective autophagic turnover of protein aggregates directly contributes to the development of these conditions (Filimonenko et al., 2007; Rusten et al., 2008), however the broader role of ESCRT and MVB pathways in selective autophagy is poorly understood.

1.2.5. The COS proteins

The yeast Cos protein family is a group of MVB sorting factors that functionally resemble mammalian tetraspanins, a major constituent of intralumenal vesicles (ILVs) (Pols & Klumperman, 2009; Wubbolts *et al*, 2003; MacDonald *et al*, 2015). The budding yeast genome encodes 11 Cos proteins

from highly similar genes all located in sub-telomeric DNA; and several of these genes are the first or last ORF on a given chromosome. Similar to other genes with these regions of the chromosomes, the *COS* genes are transcriptionally repressed by Sir2 and activated by Rpd3 – both histone deacetylases (Bernstein *et al*, 2000; MacDonald *et al*, 2015). The structure of the Cos proteins are made up of around 400 resides which form four membrane-spanning domains, and GFP tagged Cos proteins have been found to be targeted within the vacuole lumen, as well as enriched at the extracellular membrane (Huh *et al*, 2003; MacDonald *et al*, 2015). All Cos proteins were found the be strongly ubiquitinated in mass spectrometry experiments (Hitchcock *et al*, 2003; Peng *et al*, 2003).

Despite the high similarity in sequence and amino acid composition between the various Cos proteins, distinct roles have been identified for the various Cos proteins. Early studies found that Cos8 was enriched at the nuclear membrane and was transcriptionally regulated by the Hac1 transcription factor – a master regulator of the unfolded protein response (Spode *et al*, 2002). High-throughput synthetic genetic array studies confirmed a genetic interaction between Cos8 and genes associated with the nuclear membrane while the Cos7 protein was identified as interacting with an extensive network of mitochondrial genes (Costanzo *et al*, 2016).

The first reports of a biological function shared by most of the Cos proteins found that endosomal sorting of plasma membrane proteins into the vacuole was dependent on the Cos activity and specifically the ubiquitinated state of the proteins (MacDonald *et al*, 2015). Interestingly this effect was particularly obvious following nutrient starvation as MVB sorting is a major pathway contributing to proteome remodeling following metabolic stress. By forming microdomains within endosomal membranes, Cos proteins provided a concentrated ubiquitin signal which promoted the sorting of specific cargos into MVB and ultimately degradation in the vacuole (MacDonald *et al*, 2015).

As these proteins are predicted to be located at other cellular membranes, it is unknow if there also a similar mechanism of forming microdomains and promoting protein sorting takes place. Furthermore, the exact mechanism linking metabolic state to the regulation of Cos proteins in unclear.

1.3. Chromatin control of transcription

1.3.1. Chromatin context of DNA

The eukaryotic genome can reach several meters in length; however, it must be packaged into the relatively small volume of the nucleus. This is achieved through the "wrapping" of DNA around a series of proteins that impart structure to the genome. In combination with other DNA-binding proteins which facilitate DNA folding and looping, the genome is organised into increasingly higher orders of structure. The combined complex of DNA and its associated organising proteins is called *chromatin*.

Histones are proteins that represent the core of this organisation. DNA is wrapped around histone octamers such that roughly 147 base pairs (bp) of DNA coil around the histone forming a *nucleosome* (Figure 1.4A). The most common composition of the octamer is made up of two dimers of histone H3-H4 arranged as a tetramer and flanked by two H2A/H2B dimers (Figure 1.4B) (Luger et al., 1997; Campos and Reinberg, 2009). DNA spanning between two nucleosomes is called internucleosomal linker DNA and is protected by the linker histone H1. On average linker DNA in *S. cerevisiae* is around 18 bp, and in humans around 38 bp (Lee et al., 2007; Schones et al., 2008).

The composition of individual histone octamer can vary, and all eukaryotes possess histone variants, examples of which include H2A.Z and in mammals H2AX. H2A.Z is a variant which replaces the H2A protein and is frequently found in nucleosomes arranged at the beginning of genes at what is referred to as the transcriptional start site (TSS) (Raisner et al., 2005).

The coiling of DNA around histones facilitates its compaction and packaging into the nucleus, but simultaneously physically restricts access to the DNA. For instance, nucleosomes present a barrier to transcriptional machinery, and *in vitro* studies demonstrate that even a single nucleosome can inhibit RNA transcription (Izban and Luse, 1992; Lorch et al., 1987). A wide range of proteins have evolved to interact with histones and thereby regulate the chromatin structure of the genome to control access to DNA.

Most of such interactions are mediated by chromatin-regulating enzymes that recognise and bind the N-terminal domains (NTDs) of various histones. These 'histone tails' protrude from the globular histone domain of the eight subunits and are frequently marked by post-translational modifications (PTMs) (Figure 1.4C) (Hacques et al., 1990; Luger et al., 1997).

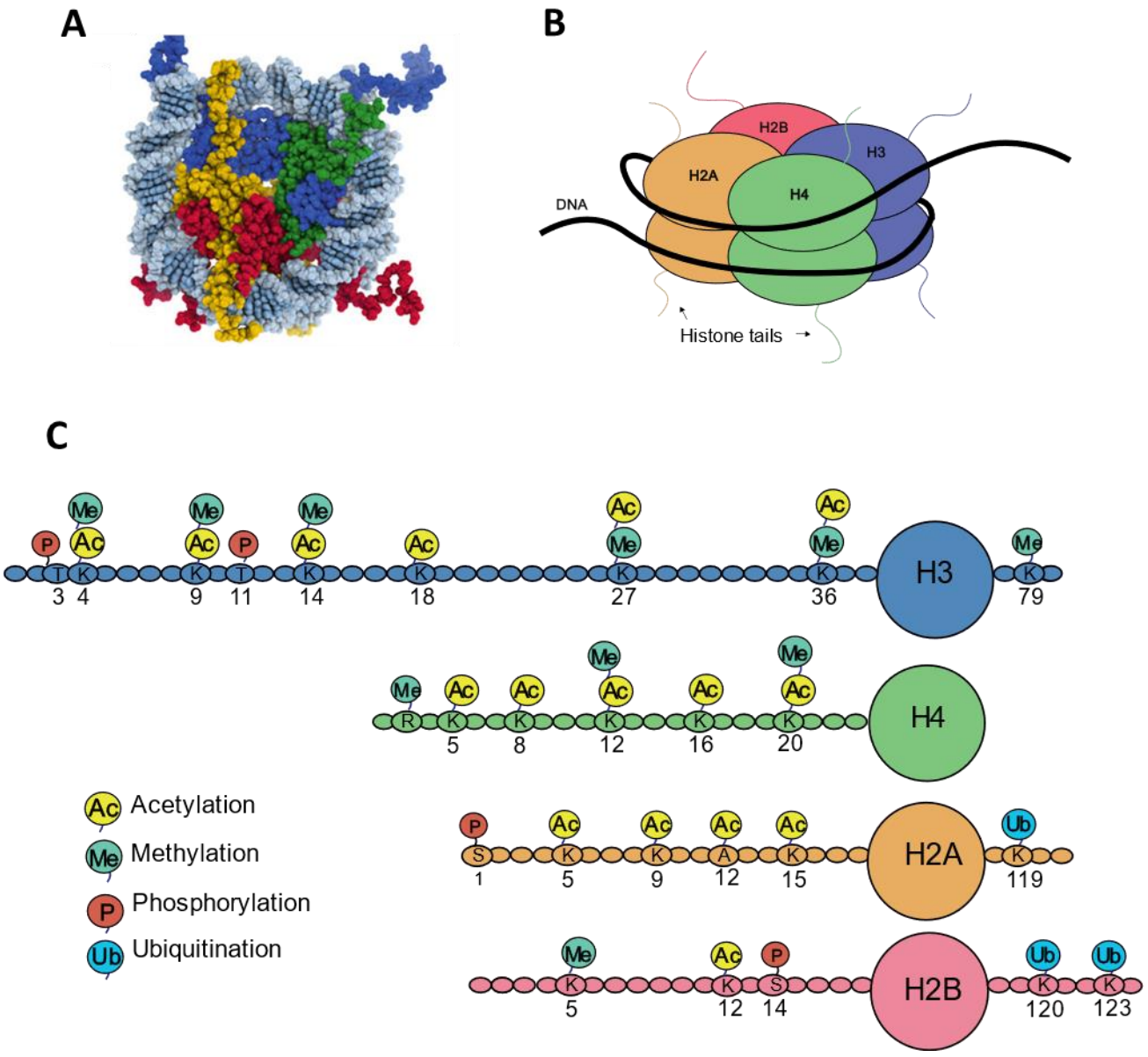

Figure 1.4. Nucleosome structure and modifications. (A) Crystal structure of DNA wrapped around the histone octamer. Histone H4 (green), H3 (blue), H2A (yellow), H2B (red) and DNA (light blue). (adapted from Workman and Abmayr 2014). **(B)** A scheme of the organisation of the histone octamer core particle and relative positions of the histone subunits. Dimers of H2A, H2B, H3 and H4 are wrapped by around 147 bp of DNA. N-terminal histone tails protrude from the core complex. **(C)** A scheme of common, but not all, histone post-translational modification. Sites which can be marked by different modification have the modification stacked above one another, however these are mutually exclusive.

The arrangement of nucleosomes along a given length of DNA can initially appear irregular and dissimilar between genes. However, high-throughput assays of nucleosome occupancy had

demonstrated that their organisation correlates with features of the underlying DNA. In nearly all genes, the position of the first nucleosome after the TSS (the +1 nucleosome) is almost invariable between different cells (Mavrich et al., 2008; Schones et al., 2008). Furthermore, these +1 nucleosomes are preceded by a characteristic nucleosome-free regions (NFR) of around 140 bp and a consistently positioned -1 nucleosome.

The NFR is established by the activity of DNA binding proteins and by the underlying sequence of DNA within NFR, which has inherently lower affinity for histones (Struhl, 1985; Anderson and Widom, 2001). Maintaining the NFR allows for the binding of transcriptional activators that subsequently facilitate gene expression.

At a genome-wide scale, the compactness of nucleosome organisation (the amount of accessible DNA to DNA-binding enzymes) can be found to divide the genome into two subsets of organisation. The less condensed, more accessible, and more transcriptionally active *euchromatin*, and the denser, more compacted, and less transcriptionally active *heterochromatin.*

1.3.2. Histones' role as signalling hubs from chromatin modifying enzymes

The N-terminal histone tails which protrude from the core nucleosome contain many basic residues that mediate interactions with effectors and can be modified by chemical moieties (Davey et al., 2002). Such PTMs, or histone modifications, have the effect of controlling both the recruitment and activity of chromatin-modifying proteins. These can also modify the intrinsic characteristic of the histone-DNA complex, such as the stability of contacts and the mobility of the nucleosome.

Histone modifications include, but are not limited to, the methylation and acetylation of lysine residues, the phosphorylation of threonine and serine residues, and the ubiquitination of lysine residues. Modified histone tails can be recognised by proteins containing specialised interaction domains for specific modification (commonly referred to as 'readers' of epigenetic marks) (Ruthenburg et al., 2007). Chromatin-modifying enzymes containing bromodomains or chromodomains recognise acetylated or methylated lysine residues, respectively. Furthermore, many other chromatin-interacting proteins have evolved to recognise histone modifications at specific residues, further specialising their targeting.

The recruitment of regulatory factors is an extrinsic effect of post-translationally modified histones; however, certain histone marks also have effects on the intrinsic properties of chromatin. The lysine residues of the histone tails typically have a positive charge and readily interact with negatively

charged DNA. Acetylation of lysine residues removes this charge and leads to a 'loosening' of the interaction between the histone molecule and DNA. This results in the non-liker DNA being more accessible to proteins and eliminates interactions between adjacent histones, resulting in decompaction of the chromatin fibre (Gross et al., 2015).

Due to these various properties and interacting partners, certain histone modifications have strong correlations with genomic features and transcriptional properties. Histone hyperacetylation correlates strongly with transcriptionally active regions, while hypoacetylated histones are typically found in silent chromatin. More specific examples include the trimethylation of H3K4 (H3K4me3) which is almost invariably associated with the TSS of active genes (Santos-Rosa et al., 2002; Guenther et al., 2007). Similarly, acetylation of H3K9 (H3K9ac) is found at the promoters of most active genes and directly promotes their activation (Grant et al., 1997; Syntichaki et al., 2000; Baptista et al., 2018).

H3K36me3 is also associated with active transcription and is found within gene bodies where it promotes genome stability (Kizer et al., 2005; Lee and Shilatifard, 2007). Furthermore, entire chromatin domains can be characterised as active when enriched in the acetylation of H4K16 (H4K16ac) and methylation of H3K79 (H3K79me3), or conversely inactive in their absence (Robert et al., 2004; Pokholok et al., 2005).

Similarly, differences in the composition of histone octamers also increases the functional complexity of chromatin. The initiation site of genes is flanked by nucleosomes containing the H2A.Z variant (Raisner et al., 2005; Zhang et al., 2005), while sites of DNA double strand break are marked by the phosphorylated H2AX histone variant (γH2AX) (Rogakou et al., 1998).

Through the combination of histone tail modifications and changes to nucleosome composition, histones act as signalling hubs that vastly increase the complexity of regulatory networks. Histones and their regulation and modification form the foundations of *epigenetic regulation*; the control of gene activity irrespective of the DNA sequence itself. Therefore, understanding the mechanisms controlling and responding to these processes is essential for the study of gene activity and genome stability.

1.3.3. ATP-dependent chromatin remodelling complexes

The regulation of the position and composition of individual nucleosomes, relative to the underlying sequence, has perhaps the most profound effect on DNA-dependent processes. Control of these processes is carried out by the ATP-dependent chromatin remodelling complexes. Using the energy of

ATP hydrolysis, these multisubunit protein complexes can disrupt the contacts between histone octamers and DNA, and thus slide, remove, or exchange variants composing the histone octamers. The result of this is either the exposure or obstruction of DNA binding sites caused by the sliding or eviction of nucleosomes or the change to nucleosome compositing through the exchange of various histone variants. This activity indirectly regulates the ability of various DNA binding proteins (DBPs) to interact with DNA and control transcription (Figure 1.5A). By regulating the composition of chromatin and access to DNA, ATP-dependent chromatin remodelling complexes influence nearly all aspects of nuclear biology (Badis et al., 2008; Clapier and Cairns, 2009; Peterson and Workman, 2000; Whitehouse et al., 2007).

Four major conserved families of ATP-dependent chromatin remodelling complexes exist across eukaryotes. Common among them is an ATPase domain of the Snf2-family that is flanked by different accessory domains that differentiate the different remodeller families (Figure 1.5B). In all ATP-dependent chromatin remodelling complexes, the ATPase domain translocates DNA relative to the histone octamer, which is usually recognised and bound by the other subunits of the complex (Clapier and Cairns, 2009).

The SWI/SNF family containing a Helicase-SANT (HSA) domain, which facilitates interactions with histones, actin, and actin-related proteins (ARPs) and a bromodomain which recruits the complex to acetylated histones. The SWI/SNF family is recruited to the TSS of activated genes by acetylated histone modifications such as H3K9ac, and their activity promotes the initiation of mRNA transcription and suppressing non-coding RNAs (ncRNAs).

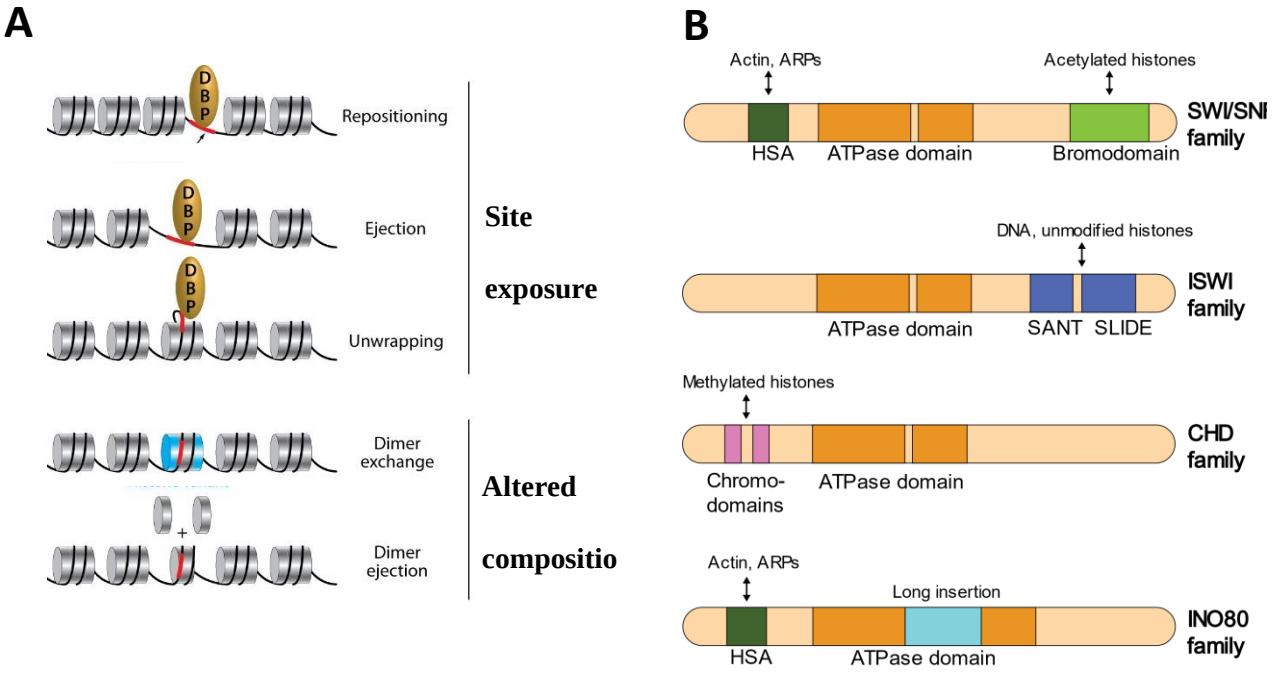

Figure 1.5. ATP-dependent chromatin remodelling complexes. (A) Summary of different functions of chromatin remodelling activity. DNA binding proteins (DBPs) are only able to interact with DNA following the repositioning or ejection of histones to reveal the binding site. Additionally, the unwrapping of DNA around histones can reveal binding sites. Histone variants can also be integrated or ejected from nucleosomes changing their structure and molecular properties. (Adapted from Clapier and Cairns, 2009). **(B)** Scheme of the Snf2 ATPase subunit of each of the four families of chromatin remodelling complexes. The unique domain architectures of each ATPase define the four families (Peterson and Workman, 2000; Whitehouse et al., 2007).

The ISWI family contains a HAND-SANT-SLIDE domain which interacts with unmodified histones and linker DNA (Figure 1.5B). This family of remodelers generally repress transcription by organising rigid nucleosome arrays, although some complexes within the ISWI family can promote mRNA transcription (Corona and Tamkun, 2004). In mammalian cells, ISWI family complexes enable DNA replication through compacted heterochromatin (Collins et al., 2002).

CHD family complexes are characterised by tandem chromodomains near the ATPase domain which enable their interaction with methylated histone residues. Much diversity exists within the CHD family, but generally these complexes can slide or evict histones thereby promoting transcription (Marfella and Imbalzano, 2007; Mills, 2017).

The INO80 family is characterised by an ATPase domain which contains a long insertion to which the Rvb1/2 helicase replated AAA-ATPase proteins bind. Additionally, the core subunit includes an HSA domain which binds actin and Arps. In budding yeast two members of the INO80 family exist, INO80 complex and SWR1 complex. SWR1 is unique among ATP-dependent chromatin remodelling complexes in that the exchange of H2A histone for the H2A.Z histone variant is the only molecular role of this complex (Krogan et al., 2003; Mizuguchi et al., 2004; Luk et al., 2010).

Unlike SWR1, the INO80 complex can slide and position nucleosomes, and it also has an opposing role to SWR1 in evicting H2A.Z from nucleosomes and promoting their exchange for H2A. Through these biochemical functions, INO80 is involved in a diverse set of cellular processes including transcription, DNA repair and DNA replication (Shen et al., 2000; Attikum et al., 2004; Papamichos-Chronakis and Peterson, 2008; Papamichos-Chronakis et al., 2011; Poli et al., 2017).

1.3.4. The INO80 complex

The INO80 ATP-dependent chromatin remodelling complex is evolutionarily conserved across all eukaryotic evolution and is involved in one of the most diverse set of functions among the chromatin remodelling complexes (Poli et al., 2017). INO80 complex activity can be divided into two primary biochemical functions, the sliding of nucleosomes and the exchange of histone dimers. Through these, the complex is involved in regulating gene transcription, DNA replication and genome stability.

In budding yeast, the complex is made up of 15 subunits: the Snf2 ATPase Ino80, three actin-related proteins (Arp4, Arp5 and Arp8), the AAA+ ATPase Rvb1/2, Taf14, Nhp10 and the Ies1-6 subunits (Shen et al., 2000, 2003). The Ino80 protein forms both the main catalytic subunit and acts as the scaffold around which the remaining subunits, divided into structural and functional modules, organise (Tosi et al., 2013; Watanabe et al., 2015; Eustermann et al., 2018).

The Ino80 subunit forms the core of the complex and is connected to the Rvb1/2 hexametric ring which forms a “head-like” module. The Nhp10 modules (made up of Nhp10, Ies1, Ies3 and Ies5) is positioned at the core of the complex. The Ies6-Arp5 modules bridges these two modules and finally the Arp8 module (Arp8, Ies4, Act1, Arp4 and Taf14) form a flexible “hinge” module completing the complex (Figure 1.6A). The long insertion with the Ino80 ATPase domain facilitates the interaction of Rvb1/2 and these proteins are required for correct complex assembly and for its chromatin remodelling activities (Figure 1.6B) (Jónsson et al., 2004; Zhou et al., 2017). The Ies2 subunit is not part of any module but interacts with the Ino80 subunit stabilising its confirmation.

Both Arp8 and Arp5 proteins are important in INO80 activity as they are critical for interaction with nucleosomes and chromatin remodelling (Shen et al., 2003; Watanabe et al., 2015). The Arp8-Arp4 module interacts with non-histone bound DNA and act as a sensor, regulating nucleosome sliding (Knoll et al., 2018). The loss of Arp8 does not compromise INO80 recognition of nucleosomes however the remodelling activity of the complex is dependent on the presence of this subunit.

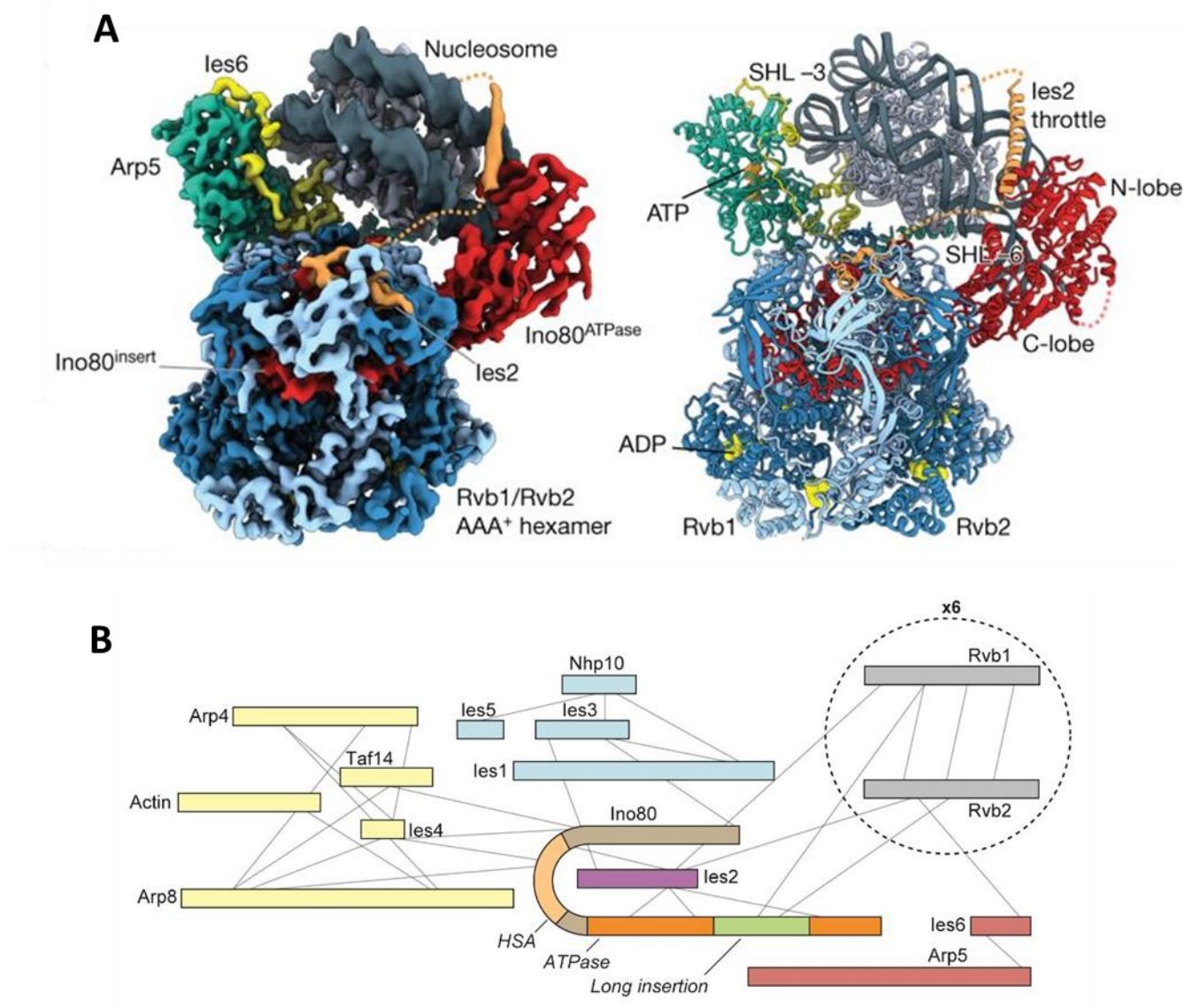

Figure 1.6. Structure and complex organisation of INO80. (A) 4.3Å Cryo-electron microscope image of the INO80 complex (excluding the Arp8 module) bound to a nucleosome. Colours are: nucleosomes (silver), Ino80 (red), Ies2 (orange), Arp5 (green), Ies6 (yellow), Rvb1/2 (Blue). ADP and ATP molecules are highlighted. (adapted from Eusterman et al 2018). **(B)** A schematic representation of the interactions between the different INO80 subunits and the central Ino80 subunit (adapted from Tosi et al 2013).

The Arp5 module binds histone H2A/H2B and maintains a "grip" on the nucleosome as ATPase activity of Ino80 pumps DNA against this, resulting in nucleosome sliding. Loss of the Arp5 subunit leads to compromised INO80 function as both nucleosome recognition and remodelling activity are severely compromised (Tosi et al., 2013; Eustermann et al., 2018).

1.3.5. Transcriptional regulation by INO80

The INO80 complex was initially discovered as a transcriptional regulator of the *INO1* gene and subsequent work also identified the *PHO5* and *GAL1* genes as targets for INO80 control (Barbaric et al., 2007; Ebbert et al., 1999; Steger et al., 2003). Measuring the genomic enrichment of INO80 by co-purifying chromatin bound Ino80 by chromatin immunoprecipitation (ChIP), found it to be most abundant around gene promoters. The enrichment of Ino80, Arp5 and Ies6 was most significant at the +1 nucleosome of the TSS and the INO80 complex was found to be capable of binding over 90% of yeast promoters (Yen et al., 2013; Yao et al., 2016). Current models suggest that INO80 preferentially recognises and binds DNA devoid of nucleosomes such as the NFR upstream of transcription initiation sites.

Studies where chromatin was reconstituted *in vitro* found that INO80 was the only chromatin remodeller capable of correctly organising the -1 and +1 nucleosomes of the NFR, relative to the TSS (Krietenstein et al., 2016). This suggests that INO80 may have a fundamental role in organising the nucleosomal architecture around the TSS of most genes. Accordingly, both SWI/SNF and INO80 were found to be required for correct promoter remodelling during gene activation (Barbaric et al., 2007; Steger et al., 2003).

The nucleosomes around the TSS are enriched for the histone variant H2A.Z, and its removal by INO80 appears to regulate the passage of transcriptional machinery past the +1 nucleosome (Weber et al., 2014).

Measurements of gene activity in yeast strains where either *Ino80* or *Arp8* subunits are deleted, found that approximately 20% of the yeast genome was significantly mis-expressed (Attikum et al., 2004). Similarly, knock down of human INO80 also identified broad changes to gene activity (Cao et al., 2015). Interestingly, in both studies, researchers found nearly equal ratios of genes being upregulated and downregulated, suggesting INO80 does not have a distinct role as a transcriptional coactivator like other chromatin remodellers (for example SWI/SNF). However, these studies only measured steady-state RNA levels, which reflect various cellular process and maynot be accurate representations of transcriptional activity. Indeed recent work has demonstrated that INO80 is involved in the regulation of transcriptional elongation and mRNA stability of certain transcripts (Luzzi et al., 2021). Quantifying

steady-state RNA does not reveal differences in the rate of nascent RNA synthesis and control of mRNA stability, instead studies using methods designed to measure nascent RNAs should be employed to study the role of INO80 in transcription (Wissink et al., 2019).

Recent transcriptome analysis of *Arp5*, *Ies6*, and *Ino80* deleted cells found that genes associated with metabolic pathways were disproportionally affected. Specifically, glycolysis-related genes were found to have reduced expression while genes of the oxidative phosphorylation pathway had increased expression (Yao et al., 2016). Subsequent work found that transcriptional changes caused by the *ino80Δ* mutation resembled the effects of TORC1 inhibition by rapamycin on gene expression, suggesting that the *ino80* deleted mutant resembled TORC1 inhibition as a result of INO80 activity promoting active TORC1 signalling (Beckwith et al., 2018). Furthermore, many TORC1 responsive genes were found to have decreased histone acetylation in the *ino80*-deficient strain. However, no direct mechanism was identified connecting INO80 to TORC1 signalling or chromatin acetylation of these genes.

More evidence connecting INO80 activity with metabolic gene regulation was identified in metabolically synchronised yeast cells. In such conditions, *S. cerevisiae* coordinate various pathways, including gene expression, with respiration and cell division (Tu et al., 2005). Mutants of the INO80 complex were found to have defective oxygen consumption patterns and failed to correctly coordinate cell division with metabolic state (Gowans et al., 2018). The YEATS domain of the Taf14 protein was found to be essential in silencing the expression of growth promoting genes during the low oxygen phase of the synchronised metabolic cycle (Gowans et al., 2019), mediated by its recruitment to modified H3K9 residue (Andrews et al., 2016). Taf14 is a subunit of various complexes, including INO80, and the study did not show this function to be dependent the INO80 complex itself. Therefore, it is still an open question whether INO80 is directly involved in this process.

Taken together, these results are suggestive of a role for INO80 in regulating metabolic gene expression, however the mechanism of this remains unknown.

1.3.6. Genome stability maintenance by INO80

The mis-regulation of chromatin-based processes or the failure to address faulty DNA-interacting machinery, can lead to potentially lethal DNA damage.

INO80 has been found to be directly involved in multiple pathways protecting genome stability. Double strand break (DSB) repair by homologous recombination involves the resection of DNA ends and INO80 is involved in this process alongside other chromatin remodellers (Attikum et al., 2007).

The loss of INO80 leads to compromised homologous recombination and sensitivity to DNA damage inducing agents (Kawashima et al., 2007; Papamichos-Chronakis et al., 2006). Furthermore, the site of a DSB is known to move within the nucleus (Dion et al., 2012; Miné-Hattab and Rothstein, 2012), predominantly to the nuclear envelope where DNA damage repair processes are believed to be favoured (Horigome et al., 2014; Nagai et al., 2008). Intriguingly, INO80 activity is required for the increased mobility and repositioning of DSB (Amitai et al., 2017; Horigome et al., 2014; Seeber et al., 2013). Whether INO80 activity similarly functions to reposition non-damaged loci is intriguing as it may be a mechanism influencing gene expression.

The stalling of DNA replication machinery or damage to the leading edge (called the replication fork) can result in DSBs and therefore must be addressed by the cell. INO80 activity was found to promote the restart of stalled replication forks through the eviction of nucleosomes downstream of the fork (Falbo et al., 2009; Papamichos-Chronakis and Peterson, 2008; Shimada et al., 2008). The recruitment of INO80 to the site of the stalled replication fork was found to be mediated by ubiquitinated histone H2B (Lee et al., 2014).

Further highlighting the connection between ubiquitin signalling and INO80, the clearance of stalled RNA polymerase II (RNAPII) complex was mediated by the complex (Lafon et al., 2015). Collisions between DNA replication and transcriptional machineries poses a threat to genome stability and the clearance of stalled RNAPII subunits from chromatin is needed for genome duplication to complete (Hamperl and Cimprich, 2016). Through interactions with Cdc48, a core component of the UPS, INO80 promotes the removal of ubiquitylated RNAPII from chromatin and its subsequent degradation in the 26S proteasome (Lafon et al., 2015).

Whether INO80's role in ubiquitin-mediated protein turnover is limited to RNAPII clearance is not yet established.

1.3.7. Crosstalk between metabolism and chromatin regulation

Recent work has begun to reveal the interconnectedness of epigenetics and metabolic state. Many of the most abundant epigenetic PTMs require the presence of metabolic intermediates and cofactors for their generation. Chromatin-modifying proteins, which mediate histone acetylation, deacetylation, methylation, and chromatin remodelling, all require metabolic intermediates as cofactors. In this way, epigenetic regulation of gene expression is sensitive to the metabolic state of the cell, acting as sensors for nutrient availability.

1.3.7.1. Acetyl-CoA

Acetyl-CoA is a critical metabolic intermediate which connects various pathways by influencing the activity of many different enzymes. Following glycolysis, pyruvate enters the TCA cycle in the form of acetyl-CoA and it is an essential precursor in the biosynthesis of lipids. Histone acetyltransferases (HATs) require acetyl-CoA for their activity as it is the only source for the acetyl moiety required for acetylation reaction on histones and elsewhere in the cell.

Cellular levels of Acetyl-CoA are a good general representation of the energetic state of a cell and physiological and environmental changes lead to considerable changes in abundance of acetyl-CoA (Pietrocola et al., 2015). Acetyl-CoA is separated between two distinct pools in the cell, the mitochondrial pool, and the nuclear/cytosolic pool. The mitochondrial acetyl-CoA pool is critical for oxidative phosphorylation and is primarily generated from metabolic breakdown of glucose, fatty acids, or ketone bodies (water soluble molecules produced from fatty acids). In the nucleus acetyl-CoA pools are primarily maintained by acetyl-CoA synthetase (Acs2 in yeast/ACSS1 in mammals) which generates acetyl-CoA from acetate (metazoans also possess the ATP-citrate lyase (ACL) which uses citrate as a substrate for acetyl-CoA production)

The loss of these genes leads to a significant decrease in histone acetylation, demonstrating the critical role these enzymes play by indirectly controlling epigenetic signalling (Wellen et al., 2009)

Increasing acetate levels by supplementing cells rescues the decreased histone acetylation levels clearly showing the potential histone acetylation has to sense the metabolic state of the cell (Takahashi et al., 2006)

As cells enter growth conditions, levels of intracellular acetyl-CoA increase, and this leads to increased histone acetylation by the HATs. As much of the subsequent acetylation occurs at the promoters of growth genes, acetyl-CoA is thought to function as a molecular rheostat co-ordinating nutrient availability with cellular growth (Cai et al., 2011).

1.3.7.2. NAD^+

Nicotinamide adenine dinucleotide (NAD^+) is both an essential cofactor for reduction-oxidation reactions, particularly during metabolism, and a critical substrate for certain enzymatic reactions. NAD is synthesised primarily from tryptophan consumed in an organism's diet, or from nicotinic acid (NA)

and nicotinamide (NAM), both forms of vitamin B_3. Lower eukaryotes and invertebrates predominantly use NA as a precursor for NAD synthesis while mammals use NAM. The NAD^+-dependent enzymes are the sirtuins (SIRs in yeast/SIRTs in mammals), poly(ADP-ribose) polymerases (PARPs) and cyclic ADP-ribose (cADPR) synthases (Verdin, 2015).

In yeast only the sirtuins are conserved and are made up of Sir2 and the Hst1-4 proteins. Sirtuins are class III histone deacetylases (HDACs) which depend on NAD^+ for their enzymatic activity (Blander and Guarente, 2004). The sirtuins catalyse the removal of the acyl groups by cleaving NAD^+ between nicotinamide and the ADP-ribose moieties. The ADP-ribose then serves as the acyl acceptor resulting in the acyl-ADP-ribose generation (Landry et al., 2000; Tanny et al., 1999).

The activity of sirtuins such as Sir2 can be enhanced through increasing NAD^+ levels by supplementing the growth media with NA or nicotinamide riboside (NR), a precursor to NAD^+ (Belenky et al., 2007). Conversely the deacetylase activity of Sir2 can be inhibited by the addition of NAM, which is a potent inhibitor of sirtuin enzymatic activity (Gallo et al., 2004) (Figure 1.7A).

Evidence shows that the activity of Sir2 is sensitive to fluctuations in cellular NAD^+ concentration brought about by changes in metabolic state (Guarente, 2000).

1.3.8. Heterochromatin and gene silencing

Eukaryotic genomes are organised between two distinct structural and functional domains; euchromatin and heterochromatin. Heterochromatin was initially described cytologically as regions of the chromosomes which remained dark and therefore compacted, throughout the cell cycle (Schultz, 1936). Subsequent work showed that common epigenetic characteristics define the state of heterochromatin across different organisms, even when cytological observation is not possible.

Heterochromatin is defined as transcriptional silent chromatin characterised by the compaction of nucleosome arrays making the DNA less accessible to nuclear process such as transcription and recombination. Heterochromatin plays an essential role in maintaining genome stability by preventing aberrant homologous recombination of repetitive elements and inhibiting the spreading of transposable elements (Allshire and Madhani, 2018). In metazoan, heterochromatin is critical throughout cell differentiation as it reinforces cell type through its silencing activity (Saksouk et al., 2015; Simon and Kingston, 2013).

In yeast, heterochromatin is found at the mating type *HM* locus, sub-telomeres and ribosomal DNA (rDNA). Silencing of these regions in *S. cerevisiae* is mediated by activity of the SIR proteins – Sir2, Sir3 and Sir4 – which form a repressive fibre which physically compacts the underlying DNA (Rine and Herskowitz, 1987; Gartenberg and Smith, 2016; Swygert et al., 2018). Furthermore, the compaction of the DNA is accompanied by the loss of H3K4 and K3K79 methylation, a process without which transcriptionally silent chromatin fails to form (van Leeuwen et al., 2002; Santos-Rosa et al., 2004; Katan-Khaykovich and Struhl, 2005; Altaf et al., 2007). The formation of heterochromatin is initiated by the recruitment of the Sir2-Sir4 complex by DNA-binding proteins such as Rap1 (at telomeres and HM mating type locus), and Orc1 and Abf1 (only found at HM mating type locus) (Diffley and Stillman, 1989; Hecht et al., 1996; Moretti et al., 1994). The NAD^+-dependant HDAC Sir2 then proceeds to deacetylate the histone tails of adjacent nucleosome. Importantly, Sir3 can bind the hypoacetylated H4K16, a well-established high-affinity interaction both *in vivo* and *in vitro* (Carmen et al., 2002; Hecht et al., 1995). This in turn recruits further Sir2-Sir4 heterodimers (Hecht et al., 1996; Imai et al., 2000; Onishi et al., 2007; Rusché et al., 2002).

Therefore, assembly and spread of the SIR complex is defined by this repeating stepwise process of recruitment, histone deacetylation, and binding of further Sir proteins.

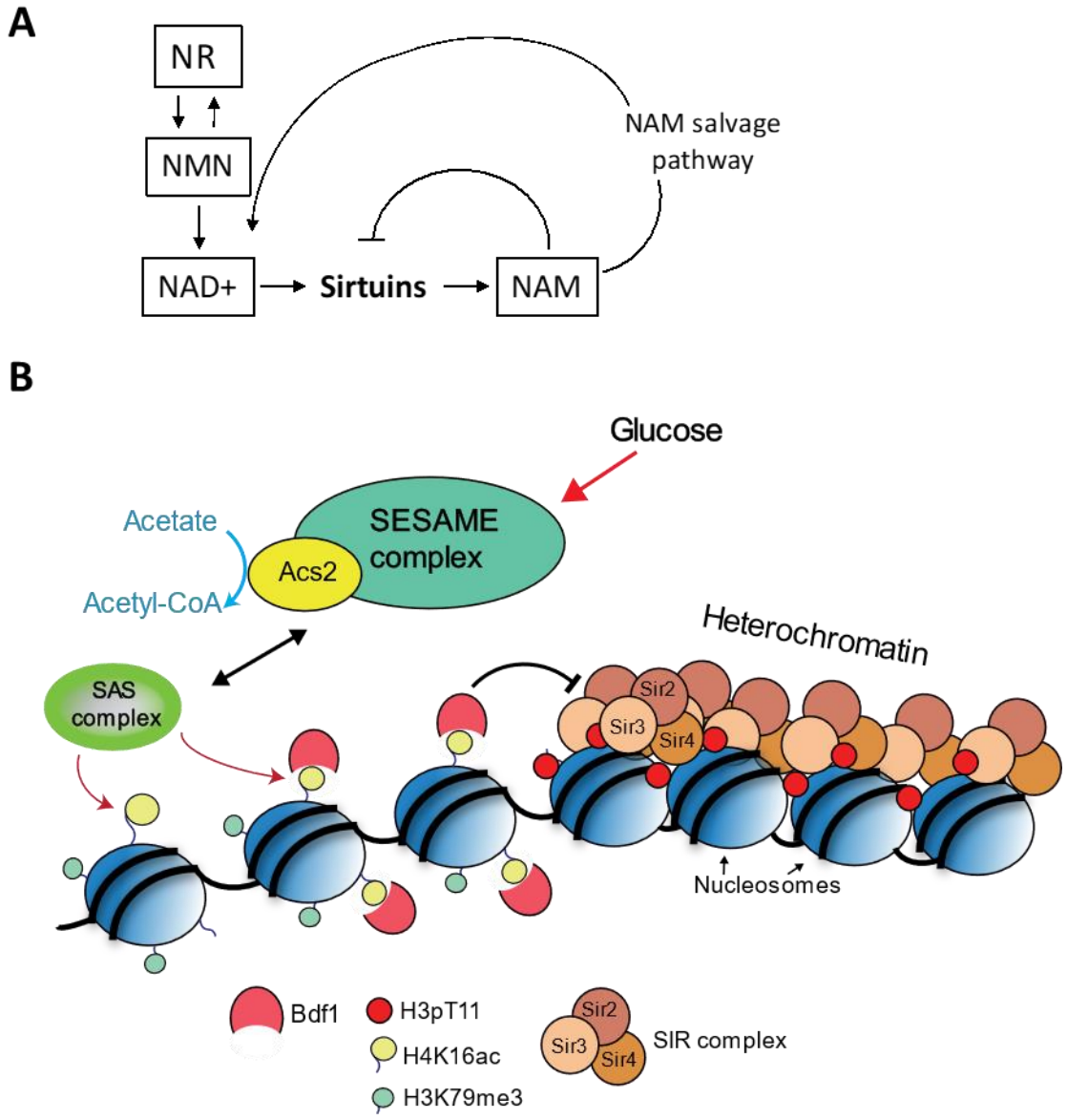

Figure 1.7. Metabolites directly affect epigenetic regulation. (A) NAD+ is consumed in Sir2-mediate deacetylation producing a molecule of nicotinamide (NAM). NAM is an inhibitor of Sir2 activity but can be converted back to NAD+. Budding yeast preferentially use nicotinic acid (NA) or nicotinamide riboside (NR) as a precursor to NAD+. **(B)** Schematic graph of the Serine-responsive SAM containing metabolic enzyme (SESAME) complex activity at subtelomeres. Red arrows indicate glucose to promote SESAME activity. Blue arrow represents enzymatic activity of Acs2. Double sided black arrow represents recruitment. Black bar representing the inhibitory action of Bdf1 on SIR complex spreading. SESAME phosphorylate H3T11 in response to high glucose levels promoting heterochromatin silencing (not indicated in the figure). Additionally, the recruitment of the SESAME subunit Acs2 to subtelomeres promotes the activity of the histone acetyl-transferase SAS complex by increasing acetyl-CoA synthesis.

1.3.9. Euchromatin-Heterochromatin boundaries

At telomeres and subtelomeric regions, ChIP experiments suggest SIR spreading continues and decreases with distance away from the telomere until approximately 6-15 kb from the telomere (Xue et al., 2015, p. 80; Hocher et al., 2018; Xue et al., 2017). Since this self-reinforcing process can theoretically propagate itself indefinitely, tight regulation of the euchromatin-heterochromatin boundary must be established by the cell.

In budding yeast, boundary formation between active and inactive chromatin is predominantly controlled by the acetylation state of H4K16 and the methylation state of H3K79. Sas2 acetyltransferase catalyses the acetylation of H4K16 acetylation, while Dot1 methyltransferase mediates H3K79 mono, di and tri-methylation. Both H3K79 methylation and H4K16 methylation inhibit Sir3 binding to chromatin and therefore halt SIR protein spreading (Figure 1.7B) (Meijsing and Ehrenhofer-Murray, 2001; Osada et al., 2001; Altaf et al., 2007; Valencia-Sánchez et al., 2021). Methylation of histone H3 in silent chromatin is controlled by the ubiquitination of H2B lysine 123 (H2BK123ub) and by the INO80 complex. Together with H4K16ac, H2BK123ub is required for Dot1 recruitment and activity (Gardner et al., 2005). INO80, instead inhibits transcription associated H3K79 methylation, thereby promoting a silent state (Xue et al., 2015).

In addition to the methylation state of H3K79, active competition between Sir2 and Sas2 over the acetylation state of H4K16 plays a vital role in creating a boundary to the spread of the SIR protein (Kimura et al., 2002). At a basic level, Sir2 activity outcompetes Sas2 near the SIR nucleation site however at increasing distance from the telomere Sas2 acetylation activity takes precedence. Additionally counteracting the expansion of SIR proteins are the bromodomain containing Bdf1 and Yta7 proteins, which bind to H4K16ac (Ladurner et al., 2003; Jambunathan et al., 2005; Tackett et al., 2005). H4K16ac promotes the incorporation of the H2A.Z variant into nucleosomes at the boundary with heterochromatin, and this further inhibits heterochromatin spreading (Meneghini et al., 2003; Shia et al., 2006).

Finally, strong promoters and discontinuities in the nucleosome array, and particularly the establishment of NFRs, acts as a strong barrier to SIR spreading (Bi and Broach, 1999; Bi et al., 2004b; Simms et al., 2008; Dhillon et al., 2009).

1.3.10. Heterochromatin dynamics

Despite the various reinforcing mechanisms to ensure its stability, heterochromatin responds to various internal and external stimuli (Wang et al., 2016).

Aging leads to a global loss of heterochromatin in various eukaryotic organisms (Zhang et al., 2015). In yeast, changes to temperature lead to increased telomere silencing (Bi et al., 2004a). In addition, cell metabolic state has been shown to have extensive effects on chromatin. Changes to the carbon source have significant effects on telomere silencing. When glucose is replaced by galactose telomeric silencing is reduced however the change from glucose to glycerol leads to increased telomere silencing (Jacobson and Pillus, 2009; Vall-llaura et al., 2019). Additional glucose starvation leads to increased NAD^+ levels and the resulting enhancement of Sir2 activity promotes telomere silencing (Lin et al., 2002).

Sub-telomeric heterochromatin DNA is not devoid of genes and instead this region of the genome was found to contain a surprising amount of stress response genes in various yeast strains (Ai et al., 2002; De Las Peñas et al., 2015; Jethmalani et al., 2021). Two such gene families found in yeast are the *PAU* and *COS* gene families, both of which have over 10 members predominantly located within 10 kb of chromosome ends (Spode et al., 2002; Viswanathan et al., 1994). Both gene families have been implicated in metabolic regulation (Rachidi et al., 2000; Ai et al., 2002; MacDonald et al., 2015).

However, the exact mechanism by which telomeric genes can escape silencing and respond to metabolic, and stress, stimuli, is poorly understood.

1.3.11. The SESAME complex and Acs2

Recent work has increasingly found more connections between metabolic state of the cell and the regulation of heterochromatic gene expression.

The Serine-responsive SAM-containing Metabolic Enzyme complex (SESAME) is an example of a newly described mechanism directly linking metabolism with chromatin silencing (Li et al., 2015). The pyruvate kinase Pyk1 is a key enzyme during glycolysis and forms the SESAME complex together with the acetyl-CoA synthase Acs2 and other accessory proteins. The SESAME complex responds to glucose levels and at high glucose levels leads to the phosphorylation of histone H3T11 (H3pT11) within telomeres. The presence of H3pT11 increases Sir2 occupancy at telomeric DNA and increases gene silencing (Zhang et al., 2021). Set1-mediated H3K4 methylation promotes the recruitment of SESAME to active genes however SESAME recruitment and H3pT11 enrichment at sub-telomeric heterochromatin was unaffected in *set1Δ* (Zhang et al., 2021). This suggests that SESAME recruitment to heterochromatin is independent on H3K4me and the mechanism controlling this pathway remains unclear.

The SESAME complex interacts with the SAS acetyl-transferase complex and promotes SAS-mediated H4K16 acetylation at sub-telomeric chromatin (Figure 1.7B) (Chen et al., 2021).

The conversion of acetate to acetyl-CoA by Acs2 directly enhances H4K16 acetylation by increasing local acetyl-CoA concentrations and counteracting SIR spreading through increasing Bdf1 occupancy at the boundary (Chen et al., 2021). The authors did not investigate the effect of SESAME on the acetylation of other histone residues and whether SESAME promotes all histone acetylation is an open question. Similarly, whether Acs2 recruitment and activity is dependent on SESAME complex is not clear.

The SESAME complex is an intriguing example of how cells incorporate metabolic state such as sensing glucose and acetate availability, with regulation of heterochromatin.

What additional mechanisms control this pathway, and whether SESAME recruitment specifically regulates biological pathways through its function at sub-telomeres is not clear.

1.4. Aim of this study

The role for INO80 in *Saccharomyces cerevisiae* metabolic gene regulation is supported by various experimental studies, however the mechanism of this process is not established. Furthermore, the significance of INO80 regulation of metabolic processes is still poorly understood. Whether INO80 activity is involved in the cellular response to metabolic stress is not known.

The aim of this study is to characterise the role of INO80 in metabolism by studying the role the complex plays in the metabolic stress response. The mechanism for INO80 regulation of metabolic gene activity is not known and we set out to test how loss of *Ino80* affects gene expression following metabolic stress.

Finally, recent evidence has implicated INO80 in regulating the turnover of ubiquitinated proteins on chromatin. Whether INO80 is involved in global protein turnover or if this is limited to chromatin bound factors is not known.

In summary, this thesis aims to characterise the role of INO80 in metabolic stress response, investigate the role of INO80 in protein turnover, and investigate the molecular mechanism of INO80 metabolic gene regulation in *Saccharomyces cerevisiae*.

Chapter 2

Chapter 2. Materials and Methods

2.1. General yeast cell culture

All strains used in this study are derivatives of LS20, S288C and BY4741 genetic backgrounds (Table 2.1).

The culture of yeast strains was done following standard protocols (Longtine et al., 1998). Culture was carried out in rich media (YPD: 1% yeast extract, 2% peptone, 2% glucose) or synthetic complete media (SC/CSM: 0.13 % CSM powder, 0.17 % yeast nitrogen base, 2 % glucose, 0.5 % ammonium sulphate) (all medias used are listed in Table 2.2). If an auxotroph was used for selection, the SC medium was made using the appropriate drop-out mix. During experiments, the cultures were always grown at 30°C and allowed to double once before use in any downstream work. Generally, yeast cultures were seeded at OD_{600} 0.25-0.3 harvested at OD_{600} 0.7-0.8 (unless otherwise specified).

Table 2.1 Yeast strains used in this study

Strain	Referred as	Genotype	Source
YM50	WT/Untagged	LS20 [*MatΔ ade2 can1r cyh2r lys S URA3-52 trp1Δ his3-Δ200GAL:HO leu 2Δ]*	(Sandell and Zakian, 1993)
YM157	Ino80-HA	LS20 INO80-3HA::KANMX POL1-13Myc::TRP1 bar1Δ::HisG-URA3	(Papamichos-Chronakis et al., 2011a)
YM85	*ino80Δ*	LS20 *ino80Δ::*KANMX	(Papamichos-Chronakis and Peterson, 2008a)
YM181	*arp8Δ*	LS20 *arp8Δ::*KANMX	(Papamichos-Chronakis et al., 2011a)
YM899	Ino80-FLAG	BY4741 *INO80-5XFLAG::*NATMX	(Lafon et al., 2015)
YM933	*atg1Δ*	LS20 *atg1Δ::*KANMX	This study

YM1252	*atg1Δarp8Δ*	LS20 *atg1Δ::*KANMX *arp8Δ*::HPHMX	This study
YM1310	WT	BY4742 (MATa his3Δ0 leu2Δ0 lys2Δ0 ura3Δ0)	Gift from Piper R (MacDonald et al., 2015)
YM1277	*cosΔ*	BY4742, *cos1Δ cos2Δ cos3Δ cos4Δ cos5Δ cos6Δ cos7Δ cos8Δ cos9Δ cos10Δ cos12Δ yhl042wΔ yhl043wΔ yhl044wΔ yir043cΔ yir044cΔ* **	Gift from Piper R (MacDonald et al., 2015)
YM941	Idh1-GFP WT	BY4741 ATG8 wt-T-P-kanMX IDH1-EGFP-natNT2	Gift from Nakatogawa H (Mochida et al., 2015)
YM942	Idh1-GFP *atg1Δ*	BY4741 ATG8 wt-T-P-kanMX IDH1-EGFP-natNT2 *atg1Δ::zeoNT3*	Gift from Nakatogawa H(Mochida et al., 2015)
YM1304	Idh1-GFP *cosΔ*	IDH1-GFP::KANMX *cos1Δ cos2Δ cos3Δ cos4Δ cos5Δ cos6Δ cos7Δ cos8Δ cos9Δ cos10Δ cos12Δ yhl042wΔ yhl043wΔ yhl044wΔ yir043cΔ yir044cΔ*	This study
YM0965	Idh1-GFP *ino80Δ*	BY4741 ATG8 wt-T-P-kanMX IDH1-EGFP-natNT2 *ino80Δ::HPHMX*	This study

YM969	Sec63-GFP WT	S288C SEC63-GFP::KANMX	This study
YM970	Sec63-GFP *ino80Δ*	S288C SEC63-GFP *ino80Δ::HPHMX*	This study
YM1302	Sec63-GFP *cosΔ*	BY4742 SEC63-GFP::KANMX *cos1Δ cos2Δ cos3Δ cos4Δ cos5Δ cos6Δ cos7Δ cos8Δ cos9Δ cos10Δ cos12Δ yhl042wΔ yhl043wΔ yhl044wΔ yir043cΔ yir044cΔ*	This study
YM955	Sec63-GFP *atg1Δ*	S288C SEC63-GFP** *atg1Δ::HPHMX*	This study
YM490	WT	S288C (*MATα SUC2 gal2 mal2 mel flo1 flo8-1 hap1 ho bio1 bio6*)	Gift from A. Peyroche (CEA)
	atg5Δ	S288C *atg5Δ::KanMX*	
YM1358	WT	BY4741 WT (MATalpha his3Δ0 leu2Δ0 lys2Δ0 ura3Δ0)	(Xue et al., 2015)
YM1359	*arp5Δ*	BY4741 *arp5Δ::KANMX*	(Xue et al., 2015)
YM1360	*sir3Δ*	BY4741 *sir3Δ::HPHMX*	(Xue et al., 2015)
YM1361	*sir3Δarp5Δ*	BY4741 *arp5Δ::HISMX sir3Δ::HPHMX*	(Xue et al., 2015)
YM1384	*sir2Δ*	LS20 *sir2Δ::KANMX*	This study
YM1396	*Sir2Δarp8Δ*	LS20 *sir2Δ::KANMX arp8::HPHMX*	This study
YM1431	Sir3-HA	LS20 Sir3-HA::KANMX	This study
YM1444	Sir3-HA *io80Δ*	LS20 Sir3HA::KANMX *ino80Δ::*HPHMX	This study

Table 2.2 – Medias used in this study

Name	Composition
YPD/YEPD	1% yeast extract, 2% peptone, 2% glucose
YP-Gal	1% yeast extract, 2% peptone, 2% galactose
SC/CSM	0.13 % CSM powder, 0.17 % yeast nitrogen base, 2 % glucose, 0.5 % ammonium sulphate
Drop-out media	0.13 % drop-out CSM powder, 0.17 % yeast nitrogen base, 2 % glucose, 0.5 % ammonium sulphate
SC-G	0.13 % CSM powder, 0.17 % yeast nitrogen base, 3 % glycerol, 0.5 % ammonium sulphate
SD-N	0.17% yeast nitrogen base, 2% glucose
SG-N	0.17% yeast nitrogen base, 3% glycerol

2.2. Yeast transformation protocol

Yeast transformation was achieved using standard lithium acetate (LiAc)-based protocols (Schiestl and Gietz, 1989). Briefly, exponentially growing yeast would be washed with water and 0.1 M LiAc. A transformation mis consisting of DNA, PEG, 1 M LiAc and salmon sperm carrier DNA was prepared and incubated with cells for 23 minutes at 42°C. The transformed yeast was first seeded in nonselective media and 24 hours were transferred to antibiotic-containing plates for selection of transformed clones.

2.3. Knock-out mutant generation and protein tagging

For gene deletion, open-reading frames (ORFs) with either the KANMX gene (taken from a pFA6a plasmid) or the HPHMX gene (from a pAG32 plasmid) was employed. The KANMX or HPHMX genes were amplified by PCR with primers that incorporated homology to the required gene. The yeast cells were transformed with the resulting PCR sample and deletion occurred by homologous recombination. The transformants were then tested for drug resistance on agar plates and genomic DNA was extracted from potential clones. PCR amplification from genomic DNA followed by

separation by gel electrophoresis was used to confirm gene deletions. Screening primers were designed to amplify from upstream of the target gene ORF and from within the antibiotic resistance gene (a band is expected when the gene is deleted). A second pair was designed to amplify from upstream of the target gene ORF and within the gene ORF (a successful gene deletion should not produce a band). Standard protocols followed (Longtine et al., 1998; Tong et al., 2001).

Table 2.3 Plasmids used in this study

Name	Plasmid	Application	Source
MP07	pPRS416-URA3	Empty vector	Addgene
MP13	pFA6a- 3HA-KANMX	Protein tagging	Gift from M. Longtine
MP16	pFA6a- KANMX	Gene deletion	Gift from M. Longtine
MP22	pFA6a- 3HA-HIS3	Protein tagging	Gift from M. Longtine
MP28	pAG32- HPHMX	Gene deletion	Euroscarf
MP34	pRS416- INO80-URA3	Ino80 gene	(Lafon et al., 2015)
MP39	pRS416- INO80(K737A)-URA3	INO80 activity assay	(Lafon et al., 2015)
MP160	pRS416- GFP-ATG8 – URA3	Autophagy assay	Gift from S. West
MP169	pFA6a – GFP(S65T) – HIS3MX	GFP protein tagging	Gift from D. Lydall

2.4. Autophagy induction (nitrogen starvation)

To study the response to nitrogen starvation, yeast strains were grown in synthetic complete medium (SC medium: 0.13% complete CSM mixture, 0.17% yeast nitrogen base, 2% glucose, 0.5% ammonium sulphate) to mid/late log phase (OD_{600} 0.8 – 1) at 30ºC. These were then washed twice in dH_2O and

transferred to nitrogen starvation medium (SD-N medium: 0.17% yeast nitrogen base without amino acids and ammonium sulphate and 2% glucose).

2.5. Mitophagy induction

The yeast was grown to OD_{600} 0.7-0.8 in SC medium and harvested by centrifugation. Cells were washed twice with dH20 and left in sterile water for 10 minutes to further deplete glucose. Cultures were then resuspended in SC-G media (0.13 % dropout of CSM powder, 0.17 % yeast nitrogen base, 3 % glycerol, 0.5 % ammonium sulphate) at $OD_{600\ 0.5.}$ Mitophagy was tested 24 and 48 hours following the switch to SC-G.

2.6. Measuring autophagy

Autophagic activity was measured in S288C WT, *atg5Δ* (S288C *atg5Δ::KanMX*), LS20 WT, *ino80Δ* (LS20 *ino80Δ::HphMX*), BY4742 WT and *cosΔ* (BY4742*, cos1Δ cos2Δ cos3Δ cos4Δ cos5Δ cos6Δ cos7Δ cos8Δ cos9Δ cos10Δ cos12Δ yhl042wΔ yhl043wΔ yhl044wΔ yir043cΔ yir044cΔ*). The indicated strains were transformed with pRS416-GFP-ATG8 (416 - Gift from Steve West (Yuce and West, MCB 2013) addgene ID: 49425) plasmid or empty vector pRS416 (adggene). The transformed strains were cultured in SC-uracil and switched to SD-N according to the standard protocol. Samples were collected before the switch to SD-N (0 h) and at the indicated time point after the switch Samples equivalent to 5 ml at OD_{600} 1 were collected and protein extraction by TCA and immunoblot analysis was performed. Vacuolar membrane staining was performed by incubating cells in 5 µg/mL of FM™ 4-64 dye (Invitrogen), gently mixing by inverting and applying the cells to microscope slides (VWR). Image evaluation of GFP-Atg8 localisation was performed using a Nikon eclipse 50i.

2.7. Spot-test assay

Cultures were processed for the spot test assay 5-10 days after the switch to growth in SD-N medium. Following the indicated time point, the cells were washed with dH20 and the concentrations of individual strains were equalised by OD_{600} 0.5. Samples were spotted on to YPD plates (1% yeast extract, 2% peptone, 2% glucose and 2% agar) in a 5-fold serial dilution. The plates were grown at 30 ° C for 48 – 72 hours and imaged on a G-box transilluminator (Syngene).

2.8. Growth on rapamycin plates

The S288C strains (WT and *ino80Δ*::HphMX), BY4741 strains (WT and *ino80Δ:HphMX*) and LS20 strains (WT and *ino80Δ::HphMX*) strains were grown to the mid-log phase (OD_{600} 0.6-0.8) and the concentrations were equalised by diluting with OD_{600}. Samples were washed with dH_20, and five-fold serial dilutions were then spotted to YPD plates or YPD plates containing rapamycin (1% yeast extract, 2% peptone, 2% glucose, 2% agar and 20 mM rapamycin). Additionally, the samples were spotted to synthetic complete plates (SC medium: 0.13% drop-out mix, 0.17% yeast nitrogen base, 2% glucose, 0.5% ammonium sulphate and 2% agar) either containing or lacking 20 mM rapamycin. The plates were incubated at 30°C for 72 hours and imaged in a G-box transilluminator (Syngene).

2.9. Phloxine B viability assay

Cells were collected after 0, 1, 3, 5, 7 and 10 days after the switch to growth in SD-N medium. Cells were pelleted and resuspended in fresh media containing 2 µg/mL Phloxine B. The cells were mixed by inverting and incubated for 5 minutes. The cells were then spun and washed twice in dH_20 followed by mounting on slides (VWR). Images were obtained with a 40x objective, using a Nikon eclipse 50i. The images were quantified using Fiji (Ver. 1.53c). For each condition >200 cells were counted, and the percentage of stained cells was determined. Each condition was repeated 3 or more times in independent biological replicates.

2.10. Growth curve analysis

Cells were seeded in a 96-well plate in YPD medium (YPD broth (Formedium)(1% yeast extract, 2% peptone, 2% glucose)) at an OD_{600} of 0.1. Cultures were made up to a volume of 150 µl and covered with Breathe-Easy® breathable films (Sigma-Aldrich). Cells were grown at 30°C and plates were agitated with shaking at 1000 rpm for 1 minute every 30 minutes. OD_{600} was measured using the CG-12 robot (S&P Robotics Inc.) every hour. Rapamycin was used at a final concentration of 20 mM. Hydroxyurea was used at a final concentration of 5 mM. To calculate the doubling time of each strain at the relevant time, the OD_{600} values were transformed into log2 and a line was plotted to the exponential phase of growth. The doubling time was then determined by using the equation of the line.

2.11. NAD^+ and NADH measurements

Measurement of NAD^+ and NADH levels in yeast whole cell extracts was carried out as described here (Kataura et al., 2022).

Briefly, cytoplasmic extracts were generated using either an acid solution (20% TCA) (for NAD^+) or a basic solution (0.5M sodium hydroxide (NaOH), 5 mM EDTA)) (for NADH). Subsequently, concentrated (5x) stocks of both acidic and basic solutions were added to the cytoplasmic extracts to extract NAD^+ and NADH. Samples were adjusted to pH 8. The levels of NAD^+ and NADH were measured by quantifying the fluorescence of resorufin produced by an enzymatic cycling reaction using resazurin, riboflavin 5' monophosphate, alcohol dehydrogenase and diaphorase. Fluorescence measurements were taken once a minute for 1 hour using a microplate reader (FLUstar Omega, BMG Labtech).The values of NAD^+ and NADH were determined using a β-NAD standard curve and normalised relative to measured protein concentration of each sample.

2.12. Western Blot analysis

2.12.1.1. Protein purification

Whole cell protein extracts were generated following the TCA protein extraction protocol (based on (Keogh et al., 2006)). Cultures were collected to an equivalent of 5 ml at OD_{600} 1, and harvested by centrifugation. All steps were performed on ice and with prechilled solutions. Cells were washed with 20% TCA (sigma-aldrich) and resuspended in 100 µL of 20% TCA. Cells were lysed for mechanical disruption of the cell wall using glass beads and a Precelly 24 homogeniser (Bertin Technologies). Disruption was achieved with three cycles at 6500 rpm for 30 seconds followed by a 2 minute pause. The samples were diluted by adding 200 µL of 5% TCA and centrifuged for 15 minutes at 13200 rpm at 4 °C. The pellets were solubilised in 30 µL 2M Tris pH 8.0 and 70 µL 3X SDS loading buffer (100 mM Tris-HCL pH 6.8, 4% SDS, 20% Glycerol, 200 mM DTT, bromophenol blue) and denatured at 95 °C 8 minutes and the insoluble material was removed by centrifugation. The material was kept at -20 °C or at room temperature prior onto loading to polyacrylamide gels.

2.12.1.2. SDS-PAGE

Polyacrylamide gels were cast by hand using APS/TEMED initiated reactions. The polyacrylamide concentration varied between 7.5% and 10% depending on the size of the target to be resolved.

2.12.1.3. Western Blotting

Polyacrylamide gel resolved samples were transferred to PVDF membranes (Biorad) using the Trans-Blot® Turbo™ transfer system (Biorad) at 1.3A / 25V for 8 minutes (immunoblot against GFP-Atg8) or 10 minutes (all other applications). The samples were blocked in 4% EveryBlott blocking buffer (Biorad) diluted in 1X PBS for 1 hour at room temperature. Primary antibodies were diluted in 4% blocking buffer and incubated overnight at 4 °C (Table 2.4). The membranes were washed with PBST (PBS ontaining 0.05% Tween 20 (Sigma)). Incubation with secondary antibodies was performed for 45 minutes at room temperature (Table 2.6). Protein detection was performed using enhanced chemiluminescence (ECL) (Life Technologies) and exposure and image capture was performed using the G-box transilluminator (syngene). GeneSys software (V1.5.4.0) was used to achieve correct exposure and image capture. Protein quantification and quantitative analysis was performed using Fiji software (version 1.53c).

Table 2.4 Primary antibodies used in this study

Target	**Animal origin**	**Dilution**	**Source**
Anti-GFP	Rabbit	1:1000	Cell signalling #2555
Anti-FLAG	Rabbit	1:2000	Cell signalling #
Anti-HA	Rabbit	1:1000	Abcam #9110
Anti-Ubiquitin (P4D1)	Mouse	1:1000	Cell Signalling #3936
Anti-Histone H3	Rabbit	1:5000	Abcam #1791
Anti-H3K9ac	Rabbit	1:2000	Abcam #4441
Anti-G6PDH	Rabbit	1:5000	Invitrogen PA5-27359
Anti-Acs2	Mouse	1:500	Gift from Boeke lab
Anti-Pgk1	Mouse	1:2000	Abcam #113687

Table 2.5 Secondary antibodies used in this study

Antibody	Dilution	Source
Anti-Rat IgG HRP conjugate	1:7500-1:20000	Santa-Cruz (sc-2032)
Anti-Mouse IgG HRP conjugate	1:7500-1:20000	Promega (W4021)
Anti-Rabbit IgG HRP conjugate	1:7500-1:20000	Promega (W4011)

2.13. Chromatin Immunoprecipitation

The relevant strains were diluted to an OD_{600} of 0.2 and cultured in 150 ml of SC media (0.13% complete CSM mixture, 0.17% yeast nitrogen base, 2% glucose, 0.5% ammonium sulphate) at 30 °C to an OD_{600} of 0.6. Samples that were to be switched to SD-N for nitrogen starvation were cultured at mid/late log (OD_{600} 0.8 - 1) prior to the switch to starvation medium. The switch to starvation medium followed previously described methods. Chromatin crosslinking was done using 1% formaldehyde (Sigma Aldrich) for 15 minutes (H3K9ac analysis), 30 minutes (Acs2 analysis), 45 minutes (Ino80-HA analysis) or 60 minutes (Sir3-HA analysis). The cross-linking reaction was quenched by using 150 mM Glycine (Promega) to neutralise the formaldehyde. Cells were harvested by centrifugation at 4 °C for 5 minutes at 3500 rpm, followed by three washes in pre-chilled 1X TBS buffer (Tris-HCL pH 7.6, NaCl 150 mM). The wanded cell pellets were resuspended in 400 µL of FA-lysis buffer (50 mM Hepes-KOH pH 7.5, 140 mM NaCl, 1 mM EDTA, 1% Triton X-100, 0.1% deoxycholate, 1X protease inhibitor cocktail) and lysed using Precellys 24 homogeniser (Bertin Technologies) using 4 cycles of 6500 rpm for 30 seconds and 2 minutes of pause. The lysed samples were then sheared at 4 °C using the Bioruptor® Plus sonication device (Diagenode) using cycles of 30 seconds maximum intensity sonication followed by 30 second pause. The sonication cycles used varied between 12 cycles (Ino80-HA ChIP, H3K9ac and Acs2 analysis) and 14 cycles (Sir3-HA analysis). After sonication, samples were diluted in 1 ml of FA-lysis buffer and centrifuged for 30 minutes at 13200 rpm and 4 °C. The supernatant was transferred to a new pre-chilled tube and the sample was centrifuged for an additional hour, at 4°C and 13200 rpm. The supernatant was then considered the 'input' and 10 µL of this was diluted in 450 µL of Tris-EDTA and set aside for to act as the input control. For immunoprecipitation, 150 µL of input chromatin was diluted in 250 µL of FA-lysis buffer and 6 µL of antibody (except ChIP for H3K9ac; 100 µL of input diluted in 300 µL FA-lysis buffer and 2 µL of antibody were used). The immunoprecipitation was then carried out at 4°C overnight on a rotating wheel, followed by a further 2 hours with the addition of 36 µL of Protein-A Sepharose beads (Invitrogen). The samples were then

washed for 5 minutes on a rotating wheel using 1.5 ml of FA-lysis buffer, FA-500 buffer (50 mM Hepes-KOH pH 7.5, 500 mM NaCl, 1 mM EDTA, 1% Triton X-100, 0.1% deoxycholate), LiCl buffer (10 mM Tris-HCL pH 8.0, 250 mM LiCl, 1 mM EDTA, 0.5% NP40, 0.5% deoxycholate) and finally Tris-EDTA. Following the final wash, the samples were resuspended in 250 µL of elution buffer (50 mM Tris-HCL pH 7.5, 10 mM EDTA, 1% SDS) and placed on a thermocycler at 65 °C for 15 minutes and shaking at 1200 rpm. The immunoprecipitated (IP) and input (IN) samples were then incubated with 100 µg of Proteinase K (Sigma-Aldrich) at 42 °C for 2 hours followed by another 2 hours at 70 ° C to heat inactivate Proteinase K and reverse crosslinking. The DNA samples were then purified by phenol-chloroform extraction and precipitated with 2.5 volume of 96% EtOH, 0.1 volume of 3M AcONa and 5 µg Glycogen (Life Technologies) for 30 minutes at -80°C. The precipitated samples were centrifuged at 4 °C and 13200 rpm for 30 minutes. The pellets were dried for 5 – 10 minutes and resuspended in 100 µL (IP) or 500 µL (IN) of nuclease-free water.

IP and IN DNA was measured using the Platinum® SYBR® Green qPCR Super-Mix UDG kit (Life Technologies) in 10 µL reactions. An Applied Biosystem Step-one Plus thermocycler was used and the programmes were performed following the recommended protocols for the kit and machine. Standard curves were measured and used to determine the abundance of DNA in each sample. IP/input values would then be normalised to an internal control and relative values presented.

2.14. RNA and qPCR

2.14.1.1. RNA extraction

The appropriate strains were grown to mid log phase (OD_{600} 0.6-08) and harvested by centrifugation at 4°C for 5 minutes at 1,800g. Samples were washed twice with pre-chilled dH_20 and snap frozen in liquid nitrogen. Cell pellets were thawed on ice and resuspended in 350 µL of pre-chilled TES buffer (10 mM Tris-HCL pH 7.5, 5 mM EDTA, 1% SDS). The purification of the RNA was done using the hot acid phenol purification process. An equal volume of pH 4.7 phenol acid solution was added to the cell lysates and incubated at 65 ° C for 20 minutes at constant shaking of 1400 rpm. The samples were then snap frozen in liquid nitrogen and immediately thawed again by centrifugation at 13000 rpm at room temperature for 15 minutes. The top aqueous phase was transferred to new tubes and precipitated by adding 3 volumes of 100% EtOH and incubation at -80°C for 30 minutes. The precipitate RNA was collected by centrifugation at 13000 rpm at 4°C for 30 minutes. The supernatant was removed and the pellets dried for 5 –10 minutes at room temperature. The pellet was resuspended in 50 µL of nuclease-

free water and the RNA concentration was determined using a Nanodrop 2000c spectrophotometer (Thermo Fisher Scientific).

2.14.1.2. RT-qPCR

The purified RNA samples were diluted to 70 ng/µL and the abundance of RNA was measured using the SuperScript® III Platinum SYBR Green one-step qRT-PCR kit (life technologies). Reactions were carried out in 10 µL volumes with specific primers to the targets, designed to amplify fragments 80 – 180 bp in length (Table 2.6). An Applied Biosystem Step-one Plus thermocycler was used and the programs were done following the recommended protocols for the kit and machine. Each sample was assayed in triplicate and the average value was used. For every pair of primers, a standard curve was generated using either known concentrations of standards or serial dilutions of input RNA. The abundance of RNA within each sample was quantified with reference to the standard curve and normalised against an internal control.

Table 2.6 qPCR primers used in this study

Primers	**Sequence**	**Target**
COS1 forward	AAAAGACGAAGCTGCCAAGG	*COS1* (TSS+517 to TSS +646)
COS1 reverse	TAGCATCTTCCAGGCCAACA	
COS5 forward	AAAAGACGAAGCTGCCAAGG	*COS5* (TSS+516 to TSS+668
COS5 reverse	TCCTTGGGAAGCTGAACGTC	
COS7 forward	AAAGTGGTGCGAATGGATGG	*COS7* (TSS+924 to TSS+1012)
COS7 reverse	CACAGTCAATCCCGTCGAAG	
COS8 forward	CACGTCTGGAAATGCTGACC	*COS8* (TSS+749 to TSS+913)
COS8 reverse	ATTTCGTCCCATCCATTCGC	
COSp forward	CCTCGAACTGCCATCTCACT	TSS of 7 *COS* genes (~TSS-27 to TSS+114)
COSp reverse	ACCAGGTAAAGCTGCTTCTG	

GAL1 forward	TGGAAAAGCTGCATAACCAC	*GAL1* (TSS-345 to TSS-173)
GAL1 reverse	ACTTTTCGGCCAATGGTCTT	
ACT1 forward	CGTTCCAATTTACGCTGGTT	*ACT1* (TSS+794 to TSS+999)
ACT1 reverse	AGCGGTTTGCATTTCTTGTT	
INO1 forward	GTGCACGTACAAGGACAACG	*INO1* (TSS+54 to TSS+235)
INO1 reverse	AGCCATTGTTGCCACCTAAC	
TEL0.5 forward	GACAAATAAAAATTCAGCTTTTTCAAG	Chr06: 269468 - 269494
TEL0.5 reverse	GTTCGAATCCTTAAGTAAAACACATTC	
TEL7.5 forward	GTGGAAAGTATCGAGTTATGTGTACCT	Chr06: 262659 - 262685
TEL7.5 reverse	GTCATTCAAATACAGTGGGAAGTCTAC	
SCR1 forward	GGCAGGAGGCGTGAGGAATC	*SCR1* (7S)
SCR1 reverse	CCTAACAGCGGTGAAGGTGGAG	
MET6 forward	TGGAAGCTGCCGGTATCAAG	*MET6* (TSS+1801 to TSS+1905)
MET6 reverse	AGCCCAGGTGTAGTAAGCAG	
ARG4 forward	TGGAAGCTGCTCTCACGATG	*ARG4* (TSS+1084 to TSS+1197)

2.15. Total RNA sequencing

Total RNA sequencing was performed by Anne Lafon, a former member of the lab, in collaboration with the Morrilon Lab at the Institut Curie. The protocol followed was based on (Luzzi et al., 2021).

2.16. Nascent RNA measurement by 4tU-sequncing

4tU sequencing was performed by Kenny Schumacher and the Devys lab. The protocol followed is described here (Luzzi et al., 2021).

2.17. Bioinformatic and statistical analysis

All bioinformatics analysis was carried out by Ugo Szachnowski and Camille Gautier. All figures were produced under my direction. All experiments were repeated performed as 3 or more biological repeats. Error bars denote +/- s.e.m. unless otherwise stated, the *P* value was calculated using the Student's *t* test (two-tailed, unpaired) between two groups or one-way ANOVA. In Figure 3.2 statistical significance was determined by finding a difference of more than two confidence intervals ($p>0.05$) between each of the time points. For differences in doubling time of strains in Figures 3.3 and 3.4, significance was determined by plotting linear regression of the exponential phase of growth and determining whether the regression coefficient of the two conditions was different by more than two confidence intervals ($p<0.05$). For determining the significance of changes in doubling times, a chi-squared test was used wherein the expected value was calculated as the untreated doubling time of a given mutant multiplied by the fold change observed for WT when treated by the relevant drug. Significance is indicated as follows: *, $p<0.05$; **. $p<0.01$; ***, $p<0.001$.

Table 2.7 Materials

NAME	COMPANY	CAT #
Drop-out CSM powder (-URA)	Formedium	cat# DCS0351
Complete CSM mixture	Formedium	DCS0011
yeast nitrogen base without amino acids	Formedium	Cat#CYN0401
D-glucose	Formedium	Cat#GLU02
Ammonium sulphate	Sigma-Aldrich	Cat#A2939
Yeast extract	Formedium	Cat#YEA02
Agar	Formedium	Cat#AGA02
Nicotinamide (NAM)	Sigma-Aldrich	Cat#N0636; CAS: 98-92-0

Nicotinamide riboside (NR)	Provided from ChromaDex	N/A
Phloxine B	Sigma-Aldrich	Cat#P2759
Trichloroacetic acid (TCA)	Sigma-Aldrich	Cat#T4885
Sodium hydroxide	Sigma-Aldrich	Cat#S5881
EDTA	Fisher scientific	Cat#BP120-500
NAD/NADH Quantitation Colorimetric Kit	BioVision	Cat#K337
SDS	Sigma-Aldrich	Cat#436143
Glycerol	Sigma-Aldrich	Cat#G2025
APS	Sigma-Aldrich	Cat# 215589
TEMED	Thermo Scientific	17919
Tween 20	Sigma-Aldrich	V900548
Rapamycin	Invitrogen	PHZ1235
Glycine	Promega	H5073
40% Formaldehyde	Sigma-Aldrich	252549
Sodium chloride	Sigma-Aldrich	Cat# S9888
Protease inhibitor cocktail (PIS)	Roche	11836153001
Protein A - Sepharose™ 4B	Invitrogen	Cat# 101041
Proteinase K	Sigma-Aldrich	1073930010

ERCC RNA Spike-in control mixes	Ambion	#4456740
Microscope slides	VWR	631-0116
Platinum SYBR Green One-step qRT-PCR	Invitrogen	Cat# 11736059
SYBR™ Green qPCR SuperMix-UDG	Invitrogen	Cat# 11733038

Chapter 3

Chapter 3. INO80 promotes selective autophagy

3.1. Introduction

Abrupt changes to metabolic state require organisms such as budding yeast to respond aptly, a process predominantly mediated by co-ordinated changes in gene expression (louis Lopez Moury 2008). Such adaption to metabolic changes usually results in increased cell survival under the metabolic stress. Regulating and co-ordinating large-scale changes to the transcriptional program of a cell is therefore of critical importance in such situations.

Epigenetic factors are capable of imparting control over broad and spatially distant groups of genes, making them well suited for controlling rapid large-scale alterations in gene expression.

Many epigenetic factors are dependent on the availability of metabolites or metabolic intermediates (Li et al., 2018). For example, ATP and Acetyl-CoA act as essential co-factors for ATP-dependent chromatin remodelling complexes and histone acetylasetransferases respectively.

Such reliance on the availability of various metabolites intimately connects epigenetic factors to the metabolic state of the cell by decreasing their reliance on intermediate sensors.

The Ino80, the catalytic subunit of the INO80 chromatin remodelling complex, was initially discovered through work on the regulation of inositol metabolism and phospholipid biosynthesis (Ebbert 1999). The initial discovery of the complex as a regulator of phospholipid biosynthesis suggested a role for the complex in cellular metabolic regulation. Additionally, INO80 subunits, Ies6 and Arp5 were found to be enriched at genes associated with energy metabolism (Yao 2016), and disruption to the Arp5 subunit led to a decoupling of cellular respiration and cell division (Gowans et al 2017), indicating a central role for INO80 in cellular metabolism (Morrison, 2020).

Despite recent advances, the precise mechanism of INO80 regulation of metabolic states remains poorly understood. Furthermore, the role of the complex as either a regulator of general homeostasis or stress response factor is unclear. Recent work from the Morrison lab showed that mutants of the Ino80 subunit produced a similar transcriptome to that of wild-type (WT) budding yeast cells treated with the TOR complex (TORC) inhibitor, Rapamycin (Beckwith et al, 2018). The authors therefore proposed that INO80 is promoting TOR signalling under normal growth conditions and argued that *ino80Δ* mutants resemble TOR inhibition and are therefore resistant to metabolic conditions which naturally lead to this state.

Other work on INO80 identified the complex as functioning in concert with the ubiquitin-proteasome system (UPS), in targeting stalled RNA polymerase II (RNAPII) for degradation (Lafon et al., 2015). The involvement role of INO80 in mediating ubiquitin-dependant protein turnover raised the question of whether the INO80's role was limited to RNAPII, or if the complex played a general role in catabolic processes across the cell.

Protein catabolism can be generally divided between proteasomal degradation via the UPS, and vacuolar (lysosomal in higher eukaryotes) degradation (Dikic, 2017). The UPS pathway is capable of temporal regulation of protein stability, typically of short-lived factors, however most large-scale proteome remodelling is associated with catabolic pathways converging on the vacuole/lysosomes. Importantly, both catabolic pathways relied on signal molecules, including ubiquitin, to mark substrates for degradation (Chen et al., 2019).

Metabolic stresses such as nitrogen starvation pose danger to organisms as cells lose the ability to synthesise new proteins and sustain growth. For this reason, proteome remodelling – mediated in part by catabolism – away from a growth state and towards a stress response and survival state is critical.

In an attempt to better understand the pathways linking INO80 to cellular metabolic regulation and stress response, we decided to characterise the role of INO80 in conditions of metabolic stress, and investigate the role of the complex in protein turnover.

3.2. Results

3.2.1. Loss of Ino80 leads to sensitivity to nitrogen starvation and a loss of viability

The ability of budding yeast to tolerate nitrogen starvation depends on multiple overlapping metabolic stress response pathways (Gross and Graef, 2020). Wild-type (WT) yeast cells can survive and recover from prolonged starvation by upregulating stress response associated transcriptional pathways (Miles et al., 2021). We therefore asked how loss of Ino80 would affect this process.

Cell viability and growth response was evaluated by initially growing WT and *ino80Δ* cells in complete minimal media (CSM) and then washing and shifting the cells to a nitrogen starvation medium (SD-N). The effect of starvation on cell recovery following growth in the absence of nitrogen was measured by plating serial dilutions of WT and *ino80Δ* cells onto rich media (YPD).

Prolonged periods of up to 6 days in nitrogen starvation medium (SD-N) were found to have little to no effect on the ability of WT colonies to form (Figure 3.1A). On the contrary, the loss of Ino80 led to a profound loss of viability indicating that *ino80Δ* cells are unable to endure the same period in the starvation conditions (Figure 3.1A). Across multiple repeats and differing time scales, we found that in the initial 48 hours, the *ino80Δ* mutant showed only minor difference in its colony forming potential – and therefore survival – compared to that of WT cells. However, following 72 hours in SD-N, the absence of INO80 correlated with a severe loss of viability. The result suggests that INO80 promotes cellular pathways protecting budding yeast cells from the effects of starvation.

To confirm that deletion of *Ino80* was specifically contributing to decreased cell survival, we tested whether the growth defect of *ino80Δ* cells could be rescued by exogenously providing the INO80 gene to *ino80Δ* cells. By supplementing the *ino80Δ* strain with a plasmid expressing the INO80 gene, we found that, like the WT, the mutant was now able to survive prolonged starvation (Figure 3.1B). Consistent with a role for the INO80 gene in the observed effect; *ino80Δ* cells transformed with the plasmid backbone without the INO80 gene, showed similar loss in viability to *ino80Δ*. We concluded that INO80 is required for the survival of budding yeast in nitrogen starvation.

We next asked if INO80 activity was promoting survival through a mechanistically direct role during the nitrogen starvation response or if the phenotype was instead a secondary effect caused by the loss of *Ino80*.

To test this, we used a strain where the INO80 gene was under the control of the inducible *GAL1* promoter. This allowed the control of Ino80 expression by the addition or removal of galactose from the growing media. In this manner we avoided generating full deletion mutants of INO80, which may

have secondary phenotypes unrelated to INO80's function. Additionally, it allowed for control over the timing of expression. By using this strain, it was possible to test the effects of INO80 in starvation condition, within the same budding yeast strain.

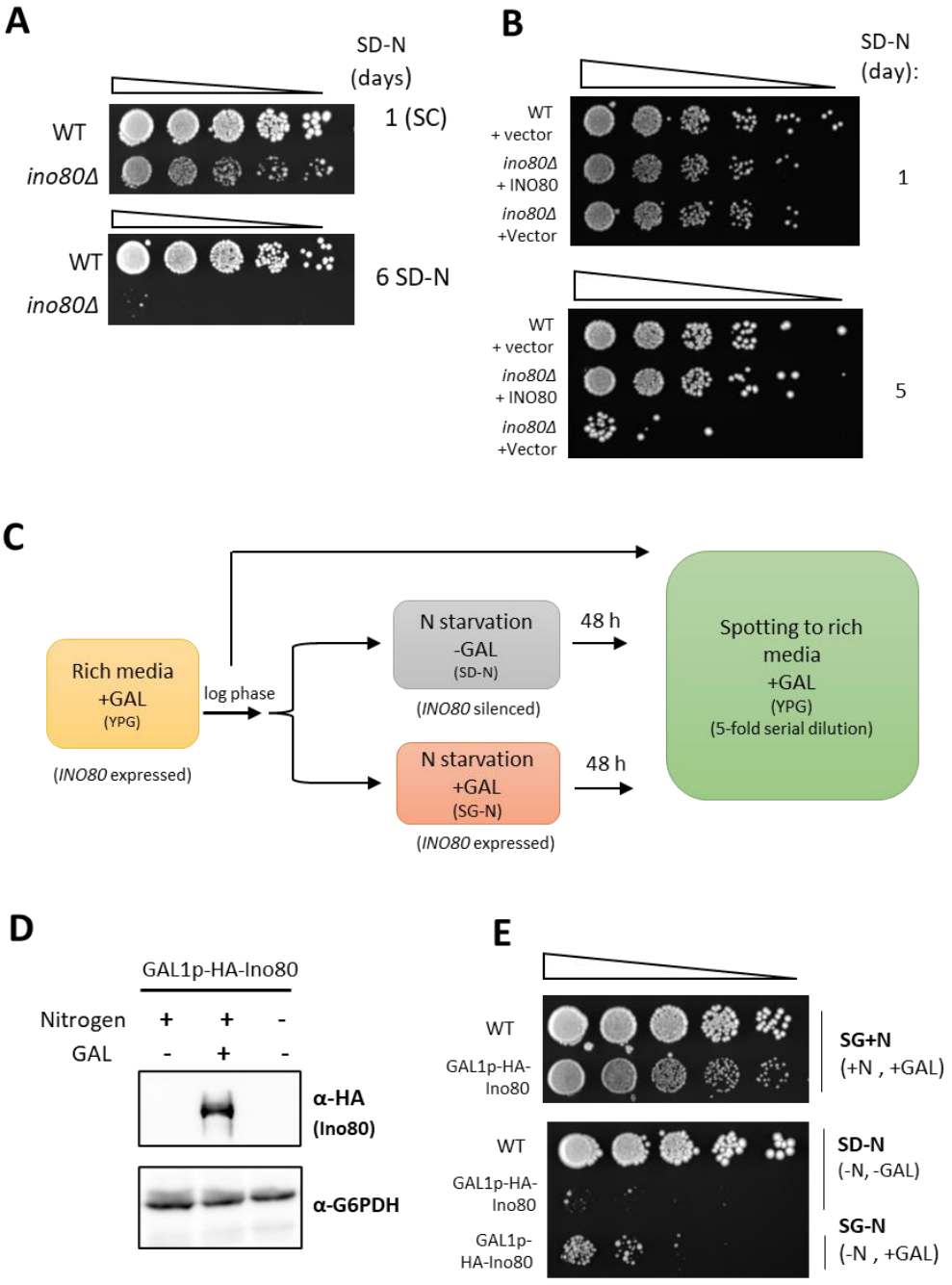

Figure 3.1. INO80 promotes cell survival in nitrogen starvation. (A) Spot-test analysis of WT and ino80Δ viability following a switch to nitrogen starvation. Equal cell concentrations were taken at the indicated time points and spotted to YPD plates in a five-fold serial dilution. Plates were grown at 30°C for 2 days. **(B)** Exogenously provided INO80 rescues ino80Δ defect. Five-fold serial dilution spotted to YPD for 1 or 5 days following shift to SD-N. Cells were either transformed with pRS416 backbone (vector) or INO80 expressing

plasmid (INO80). **(C)** A scheme of the experimental process involved in producing (D) and (E). **(D)** Immunoblot against HA to measure inducible Ino80 expression. A immunostaining against G6PDH was used as a control for equal loading. **(E)** Fivefold serial dilution of GAL1p-HA-Ino80 strain spotted to YP-Gal plates following 48 hours in the described growth conditions (right of image).

To ensure Ino80 was present at the start of the experiment, cells were initially cultured in rich media containing galactose (YP-Gal), and only after 24 hours, this was split between the two experimental conditions: either YP-GAL medium or media lacking galactose (YPD) (Figure 3.1C). Protein samples were collected once the cells reached mid to late log phase and expression of HA-Ino80 was confirmed to only be detectable in the presence of galactose. Growth in YPD showed a near complete knock-down of Ino80 (Figure 3.1D).

To determine whether INO80 has a mechanistic role in promoting survival during nitrogen starvation, the GAL1p-HA-Ino80 strain was precultured in galactose-containing medium for 24 hours and then divided between nitrogen starvation medium containing glucose (SD-N) or galactose (SG-N). After 48 hours, equal numbers of cells were plated on a galactose-containing rich medium plates and the ability of the different strains to grow was compared. As a control, the GAL1p-HA-Ino80 strain was grown in galactose and nitrogen-containing media prior to spotting to galactose-containing rich media plates (Figure 3.1E). This allowed us to generate an acute knock-down mutants of Ino80 and thus increase our confidence that any observed phenotype is not caused by a secondary effect which is mechanistically unrelated to INO80 function. In the presence of galactose and, therefore, Ino80, the growth of the GAL1p-HA-Ino80 strain closely resembled wild-type when in nitrogen-containing media, indicating functional expression of the HA-Ino80 from the galactose-inducible promoter. In nitrogen starvation conditions, and in the presence of glucose in the medium, when the *GAL1* promoter is silenced and INO80 is not expressed, the GAL1p-HA-Ino80 strain was almost entirely unable to form colonies following only 48 hours. Interestingly, this is a significantly earlier time point relative to the *ino80Δ* strain grown in SD-N. Importantly, when the GAL1p-HA-Ino80 strain was cultured in SG-N (nitrogen starvation medium where galactose is the only carbon source) we found the strain was able to outgrow the SD-N conditions (Figure 3.1E, bottom panel). The reduced growth relative to WT may be due to weaker INO80 expression from the GAL1 promoter but we are unable to conclude definitively without confirming Ino80 protein levels by immunoblot. In addition, the absence of a control condition which included nitrogen but lacked galactose (SD+N), made it impossible to conclude whether the observed phenotype was due to the loss of Ino80 alone or directly to nitrogen starvation. Our evidence is strongly suggestive of a directly mechanistic role for INO80 activity in

promoting the cellular response to nitrogen starvation and a mechanistically direct role in promoting survival in nitrogen deplete conditions.

The inability of *ino80Δ* mutants to form colonies following nitrogen starvation could be explained either by cell death or by failure of live cells to re-enter the cell cycle following plating.

To distinguish between these two possibilities, we used the dye Phloxine B, which stains dead *S. cerevisiae* cells as they lose membrane integrity (Noda 2005). As before, cells were grown in SD-N for the indicated time before being collected and incubated briefly with the dye.

For each condition and time point images of at least 200 cells were collected by microscopy. Total cells were counted and the ratio of stained (dead) to unstained (live) cells was determined and plotted as a percentage relative to the viability prior to growth in SD-N (Figure 3.2A)

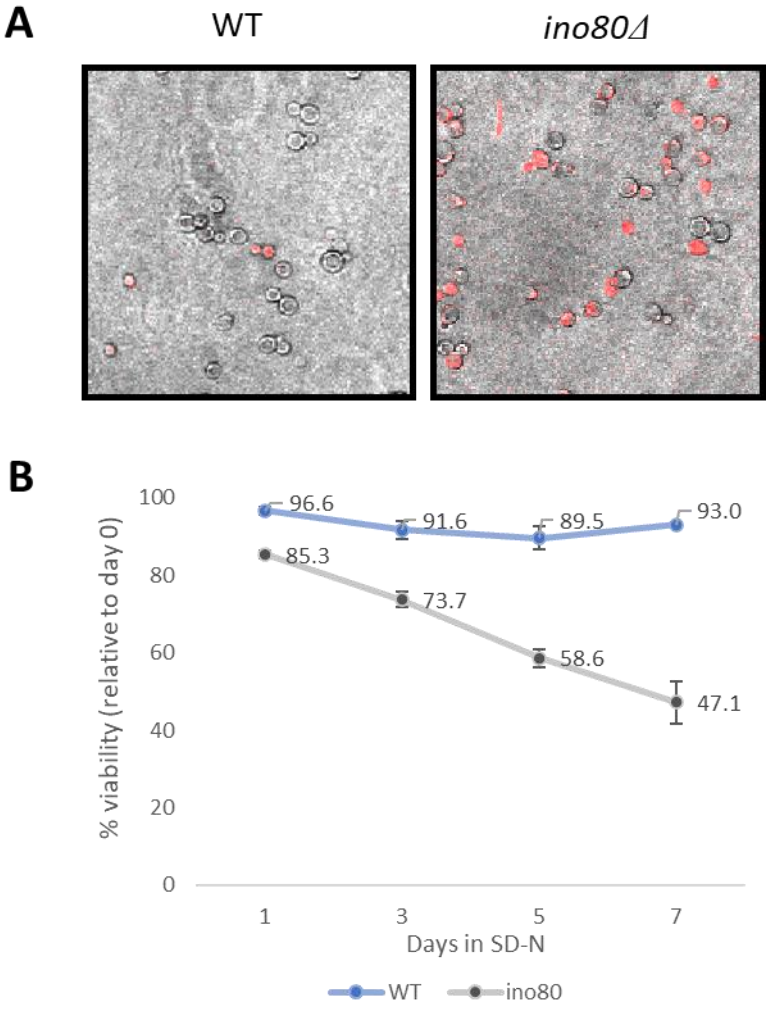

Figure 3.2. INO80 promotes cell survival in nitrogen starvation. (A) Representative images of WT and ino80Δ cells stained with Phloxine B. Images are of samples 7 days after the switch to SD-N. Overlays of

brightfield and fluorescence images. **(B)** Quantification of cell viability. Values prior to switch SD-N were calculated and percentage decrease from this number was determined. For each time point >200 cells were counted. Error bars represent s.e.m (n=3).

The WT strain displayed a mild loss of viability in response to nitrogen starvation, however maintained a significantly higher viability throughout and did not progressively lose viability over the experiment SD-N. In contrast, we found that SD-N led to a significant loss in viability of the *ino80Δ* strain within 24 hours and the percentage of viable cells continued to fall to 60% by day 5 and below 50% by day 7 (Figure 3.2B). We conclude that INO80 promotes cell survival in SD-N as the loss of the complex led to significant cell death compared to the wild-type.

Taken together we conclude that INO80 complex promotes cell viability in nitrogen starvation.

3.2.2. INO80 complex promotes survival in rapamycin

The inhibition of the TORC complex in response to nitrogen starvation is a crucial step preceding most of the downstream stress response to nitrogen starvation. To better understand how INO80 protects cells during nitrogen starvation, we examined if the complex functioned prior to or after TORC inhibition.

It has been recently shown that loss of INO80 both transcriptionally and phenotypically resembled TORC inhibited cells. Based on this findings it was suggested that INO80 was a downstream mediator of active TORC signalling (Beckwith et al., 2018). Supporting this, *ino80Δ* was shown to outgrow WT cell when both were cultured on rapamycin containing medium. Our finding that *ino80Δ* strain was sensitive to nitrogen starvation (which leads to TORC inhibition) contradicted this assumption as it suggested INO80 was involved downstream of TORC inhibited signalling. If the *ino80Δ* mutant transcriptionally and phenotypically resembled TORC inhibition, sensitivity to the stress condition would not be necessarily expected and as Beckwith *et al* argue; one would expect the cells to be "primed" for the consequence of nitrogen starvation and be somewhat resistant.

To test if INO80 acts downstream of TORC inhibition, rapamycin was used to artificially inhibit the TORC complex of WT and *ino80Δ* cells. While resembling nitrogen starvation functionally, this condition does not impart the same metabolic stress to the cells that is caused by the lack of nitrogen. Thus, we compared the effect of TORC inhibition in the presence and absence of Ino80.

When spotting 5-fold serial dilutions of wild-type or *ino80Δ* cells to YPD plates containing rapamycin, very little effect on the growth of wild-type budding yeast cells was observed. Mutants lacking Ino80

did show some sensitivity to the presence of rapamycin and unlike the results of Beckwith et al., never outgrew wild-type cells in this condition (Figure 3.3A). Various *S. cerevisiae* wild-type genetic backgrounds are available to researchers, and these vary in their tolerance of the *ino80Δ* deletion. One explanation for the differing phenotypes of *ino80*Δ we and others have observed following TORC inhibition, could be due to this variation in wild-type strains. To investigate whether the genetic background of the strain was affecting the sensitivity we observed, we tested three commonly used lab strains and found in all cases the presence of rapamycin had a stronger negative effect on *ino80Δ* cells that wild-type (Figure 3.3A & B).

We suspected the relatively mild effect of rapamycin on the wild-type strain may be due to the plates being composed of rich medium and so we switched to minimal synthetic complete (SC) plates. Here we observed a much clearer, strain-specific sensitivity to rapamycin by the wild-type yeast. Importantly, *ino80Δ* was more sensitive to rapamycin than wild-type (Figure 3.3B), displaying a severe growth defect in every strain background tested. This result therefore indicates that Ino80 is contributing to the ability of wild-type cells to sustain growth in TORC-inhibiting conditions and that, unlike the Morrison lab, we conclude that Ino80 deletion does not lead to a "rescue" of wild-type sensitivity to rapamycin.

Since budding yeast grown on agar plates require roughly 2-3 days of growth at 30°C to produce visible colonies, the effect we have been measuring is specific to prolonged growth in the presence of rapamycin.

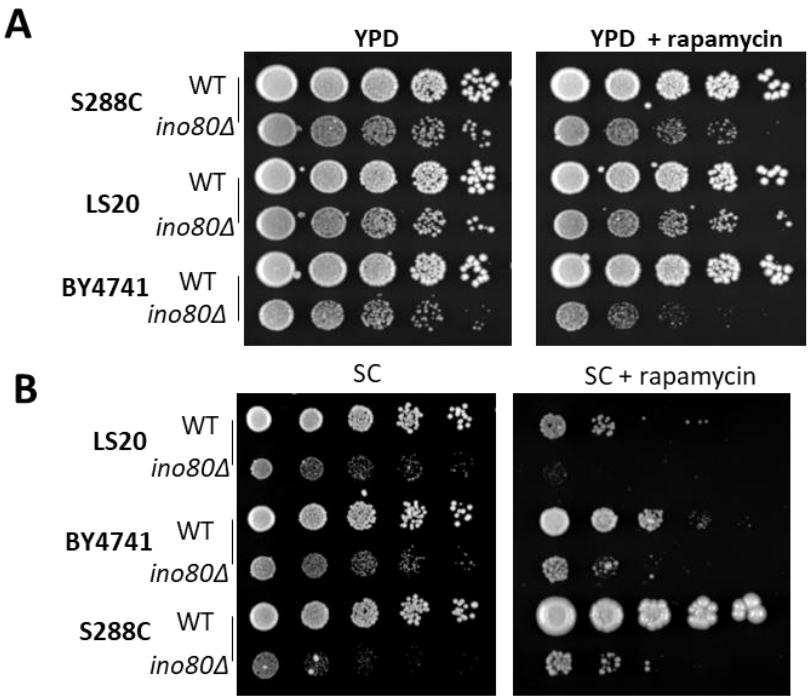

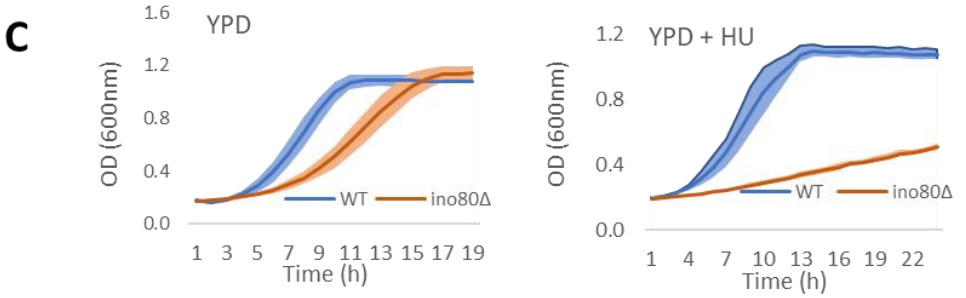

	Doubling (h)		
	-HU	+HU	FC
wt	2.60	3.40	*1.31*
ino80Δ	4.04	21.32	*5.28*

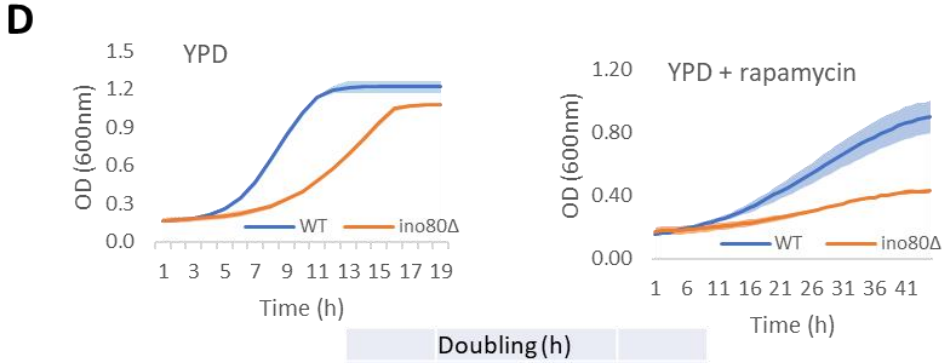

	Doubling (h)		
	- rap	+ rap	F.C.
WT	2.2	12.7	5.6
ino80Δ	3.9	25.8	6.6

Figure 3.3 (legend overleaf)

Figure 3.3 Rapamycin leads to compromised ino80Δ growth. (A) Strains were cultured in YPD before plating five-fold serial dilutions to YPD or YPD containing 20nM Rapamycin. Plates were grown at 30°C for 48 hours prior to imaging. **(B)** Strains were treated as above and plated to SC or SC containing 25 nM rapamycin. Plates were grown at 30°C for 48 hours prior to imaging. **(C)** WT and ino80Δ were cultured to in YPD or YPD containing 5 mM HU and optical density (OD600) readings were collected every hour. Three biological repeats were done, mean OD plotted and shaded areas represent SEM. Doubling times were calculated by plotting a straight line to the exponential phase of growth for each strain and doubling calculated from this straight line. Fold-change (FC) was calculated by dividing the doubling time of the +HU condition by the doubling time of the -HU condition for each strain. Change in growth on *ino80Δ* was significantly ($p > 0.001$) different than WT. **(D)** As (C) except the strains were cultured either YPD or YPD containing 50 nM Rapamycin (+/- Rap). FC was calculated by dividing the doubling time of the +rap condition by the doubling time of the -rap condition. All differences in growth were significantly ($p > 0.001$) different relative to corresponding WT control.

We wondered whether the sensitivity we observed was caused by *ino80Δ* leading to defects in pathways related to survival in prolonged growth arrest or whether it was associated with the acute effect of TORC inhibition. To assay this, we used an automated system that enabled us to culture the two strains in liquid media, with the system agitating the cells and quantifying cell density by spectroscopy at regular intervals. Thus, we could measure the immediate response to the addition of rapamycin and not bias our results to the effects of prolonged growth as might be the case when growth on solid media is used as an assay. To validate the method, we grew WT and *ino80Δ* cells in media either lacking or containing the replication-stress inducing drug hydroxyurea (HU), as *ino80Δ* are sensitive to replication stresses (Papamichos-Chronakis and Peterson, 2008b). The experimented acted as a control to validate the assay. Plotting the hourly measurements of optical density, it was visibly clear that while the growth curve of the wild-type cells was relatively unaffected, *ino80Δ* grew significantly slower (Figure 3.3C). Furthermore, by taking the exponential phase of growth and calculating the equation for the straight line, we were able to determine a doubling time, showing that *ino80Δ* cells grew more than 5 times slower than wild-type in the presence of HU. Doing so clearly showed the sensitivity of INO80 to HU and the relatively little effect the drug had on WT cells (Figure 3.3C).

Next, we employed the same method but compared the effects of Rapamycin on WT and *ino80Δ* strains. It was clear that unlike HU, rapamycin had a significantly more pronounced effect on wild-type budding yeast. However, growth in rapamycin produced a pronounced effect in *ino80Δ* cells, compromising their growth rate and leading to a pattern reminiscent to the effect of HU on *ino80Δ* (Figure 3.3D).

The most striking difference was that unlike in rich media, where both strains grew to an OD of over 1, in the presence of rapamycin the wild-type strain was able to grow to a higher OD, around double that of *ino80Δ* (Figure 3.3D). This indicates that in the experimental conditions the wild-type yeast can go through two cell cycles, doubling twice from an OD of 0.2 to around 0.8. Conversely, the *ino80Δ* only reaches an OD of 0.4, indicating that cells lacking INO80 arrest in the presence of rapamycin. We conclude that either INO80 promotes cell growth and division in the presence rapamycin.

Further demonstrating a role for INO80 supporting growth in the presence of rapamycin was calculations of doubling times which showed that the presence of Ino80 led to a lesser fold change increase in doubling time compared to WT, from 5.6 slower in wild-type to 6.6 times slower in the absence of Ino80. Furthermore, the difference between doubling time of *ino80Δ* and WT increased from 1.7-fold difference in rich media to 2-fold in rapamycin. Together this evidence shows that INO80 functions to facilitate growth both in the acute response to rapamycin and in prolonged presence of the drug on solid media plates. It supports our conclusion that *ino80Δ* does not produce a phenotype that facilitates protective adaption to mTOR inhibition as has been previously suggested (Beckwith et al 2018). The finding that upon addition rapamycin INO80 promotes cell growth suggests that while INO80 may function in promoting active TOR signalling, it may have an equal or greater role in promoting signalling associated with TORC inhibition.

3.2.3. Mutants of INO80 subunits, Arp5 and Arp8, are sensitive to TORC inhibition

The INO80 complex is composed of several actin-related protein subunits which are critical to its ability to carry out chromatin remodelling (Dion et al., 2010). The Arp5 and Arp8 subunits are two such subunits, which facilitate enzymatic activity and nucleosome recognition, and the loss of which severely impairs complex activity (Eustermann et al., 2018a; Shen et al., 2003a; Tosi et al., 2013).

To further validate the role of the INO80 complex in regulating the response to TORC1 inhibition and stress response we assessed the effect of TORC1 inhibition on the deletion mutants *arp5Δ* and *arp8Δ*. Growing the *arp5Δ* and *arp8Δ* strains in SD-N we measured viability by spotting the cells back to rich plates following starvation. Wild-type cells were able to grow despite the conditions however in both *arp5Δ* and *arp8Δ* cells we observed a clear loss in viability, resembling *ino80Δ*, albeit occurring after a longer period – around 10 days of nitrogen starvation compared to 6 to 8 days in the *ino80Δ* (Figure 3.4A).

Next, we investigated whether the finding that *ino80Δ* strain is sensitive to rapamycin is supported by a similar finding in mutants of INO80 subunits. We again used an automated system for liquid growth culture, allowing us to measure the acute response to growth in rapamycin. We found the growth rate of *arp8Δ* mutant to be negatively affected by the addition of rapamycin, and to maintain a slower growth rate compared to WT (Figure 3.4B). By calculating the doubling time, we found that *arp8Δ* underwent a greater fold-change decrease in doubling time than WT, suggesting the absence of *Arp8* leads to a severe rapamycin-related effect, as previously observed in *ino80Δ* cells. We also observed an inability to grow to cell densities resembling WT, suggesting that like *ino80Δ* cells and unlike WT, *arp8Δ* cells arrest their cell cycle in rapamycin.

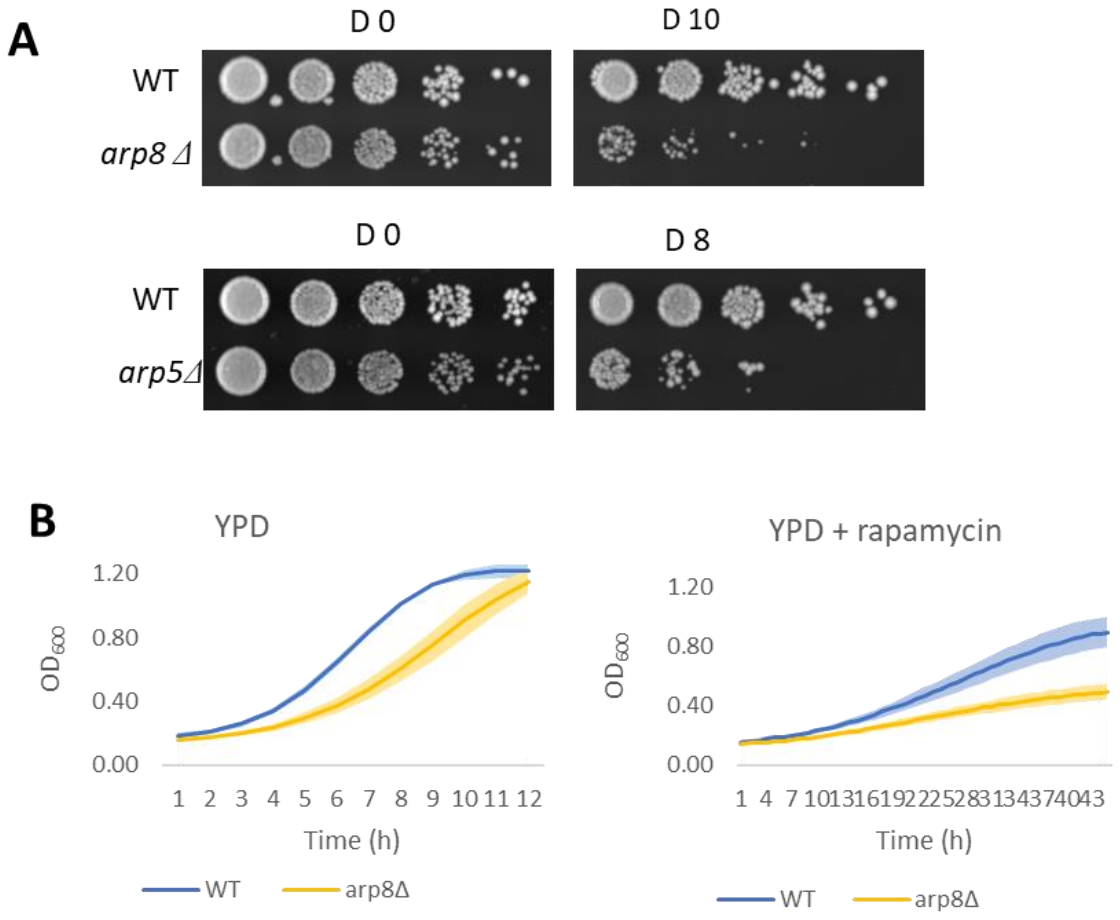

	Doubling time (h)		
	(-) rap	(+) rap	*F.C.*
wt	2.24	12.66	*5.65*
arp8	3.06	18.83	*6.15*

Figure 3.4. Deletion of INO80 subunits lead compromised viability in nitrogen starvation. (A) Five-fold serial dilutions of WT and arp8Δ spotted to YPD plates either before switch to SD-N (D 0) or after 8

(D 8) or 10 (D 10) days post switch to SD-N. Plates were incubated at 30°C for 48 hours. **(B)** WT and arp8Δ were cultured in YPD or YPD containing 50 nM rapamycin and OD was recorded at 600nm every hour. The mean of 3 experiments is plotted and the shaded areas represent SEM. Doubling times were calculated by plotting a straight line to the exponential phase of growth for each strain and doubling calculated from this straight line. Differences in doubling time between the strains and conditions are all statistically significant ($p > 0.005$).Since both subunits are crucial for complex activity, the finding that both *arp8Δ* and *arp5Δ* mutants are sensitive to TORC1 inhibition further supports the conclusion that INO80 complex activity is required for growth and survival during metabolic stress response. We therefore conclude that the INO80 complex is an important component responding to metabolic stress and sought to determine which specific stress response pathways may be associated with this effect.

3.2.4. INO80 complex and Autophagy factors show genetic interaction in response to TORC inhibition

Metabolic stress response in Eukaryotes is characterised by a broad remodelling of the proteome, primarily consisting of reduced gene expression and increased protein turnover.

The catabolic activity of the autophagy pathway is central to this process as it allows cells to reuse cellular components such as amino acids (Gross and Graef, 2020). The initiation of the autophagy pathway is dependent on the activity of the Atg1 protein and mutants lacking *Atg1* fail to perform any autophagic degradation.

We asked whether the phenotype we had observed in mutants of the INO80 complex was associated to defects in the autophagy pathway. To investigate this, a double mutant for both the *ATG1* gene and *ARP8*, was created. We reasoned that if INO80 was to promote Atg1 function, the double mutant would likely display an epistatic phenotype as this may suggest the two genes function in the same pathway. Alternatively, if the double mutant was synthetically sick to a greater degree than would be expected from the two individual deletions alone then it would imply that the two proteins function in complementary pathways in stress response.

The effect nitrogen starvation has on the survival of the double mutant was measured by growing it in SD-N media and subsequently spotting back to rich media plates to assess survival. Prior to growth in nitrogen starvation, we noted that the double mutant was slower growing than either of the single mutants, but the difference was mild. Following 5 days of nitrogen starvation, a time point at which WT cell growth is unaffected but *ino80Δ* show a strong growth retardation, both *arp8Δ* and *atg1Δ* start to lose viability relative to wild type (Figure 3.5A). At this same time-point, the growth of *atg1Δarp8Δ*

double mutant was repeatedly seen to be severely affected relative to the individual single mutant strains, suggesting that the two mutations may be producing a synthetic lethal effect in this assay (Figure 3.5A). The semi-quantitative nature of the spot-test assay made it difficult to conclude whether the effect was indeed more that would be expected from a combination of the effects seen in the single mutants.

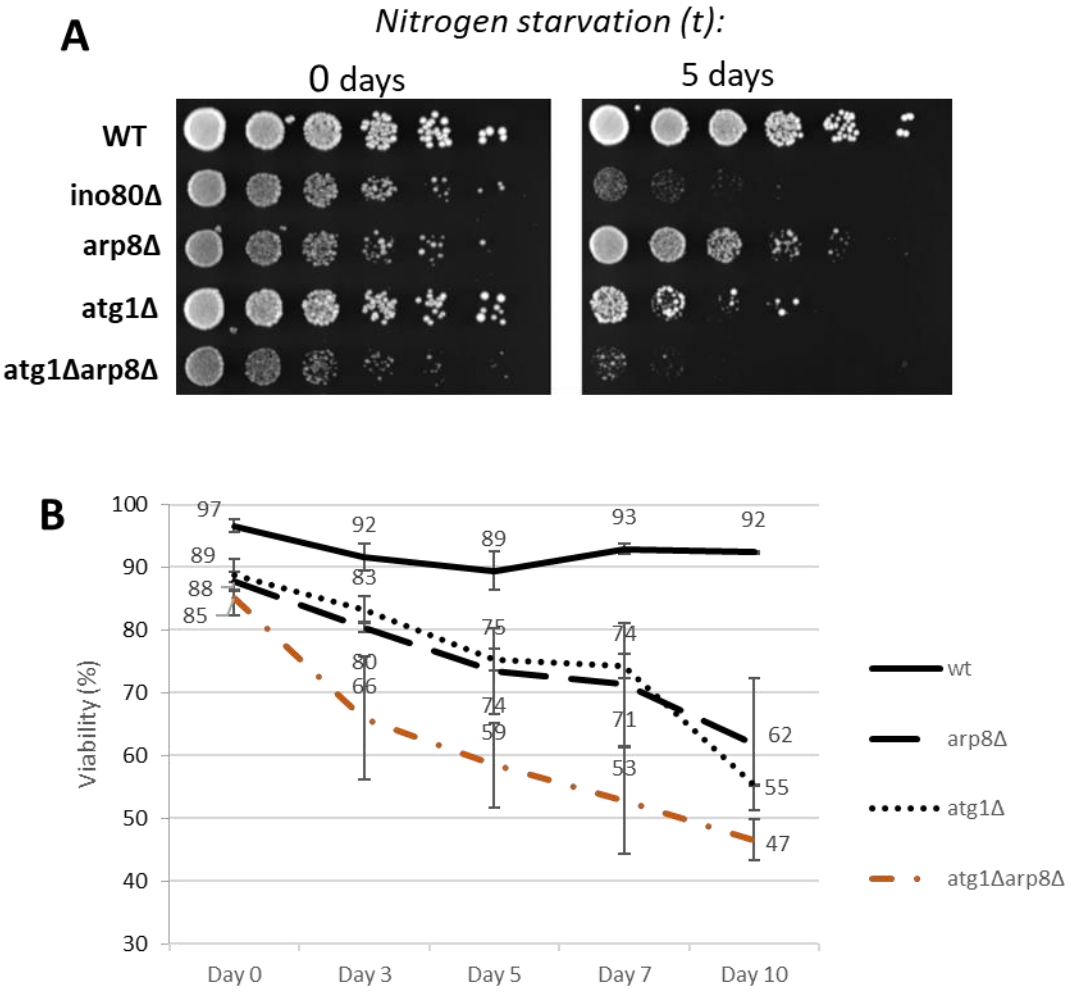

Figure 3.5. Genetic interaction between INO80 and autophagy pathway. **(A)** The indicated strains were cultured in SD-N for the listed time period. Subsequently, five-fold serial dilutions were plated on YPD and growth assessed following 48 hours of culture at 30°C. **(B)** Indicated strains were cultured in SD-N and viability measured by Phloxine B at the stated time points. Stained cells were imaged and the ratio of dead to live cells counted. Each biological replicate was based on a minimum of 200 imaged cells and the experiment was repeated 3 times. Error bars represent SEM.

To measure viability more quantitively, we measured percentages of live anddead *atg1Δarp8Δ* cells directly by using the viability dye Phloxine B. While wild-type cells maintained a viability of 90% throughout the experiment, we found that the combination of the two mutations led to a rapid decrease

to around 70% viable cells in the first 3 days and further dropping to 50% viable cells around days 7 – 10 (Figure 3.5B).

However, similar rapid drops in viability were observed in the single mutants assayed, and the high variation in individual experiments meant that there was no significant difference between the double mutant and the individual single mutation strains (Figure 3.5B). As no significant difference was observed in the effect of nitrogen starvation, we concluded that the two mutations produced an epistatic genetic effect in regard to cell viability during metabolic stress conditions. This suggested that both Arp8 and Atg1 function in the same pathway when promoting viability in response to nitrogen starvation.

The severe growth defect observed in the double mutant indicated that the INO80 regulation may complement the autophagy response in promoting cell growth following nitrogen starvation. However, our data suggests that different pathways may be regulating recovery from nitrogen starvation on the one hand and promoting viability in nitrogen starvation on the other. The epistatic nature of cell viability when comparing *arp8Δ* and *atg1Δ* to the double mutation, led us to conclude that during nitrogen starvation, INO80 complex promotes viability through a function associated with autophagy.

3.2.5. INO80 promotes the clearance of ubiquitin-conjugates

Our data revealed a genetic interaction between INO80 subunits and components of the autophagy pathways. Previous work had identified INO80 as an essential component of the degradation of ubiquitinated RNAPII. We wondered whether INO80 may have a broader role in cellular protein turnover than previously identified. The failure to clear superfluous proteins contributes so cell death in autophagy mutants and we hypothesised that the same may be the case for *ino80Δ*.

To address the hypothesis that cell death in *Ino80* deleted cells is associated with defective protein turnover, protein accumulation was tested in the following experiment, performed by Anne Lafon, a former member of the lab, and subsequently repeated and confirmed by me.

To understand the extent of the defect in ubiquitin-conjugate turnover, protein samples were prepared from whole cell extracts (WCEs) of WT, *ino80Δ* and catalytically dead mutant of INO80; *K373A*. Alongside these, proteins from the soluble and insoluble fraction of the cells were also prepared. The soluble fraction corresponds to non-membrane integrated proteins, usually of cytoplasmic origin and which are also not associated with chromatin. Conversely, membrane-integrated or chromatin-bound proteins remain within the insoluble fraction, alongside large protein aggregates (Alberts et al., 2002).

The protein samples were run on a polyacrylamide gel and immunoblotted against ubiquitin. The antibody used did not recognise a specific linkage and instead could recognise ubiquitin, polyubiquitin and ubiquitinated proteins. Histone H3 was used as a quantitative and qualitative control of the fractionation experiment, as it is not found in the soluble (cytoplasmic) fraction. The largely cytoplasmic Pgk1 protein was used as a second loading control. In WCE, the immunoblots revealed a clear accumulation of ubiquitin conjugates in the absence of *Ino80* protein or when Ino80 catalytic activity was compromised (Figure 3.6A, lanes 2-3 and 5-6). Notably, this accumulation was most pronounced in the insoluble fraction of proteins. In the soluble fraction we found less ubiquitinated protein accumulation in *ino80Δ* or catalytically dead *Ino80*, compared to WT (Figure 3.6A, lanes 7-9). The differential accumulation of ubiquitinated proteins in the insoluble fractions suggests that INO80 alleviates accumulation of ubiquitinated proteins originating predominantly from protein aggregates, chromatin-bound proteins, or membrane-bound proteins. Additionally,INO80 activity inhibits the clearance of ubiquitinated soluble fraction, representing cytoplasmic or non-chromatin bound nuclear proteins.

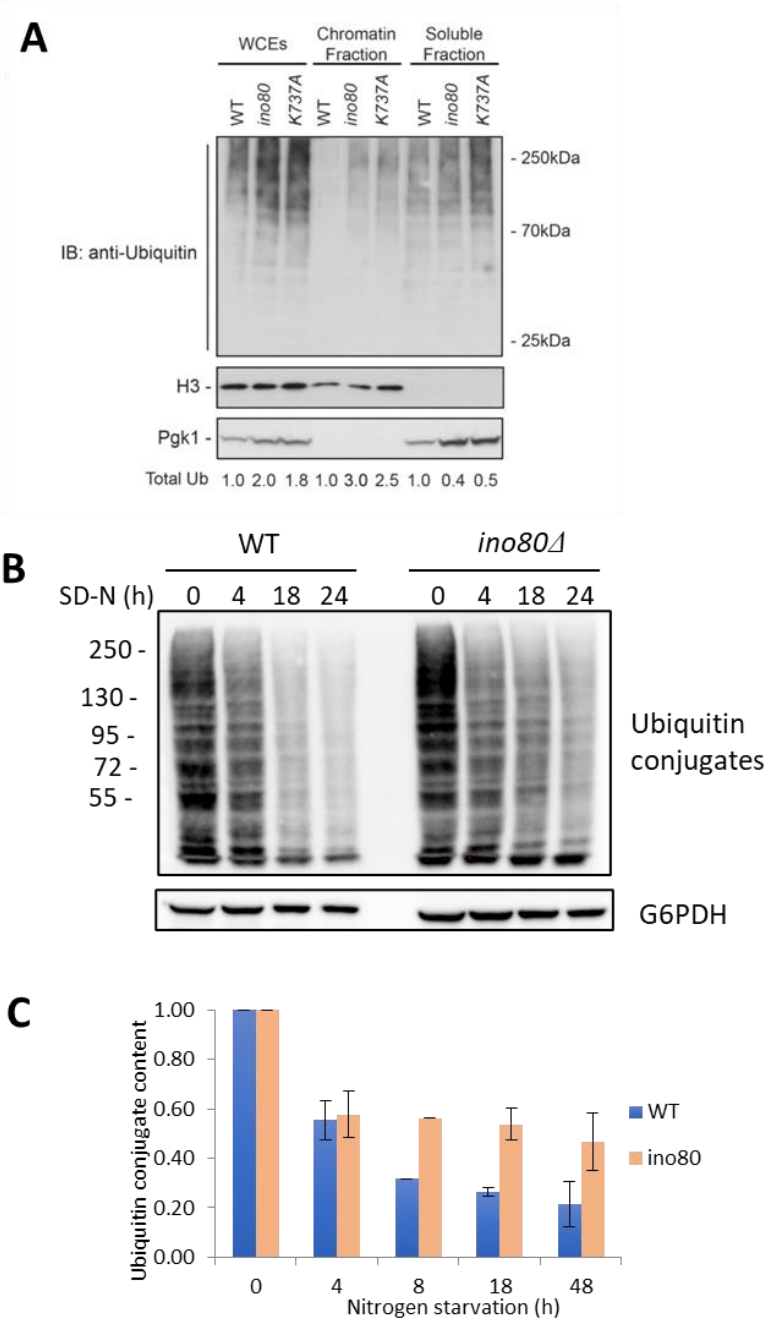

Figure 3.6. Accumulation of ubiquitin conjugates is a hallmark of INO80 loss. (A) Ubiquitinated protein abundance. Whole cell protein extracts (WCE) from WT, ino80Δ and catalytically 'dead' Ino80 (K737A) were produced from exponentially growing cells In YPD. The soluble and insoluble ('Chromatin') fractions were generated by fractionation and immunoblotted against ubiquitin (Ub), Histone H3 and Pgk1. Intensities of WT bands were calculated using Fiji and relative amounts of each mutant was calculated against the relative WT. **(B)** Ubiquitin conjugate turnover following SD-N. WT and ino80Δ were shifted to SD-N and WCE were produced and immunoblot with antibodies against Ub and G6PDH. **(C)** Ubiquitin conjugate levels were calculated from immunoblot band intensities and plotted as a fraction of Ub levels before the switch to SD-N. Error bars represent s.e.m (n=3).

Focusing on the insoluble proteins, work by Anne Lafon confirmed that the accumulating ubiquitin conjugates are not chromatin bound proteins as the incubation of the insoluble fraction with the nuclease, Benzonase, did not "release" the conjugates into the soluble fraction (data not shown). To better understand the identity of the ubiquitin conjugates, the lab performed a stable isotope labelling with amino acids in cell culture (SILAC) to generate a quantitative overview of the ubiquitinated proteome (ubiquitome) in *ino80Δ* relative to WT. The biochemical experiments were conducted by Anne Lafon in collaboration with Petra Belli lab at the Institute of Molecular Biology, Mainz. The proteomic data generated by these experiments was subsequently analysed by me. The *ino80Δ* ubiquitome was found to be particularly enriched in proteins from various membrane bound organelles, in particular the Endoplasmic Reticulum (ER), Nuclear outer membrane, Golgi apparatus and the Vacuole (Table 3.1). This was interesting since unlike soluble proteins, membrane bound proteins such as those observed to be enriched, are not common targets of the ubiquitin-proteasomal system (UPS) (Dikic, 2017). Instead, their turnover and that of organelle structures in general, is dependent on the autophagy pathway and associated selective autophagy pathways.

Feature	FDR	Genes in network	Genes in genome
endoplasmic reticulum part	3.13E-08	33	212
nuclear outer membrane-endoplasmic reticulum membrane network	2.96E-06	28	194
membrane region	2.96E-06	28	194
lipid metabolic process	2.00E-05	32	270
endoplasmic reticulum membrane	2.00E-05	25	176
endoplasmic reticulum organization	3.58E-05	10	27
lytic vacuole	7.10E-05	29	250
fungal-type vacuole	7.10E-05	29	250
storage vacuole	7.10E-05	29	250
vacuole	7.10E-05	30	265
ion transmembrane transporter activity	7.95E-05	26	212
ion transport	7.95E-05	27	225
lipid biosynthetic process	7.95E-05	23	170
transferase activity. transferring hexosyl groups	7.95E-05	15	76
cellular lipid metabolic process	1.12E-04	27	231
Golgi apparatus	1.34E-04	22	164
divalent inorganic cation transmembrane transporter activity	2.46E-04	8	21
transferase activity. transferring glycosyl groups	2.72E-04	16	96
carbohydrate derivative biosynthetic process	4.90E-04	23	193
vacuole fusion	4.90E-04	10	39

Table 3.1 Accumulating ubiquitinated proteins in *ino80Δ*. (Legend overleaf).

Table 3.1 Accumulating ubiquitinated proteins in *ino80Δ* Membrane bound proteins and autophagic targets accumulate in ino80Δ. SILAC mass spec was performed on ubiquitin pull-downs from WT and ino80Δ strains. Differential accumulation of ubiquitin conjugates in the absence of Ino80 was assessed and a summary of the 20 top GO terms associated with accumulated ubiquitination targets is presented.

The over representation of organelle-associated proteins in the *ino80Δ* ubiquitome suggested that loss of INO80 function led to accumulation of damaged organelles and generation of protein aggregates. Nitrogen starvation induces the clearance of ubiquitinated proteins, primarily aggregates, in an autophagy dependent manner called aggrephagy (Lu et al., 2014). To investigate whether INO80 functioned within this pathway, we generated protein extracts from cells following nitrogen starvation. Immunoblotting with antibodies against ubiquitin we again observed the accumulation of ubiquitin conjugates in *ino80Δ* compared to WT (Figure 3.6B, lanes 1 and 5). Strikingly, this difference was significantly more profound following 4 and 24 hours in nitrogen starvation, showing a clear accumulation of proteins in *ino80Δ* (Figure 3.6B, lanes 2-4 and 6-8). Nitrogen starvation induced autophagic clearance of protein aggregates can be observed in our results from WT cells, but not in the *ino80Δ*. The experiment was repeated, and signal intensities of each lane were quantified and normalised to a loading control, G6PDH. Doing so, we observed nitrogen starvation leading to an 80% decrease in levels of ubiquitin conjugates following 24 hours (Figure 3.6C).

Our results show that INO80 catalytic activity is involved in proteomic homeostasis. The loss of INO80 increases ubiquitinated organelle proteins, mostly in the form of aggregates. This accumulation persists even following nitrogen starvation. This result suggests that while nitrogen starvation leads WT cells to turnover ubiquitinated proteins and aggregates through aggrephagy, this pathway is compromised in the absence of *Ino80*.

3.2.6. INO80 promotes selective autophagy of mitochondria and ER

The possible connection to defective protein turnover, as well as the sensitivity of *ino80Δ* mutants to nitrogen starvation, led us to question whether the autophagy pathway was functional in the absence of the INO80 complex.

Autophagy is generally divided between “bulk” and “selective” autophagy. Bulk autophagy refers to a non-specific catabolism that targets cytoplasmic constituents in response to TORC1 inhibition. In order to assess the activity of this pathway, one can use a c-terminus fusion of the essential autophagy protein Atg8 to GFP (Nair et al., 2011). In doing so, autophagic delivery of GFP-Atg8 to the vacuole

leads to the accumulation of free GFP upon hydrolysis and the destruction of the bond. Strains that harbour mutations leading to defective autophagy, such as *atg5Δ* will not show accumulation of free GFP (Figure 3.7A).

We employed this approach in the *ino80Δ* background and found that free GFP accumulated readily when shifted to nitrogen starvation, mimicking the behaviour of wild-type cells. This indicated that bulk autophagy was activated appropriately upon TORC1 inhibition (Figure 3.7B). To further confirm that the observed free GFP protein was accumulating within the vacuole, we used fluorescent microscopy in conjunction with the vacuolar dye FM4-64 (Zal et al., 2006), finding that indeed the GFP signal accumulated inside the vacuolar membrane in both WT and *ino80Δ* strains when the cells were starved in SD-N medium (Figure 3.7C).

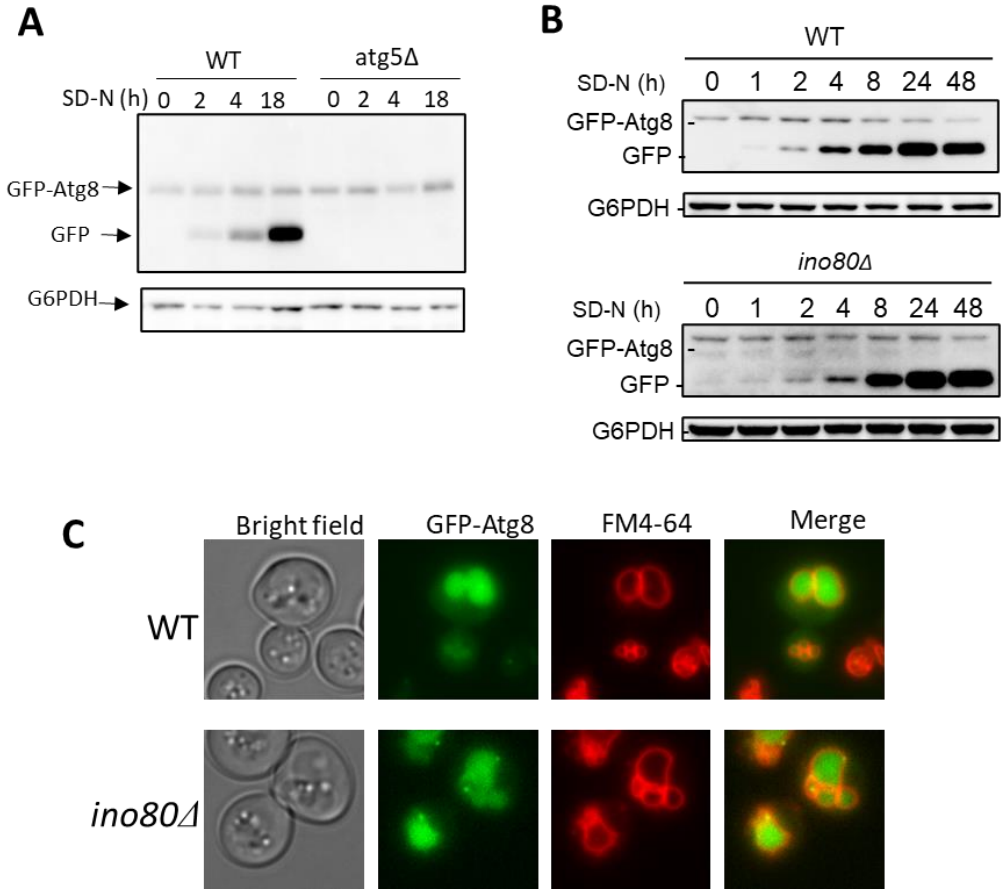

Figure 3.7. INO80 activity does not promote bulk autophagy. (A) Generation of free GFP following autophagy induction. WT and atg5Δ strains were shifted to SD-N and acid-extracted protein samples were collected at the indicated time points. GFP accumulation was measured by immunoblot with antibodies against GFP and loading assayed using antibodies against G6PDH. **(B)** Autophagy induction in WT and ino80Δ. Samples were prepared as above using the additional timepoints listed. **(C)** Functional autophagic delivery to

the vacuole. Exponentially growing WT and ino80Δ cells. transformed with a GFP-Atg8 expression plasmid. were shifted to SD-N for 2 hours and then stained with FM4-64 and imaged by fluorescent microscopy. Images show cells following 2 hours in SD-N

Together, these results suggest that INO80 is not essential for the functioning of bulk autophagy in response to nitrogen starvation.

While INO80 function was not required for the general activity of the autophagy pathway, much of the *ino80Δ* ubiquitome was enriched in proteins of various membrane bound organelles. Selective autophagy pathways use various receptor-mediated mechanisms to selectively target specific cellular constituents and compartments for turnover, such as organelles (Farré and Subramani, 2016). To investigate whether INO80 activity was required for selective autophagy of specific organelles, we assessed the activity of these pathways by measuring the targeting of various organelles to degradation in the vacuole. To do this, protein markers of specific organelles, usually membrane-integrated proteins essential to the function of the organelle, were GFP tagged. By measuring the generation of free GFP, indicative of autophagic degradation, the activity of the relevant selective autophagy pathway could be assessed (Stolz et al., 2014).

We sought to investigate the activity of the pexophagy, and reticulophagy (or ER-phagy) and the mitophagy pathways, given that proteins of these organelles were found to be hyper-ubiquitinated in *ino80Δ*.

The abundance of peroxisomes is dynamically regulated in response to metabolic conditions and nitrogen starvation induces the selective degradation of these organelles by Pexophagy. Using Pex11-GFP fusion as a marker, we found that Pexophagy was unaffected by the loss of *Ino80*, suggesting INO80 does not regulate the pathway (data not shown).

Reticulophagy, is a selective autophagy pathway that is activated in response to ER stress and the unfolded protein response (UPR) (Yang et al., 2021). To address whether ER-phagy was compromised in the absence of *Ino80,* we used a strain which expressed the ER membrane transporter protein Sec63 fused to GFP (Schuck et al., 2014). Nutrient starvation is one of several strategies to induce this selective autophagy pathway, and accordingly WT, *atg1Δ* and *ino80Δ* SEC63-GFP strains were cultured in SD-N and protein samples were collected. Immunoblotting against GFP showed the accumulation of free GFP was present in the WT but clearly defective in the autophagy compromised *atg1Δ* (Figure 3.8A). The *ino80Δ* mutant resembled *atg1Δ* cell and was compromised in its ability to deliver components of the ER membrane to the vacuole - only a very faint band corresponding to the size of GFP could be observed (Figure 3.8A). Since the severely reduced GFP signal implied a failure

to deliver ER membrane to the vacuole, we concluded that INO80 activity was promoting the reticulophagy pathway and the associated specific degradation of ER membrane.

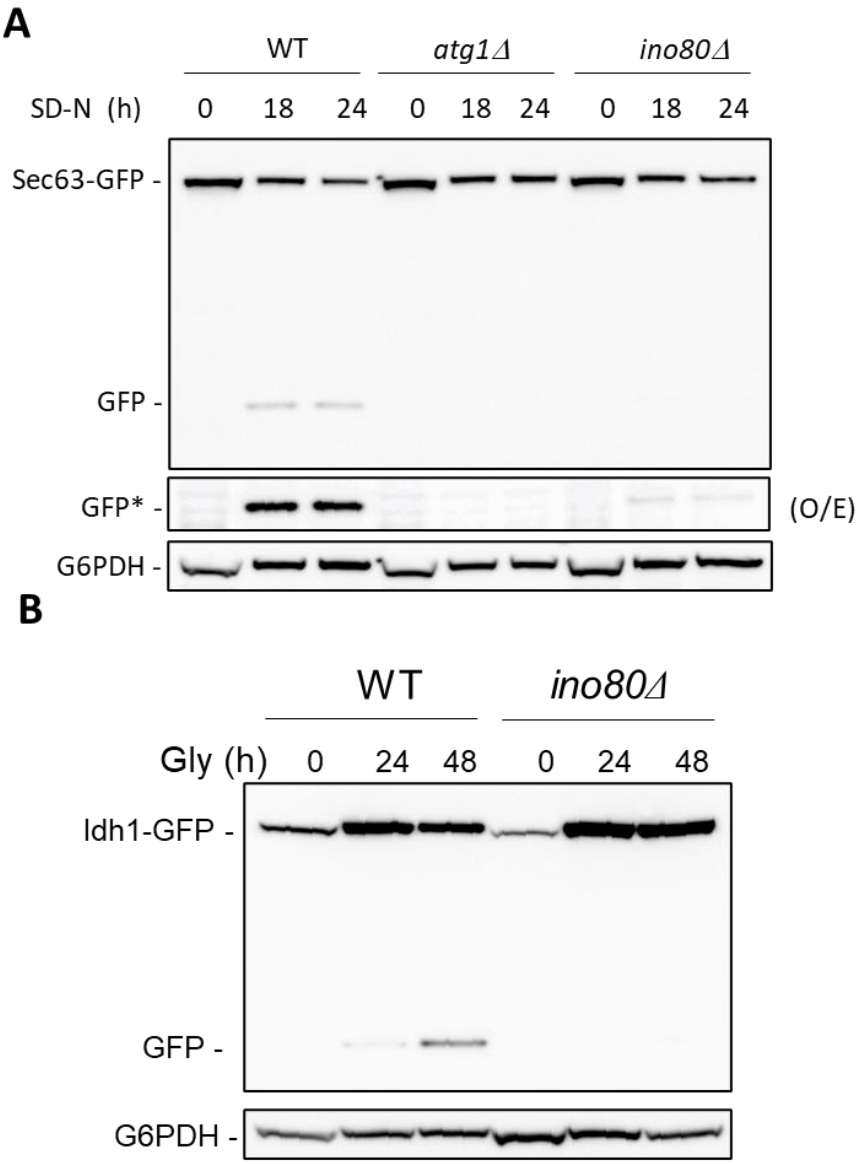

Figure 3.8. INO80 promotes selective autophagy of Mitochondria and ER. (A-B). Wild-type cells together with Atg1 and Ino80-deficient cells expressing the ER or mitochondrial markers (Sec63 or Idh1-GFP) fusion were grown to exponential phase and subsequently shifted to media lacking nitrogen in the case of Sec63. and media where glycerol is the sugar source in the case of Idh1. At the indicated times protein extracts were taken and analysed by western blot using antibodies against GFP.

Finally, we assessed Mitophagy activity, a quality control pathway for removing damaged or superfluous mitochondria. To evaluate this pathway, budding yeast was grown in the presence of a non-fermentable carbon source, glycerol. The resulting shift to aerobic respiration places a burden on mitochondria and increases the need for quality control and the turnover of damaged organelles (Eiyama and Okamoto, 2017). To determine activity of the pathway, we used a strain where the mitochondrial protein Idh1 is fused to GFP. Culturing WT and *ino80Δ* IDH1-GFP strains in glycerol and collecting total protein, we noted that by 24 hours in glycerol, and more clearly after 48 hours; free GFP began to accumulate in the WT strain indicating mitochondrial delivery to the vacuole. However, GFP was not observed in the *ino80Δ* cells (Figure 3.8B), suggesting the mitochondrial delivery to the vacuole was dependant on INO80. This strongly suggests that INO80 activity is promoting Mitophagy.

Taken together, these results indicate a role for the INO80 complex in regulating specific selective autophagy pathways. We concluded that INO80 activity was promoting selective autophagy of the ER and the mitochondria, potentially through a novel transcriptional pathway.

3.2.7. INO80 regulated transcriptome resembles nitrogen starved cells

The chromatin remodelling activity of the INO80 complex has wide-ranging effects on transcription, and mutants lacking the complex display extensive transcriptional mis-regulation (Poli et al., 2017a). We thus hypothesized that INO80 might regulate a selective autophagy-promoting transcriptional program in response to metabolic stress.

To investigate the role of INO80 in the transcriptional response to starvation, total RNA extraction followed by high throughput sequencing (RNA-seq) was performed by Anne Lafon. The sequencing and raw read analysis was performed in collaboration with the Morillon lab by Ugo Szachnowski. WT and *ino80Δ* strains were grown in CSM before shifting to nitrogen starvation conditions and samples were collected and sequenced before and 2 hours following nitrogen starvation. The samples included ERCC RNA ‘spike-in’ of a known amount allowing for normalisation between samples and subsequent comparisons between the WT and *ino80Δ* strains. Transcription profile expression analysis was performed by myself, and figures were generated by Ugo Szachnowski under my direction.

A previous RNA-seq study investigated changes to the WT and *ino80Δ* transcriptomes caused by Rapamycin and concluded that the *ino80Δ* transcriptome resembles TORC1 inhibited cells (Beckwith et al., 2018). The authors concluded that INO80 was mediating active TORC1 signalling and was

therefore a transcriptional effector of the TORC1 pathway. Our own results contradicted some of the other findings of their study, in particular the rescue of WT growth defect in rapamycin by *ino80Δ*. Therefore, before investigating whether INO80 regulated an autophagy-associated transcriptional program (following TORC1-inhibition), we decided to replicate their transcriptomic analysis using our own RNA data set.

We compared the transcriptional effect of *Ino80* loss against the effect of shifting exponentially growing cells to nitrogen starvation for 2 hours. While the original study used rapamycin to inhibit TORC1 signalling, we reasoned that the effect of nitrogen starvation should be nearly identical (Klosinska et al., 2011).

We calculated the fold-change (FC) between log transformed RNA values for all mRNA genes in WT nitrogen starved cells against the non-starved transcriptome. The FC for each gene was then compared to the FC observed when the exponentially growing *ino80Δ* transcriptome was compared to WT, non-starved, transcriptome. Such comparisons allowed us to measure concordance in transcriptional effect between nitrogen starvation and loss of *Ino80*. Although the correlation was not particularly strong, showing a Pearson's correlation coefficient of 0.296, we did observe a statistically significant positive correlation between differentially expressed genes in *ino80Δ* and nitrogen starved WT cells (Figure 3.9A). A similar analysis was done for down-regulated genes, again finding a statistically significant positive correlation, with a Pearson's correlation coefficient of below 0.3 (data not shown). We concluded that changes to the transcriptome caused by loss of *Ino80* did resemble the effect of nitrogen starvation. Because the genome wide correlation was relatively weak, we decided to investigate the correlations between subsets of TORC1 regulated genes.

We observed that the clearest correlation was for nitrogen responsive genes, with a strong and significant Pearson's correlation coefficient of 0.706 among up and down regulated genes (Figure 3.9B). This suggests that loss of INO80 leads to the same transcriptional up regulation and down regulation as observed following nitrogen starvation. This indicated that INO80 may be regulating the nitrogen responsive pathway during active TORC1 signalling, and nitrogen repression leads to its de-regulation which mimics the loss of the complex.

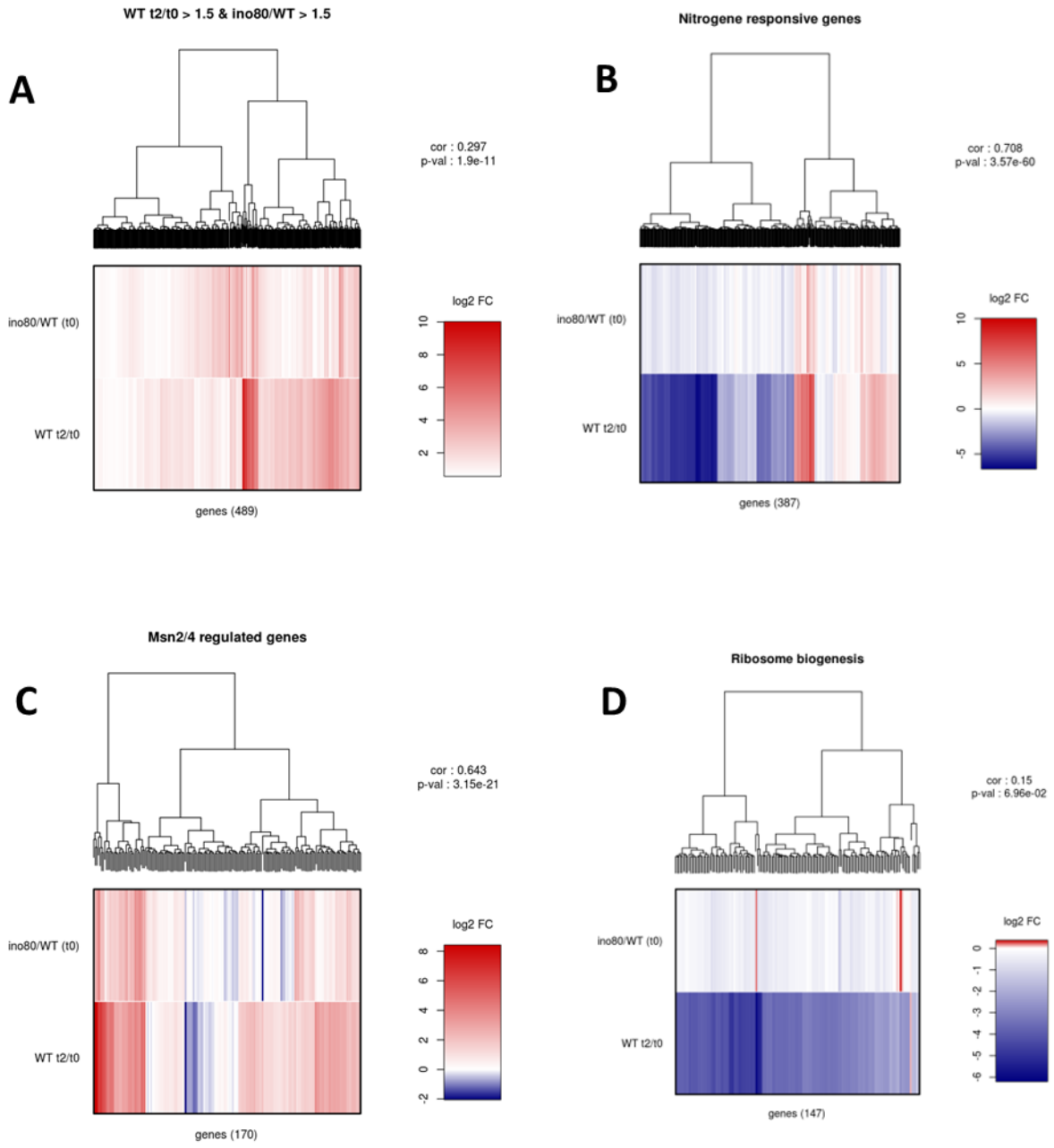

Figure 3.9. INO80 regulated transcriptome resembles nitrogen starved cells. (A) Log-transformed expression fold-change (FC) between nitrogen starved and non-starved WT and ino80Δ. Shown is the comparison non-starved ino80Δ and nitrogen starved WT cells. Plotted are only genes with FC of over 1.5 and Pearson correlations (Cor) and p-values (p-val) are calculated for the plotted genes. **(B)** Plotted as above. but only genes involved mTOR regulation of nitrogen availability response (Scherens et al 2006). **(C)** Plotted as above. only shown are Msn2/4 regulated stress response genes (Gasch et al 2000). **(D)** Plotted as above. only shown are ribosome biogenesis genes (Jorgensen et al 2004).

The transcription factors MSN2 and MSN4 are two major effectors of the TORC1 inhibition and activate a wide range of genes in response to metabolic stress (Beck and Hall, 1999; Kim and Guan, 2019). We continued the comparison between the effect of *Ino80* loss and the effect of nitrogen starvation relative to WT transcriptome. We compared fold-change in the expression of Msn2/4 regulated genes in the starved cells and again found a highly significant positive correlation (r=0.643) with cells lacking INO80 (Figure 3.9C). The transcription factors MSN2 and MSN4 are two major effectors of the TORC1 inhibition and activate a wide range of genes in response to metabolic stress. Since TORC1 inhibition leads to the activation of MSN2/4 regulated genes, the correlation between *ino80Δ* transcriptome and that of nitrogen starved cells strongly suggests that INO80 activity is involved in repressing MSN2/4 transcriptional pathway during cell growth and active TORC1 signalling. This agrees with the findings of Beckwith *et al* (2018).

Finally, we compared differences in the expression of ribosome biogenesis genes, as the silencing of this group of genes is a hallmark of the transcriptional response to nitrogen starvation. As previously seen, loss of INO80 led to a transcriptome that was positively correlated with nitrogen starved wild-type cells however changes to this group of genes was less similar to the effect of nitrogen starvation than the other reported groups of genes (Figure 3.9D). The results suggest that loss of INO80 does lead to slight repression of ribosome biogenesis genes however this is of only weak correlation to the effects of nitrogen starvation (Pearson correlation 0.15).

Ultimately our results concord with the data presented by Beckwith et al. (2018), with some variation regarding the extent of correlations. Taken together, we conclude that INO80 mediates active TORC1 signalling, however, to what degree this is the case and how directly INO80 is involved remains unclear. While we generally see the transcriptional effect of nitrogen starvation resembling the transcriptome of Ino80 deleted cells, the magnitude of the differential expression is generally smaller following loss of *Ino80* compared to nitrogen starvation. This may be the result of INO80 being one of a set of regulatory factors promoting TORC1 signalling through this pathway.

3.2.8. INO80 regulates transcription of protein sorting genes in response to nitrogen starvation

The finding that INO80 activity leads to a transcriptional program associated with active TORC1 signalling fails to account for our previous findings that INO80 regulates pathways responding to nutrient starvation. Therefore, we asked whether INO80 activity is required for establishing the transcriptional response to nitrogen starvation. Focussing again on key transcriptional pathways, we compared changes in gene expression after nitrogen starvation in the presence and absence of *Ino80*.

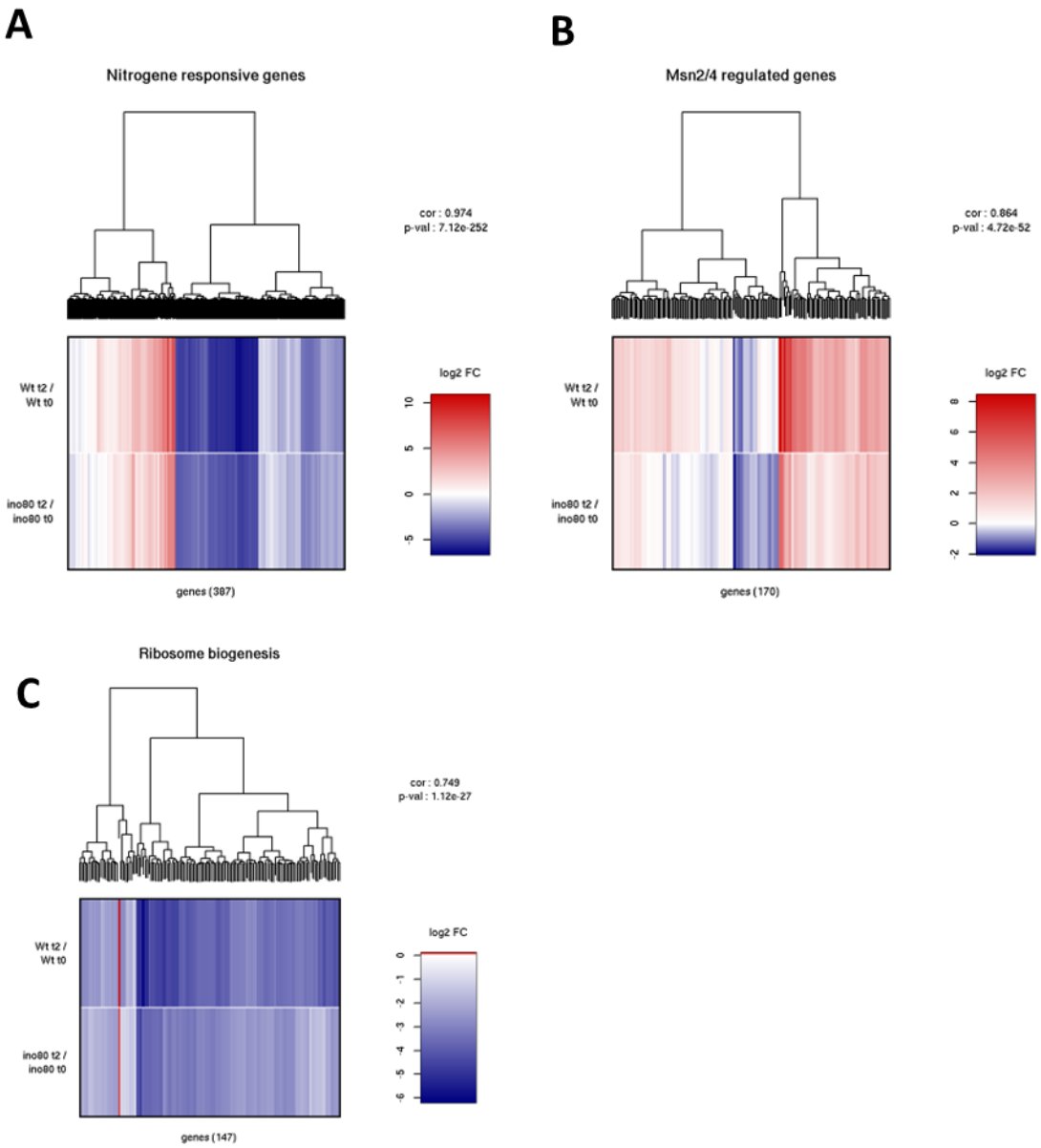

Figure 3.10 Wild-type and *ino80Δ* transcriptomes undergo similar changes in response to nitrogen starvation. **(A)** Log-transformed expression fold change (FC) between nitrogen starved and non-starved WT and ino80Δ. Plotted are only genes with FC of over 1.5 and Pearson correlations coefficient (Cor) for the corelation and p-values (p-val) are calculated for the plotted genes. **(B)** Plotted as described in (A) only shown are Msn2/4 regulated stress response genes (Gasch et al 2000). **(C)** Plotted as described in (A) only shown are ribosome biogenesis genes (Jorgensen et al 2004).

We compared the effect of *Ino80* loss similarly to the process described above, this time comparing the FC effect of nitrogen starvation in WT cells (WT SD-N/WT) against the effect in *ino80Δ* (*ino80Δ* SD-N/ *ino80Δ*). We first compared changes to the expression of nitrogen-responsive genes following

starvation and found that both strains underwent highly similar changes with a Pearson's correlation coefficient of 0.974 (Figure 3.10A). This meant that despite the previously identified similarity between *ino80Δ* and nitrogen starved transcriptomes, INO80 was not required for transcription of nitrogen responsive genes following TORC1 inhibition. Next we performed the same analysis on Msn2/4 regulated genes and found a strong correlation between the transcriptional changes, irrespective of whether the *INO80* gene was present (Pearson's correlation coefficient of 0.864) (Figure 3.10B). Finally, we compared the transcription of ribosome biogenesis genes, again finding that the transcriptional changes significantly correlated irrespective of the strain, and this group of genes having a Pearson's correlation coefficient of 0.749 (Figure 3.10C).

The results indicate that INO80 was not essential for the establishment of a TOR inhibited transcriptional program, as there was a high correlation between the two transcriptomes. However, the heatmaps show clusters of genes to be mis regulated in different groups, such as nitrogen-responsive genes which fail to be up regulated in the absence of *Ino80* (Figure 3.9A). Similarly, some Msn2/4 gene can be seen to be up-regulated in response to nitrogen starvation in the WT, but down-regulated in the absence of *Ino80* (Figure 3.10B).

Therefore, we conclude that while broadly the transcriptional response to nitrogen is independent of INO80, specific genes may require INO80 activity for correct expression following nitrogen starvation. We hypothesised that the regulation of specific genes may be causing the defective selective autophagy we observed in *ino80Δ*.

We decided to focus on the most differentially expressed genes in the mutant. RNA-seq analysis after 2 hours of nitrogen starvation showed that 661 mRNA genes had significant differential expression greater than 1.5-fold higher in WT relative to *ino80Δ.* This suggested that INO80 was required for promoting their expression. Since *Ino80* deletion leads to wide ranging transcriptional changes independent of starvation, we asked how many of these differentially expressed genes were also found to be mis-regulated prior to starvation. Notably, the majority, 518, were not differentially expressed prior to nitrogen starvation, suggesting that the mis-regulation of these genes is due to the loss of a starvation specific INO80 function (data not shown).

We asked if any known or core autophagy genes were found in this group of genes and discovered that only *ATG10* was differentially expressed, being expressed 1.9-fold higher in WT than *ino80Δ*. Atg10 is a core and essential autophagy protein (Shintani et al., 1999). Since our functional analysis of the autophagy pathway in *ino80Δ* showed that bulk autophagy was not INO80-dependant, we concluded that mis-regulation of *ATG10* was likely not a major contributor to the phenotypes of *ino80Δ*.

To increase our stringency, the analysis was restricted to genes with two-fold or greater expression in WT relative to *ino80Δ* (249 genes) and we asked whether the genes were enriched for any statistically significant biological process Gene Ontology (GO) terms.

Applying this, we discovered a statistically significant enrichment for gene ontology terms associated with catabolic processes (p value = 6.2 x 10^{-9}), these were concentrated around protein sorting and delivery to the vacuole (Table 3.2 and Figure 3.10).

Gene Set	Description	Size	Expect	Ratio	P Value	↑ FDR
GO:0043328	protein transport to vacuole involved in ubiquitin-dependent protein catabolic process via the multivesicular body sorting pathway	25	0.65046	13.836	6.1759e-9	0.000023184
GO:0043162	ubiquitin-dependent protein catabolic process via the multivesicular body sorting pathway	35	0.91065	9.8831	1.7083e-7	0.00032064
GO:0032511	late endosome to vacuole transport via multivesicular body sorting pathway	45	1.1708	7.6868	0.0000017163	0.0021476
GO:0032509	endosome transport via multivesicular body sorting pathway	51	1.3269	6.7825	0.0000051563	0.0045788
GO:0071985	multivesicular body sorting pathway	52	1.3530	6.6521	0.0000060985	0.0045788
GO:0072666	establishment of protein localization to vacuole	68	1.7693	5.6521	0.0000084193	0.0052677
GO:0008324	cation transmembrane transporter activity	196	5.0996	3.3336	0.000010976	0.0058861
GO:0045324	late endosome to vacuole transport	60	1.5611	5.7651	0.000020515	0.0096269
GO:1904659	glucose transmembrane transport	24	0.62444	9.6086	0.000025672	0.010708
GO:0008645	hexose transmembrane transport	25	0.65046	9.2242	0.000033059	0.011282

Table 3.2 – Gene ontology of differentially expressed genes following 2 hours of nitrogen starvation. Functional gene set analysis of mRNA genes identified to be have 2-fold greater expression in WT relative to ino80Δ following nitrogen starvation (FC > 2. WT/ino80Δ) . Listed are enriched pathways identified to be mis-regulated in the deletion mutant. Most significantly enriched terms are placed at the top of the table. "Size" refers to number of genes from the set of 249 that fall into that group. "expect" is the number of genes expected to be found in a random sample of genes. (http://www.webgestalt.org/)

Gene Set	Description	Size	Expect	Ratio	P Value	↑ FDR
GO:0043328	protein transport to vacuole involved in ubiquitin-dependent protein catabolic process via the multivesicular body sorting pathway	25	0.65046	13.836	6.1759e-9	0.000023184
GO:0072666	establishment of protein localization to vacuole	68	1.7693	5.6521	0.0000084193	0.0052677
GO:1904659	glucose transmembrane transport	24	0.62444	9.6086	0.000025672	0.010708

Table 3.3 – Gene ontology terms of differentially expressed genes following 2 hours of nitrogen starvation and the removal of redundant terms. Weighted set cover was applied to the significantly enriched GO terms of top differentially expressed genes (FC > 2. WT/ino80Δ) after 2 hours of nitrogen starvation.

By using an additional analysis of weighted set cover to reduce redundancy in the gene ontology terms being enriched (due to the same genes being given association with multiple terms), three GO terms remained (Table 3.3). We found glucose transmembrane transport genes to be significantly enriched (p value = 2 x 10^{-5}). We reasoned that the failure to correctly up-regulate processes for sugar intake may be a contributing factor to the sensitivity of *ino80Δ* to nitrogen starvation.

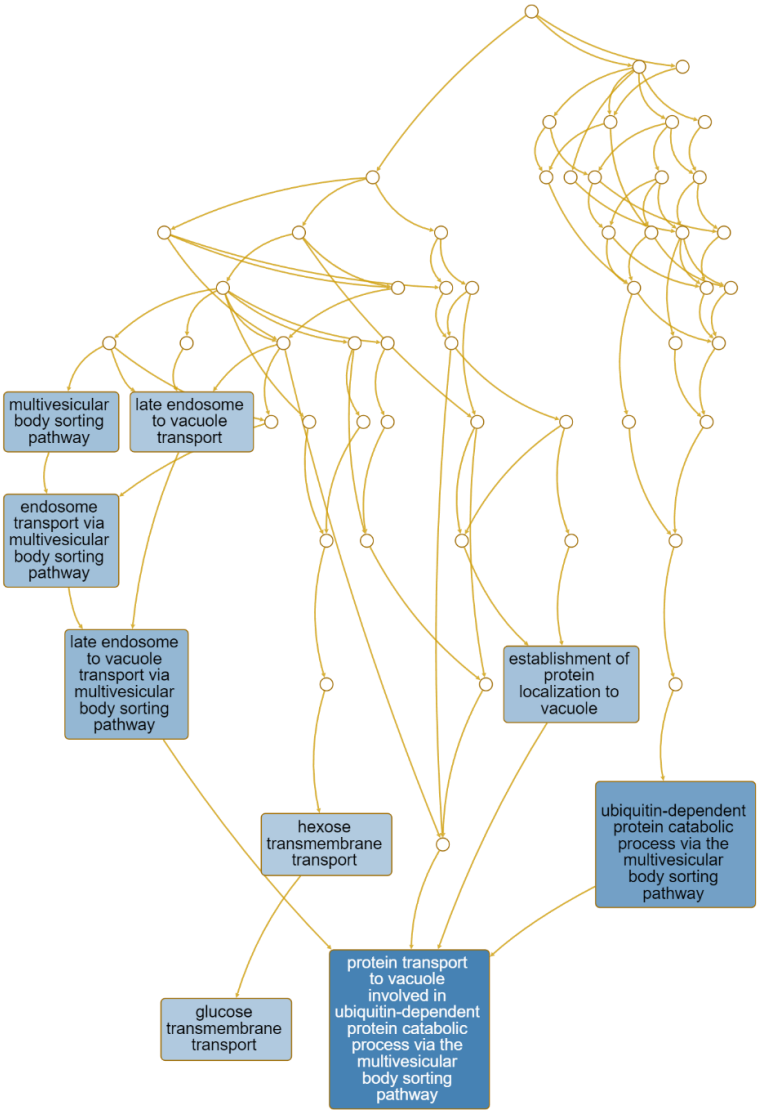

Figure 3.11. A gene ontology directed acyclic graph (DAG). Gene ontology (GO) of all top differentially expressed genes (FC > 2. WT/ino80Δ). Each node represents a GO term. arrows represent 'part-of' and 'is-a' relationships between GO terms. Blue boxes highlight most significantly over-represented GO terms (Aranguren et al., 2007; Goeman and Mansmann, 2008).

Finally, investigating the genes associated with the most significant GO terms, we found that many shared the same group of related genes, namely *COS1*, *COS2*, *COS5*, *COS7*, *COS8*, *COS10* and *COS12*

(Table 3.4). We conclude that INO80 activity is required for the regulation of transcriptional pathways associated with ubiquitin-dependent vacuolar protein sorting, and glucose transmembrane transport. We speculated that this may be contributing to the inability of *ino80Δ* to clear ubiquitin conjugates as previously observed as well as contributing to the growth defect. Furthermore, we wondered if failure to express genes involved in delivery to the vacuole may be contributing the defective selective autophagy pathways. The results strongly implied that INO80 activity promoted a specific transcriptional network regulating protein sorting and turnover in response to nitrogen starvation.

Gene	log2 FC	padj
COS12	4.409	3.65E-24
COS8	3.862	2.82E-87
COS2	2.821	1.49E-45
COS3	2.543	2.6E-112
COS1	2.440	2.48E-83
COS5	2.430	5.48E-34
COS7	2.283	5.66E-49
COS10	1.889	7.69E-24

Table 3.4. GO modification-dependent protein catabolic process. Genes found in the top enriched GO term groups. 'Log2FC' refers to log2-transformed fold change value (WT/ino80Δ). 'padj' refers to adjusted p-value.

3.2.9. INO80 represses the expression of genes involved in yeast reproductive processes during nitrogen starvation

We next investigated what genes are transcriptional activated in the absence of INO80 by comparing the 2-hour nitrogen starvation time point between WT and *ino80Δ*. We reasoned that any genes which has a significant fold change increase in the *ino80Δ* relative to WT, are likely targets of INO80-mediated silencing in nitrogen starvation. We chose a 2-fold increase in *ino80Δ* relative to WT and

identified 128 genes which were hyper-activated in the absence of INO80. To understand whether any biological processes were enriched within this set of genes we ran an over-representation analysis (ORA) for gene ontology terms associated with these 128 genes. We found budding yeast reproductive processes to be significantly enriched ($p = 1.4 \times 10^{-14}$), with many of the genes falling into gene ontology groups such as meiotic cell cycle (GO:0051321, $p = 3.9 \times 10^{-12}$) and spore wall assembly (GO:0042244, $p = 1.03 \times 10^{-13}$) (Table 3.5). When a weighted set cover was applied to the analysis, identifying the top non-redundant gene sets, only 'reproductive processes' (GO:0022414) was found to be enriched, suggesting all the other significantly enriched gene ontology terms were closely associated with this process.

Gene Set	Description	Size	Expect	Ratio	P Value	↑ FDR
GO:1903046	meiotic cell cycle process	269	3.9166	6.8938	2.2204e-16	6.4704e-13
GO:0051321	meiotic cell cycle	319	4.6446	6.0285	1.8874e-15	2.7499e-12
GO:0022414	reproductive process	462	6.7266	4.7572	9.7700e-15	9.4899e-12
GO:0000003	reproduction	480	6.9887	4.5788	2.8977e-14	2.1110e-11
GO:0010927	cellular component assembly involved in morphogenesis	73	1.0629	14.113	5.7732e-14	2.5720e-11
GO:0030435	sporulation resulting in formation of a cellular spore	164	2.3878	8.3759	8.5709e-14	2.5720e-11
GO:0030476	ascospore wall assembly	49	0.71343	18.222	8.8263e-14	2.5720e-11
GO:0042244	spore wall assembly	49	0.71343	18.222	8.8263e-14	2.5720e-11
GO:0070590	spore wall biogenesis	49	0.71343	18.222	8.8263e-14	2.5720e-11
GO:0070591	ascospore wall biogenesis	49	0.71343	18.222	8.8263e-14	2.5720e-11

Table 3.5. Gene ontology of differentially expressed genes following 2 hours of nitrogen starvation. Gene set enrichment analysis of all genes found to have > 2-fold higher expression in the ino80Δ relative to WT following nitrogen starvation (FC > 2. ino80Δ/WT). Most significantly enriched terms are placed at the top of the table. "Size" refers to number of genes from the set of 249 that fall into that group. "expect" is the number of genes expected to be found in a random sample of genes. (http://www.webgestalt.org/)

Nitrogen starvation induces diploid yeast to initiate meiosis and leads to gametogenesis (referred to as sporulation in yeast) and the formation of pseudohyphae as part of the stress response (van Werven and Amon, 2011). This process is controlled by the master regulator IME1, which induces the expression of many genes involved in meiotic DNA replication and the initiation of sporulation (Kassir et al., 1988). We wondered if loss of *Ino80* might be controlling the transcription of the *IME1* gene and investigated using the data from our RNA-seq dataset. Comparing *IME1* RNA tag densities for *ino80Δ* cells we found that nitrogen starvation led to 3.2-fold higher expression of the gene relative to WT (Figure 3.12A). *IME1* RNA levels continued to increase following 4 hours of nitrogen starvation to 3.7-fold relative to WT (Figure 3.12A). IME1 expression activates the transcription of many 'early' sporulation genes including *NDT80*, which is a transcription factor controlling the expression of 'middle' sporulation genes involved in meiosis and gamete formation (Chu and Herskowitz, 1998, p. 10). Consistent with a de-repression of *IME1* gene, we found that *NDT80* expression was also increased 3-fold in *ino80Δ* relative to WT after 2 hours of nitrogen starvation and 6-fold increased after 4 hours of nitrogen starvation (Figure 3.12B).

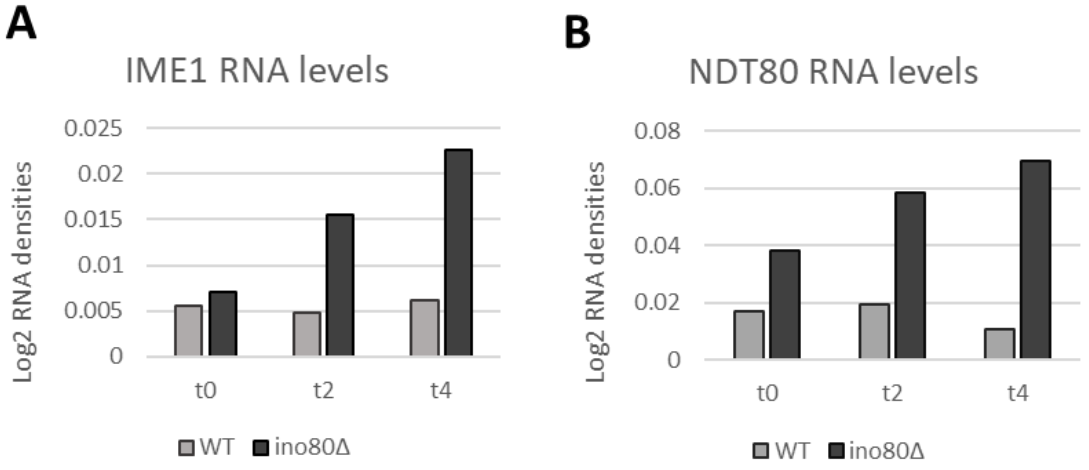

Figure 3.12. INO80 inhibits the expression of sporulation master regulators in nitrogen starvation. (A-B) Average RNA log2 tag densities measured in the RNA-seq were plotted for the IME1 and NDT80 genes. Values for prior to starvation (t0). following 2 hours (t2) and 4 hours (t4) of starvation are plotted.

Ndt80 expression was already increased relative to WT prior starvation and before to the induction of *IME1* gene, arguing that the regulation of these two genes may not be directly related to the role of INO80 during nitrogen starvation. We conclude that the over-representation of derepressed genes

associated with reproductive processes is the result of increased Ime1 and Ndt80 expression in the absence of *Ino80*. However, further work is needed to understand what role INO80 activity plays in budding yeast sporulation since the genetic background of an experimental yeast strain plays a significant role in how proficient a given yeast is at performing sporulation (Dirick et al., 1998).

3.2.10. The COS genes are targets for INO80 regulation upon nitrogen starvation

Our results so far have suggested INO80 regulates specific selective autophagy pathways. We reasoned that the failure to upregulate genes associated with catabolic processes and protein sorting (Table 3.3), is a likely pathway causing this defect. We decided to focus on transcriptional pathways that required INO80 activity for their expression following nitrogen starvation.

To investigate what genes are most dependent on INO80 activity, we plotted the log_2 transformed fold-change against significance ($-Log_{10}$). Intriguingly, eight of the most INO80-dependant genes belong to a single genes family, expressing the highly ubiquitinated tetraspan Cos proteins (Figure 3.13A) (MacDonald et al., 2015). The gene family comprises of 11 members, named COS1-10 and COS12 as well as an additional, related gene YIR042C, all members of the DUP380 subfamily, an evolutionarily conserved structural family found in multiple yeast species (Despons et al., 2006; Spode et al., 2002). The different Cos proteins are found enriched at different membranes in the cells, with COS8 primarily enriched at the nuclear membrane (Spode et al., 2002), Cos5 at the extracellular membrane and Cos7 predicted to reside in the mitochondrial membrane (MacDonald et al., 2015).The function of Cos proteins is not well understood but has been demonstrated to be critical for endosomal sorting through the multi-vesicular body (MVB) pathway (MacDonald et al., 2015). Nutrient depletion leads to protein turnover of membrane-integrated proteins, and Cos5 and other Cos proteins have been demonstrated to mediate this process (MacDonald et al., 2015).

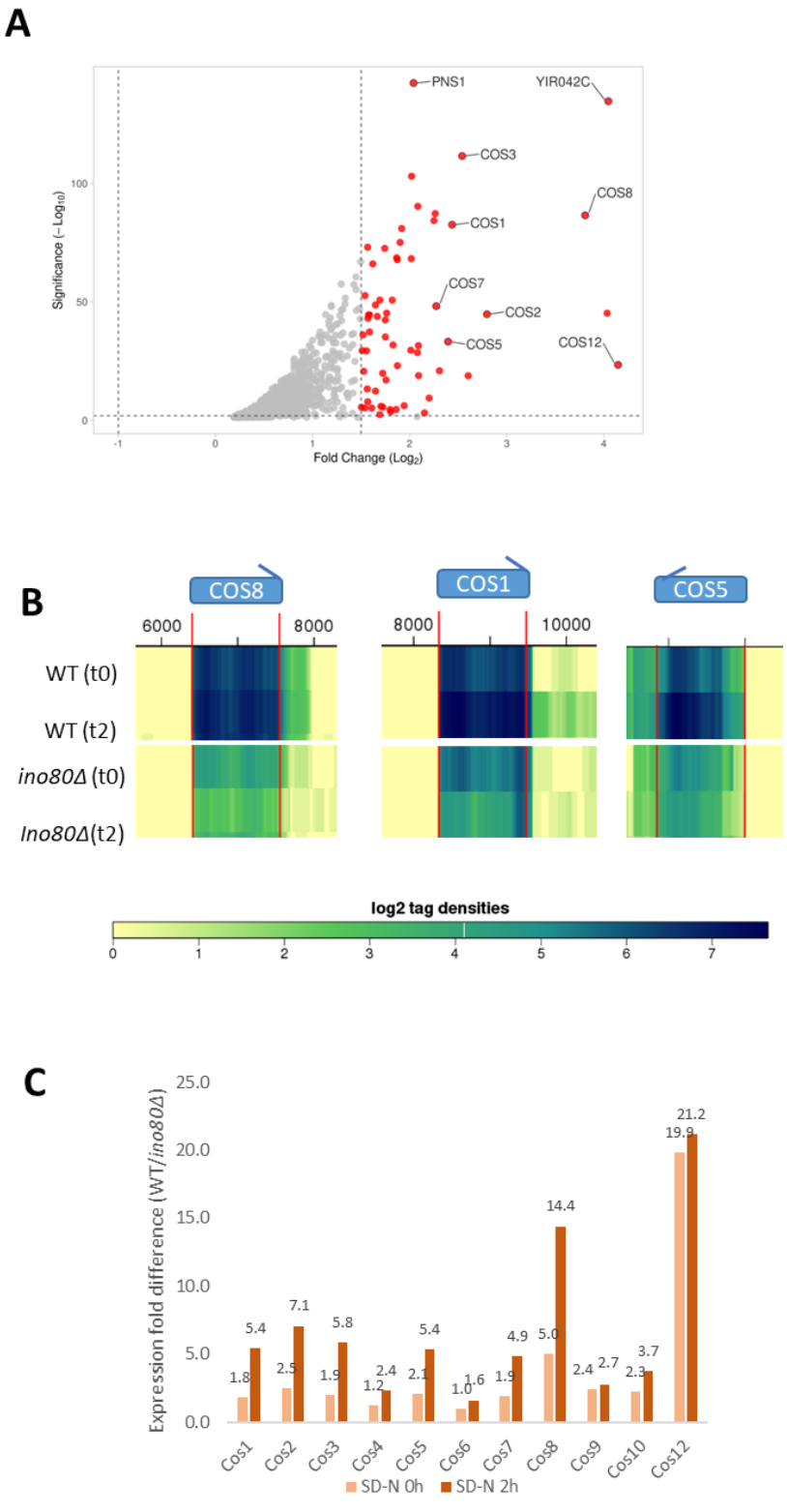

Figure 3.13. INO80 promotes the expression of multiple COS genes in nitrogen starved conditions. (A) Volcano plot of overall differential expression in RNA-seq between WT and ino80Δ following 2 hours of culture in SD-N. Only shown are genes found to be repressed in ino80Δ. The cut-off on the x-axis

represents a fold-change of > 2.5. and on the y-axis represents a significance of $p < 0.01$. **(B)** Heatmaps of RNA-seq generated log2 tag densities mapped to COS8, COS1 and COS5. **(C)** RNA-seq log2 tag density averages over every COS gene were calculated and FC (WT/ino80Δ) plotted for before switch to starvation media ('SD-N 0h') and following 2 hours of nitrogen starvation ('SD-N 2h'). FC data is present above each relative bar in the plot.

By plotting read densities as heatmaps along a reference genome, we observed that loss of INO80 led to decreased expression of COS genes both before and after nitrogen starvation (Figure 3.13B). We noticed that for many of the COS genes, two hours of nitrogen starvation led to an increase of RNA expression relative to non-starved conditions (Figure 3.13B). Strikingly, *ino80Δ* cells were unable to upregulate the expression of these genes following nitrogen starvation and for several *COS* genes, nitrogen starvation led to repression in cells lacking *ino80Δ* (Figure 3.13B). Comparing differential expression between WT and *ino80Δ* before and after nitrogen starvation, we observed that nitrogen starvation led to a greater difference in expression levels (Figure 3.13C). We concluded that INO80 promotes the expression of the *COS* genes in normal conditions and that in addition to this, nitrogen starvation leads to the upregulation of *COS* transcription in an INO80 dependent process.

To confirm our observation that INO80 regulated the expression of COS genes, WT and *ino80Δ* cells were cultured in; rich media, SD-N or on a non-fermentable carbon source, glycerol. RNA was purified and the expression of 4 COS genes, the INO1 gene and the non-coding (nc)RNA SCR1 were measured using reverse-transcriptase quantitative polymerase-chain reaction (RT-qPCR). As the expression of SCR1 is not affected by the loss of INO80 or the change of growth media the amount of this ncRNA was used as an internal control by which the levels of the other genes were normalised. The INO1 gene activity is a well-established target of INO80 activity and served as a positive control (Ebbert et al., 1999). As expected, relative INO1 RNA was found to be reduced in *ino80Δ*, particularly following nitrogen starvation and growth in glycerol (Figure 3.14A). Next we observed that, in agreement with the RNA-seq results, when the cells were grown in SD-N, the expression of COS1, 5, 7 and 8 was reduced in *ino80Δ* relative to wild-type (Figure 3.14A). COS1,5,7 and 8 RNA levels were similarly lower when *ino80Δ* was cultured in glycerol, however the differential expression resembled levels found in rich media more so than nitrogen starvation.

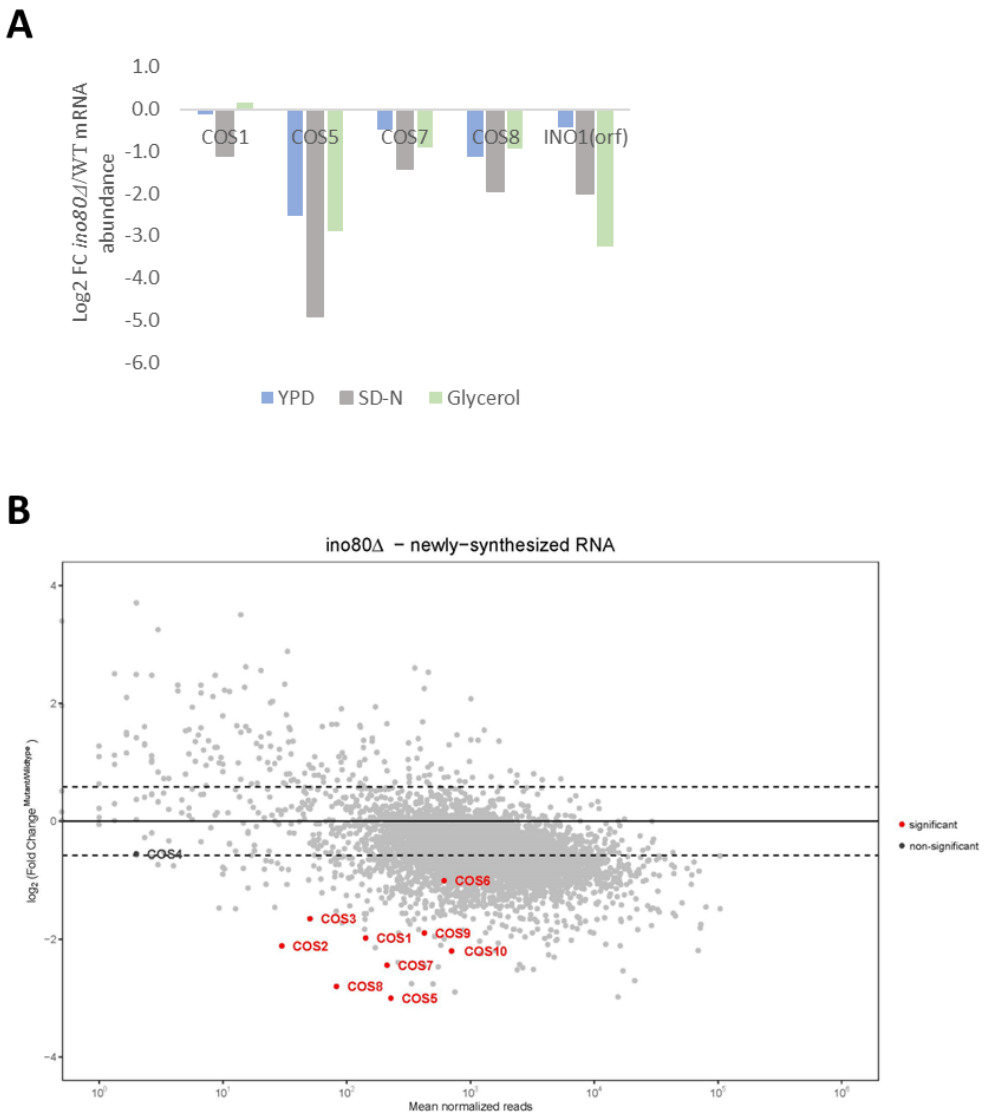

Figure 3.14. The COS gene family transcription is regulated by INO80. (A) RT-qPCR measurement of relative RNA abundance (normalised to Scr1). Plotted is the log2-transformed FC ino80Δ/WT. Samples were nitrogen starved for 2 hours (SD-N) or switched to glycerol for 24 hours. prior to sample collection and RNA purification. Experiment is a single biological repeat. **(B)** Newly synthesised RNA by 4tU-sequencing. Scatter plot analysis for the log2 fold change (ino80Δ/WT) of nascent RNA synthesis is plotted. Dashed line represents 1.5 fold change. Differentially expressed COS genes (significant, $p < 0.05$) are highlighted in red.

As this experiment was only performed once, we were unable to draw conclusion from it alone and further repeats are needed. However, the results did add further support to our previous conclusion that INO80 regulated COS RNA levels.

RNA-seq experiment represents a ‘snap-shot’ of RNA levels at steady state at a given time point. Therefore, this approach alone is unable to differentiate whether INO80 is promoting the expression of more COS RNA or increasing the stability of existing RNA.Our data supported a model where INO80 promoted the expression of COS RNA, but we were unable to distinguish between a model where INO80 regulated the transcriptional activation of COS genes or regulated the stability – and therefore steady-state availability – of COS RNA. A potential strategy to address this question would be to measure rates of nascent RNA synthesis and compare these between WT and *ino80Δ*. If INO80 activity regulated the transcription of the RNA, nascent RNA levels of COS genes would be expected to be reduced relative to WT. Alternatively, if INO80 only regulated post-transcriptional stability of COS RNA, no difference would be expected to nascent RNA levels.

One assay capable of addressing this question is the high-throughput sequencing of nascent RNA labelled *in vivo* by 4-thiouracil (4tU). Supplementing growth medium with 4tU leads cells to process it to 4-thiouridine monophosphate which is incorporated into synthesising RNA (Zeiner et al., 2008). RNA can be tagged and purified based on the presence of 4tU, allowing for the high-throughput measurement of RNA synthesis and decay rates when the 4tU is provided for a short duration of time, known as pulse/chase. In collaboration with the lab of Laszlo Tora, 4tU-seq was conducted by Kenny Schumacher in WT and *ino80Δ*. Analysis of the nascent RNA sequencing data revealed that, RNA synthesis was significantly reduced in *ino80Δ* for all COS genes except COS4 (Figure 3.14B). Furthermore, the synthesis of *COS5* and *COS8* RNA was observed to be some of the most decreased out of all genes in the *ino80Δ* samples, and in agreement with our previous RT-qPCR data. We therefore conclude that the transcription of most of the *COS* genes is INO80-dependant. Although the 4TU-seq data set was only performed in a non-starvation medium, we reasoned that such a significant dependence on INO80 for transcription was likely to also be the cause of the drastically reduced levels observed following nitrogen starvation.

3.2.11. The COS genes are novel regulators of Mitophagy

Previous work on the COS genes has found the gene family to be involved in selectively targeting membrane-integrated proteins to the vacuole (MacDonald et al., 2015). We hypothesised that the Cos proteins may function within other pathways and promote protein delivery to the vacuole. We asked whether our previously observed defects in the absence of *Ino80*; namely compromised ubiquitin-conjugate turnover and defective selective autophagy, was mediated by the loss of Cos protein activity.

To investigate this, we employed yeast strain where all of the *COS* genes and the *YIR042C* pseudo gene were all partially or fully deleted, referred to as *cosΔ* (MacDonald et al., 2015).

Due to the repetitive nature of these genes, the authors could not comprehensively delete the entirety of the coding sequence of every *COS* gene and so the majority are only partially deleted. The similarity the *COS* genes share with one another meant that it was difficult to fully ensure no expression was taking place. RNA-seq confirmed that the genes were still partially expressed (MacDonald et al., 2015).

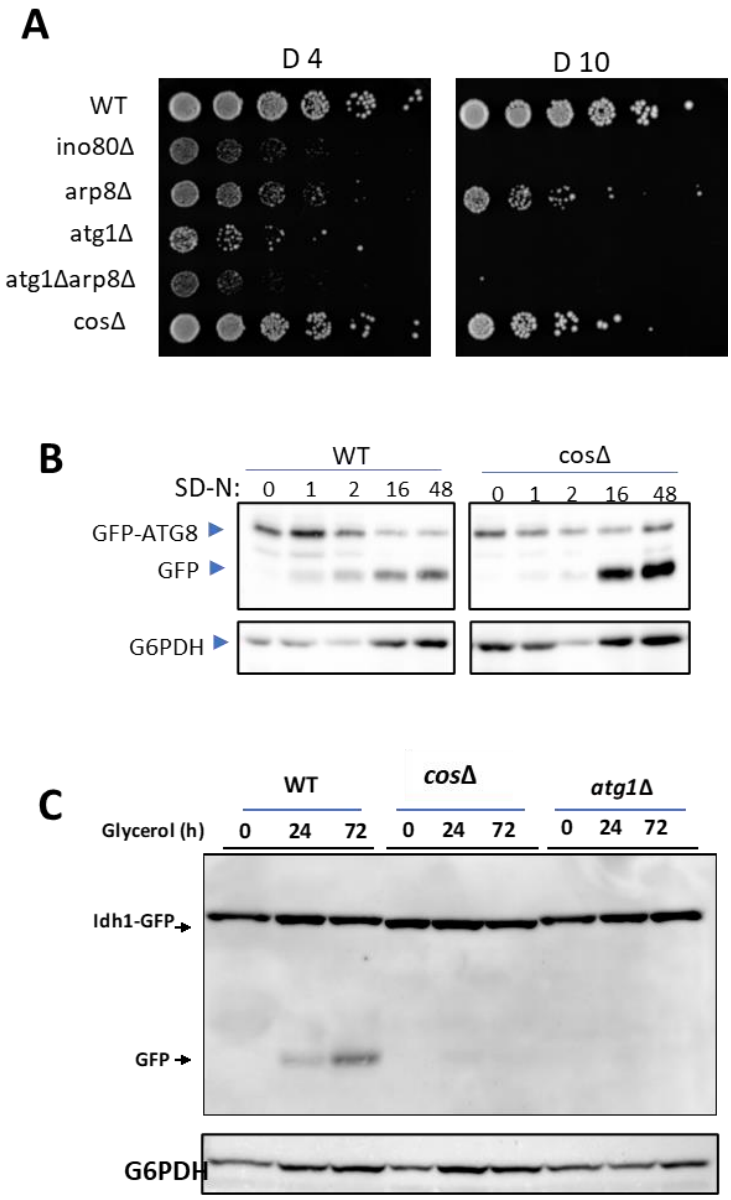

Figure 3.15. Correct COS expression is required for active mitophagy. (A) Loss of COS genes has a mild effect on growth in SD-N. Five-fold serial dilutions of SD-N grown samples (4 days in SD-N after switch (D 4) and 10 days after switch (D 10) spotted to rich media plates. Growth was assessed after 2 days of growth

at 30°C. **(B)** Bulk autophagy does not require Cos activity. Immunoblot measurement of autophagy activity in WT and cosΔ cells transformed with GFP-Atg8 expressing plasmid. Time post switch to SD-N indicated in days. **(C)** Mitophagy assay. Idh1-GFP expressing WT, cosΔ and atg1Δ strains were switched to YPG medium for the indicated. Mitophagy was assessed by immunoblot against GFP.

First, we asked if the *cosΔ* strain resembled the *ino80Δ* mutant in its sensitivity to nitrogen starvation. The strain was cultured in SD-N and fitness was quantified by performing spot tests of five-fold serial dilutions on rich media plates. We found that like the WT, *cosΔ* was able to resume growth after 5 days of nitrogen starvation and did not resemble the sensitivity of *ino80Δ* at this time-point (Figure 3.15A). However, following 10 days of nitrogen starvation, while the WT remained un-affected, the viability of *cosΔ* begun to decrease, roughly by a factor of 10 – 20-fold relative to WT (Figure 3.15A). We concluded that Cos proteins were likely contributing to cell fitness in nitrogen starvation however their loss was not responsible for the sensitivity observed in *ino80Δ*.

We next asked if bulk autophagy was functional in the *cosΔ* strain. After transforming the strain with a GFP-Atg8 expressing plasmid, we shifted the cells to nitrogen starvation media and found that free GFP begun to accumulate around 2 hours and was very clear by 16 hours, suggesting functioning autophagy pathway (Figure 3.15B). This indicated that the (potentially partial) loss of the Cos proteins did not affect the core autophagy pathway and bulk autophagy was still able to deliver autophagosomes to the vacuole in the absence of most Cos function.

Finally, we tested the function of mitophagy in the *cosΔ* mutant strain by first tagging the mitochondrial protein Idh1 with GFP and then inducing mitophagy through shifting the cells to glycerol. While this treatment resulted in WT budding yeast inducing mitophagy and generating free GFP molecules, we found that the generation of free GFP, and therefore delivery of Idh1 containing mitochondrial membranes to the vacuole, to be compromised in the *cosΔ* (Figure 3.15C). The inability to carry out mitophagy was identical to the defect of autophagy deficient strain *atg1Δ* and we concluded that the Cos proteins are involved in the promotion of the mitophagy pathway. Thus, we propose that Cos proteins are novel regulators of mitophagy and that INO80 controls the mitophagy pathway, in part through regulating *COS* transcription.

In conclusion, we have found that loss of *Ino80* leads to cell death following nitrogen starvation and this correlates with compromised selective autophagic degradation of ER, mitochondria, and protein aggregates. Transcriptionally INO80 activity promotes the expression of a family of genes associated with protein targeting for vacuolar degradation, the *COS* gene family. And mechanistically these genes promote the autophagic degradation of mitochondria.

3.2.12. COS genes promote ER-phagy activity

The finding that mitophagy was compromised in the *cosΔ* strain led us to ask whether other INO80-dependent selective autophagy pathways are defective when Cos activity is missing. To test this, we GFP tagged the Sec63 protein in the *cosΔ* background. This ER membrane integrated protein then served as a marker for ER-phagy and generation of free GFP was indicative of functional ER-phagy. We found that 24 and 48 hours of nitrogen starvation was sufficient to induce ER-phagy in the WT strain, and this was compromised in the autophagy deficient *atg1Δ* strain (Figure 3.16, lanes 1 – 6). The same conditions led to decreased free GFP accumulation relative to WT when *cosΔ* strain was tested (Figure 3.16, lanes 7-9). We found this decrease to be consistent across multiple experiments but concluded that Cos activity is not essential for functional ER-phagy. However, we do find that the loss of Cos proteins leads to decreased ER-phagy and therefore we conclude that Cos activity may also be involved in promoting the autophagic turnover of ER.

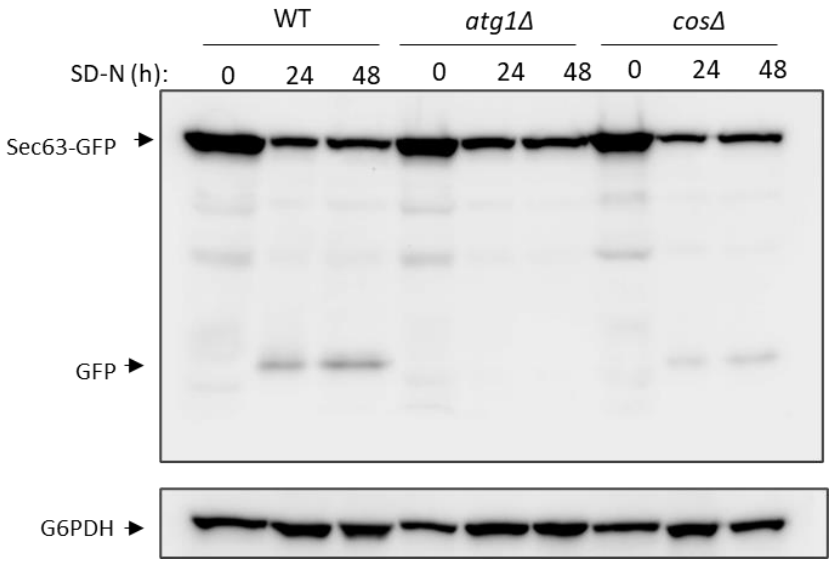

Figure 3.16. Cos activity promotes ER-phagy. Sec63-GFP expressing strains were grown in SD-N for 24 and 48 hours to induce mitophagy. WCE were immunoblot against GFP to measure autophagic turnover of ER. Immunoblot against G6PDH was used as a loading control.

3.3. Summary and Conclusions

We present data that demonstrates a role for INO80 in the metabolic stress response. We find that cells lacking a functional INO80 complex exhibit a loss of viability and that this defect is associated with the autophagy pathway. The core autophagy pathway does not require INO80 activity however we find that INO80 promotes several selective autophagy pathways. We identify that the autophagic turnover of protein aggregates, mitochondria, and the ER, requires INO80. We conclude that INO80 promotes viability in nitrogen starvation by regulating selective autophagy and promoting the turnover of protein aggregates and defective organelles.

Our transcriptomic analysis of *ino80Δ* cells in nitrogen starvation found that gene expression of only a few biological pathways was significantly over-represented among misregulated genes in the absence of *ino80Δ*. Specifically these were genes involved in ubiquitin dependent MVB pathway protein sorting, and the uptake of glucose. Importantly we find that the MVB associated *COS* genes promote mitophagy. This finding highlights a previously unknown regulatory mechanism involved in the control of the selective turnover of mitochondria. Additionally, our data suggested that Cos activity promotes selective autophagy of ER, although we found that the pathway was still functional in the absence of the *COS* genes. This may be due to the *cosΔ* strain only being partially deleted for each *COS* gene (MacDonald et al., 2015) We therefore propose that INO80 promotes mitophagy by controlling the transcriptional activity of *COS* genes. More generally, we speculate the Cos activity and the MVB pathway may be involved in selective autophagy of multiple organelles.

Biochemical studies of the COS genes would help better explain how these proteins function in the mitophagy pathway. Whether the proteins are localised to the membranes of mitochondria and ER would help determine what role they may be playing in autophagic turnover of these organelles.

Chapter 4

Chapter 4. INO80 counteracts Sir-dependent silencing at subtelomeres

4.1. Introduction

We have previously found that following metabolic stress, INO80 activity regulates selective autophagy of mitochondria and the turnover of ubiquitinated proteins. Additionally, we found that loss of *Ino80* led to severe growth defect in nutrient starvation. Our transcriptomic analysis revealed that the *COS* gene family depends on INO80 for transcriptional activation following nitrogen starvation. Importantly, mutation in the coding sequences of *COS* genes results in compromised mitophagy.

The location of *COS* genes within a 10 – 20 kilobase (kB) region from the telomeres places the genes within what is described as sub-telomeric chromatin. The silent information regulator (SIR) complex assembles a heterochromatin like structure which nucleates from telomeric repeats and spreads through subtelomeric chromatin (Hecht et al., 1996; Tanny et al., 1999). Importantly, this spreading mediates chromatin silencing.

The repressive SIR complex functions through the NAD^+-dependent deacetylase activity of Sir2 and the subsequent binding of Sir3 to hypoacetylated nucleosomes (Carmen et al., 2002; Hecht et al., 1995). Together with Sir4, these proteins form a repressive structure which both physically compacts chromatin and epigenetically silences it (Kueng et al., 2013). Histone modification play a central role in this process and the maintenance of a silenced or active chromatin state. The hypoacetylation of histones H4 and H3 N-terminal tails strongly correlates with gene repression, particularly the H4 lysine 16 (H4K16) and H3 lysine 9 (H3K9) residues. Both of these residues are deacetylated by the Sir2 enzyme.

Counter acting the silencing activity of the SIR complex are other chromatin modifying enzymes. These include histone acetyltransferases (HATs), however these enzymes require acetyl-CoA as a substrate in order to catalyse the acetylation of histones (Takahashi et al., 2006a). In *Saccharomyces cerevisiae* the synthesis of nuclear acetyl-CoA is mediated by the Acs2 enzyme (Takahashi et al., 2006a). Recently, the recruitment of Acs2 to subtelomeric chromatin was shown to be important for counteracting of SIR spreading and the activation of subtelomeric genes (Chen et al., 2021).

Previous studies have identified the *COS* to be silenced by Sir2 activity and activated in response to nutrient starvation, however the mechanism of activating these genes was not clear (MacDonald et al., 2015). Considering the subtelomeric localisation of *COS* genes, we wondered how their transcription was ensured following starvation. Our results suggested that the correct regulation of *COS* genes was

an important process during metabolic stress. Therefore, we decided to further investigate how INO80 activity regulates the *COS* genes expression.

4.2. RESULTS

4.2.1. The subtelomeric COS genes silenced by the SIR complex

Chromatin remodelling by INO80 has wide-ranging effects on the transcriptional activity of many genes (Poli et al., 2017b). We have found that the COS gene family is regulated by the INO80 complex, particularly following nitrogen starvation. However, the mechanism by which INO80 promotes the expression of the COS genes remained unclear. We therefore decided to focus on the chromatin environment of *COS* genes to better understand their regulation.

The COS genes are members of the DUP380 subfamily of sub-telomeric genes and all members of the family are located in sub-telomeric DNA (Despons et al., 2006). Budding yeast sub-telomeric DNA has relatively lower transcription compared to other regions of the genome (Thurtle and Rine, 2014). Epigenetic regulation of sub telomere silencing is mediated by the SIR complex and the activity of the NAD^+-dependent histone deacetylase Sir2 has been previously shown to negatively regulate *COS* expression (MacDonald et al., 2015).

We previously noted that nitrogen starvation led to increased COS gene expression, and this was compromised in the absence of Ino80. Loss of Ino80 led to reduced COS expression relative to wild type (WT) in non-starvation conditions but we were interested by the findings that in the absence of Ino80, nitrogen starvation led to further repression of these genes. (Figure 3.13, 4.1A).

We found that growth in nitrogen starvation medium (SD-N) lead to an increase in the expression of *COS* genes in WT, whereas the same conditions led to silencing of the genes in *ino80Δ* (Figure 4.1A). We therefore hypothesised that a potential role of INO80 may be to counteract a repressive environment found at sub-telomeric chromatin and thereby promote COS gene expression.

Given the role of the SIR complex in repressing *COS* gene expression, and the activating role that INO80 activity had, we decided to evaluate the relationship between these two regulatory pathways. We retrieved an RNA-seq dataset consisting of expression data for WT, SIR mutant *sir3Δ,* INO80 subunit mutant *arp5Δ,* and the double mutant *sir3Δarp5Δ* (Xue et al., 2015), and performed a meta-analysis of RNA read densities at the COS genes.

The normalised mean RNA densities over each COS gene were plotted, and the levels for WT and different mutants compared. This analysis confirmed that the loss of Sir3, the main structural component of the SIR repressive complex, led to increased COS RNA levels across all COS genes (Figure 4.1C). We also consistently saw lower expression of the *COS* genes in the *arp5Δ* cells, however the difference between WT and *arp5Δ* was not as large as what we had observed in our own data. One

possible explanation is that the RNA-seq experiment was done using yeast grown in rich media conditions which are reported to repress *COS* expression (MacDonald et al., 2015).

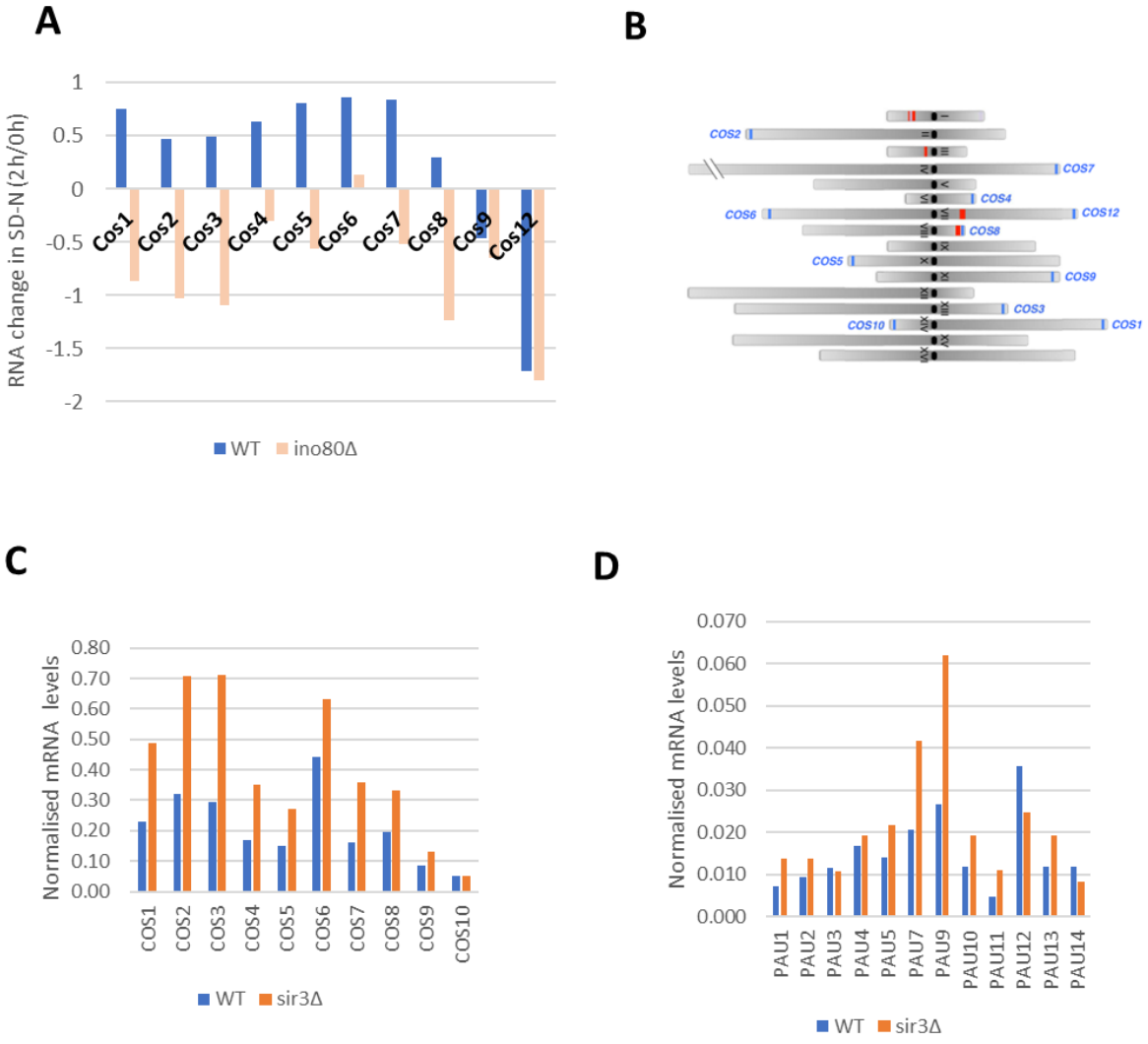

Figure 4.1 Subtemoleric COS genes are transcriptionally regulated by Sir3. (A) Change in COS RNA levels following 2 hours of nitrogen starvation. RNA-seq generated log-transformed mean RNA densities for individual COS genes were calculated for non-starved "0h" and nitrogen starved "2h". Fold-change (FC) upon starvation was determined by dividing the 2h values by 0h. **(B)** A schematic representing S. cerevisiae chromosomes and the position of all COS genes (blue lines) and COS pseudogenes (red lines). Adapted from Macdonald et al., 2015. **(C)** RNA levels of COS genes are de-repressed in sir3Δ. RNA-seq data taken from Xue et al 2015. Log-transformed mean RNA densities for individual COS genes compared between WT and sir3Δ grown in rich media. **(D)** Sir3 regulation of PAU gene RNA. Log-transformed mean RNA densities for individual PAU genes in WT and sir3Δ grown in rich media. Data analysed from (Xue et al., 2015).

Our findings that the loss of *Sir3* lead to de-repression of *COS* gene expression led us to ask whether this was specific to this family of genes or whether all sub telomeric genes were equally de-repressed in *sir3Δ*. While we were unable to address this in an unbiased manner we decided to use the expression of a similarly large gene family located in sub telomeric chromatin as a reference.

The PAU genes are one of the largest gene families in the budding yeast genome and nearly all genes are located at chromosome ends within sub-telomeric regions (Viswanathan et al., 1994). While not a conclusive analysis, we assumed that in the case of a general de-repression of sub telomeric chromatin, the PAU genes would be expected to be similarly affected.

We found that in contrast to COS genes, not all located PAU genes located at sub-telomeric chromatin were repressed by the SIR complex, and that in general the repression appeared more variable (Figure 3.1D). By calculating the fold change for each COS and subtelomeric PAU gene (*sir3Δ* mean densities/WT mean densities), we found the average fold change upon *sir3Δ* was only 1.4 for PAU genes compared to over 3-fold change for COS genes.

This was suggestive that Sir3, and therefore the SIR complex may be exerting a specific transcriptional control on the COS genes. Importantly, we also found that loss of *Ino80* or *Arp5* did not have a repressive effect on the expression of the PAU genes (data not shown), suggesting that INO80 control of *COS* expression may be specific to this family of genes.

Our analysis of transcriptional changes following loss of Sir3 further confirms previous work that Sir2 negatively regulates the COS gene expression and helps establish the SIR complex as a negative regulator of their expression. It also suggests that Sir3 regulation of *COS* genes might be specific to their expression.

4.2.2. Nitrogen starvation and loss of Ino80 leads to increased NAD+ levels

In budding yeast, the Sirtuin family of NAD^+ dependent histone deacetylases are major consumers of cellular NAD^+ (Kato and Lin, 2014). Gene silencing is mediated by the catalytic activity of the NAD^+-dependent deacetylase Sir2 (Feldman et al., 2012; Swygert et al., 2018).

We previously observed that growth in SD-N medium leads to increased silencing of *COS* genes in the absence of *Ino80* and we hypothesised that this may be associated with increased Sir2 activity.

Previous studies had demonstrated that various forms of nutrient starvation leads to increased levels of cellular NAD^+ and this leads to increased sub-telomeric silencing by Sir2 (Lin et al., 2000; Bekers et al., 2015; Lee et al., 2013).

We decided to investigate the effect nitrogen starvation and Sir-activity had on NAD^+ levels. Cellular NAD^+ levels were quantified by using a colorimetric assay to measure both NAD and NADH, and then normalised to the mass of total protein.

To understand how SIR activity affected NAD^+ levels, we compared normalised NAD^+ levels between WT (*BY4741* background) and *sir3Δ* mutant. NAD^+ levels were found to be increased by around two-fold in the absence of *Sir3* and the ratio of NAD^+/NADH increased from 14 to 30 (Figure 4.2A).

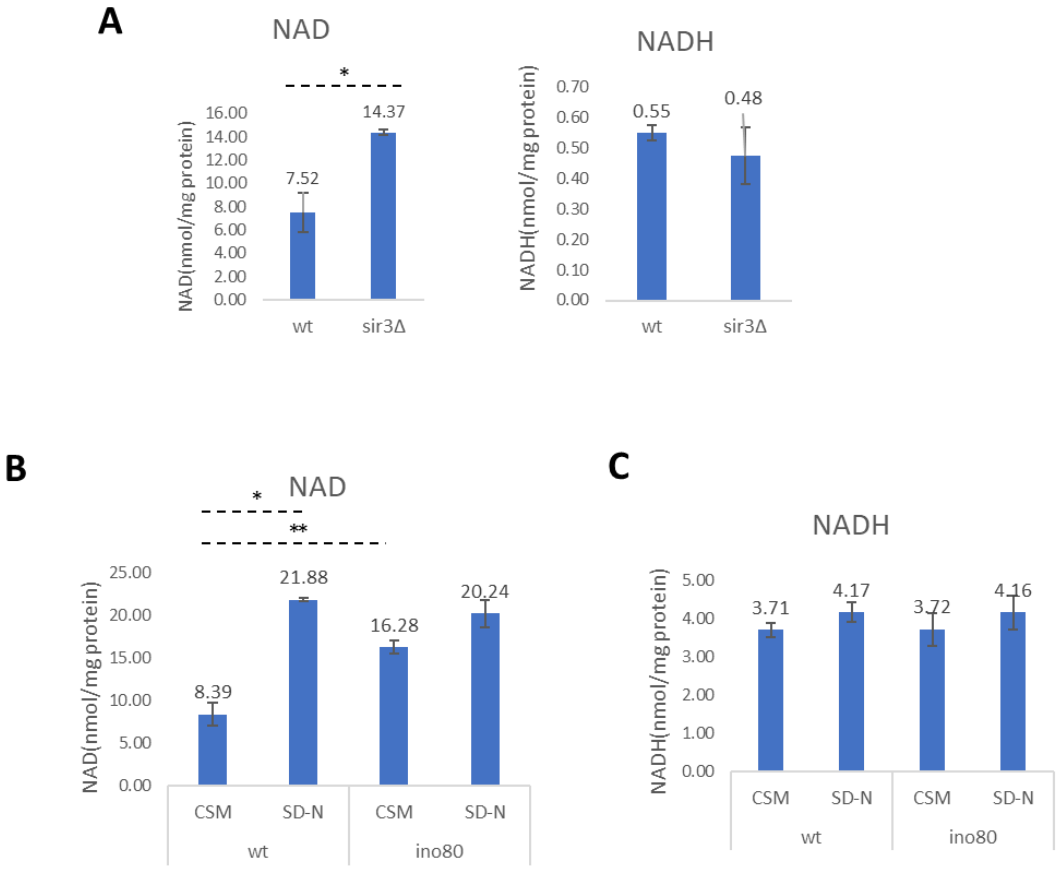

Figure 4.2. Quantification of changes to NAD+/NADH levels. (A-C) NAD levels are elevated in *ino80Δ* and resemble SD-N. WT, *ino80Δ* and *sir3Δ* strains were cultured in either complete medium (CSM) or for 2 hours in nitrogen starvation medium (SD-N). Cell lysates were generated alongside acid-purified protein and NAD and NADH was quantified by colorimetric assay. Levels were then normalised to corresponding protein levels and averages of 3 biological repeats plotted. Error bars are standard error of mean.

While Sir3 is not an NAD^+ consuming enzyme, it is essential for the formation and spreading of the SIR complex. The observed a 2-fold increase in NAD levels suggested that decreased NAD^+ consumption by Sir-mediated processes led higher cellular levels of NAD^+.

We next investigated if NAD^+ levels change in our own experimental conditions and whether the loss of *Ino80* influences the levels of NAD^+. To test this, we cultured wild-type and *ino80Δ* strains in synthetic complete media (CSM), collecting samples prior to and following a shift to SD-N. Quantifying the levels of the oxidized NAD^+, and the reduced form NADH, we found that NAD^+ levels and the relative ratio of NAD^+ to NADH significantly increased from 2.3 to 5.5, when cells were shifted to nitrogen starvation (Figure 4.2B, Table 4.1). Our assay was unable to differentiate between changes occurring in nuclear NAD^+ levels or NAD^+ originating from the mitochondria or cytoplasm.

To test if the presence of the INO80 complex altered NAD^+/NADH levels, we measure their levels in the *ino80Δ* strain before and after nitrogen starvation. The loss of INO80 led to significantly higher levels of NAD^+ and a higher NAD^+/NADH ratio of 4.4 in non-starved conditions (Figure 4.2A, Table 4.1). This finding highlighted similarities between *ino80Δ,* and nitrogen starved WT cells, both sharing increased NAD^+ levels relative to non-starved wild-type cells. In the absence of INO80, the shift from growth in CSM medium to SD-N medium did not lead to the same roughly 2-fold increase seen in WT. However, the NAD^+/NADH ratio following the loss of INO80 was similar to WT strain, a ratio of 4.9 for *ino80Δ* (Table 4.1).

Strain	**Medium**	**NAD^+ (nmol/mg protein)**	**NADH (nmol/mg protein)**	**NAD/NADH ratio**
WT (LS20)	CSM	8.39	3.71	2.3
WT (LS20)	SD-N	21.88	4.17	5.2
ino80Δ	CSM	16.28	3.72	4.4
ino80Δ	SD-N	20.24	4.16	4.9
WT (BY4741)	YPD	7.52	0.55	13.7
sir3Δ (BY4741)	YPD	14.37	0.48	30.1

Table 4.1. The effect of different conditions on the NAD^+/NADH levels of different budding yeast strains.

Taken together our data indicates that nitrogen depletion and the associated growth arrest led to increases in NAD^+ availability. However as demonstrated by the NAD^+ levels observed in mutants of *sir3Δ*, it is not possible to differentiate between whether that is due to an increase in NAD^+ production or a reduction of NAD^+ consumption.

These results suggest that the repressed silencing of *COS* genes is not the result of only increased Sir activity in nitrogen starvation, since they demonstrate that increased consumption would be expected to lower NAD^+ levels of *ino80Δ* cells. Furthermore, since *ino80Δ* NAD^+ levels do not change between non-starved and starved conditions, their changing levels cannot account for the increased silencing we observe in *ino80Δ*. The results show that both loss of Ino80 and nitrogen starvation lead to increased NAD^+ levels, however the cause of this increase is not clear.

4.2.3. INO80 complex is found enriched on COS promoters and gene bodies

Our results suggest that INO80 regulation is required to induce *COS* gene expression. The INO80 complex is recruited to many gene promoters where it controls the nucleosome organisation at the nucleosome free region (NFR). We reasoned that if INO80 activity was directly regulating the expression of the *COS* genes, INO80 would be expected to be enriched at these genes.

For this we set performed cross-linking followed by chromatin immunoprecipitation (ChIP) of Ino80, thus allowing for the detection of Ino80 bound DNA by quantitative PCR (ChIP-qPCR).

We reasoned that the more compact nature of sub-telomeric chromatin may make it more resistant to sonication. Using previously established cross-linking protocols for Ino80 (Papamichos-Chronakis et al., 2011b), we increased sonication and aimed for resulting fragments to be below 500 bp in length on average. This has the additional benefit of helping to distinguish between INO80 recruitment to the open reading frame (ORF) and the promoter of the genes. The relatively short size of COS genes – around 1.1 kB – meant that by designing primers for the promoter/transcription-start-site (TSS) and separate primers at least 500 bp into the ORF, we would be able to get some, but not definitive, differentiation between recruitment to these separate locations of the gene.

Using a standard method of 30 seconds sonication at 4°C, followed by a 30 second pause, we identified a reproducible range of cycles between 10 and 16 that reliably gave us efficient shearing of cross-linked chromatin (Figure 4.3A). Treatment with RNase A, which ensured that only DNA fragment size was being assessed, revealed that while 16 cycles of sonication produced more highly sheared DNA, the overall amount recovered was much reduced. Therefore, we decided to progress with 14 cycles as using this timing, the majority of chromatin was consistently sheared to below 500 bp in size.

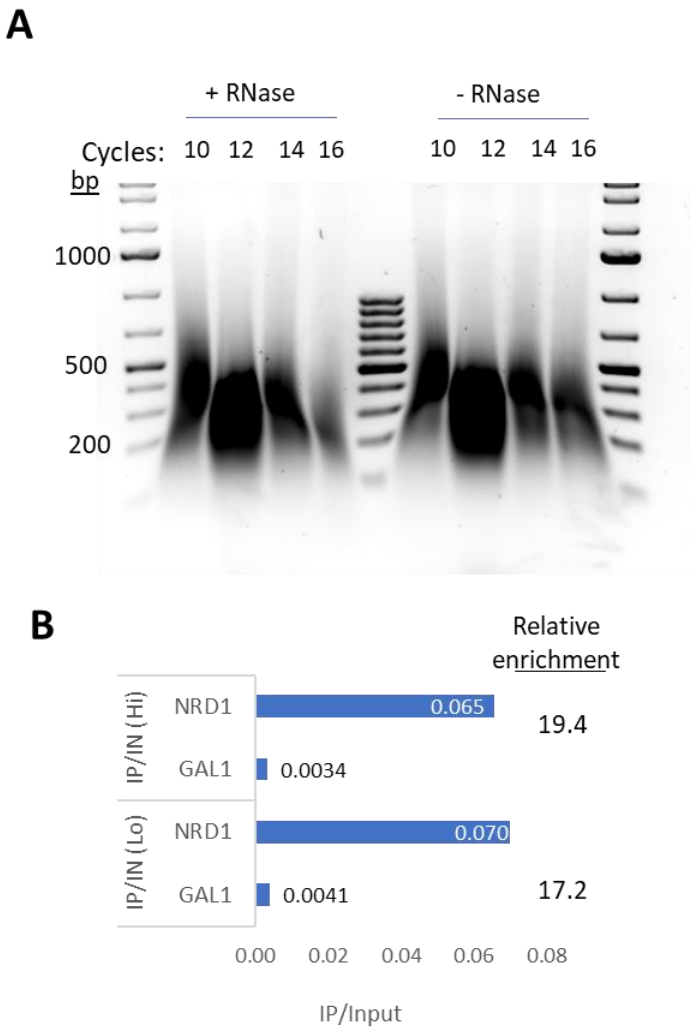

Figure 4.3. Optimisation of cross-linked chromatin shearing. **(A)** The size distribution of sheared chromatin following sonication run on agarose gels. **(B)** Enrichment of Ino80-HA at a known recruitment site (NRD1 ORF) and INO80-depleted region (GAL1 promoter). 'Hi' samples contained 50% more chromatin input to the immunoprecipitation reaction than 'Lo' samples. Enrichment at the GAL1 loci was treated as 'background' and so relative enrichment was calculated by dividing NRD1 IP/input levels by the GAL1 values.

Next, we focussed on identifying the quantities of sheared chromatin to use for the immunoprecipitation reaction for high enrichment of signal over background. A concern with increasing the amount of chromatin used in the pull-down is that enrichment will not increase proportionally and instead non-specific antibody interactions increase, thereby reducing true enrichment over the background.

To measure enrichment, primers designed to the *GAL1* promoter were used as a control for background signal. These primers were chosen as the *GAL1* promoter is only active in the presence of galactose and strongly repressed in the presence of glucose (Flick and Johnston, 1990), ensuring that in our conditions where glucose is the only carbon source, its promoter region would be inactive. Data in the lab (unpublished) has identified the TSS of the *NRD1* gene to be highly enriched by INO80 and so this was chosen as a positive control to measure enrichment with.

We tested two concentration equivalents to around 1.5-fold difference of one another, with the low and high concentrations referred to as "lo" and "hi" respectively. Performing an IP followed by qPCR on the purified DNA, we found very little difference in the background signal of *GAL1* (Figure 4.3B). Similarly, *NRD1* signal was determined to be very similar between the two amounts of chromatin used. Overall, the enrichment over background was higher in the "Hi" samples but we determined that from a single experiment we could only conclude that using larger volumes of chromatin did not clearly decrease the overall enrichment. We progressed by adopting the higher volume of chromatin in our experiments.

Using the optimised protocol and a budding yeast strain where the endogenous *INO80* gene contains a HA tag fusion, we performed four biological repeats of the Ino80-HA ChIP. The cells were grown in non-starved and nitrogen starved conditions, and samples were collected from exponentially growing cells or following 2 hours of starvation. We measured enrichment of Ino80 over several *COS* genes using qPCR and primers designed to either target the ORF or conserved sequence shared between multiple *COS* gene promoters, referred to here as *COSp*. Specifically, we designed primers to recognise a common sequence spanning the promoter region and TSS of several *COS* genes simultaneously (*COS1, COS3, COS4, COS5, COS6* and *COS7*; wherein for all genes other than *COS1* and *COS4* the resulting fragment was 142 bp while for the two outliers the fragment was 122bp). Due to the highly conserved sequence upstream of the *COS* transcription start site (TSS), it was impossible to design unique primer pairs for individual promoters or 5' ends of the ORF.

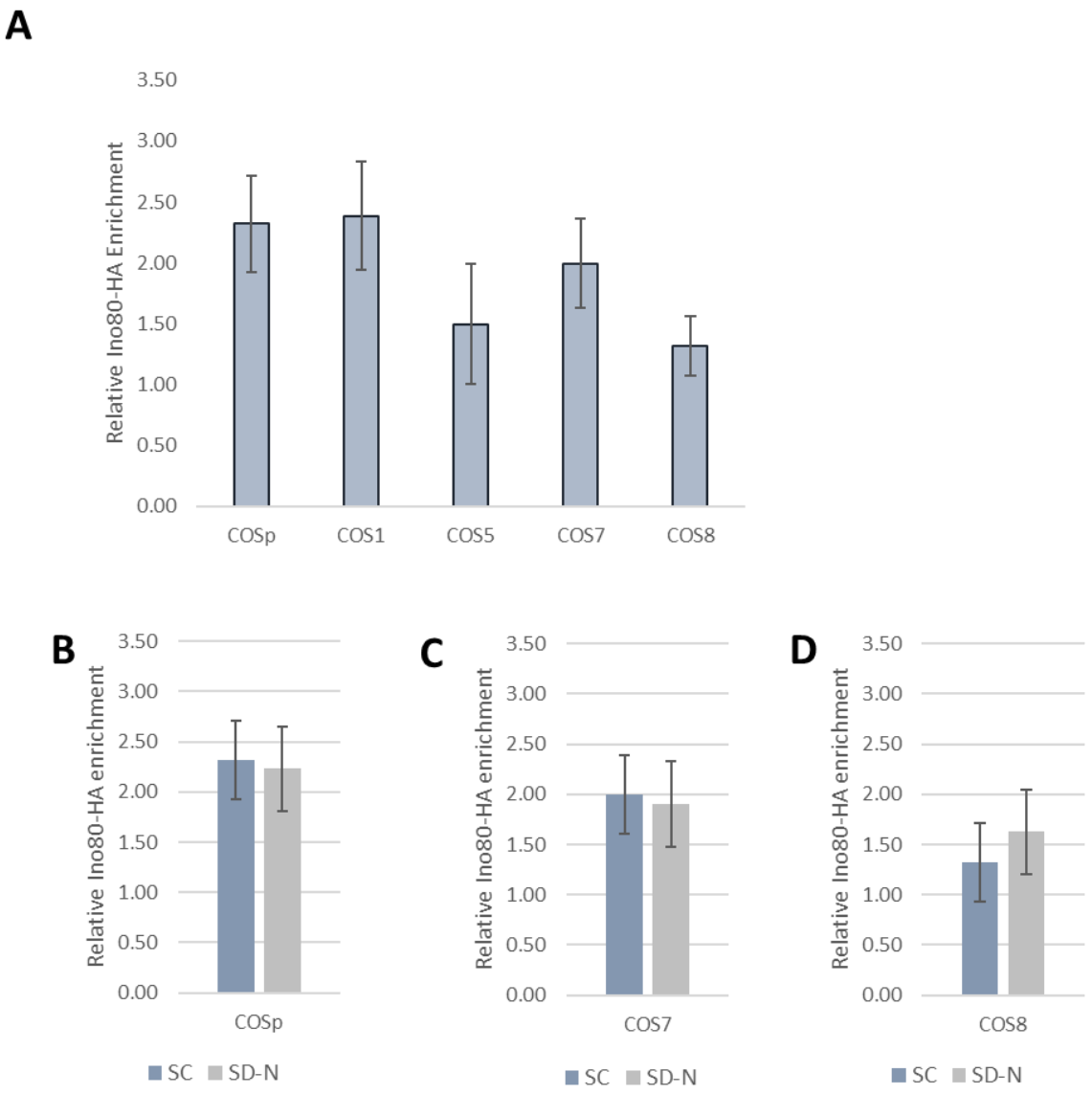

Figure 4.4. INO80 is enriched at COS genes and promoters. (A) ChIP-qPCR measurement of INO80 enrichment at COS genes and promoters. IP/input values were normalised to Ino80-HA levels at the GAL1 promoter. Experiment was repeated 4 times and error bars represent SEM. Primers of COSp were designed to target a common promoter sequence of multiple COS genes. **(B-D)** INO80 enrichment does not change in response to nitrogen starvation. Non-starved conditions (SD) and nitrogen starved (SD-N) are presented. Error bars represent s.e.m (n=4), all samples were compared to GAL1 promoter as a control to represent background.

Quantifying co-precipitated DNA by qPCR, we found a significant enrichment of Ino80 over background at the *COSp* sequence and similarly at individual *COS* gene ORFs (Figure 4.4A). We found the highest enrichment at *COS1* and *COS7* gene ORFs and the lowest at *COS8* ORF (Figure 4.4A). Similarly, Ino80 was found to be significantly enriched at the common *COS* promoter region at around 2.5-fold over background. All enrichment were statistically significant. INO80 function is well established to occur at gene promoters and therefore it is not surprising to find lower enrichment at gene ORFs, particularly since most primers were designed over 500 bp into the body of the gene. Despite the low levels of enrichment, our data indicated that INO80 is enriched at the *COS* genes under standard growth conditions and supports the hypothesis that INO80 activity regulates the activity of these genes.

Having identified INO80 enriched at these genes we asked whether nitrogen starvation affected the recruitment of the complex. Quantifying the samples taken following 2 hours of starvation and again normalised to the un-affected GAL1 promoter, we found that levels of enrichment were very consistent at the tested loci and showed no change from the levels observed in non-starved conditions (Figure 4.4B-D). We therefore concluded that INO80 is enriched at the promoters of multiple *COS* genes and this localisation is irrespective of active or inhibited mTOR signalling.

Our finding that the INO80 complex is enriched at the *COS* genes supports the hypothesis that INO80 activity within the chromatin context of these genes controls their regulation. However, finding no change in the recruitment of INO80 to these loci suggests that nitrogen starvation induced activation of *COS* gene expression is achieved through potential changes to other chromatin associated factors, or by increasing the activity of INO80 under metabolic stress conditions which may change the role of the already present INO80.

4.2.4. Loss of Sir3 rescues defective COS expression of Ino80 mutants

The COS genes appear to be simultaneously subject to SIR-mediated repression and dependent on the presence of INO80 for expression. Since INO80 is enriched at COS genes, we wondered if INO80 activity promotes COS expression by counteracting SIR-mediated repression.

If this is the case, repression of COS genes in *ino80Δ* would be dependent on a functioning SIR complex. An alternative explanation is that INO80 activity induces gene activation in a SIR-independent pathway and in such a case, the loss of Sir proteins would not be expected to affect expression levels in *ino80Δ.*

We reasoned that a strain where both INO80 and Sir activity were compromised would be able to distinguish between these two possibilities. Therefore, we created a double mutant for both INO80 and SIR complex subunits, namely *sir2Δarp8Δ*, as well as employing a published double mutant strain, *sir3Δarp5Δ* (Xue et al., 2015).

We first analysed published RNA sequencing from the *sir3Δarp5Δ* double mutant and the analogous single mutant strains in collaboration with the Antonin Morillon lab. Analysing the expression of *COS5* and *COS8* we found, as expected, that the compromise of INO80 activity in *arp5Δ* led to reduced expression, while the *sir3Δ* displayed increased expression of both genes (Figure 4.5A). Importantly, when the *arp5Δ* mutation was combined with *sir3Δ*, both *COS5* and *COS8* genes were no longer down-regulated relative to WT and instead expressed RNA to similar levels as the de-repressed *sir3Δ* (Figure 4.5A & B). Thus, the silencing of *COS5* and *COS8* in the *arp5Δ* is dependent on the presence of Sir3. Similar results could be observed across all *COS* genes further strengthening our conclusion (Figure 4.5B).

As the published RNA-seq data were from an experiment conducted in rich media (YPD), we asked if this observation is consistent for cells growing in minimal media and importantly how did the shift to nitrogen starvation affect the double mutant. We requested the use of the above strains and cultured them in SC media to late-log phase and shifted them for 2 hours to SD-N. We collected RNA from before and following the shift to SD-N, and quantified transcription using reverse transcribed (RT) quantitative (q) PCR, using ACT1 RNA levels to normalise, allowing us to compare levels between samples.

In non-starved conditions we found that *COS1* and *COS8* RNA levels were not significantly affected by the loss of *Sir3* and *Arp5* (Figure 4.5C & D). Following nitrogen starvation, the expression of both genes was significantly increased in WT, but remained unchanged in the *arp5Δ* cells (Figure 4.5C & D). The combination of *Sir3* deletion with *arp5Δ* restored the expression of *COS1* and *COS8* back to WT levels. Specifically, we observed a significant increase in the expression of *COS1* and *COS8* RNA in the *sir3Δarp5Δ* double mutant relative to *arp5Δ* in SD-N. This agrees with and supports our previous finding, and we conclude that the failure to correctly express *COS* genes, specifically *COS1* and *COS8*, in the absence of functional INO80 complex, is due to the presence of Sir3 and SIR complex activity. Our results suggest that INO80 activity functions to counteract transcriptional silencing of *COS* genes by the SIR complex following nitrogen starvation.

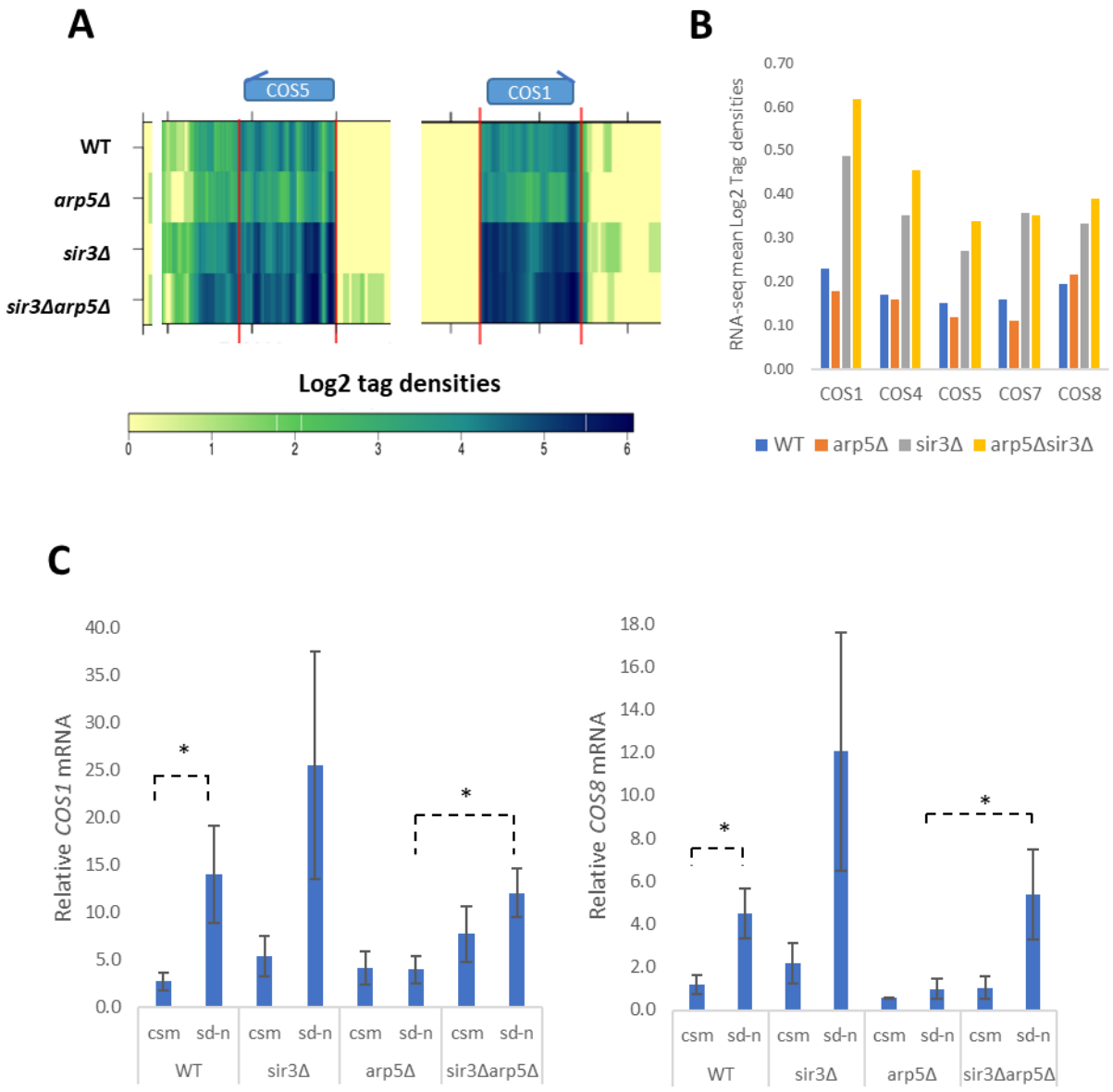

Figure 4.5. SIR complex mediates the silencing of COS genes in the absence of functional INO80. **(A)** RNA-seq results from Xue et al 2015. Log2 tag densities were mapped genome wide. Representative heatmaps of COS5 and COS1 genes. **(B)** Averaged log2 tag densities for 5 representative COS genes plotted for each strain. **(C)** RT-qPCR analysis of RNA expression of COS1 and COS8 genes in various strains. RNA was collected prior to starvation (CSM) and following 2 hours of growth in SD-N.

4.2.5. Loss of SIR activity leads to a functional rescue of Ino80 growth in nitrogen starvation

Having found that *COS* RNA levels are rescued when the loss of Ino80 activity is combined with deletions of Sir proteins, we asked whether the growth defect of *ino80Δ*, *arp5Δ* and *arp8Δ* mutants grown in SD-N, is also rescued when Sir activity is absent.

To examine the sensitivity of the double mutant to nitrogen starvation, we grew the strains to late log phase before shifting them to a nitrogen starvation medium and measuring viability and cell growth through spotting serial dilutions of cells back to rich media plates.

We found that around 10 days of growth in nitrogen starvation conditions was sufficient to severely compromise the viability of *arp5Δ* relative to WT, but not of *arp5Δsir3Δ* (Figure 4.6A). This result suggests that the growth defect seen in *arp5Δ* is in large part the result of epigenetic silencing by the SIR complex.

Next, we confirmed the result by testing whether the growth defect of the *arp8Δ* strain is rescued by combining it with a deletion of *Sir2*. The results resembled the effect previously observed in *arp5Δsir3Δ* and we observed that the *arp8Δsir2Δ* strain resembled the ability of WT yeast cells to withstand nitrogen starvation (Figure 4.6B). These two results strongly suggest that the nitrogen starvation induced lethality in the absence of a functional INO80 complex is caused by the activity of the SIR complex. The results further support a model where INO80 activity counteracts Sir-dependent silencing of chromatin. We observed differences in the severity of the starvation phenotype between *ino80Δ*, *arp5Δ* and *arp8Δ*, however we suggest that much of variability is the result of differences in the susceptibilities of the different genetic yeast strains to the loss of INO80 function (Poli et al., 2017b). Furthermore, the relatively weaker phenotype of *arp8Δ* is likely due the fact that loss of this subunit does not compromise complex structure nor recruitment to nucleosomes (Knoll et al., 2018; Shen et al., 2003b).

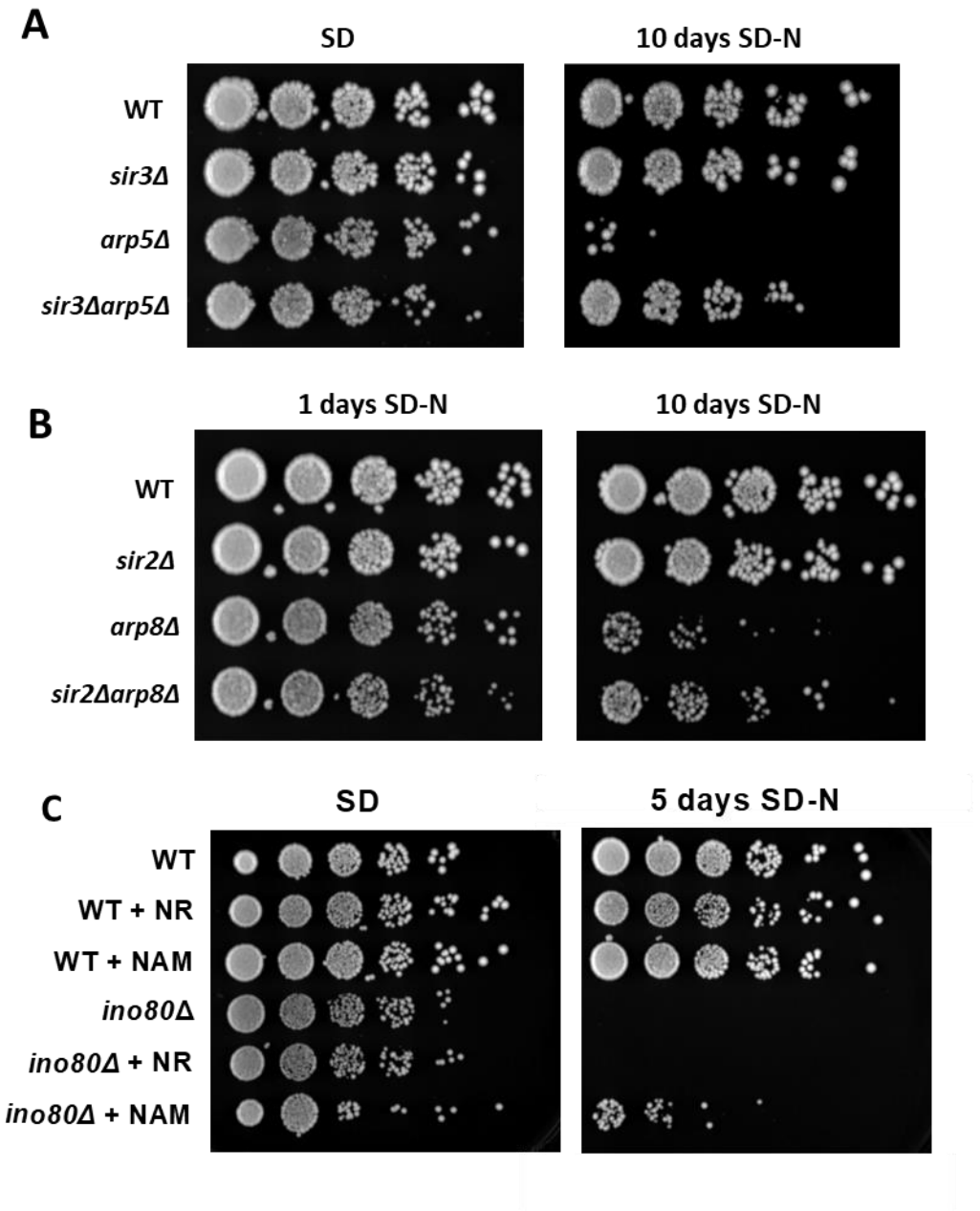

Figure 4.6. Loss or repression of SIR complex rescues growth defect of INO80 mutants. (A-B) five-fold serial dilutions of yeast from the indicated strains either directly after culture in SD (non-starvation) media or following SD-N for the indicated time. Cell number was normalised prior to plating. Representative image, experiments were repeated 3 times. **(C)** Five-fold serial dilution of WT and ino80Δ strains. SD-N medium was supplemented with either 5mM NAM or 5 mM NR at the beginning of the incubation

Next, we asked if these genetic interactions were limited to mutants of INO80 subunits or whether the loss of Sir activity would also rescue the (significantly sicker) *ino80Δ* strain when grown in nitrogen deplete conditions. Histone deacetylation by Sir2 requires NAD^+ and the reaction results in the production of acetyl-ADP-ribose and nicotinamide (NAM) (Landry et al., 2000; Tanny et al., 1999). A multi-enzyme pathway can convert NAM to NAD^+ yeast cells, however when present, NAM acts as a potent inhibitor of Sir2 activity. Yeast cells preferentially use nicotinic acid (NA) or nicotinamide riboside (NR) as a precursors for NAD^+ synthesis and the addition of either of these rapidly increases cellular NAD^+ levels (Belenky et al., 2007; Orlandi et al., 2017).

We decided to inhibit the activity of Sir2 by supplementing the starvation media with NAM. To ensure that we were not observing the effect of increased NAD^+ levels we included a control condition where NR was supplemented into the media. Since yeast convert NR to NAD^+ far more readily than NAM (Bieganowski and Brenner, 2004), we were confident that an effect observed only in NAM would not be the result of increased cellular NAD^+ levels.

Addition of NAM or NR did not affect the growth of WT budding yeast prior to or following nitrogen starvation (Figure 4.6C). When *ino80Δ* was grown in non-supplemented SD-N medium, or in medium supplemented with NR, we observed the strain loses ability to grow by day 5 -6 as previously demonstrated. However, supplementing the nitrogen starvation medium with NAM rescued the growth of the *ino80Δ* strain, partially counteracting the growth defect of Ino80 loss (Figure 4.6C). These results show the addition of NAM, but not increasing NAD^+ levels alone, can rescue the growth defect of *ino80Δ*. Taken together with our previous results, we propose that this rescue is the result of inhibiting Sir2 activity, and that therefore Sir-dependent silencing is significantly contributing to the sensitivity of *ino80Δ* to nitrogen starvation.

4.2.6. Sir activity inhibits the turnover of ubiquitin conjugates in the absence of Ino80

We wanted to understand how counteracting Sir activity was leading to the rescue of viability in strains lacking functional INO80. We previously found that loss of INO80 activity led to defective turnover over of ubiquitin conjugates following nitrogen starvation. We therefore speculated the proteotoxicity of accumulating protein aggregates and ubiquitin conjugates may be contributing to the *ino80Δ* growth defect.

The reduced sensitivity of the double mutants to nitrogen starvation led us to ask whether we observed a decrease in ubiquitin conjugate accumulation, and therefore potentially less proteotoxic stress in *sir3Δarp5Δ* strain.

We collected whole cell protein extracts from WT, *arp5Δ, sir3Δ* and *sir3Δarp5Δ* strains and ran the purified samples on SDS-PAGE gel. Using an antibody against ubiquitin we immunostained all ubiquitin conjugates present in the sample. To quantify the experiments, we used antibodies against G6PDH as a loading control. By using image analysis software, the signal intensity within each lane was calculated and normalised to the signal intensity of the G6PDH loading control.

In the WT strain, the induction of nitrogen starvation led to decreasing levels of ubiquitin conjugates within 24 hours and most clearly at 48 hours post nitrogen depletion in the WT strain (Figure 4.7A, lanes 1-3). However, little to no change in ubiquitinated protein accumulation was observed in the *arp5Δ* strain, resembling the previous observations in *ino80Δ* (Figure 4.7A, lanes 4-6). The lack of ubiquitin-conjugate turnover was however rescued when the *arp5Δ* mutation was combined with the loss of *Sir3*, and levels resembled those observed in WT (Figure 4.7A, lanes 7-9). Statistical analysis of quantified intensities of ubiquitin-conjugate accumulation from multiple experiments confirmed that the significantly difference between WT and *arp5Δ* was rescued in *sir3Δarp5Δ* (Figure 4.7B). Loss of *Sir3* alone did not have any significant effect on ubiquitinated protein levels (immunoblot not shown, quantification presented in Figure 4.7B).

Therefore, our results strongly indicate that both the sensitivity of INO80 mutants to nitrogen starvation, and the concomitant accumulation in ubiquitin conjugates, are at least in part the result of Sir activity and that the loss or inhibition of this rescues both defects.

These results suggest that Ino80 is counteracting Sir activity to promote the appropriate autophagy mediated turnover of ubiquitinated proteins. Together with our previous results this suggests that the rescue *arp5Δ* growth when combined with a deletion in *Sir3* is mediated by the rescue of defective aggrephagy.

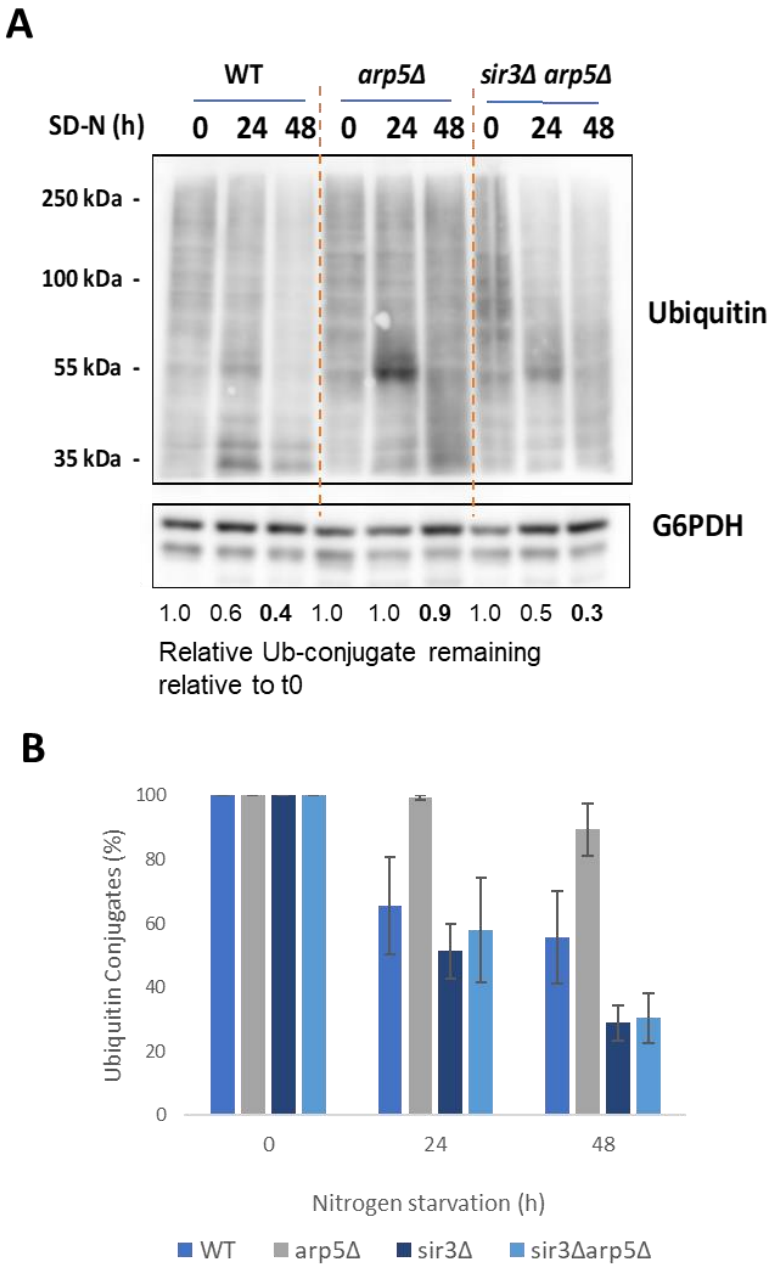

Figure 4.7. Turnover of ubiquitinated proteins is restored in INO80 mutants lacking SIR activity. (A) Turnover of ubiquitinated conjugates following nitrogen starvation. WCE were generated from WT, arp8Δ, sir3Δ (not shown) and sir3Δarp8Δ at the indicated time points and immunoblot against ubiquitin. Relative Ub-conjugate levels were calculated as a fraction of the levels in each strain prior to nitrogen starvation (t0) and were based on normalised band intensities. (B) Quantification of average ubiquitin-conjugate levels for each strain (based on intensity measurements from immunoblots against ubiquitin as in panel A). Levels prior to starvation were set to 100% and intensities after 24 and 48 hours were calculated as fractions of this. All intensities were normalised to a loading control (G6PDH). Error bars are s.e.m (n = 3).

4.2.7. Sir3 enrichment at COS genes not significantly affected by the loss of Ino80

SIR-mediated silencing of sub-telomeric DNA is induced by histone de-acetylation by Sir2; with Histones H4 lysine 16 (K16), H3 lysine 9 (K9) and H3 lysine 56 (K56) being the main targets for its activity (Oppikofer et al., 2011; Parsons et al., 2003; Xu et al., 2007). The hypoacetylated status of H4K16 is recognised by Sir3 which then recruits Sir4 and Sir1, forming a repressive structure which, in combination with hypoacetylated gene promoters, is responsible for silencing (Swygert et al., 2018)

As the COS gene expression defect in INO80 mutants is rescued by SIR deletion, we reasoned that INO80 is likely to promote *COS* expression in metabolic stress either by disrupting the recruitment/formation of Sir heterochromatin or by counteracting the histone deacetylation function of Sir2.

We began investigating whether the loss of INO80 leads to changes in the recruitment of Sir3 at *COS* genes and their promoters. To do this, we created a Sir3-HA fusion in both a WT and *ino80Δ* backgrounds (Figure 4.8A), enabling us to perform crosslinking of chromatin followed by ChIP using an antibody against the HA tag.

To specifically test for SIR3 recruitment, we adjusted the ChIP protocol for enriching heterochromatin. To gauge the efficiency of our experiments we used a combination of two primer pairs, referred to as TEL0.5 and TEL7.5, which recognised intergenic sequence 0.5 kB and 7.5 kB away from the telomere of chromosome 6R (Radman-Livaja et al., 2011). Higher relative enrichment at TEL0.5 relative to TEL7.5 indicates a higher efficiency pull down in the experiment, since Sir3 recruitment is well reported to be highest closer to the chromosome end. We found that increasing the amount of cross-linking to 60 minutes was sufficient to detect Sir3 enrichment at budding yeast sub-telomeric DNA relative to shorter crosslinking times (Figure 4.8B). Similarly, we found that Sir3 recruitment to *COS* genes and *COS* promoters was increased when crosslinking was increased to 60 minutes and so we continued with this method.

We performed the ChIP experiment in normal and nitrogen deplete conditions for two hours, using qPCR to analyse the relative amounts of purified DNA (ChIP-qPCR). We found that relative to the negative control of *GAL1* promoter, Sir3 was significantly enriched at the tested *COS1* (not shown), *COS5* and *COS7* genes, as well as at the *COSp* common promoter sequence (Figure 4.8C). Interestingly we found enrichment within gene bodies to be unchanged following 2 hours of growth in nitrogen depleted conditions, however Sir3 levels at the *COS* promoter loci were significantly decreased ($p = 0.04$) in response to nitrogen starvation (Figure 4.8C). Next we looked at Sir3 enrichment in the absence of INO80, finding that Sir3 is again significantly enriched at all analysed

genes however unlike the WT, we did not see any significant difference in Sir3 enrichment at the *COS* promoter between the normal and nitrogen deplete condition (Figure 4.8D). Finally, we directly compared Sir3 levels at the *COS* promoter across both strains and conditions, finding that there was no significant difference between WT and *ino80Δ* levels of Sir3 enrichment. Our data suggest that nitrogen starvation induces changes to Sir3 enrichment at *COS* promoters, which correlates with the activation of these genes. Our data only shows small and insignificant difference in Sir3 recruitment between WT and *ino80Δ* suggesting that the mechanism leading to the difference in *COS* expression between these two strains may not be limited to the Sir proteins.

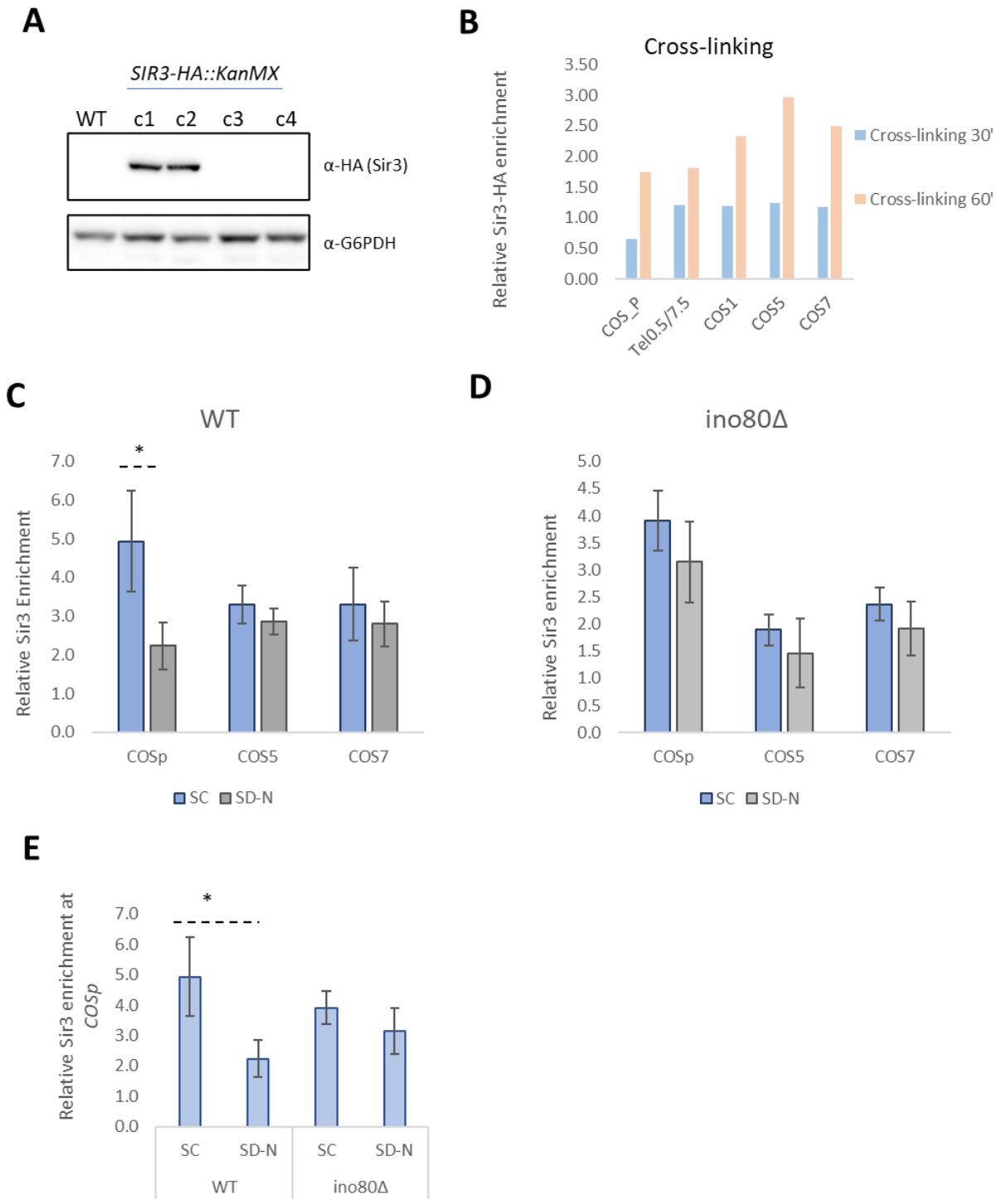

Figure 4.8. Sir3 ChIP reveals SIR enrichment at COS genes. (A) Immunoblot against HA, screening for Sir3-HA expressing clones. Immunoblot against G6PDH was used as a loading control. **(B)** ChIP enrichment was Sir3-HA measured by qPCR. Crosslinking methods were compared to identify optimal conditions. Primers against COS genes and COS promoter sequence were used. Additionally two primer pairs targeting intergenic subtelomeric DNA was used as a control to measure SIR enrichment. **(C-D)** ChIP-qPCR measurement of Sir3 enrichment at COS genes and promoters in WT yeast. All IP/input values are normalised to enrichment at the

GAL1 promoter and expressed as a ratio to this. Samples were collected from exponentially growing yeast in non-deplete condition (SC) and following 2 hours of nitrogen starvation (SD-N). Error bars are s.e.m (n = 4). **(E)** Sir3 enrichment at the COS promoter from (C) and (D) presented together.

4.2.8. Ino80 promotes Histone H3 acetylation at COS promoters

Previous work on sub-telomeric silencing in budding yeast has shown that the formation of Sir protein complex is not alone sufficient to generate a transcriptionally silenced environment. Histone H3 lysine 9 acetylation (H3K9ac) is an epigenetic mark strongly associated with active promoters and transcription (Bonnet et al., 2014; Pokholok et al., 2005; Weiner et al., 2015). H3K9ac is a major target for Sir2 deacetylation, and the resulting chromatin state reinforces the silencing of gene expression (Parsons et al., 2003).

Our data supports a model wherein INO80 counteracts Sir activity and thus de-represses genes including the *COS* proteins, thus promoting survival in nitrogen deplete conditions. We therefore wondered if the loss of INO80 would lead to a decrease of H3 acetylation at the *COS* loci, as would be expected if Sir2 activity was up-regulated.

In addition to H3K9ac, acetylated H4K16 is also a primary target for Sir2 activity (Imai et al., 2000). However, the binding of Sir3 to chromatin requires hypoacetylated H4K16 and the acetylation of this residues directly disrupts Sir3 (Carmen et al., 2002; Hecht et al., 1995; Onishi et al., 2007). Therefore our findings that Sir3 levels do no change at *COS* genes implied there may be little change to H4K16 acetylation.

Conducting qPCR with an antibody against the acetylated form of H3K9, we measured H3K9 acetylation enrichment before and after nitrogen starvation and determine the effects of Ino80 on this epigenetic mark. ChIP with an antibody against H3 allowed us to simultaneously quantify nucleosome occupancy at a given position and normalise the H3K9ac levels to the relative histone levels.

As before, Wild-type and *ino80Δ* cells were grown to late log phase and samples cross-linked before and following 2 hours of nitrogen starvation.

We first probed the *COS1* ORF, noting that nitrogen starvation led to no changes in H3K9 acetylation in the wild-type or *ino80Δ* (Figure 4.9A). However, loss of *Ino80* led to significant decreases in acetylation at the *COS1* gene relative to WT both before and after nitrogen starvation (Figure 4.9A).

Next, we investigated acetylation changes at the shared *COS* promoter sequence. At these regions, following 2 hours of nitrogen starvation, a clear and significant increase in H3K9 acetylation relative to non-starved conditions was observed in WT, coinciding with the upregulation of the COS genes (Figure 4.9B). Loss of *Ino80*, led to significant depletion of H3K9 acetylation at the COS promoters, significantly lower than levels in WT both before and after nitrogen starvation. Furthermore, no increase was detected in response to nitrogen starvation, and H3K9ac levels remained below non-starved WT. This result suggests that INO80 promotes histone H3 acetylation of COS promoters and is essential for inducing acetylation of the *COS* promoters in response to nitrogen starvation.

An alternative explanation may be that INO80 is not directly regulating *COS* genes and its loss leads to a global decrease in histone acetylation and genome wide mis-regulation of histone acetylation. To test this, we measured the enrichment of H3K9ac at euchromatic genes which are upregulated in response to nitrogen starvation in both WT and *ino80Δ*. Specifically we analysed two genes belonging to the amino acid biosynthesis pathway, *MET6* and *ARG4*. We found that both at MET6 (Figure 4.9C) and ARG4 (data not shown) no significant difference in H3K9ac enrichment between WT and *ino80Δ* was detectable following nitrogen starvation. This suggests that INO80 activity promotes the acetylation of specific genes in response to nitrogen starvation.

This further supports the conclusion that INO80 promotes H3K9 acetylation in specific genes, and we propose that it is through promoting the acetylation of the *COS* that INO80 promotes their expression in response to nitrogen starvation.

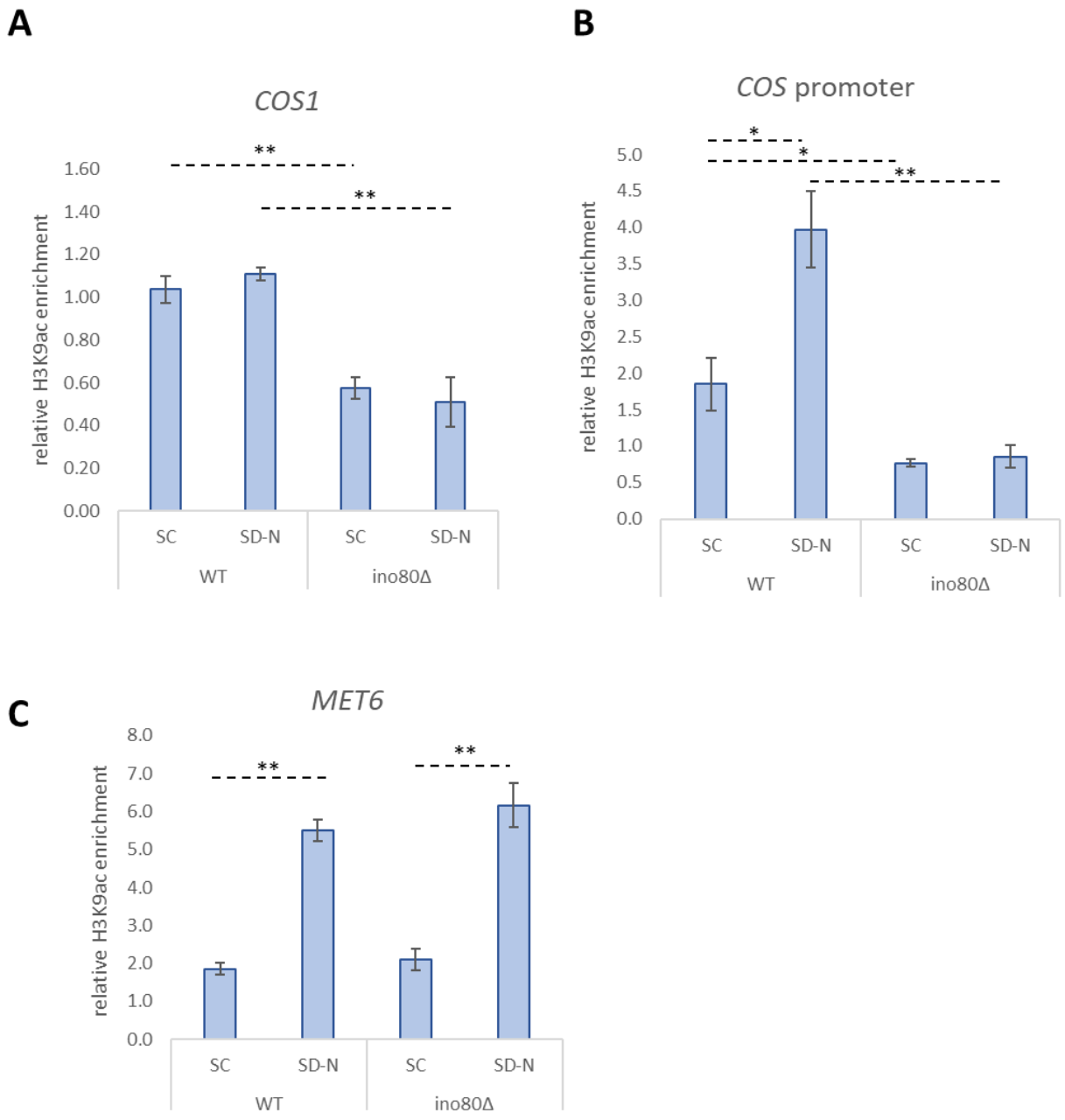

Figure 4.9. INO80 promotes H3K9 acetylation of COS genes. ChIP-qPCR measurement of H3K9ac in WT and ino80Δ before (SC) and after (SD-N) the switch to nitrogen starvation. Specific anitbodies raised against acetylated H3K9 and H3 were used. H3K9ac enrichment was normalised chromatin levels at each assayed region by normalising to H3 enrichment. All values are expressed as relative values against the ACT1 gene. Values for H3K9ac enrichment were determined using specific primer pairs against (A) COS1 gene, (B) COS promoter sequence and (C) MET6 gene. Error bars are s.e.m (n = 4).

4.2.9. Recruitment of Acs2 to COS promoters is controlled by INO80

Our previous observation that SIR occupancy is not altered in the absence of INO80 excludes the possibility that hypoacetylation of histones at the COS locus is due to increased SIR2 enrichment. Supply of acetyl-coenzyme A (CoA) is critical for acetylation as it acts as a substrate for the acetyl group used by acetyl transferases. The enzymes which synthesise acetyl-CoA such as Acs2 are therefore important factors as is exemplified by mutants lacking this protein displaying display extensive transcriptional defects, synthetic growth sickness and sensitivity to various metabolic stresses (Takahashi et al., 2006a). Acs2 is particularly significant as it is responsible for maintaining nuclear Acetyl-CoA availability and this process is suggested to be the rate limiting step for histone acetylation. Recent work with budding yeast Acs2 and the human homologues ACSS1/2 have demonstrated that the protein binds chromatin and this localisation to specific parts of the genome is linked with the its function (Chen et al., 2021; Li et al., 2017, p. 2).We thus hypothesized that INO80 activity might enable this rate limiting step by promoting the recruitment of Acs2 to hypoacetylated chromatin.

Using an antibody raised against the Acs2 protein and ChIP-qPCR, we sought to determine whether Acs2 is recruited to *COS* promoter regions in response to nitrogen starvation and whether this recruitment was mediated by INO80. WT and *ino80Δ* cells were grown in normal and nitrogen deplete conditions and Acs2 enrichment on chromatin was measured. At *COS* promoter regions we found low enrichment of Acs2 relative to the *GAL1* promoter and found that 2 hours of nitrogen starvation led to no change in the enrichment of this protein at this location (Figure 4.10A). However, despite the low enrichment, Acs2 recruitment at the COS promoter decreased by roughly 2-fold in the absence of INO80, a significant decrease relative to WT levels in nitrogen starvation. The lower enrichment of Acs2 following nitrogen starvation suggests INO80 function promotes recruitment of Acs2 to the *COS* promoter region and the loss of this recruitment correlated with lower H3K9 acetylation and transcriptional mis-regulation of these genes.

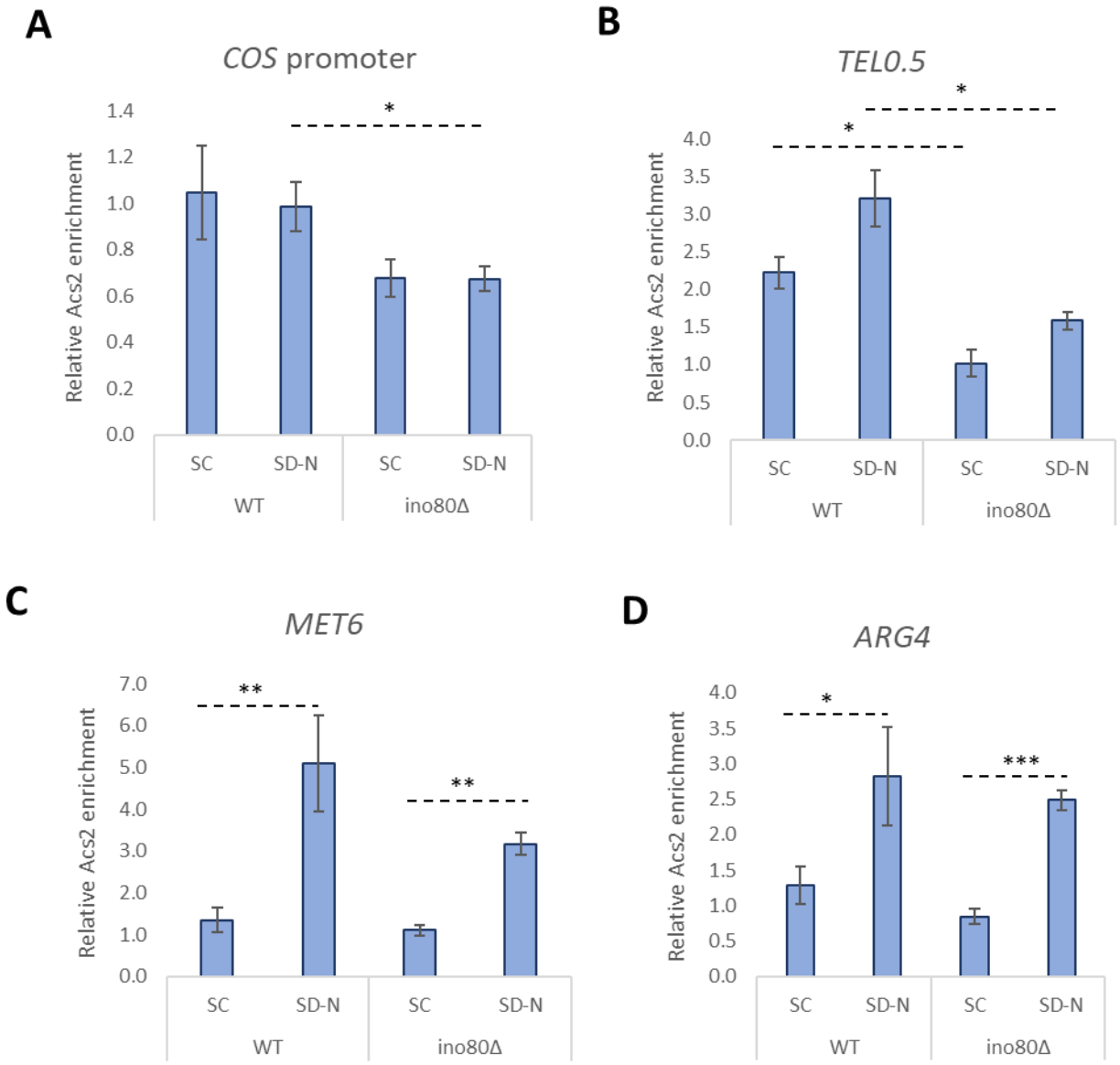

Figure 4.10. Acs2 Recruitment to COS promoters is mediated by INO80. ChIP-qPCR measuring enrichment of Acs2 at (A) COS promoter, (B) intergenic chromatin 0.5 kb from chromosome end (TEL0.5), (C) MET6 genes, and (D) ARG4 genes. An antibody raised against Acs2 was used to immunoprecipitate the chromatin. Samples were collected prior to (SC) and following (SD-N) 2-hours of nitrogen starvation. IP/input ratios were normalised against Acs2 enrichment at the ACT1 gene and relative values are plotted. Error bars represent s.e.m (n = 4).

Acs2 activity has recently been identified to regulate telomere silencing as part of the SESAME complex (Chen et al., 2021). We asked whether the mis-regulation of Acs2 recruitment to *COS* promoters was limited to this specific case or whether this may be a more general phenotype at yeast telomeres. Using the Tel0.5 primer pair which amplified an intergenic region of sub-telomeric chromatin 500 bp away from the right telomere of chromosome 6, we asked whether nitrogen starvation or INO80 induce changes in Acs2 recruitment. Interestingly, we found roughly 2–3-fold higher enrichment at the TEL0.5 region compared to the *COS* promoter DNA, suggesting the Acs2 recruitment is not strictly associated with transcriptional units (Figure 4.10B). When measuring enrichment in the absence of Ino80, we again found lower Acs2 levels and to a greater extent both before and after nitrogen depletion. Together these results implicate INO80 in the recruitment of Acs2 to the COS genes and potentially to sub-telomeric chromatin more generally.

Finally, we wanted to understand if INO80 led a general defect to Acs2 recruitment or whether the influence of INO80 is restricted to sub telomeric gene regulation. To explore this question, we picked to genes belonging to the amino acid biosynthesis pathway, *MET6* and *ARG4*, both of which are strongly induced following nitrogen starvation according to our RNA-seq experiment. Additionally, we had already confirmed the expression of these genes following nitrogen starvation to coincide with histone acetylation and so we reasoned it was likely Acs2 is recruited to these loci. Repeating the analysis as before, we found the nitrogen starvation led to a significant recruitment of Acs2 of 5-fold to the *MET6* gene as well as a 2-3-fold recruitment to *ARG4* (Figure 4.10C). No difference in Acs2 recruitment between WT and *ino80Δ* was found in normal or starved conditions (Figure 4.10C). These data shows that Acs2 is recruited at actively transcribed genes in response to nitrogen starvation. While we found that loss of *Ino80* greatly reduced Acs2 recruitment at subtelomeric chromatin, we do not see the same profound effect at actively transcribed genes.

Taken together these data suggests INO80 is a novel regulator of Acs2 and may play a significant role in controlling chromatin acetylation following nitrogen starvation by controlling Acs2 recruitment.

4.3. Summary and Conclusions

Our results suggest that INO80 promotes survival in nitrogen starvation and the selective autophagy through counteracting Sir activity at sub-telomeric chromatin. Specifically we find that the mis-regulation of the *COS* genes in the absence of INO80 is due to the presence of SIR-mediated epigenetic silencing. Our data strongly implies that in the absence of INO80, Sir-dependent silencing of the *COS* genes leads to defective selective autophagy. Mechanistically we find that INO80 promotes H3K9ac at the promoters of *COS* genes, and this correlates with the recruitment of Acs2 to the promoters of *COS* genes in nitrogen starvation conditions. Taken together, we conclude that INO80 plays an important role in regulating *S. cerevisiae* subtelomeres following nitrogen starvation and that this activity play a critical role in the metabolic stress response. We speculate that by enabling the histone acetylation of subtelomeric genes such INO80 activity protects cells during nutrient starvation. Future investigation should target the mechanism controlling Acs2 recruitment to subtelomeres and its link to INO80.

Chapter 5

Chapter 5. General Discussion and Future Work

5.1. Overview

The work presented within this thesis describes a novel gene expression pathway regulated by the ATP-dependent chromatin remodelling complex INO80 critical for the cellular response to metabolic stress. Our results demonstrate that the survival of budding yeast following nitrogen starvation is dependent on the INO80 complex and this is correlated with the activity of the complex promoting clearance of ubiquitin conjugates, and selective autophagy. Mechanistically, we show that INO80 functions to counteract NAD-dependant silencing by the SIR complex, promoting histone H3 acetylation and RNA transcription under nutrient stress conditions.

Our results suggest that INO80 promotes the expression of the heterochromatic COS gene and our findings highlight the *COS* genes as regulators of selective autophagy of mitochondria and ER.

We propose that INO80 enables *COS* expression by promoting the recruitment of the acetyl-CoA synthetase, Acs2, to *COS* promoters. This mechanism facilitates the histone acetylation of these genes despite a global cellular decrease in Acetyl-CoA levels during stress conditions. Importantly, this study reveals a mechanism for controlling the expression of genes within and adjacent to heterochromatin. Our work provides further insight into how epigenetic control of transcription is linked to metabolic stress survival.

5.2. The INO80 complex promotes growth and survival during metabolic stress response

The INO80 complex has been well established as an important factor controlling gene expression and the loss of the complex leads to widespread down- and up-regulation of mRNA levels (Attikum et al., 2004; Jónsson et al., 2004,; Mizuguchi et al., 2004). Recently, INO80 has been implicated in metabolism by controlling the expression of growth-promoting genes (Beckwith et al., 2018; Gowans et al., 2018a; Yao et al., 2016).

Our work reveals a role for INO80 in promoting survival during metabolic stress conditions, when growth is downregulated. We demonstrate that cells lacking INO80 are unable to sustain viability under nitrogen starvation conditions and rapamycin.

Nitrogen is essential for all cellular function as it is required for amino acid biogenesis and protein synthesis. The availability of nitrogen is monitored by the cell and when it is absent, TORC1 signalling is inhibited, leading growth arrest and the induction of catabolic pathways (Gross and Graef, 2020).

We found that the ability of WT cells to tolerate these conditions was dependent on a functioning INO80 complex. The role of INO80 in metabolic stress appears to be dependent on its ATP-dependent chromatin remodelling activity, as we find that loss of the individual INO80 subunits *Arp5* and *Arp8* - which are essential for nucleosome remodelling (Eustermann et al., 2018b; Shen et al., 2003a; Watanabe et al., 2015) - also exhibited a growth defect following nitrogen starvation.

The inability of INO80 mutants to tolerate these conditions was suggestive of a defect in either the arrest of cells, induction of catabolic process or another pathway associated with TORC1 inhibition.

A possible alternative explanation for the sensitivity of *ino80Δ* to metabolic stress, is that the deletion mutants have acquired secondary adaptations to compensate for the deletion of *INO80*. Such adaptations may lead to indirect effects and thus the observed phenotype may be unrelated to INO80 function. In support of this is the fact that in some *S cerevisiae* genetic backgrounds the *ino80Δ* mutation is lethal while it is not in others (Poli et al., 2017b). This may imply that certain biological adaptations must facilitate the absence of INO80 function. Therefore, it is important to confirm that the observed sensitivity is a direct consequence of INO80 loss. However, our demonstration that the growth defect following nitrogen starvation is induced by conditional repression of INO80 during stress, while it is rescued by ectopic expression of INO80, refutes this hypothesis.

Using a strain where the expression of *INO80* is controlled by the inducible *GAL1* promoter allowed for acute repression of its expression and a comparison of the effect of nitrogen starvation within the same strain. Comparing growth following nitrogen starvation either in the presence or absence of *INO80* we found a clear advantage to Ino80 expressing cells grown in the presence of galactose suggesting the expression of *INO80* gene was leading to better survival in SD-N conditions.

Importantly the effect of INO80 loss by shifting the strain away from growth in galactose containing media needs to be accounted for by including a nitrogen containing, galactose

deplete condition. This additional control would further strengthen the conclusion that the effect we observe is caused by nitrogen depletion.

A further experiment to measure the effect of losing *INO80* expression for a short period of time before regaining it by reintroduction of galactose would help strengthen the conclusion from this experiment. Such an experiment would be expected to rescue the phenotype and the condition should respond to nitrogen starvation in a similar manner to WT.

These results are strongly suggestive of a direct role for the INO80 complex in the cellular response to starvation conditions.

5.3. Cell integrity and viability in nitrogen starvation requires INO80

Various assays have been described as measuring the 'viability' of *S. cerevisiae* in nitrogen starvation. The ability of cells to grow on rich solid-media plates following starvation has been previously described as representing cell 'viability' (Matsuura et al., 1997; Suzuki et al., 2011). However, this approach suffers from its semi-quantitative nature.

By directly quantifying the percentage of live and dead cells at various time points following nitrogen depletion, we found that WT budding yeast were able to maintain a high viability for up to 10 days of nitrogen starvation. However, loss of INO80 subunits led to decreased viability which positively correlated with time in nitrogen deplete medium.

Using the Phloxine B staining as a measure of viability allowed for accurate statistics to be performed but surprisingly, we did not find a strong correlation between the two measures of viability. After 5 days in nitrogen starvation conditions, *ino80Δ* cells were unable to grow on solid media plates. However, counting of cells not stained by Phloxine B implied that over 40% of cells were still 'viable'.

One explanation of this discrepancy may be that the Phloxine B staining protocol we used was unable to stain cells which were beyond recovery and in the process of dying. This would result in many cells appearing alive despite not being able to recover. As any cell unable to recover would be expected to eventually die and lose membrane integrity, increasing the duration of the Phloxine B experiment should show progressively fewer live cells.

Alternatively, our own method may be insufficient for measuring cell death in these conditions. Supporting this is the fact that in our experiments the *atg1Δ* had a much higher viability

following 5 days of growth in SD-N medium than previously reported (Tsukada and Ohsumi, 1993). Other labs have reported the continuous culture of yeast in the presence of low concentrations of Phloxine B can be used as a strategy for measuring yeast viability. Since our method involved only a brief incubation of the cells with Phloxine B prior to analysis, increasing the duration that the molecule is incubated with the cells may give more accurate results and better reproduce published results.

We cannot exclude the possibility that the differences in viability we observed between the two methods were due to technical limitations. However, an alternative explanation is that Phloxine B staining and recovery on rich medium plates, are measuring different biological pathways.

Following starvation, growth is dependent on a cell's ability to exit the quiescent G_0 state of growth arrest, and re-enter exponential growth (An et al., 2014). Budding yeast are able to resume growth after several weeks in G_0 (Gray et al., 2004). Our data indicates that survival in G_0 state requires INO80 and it is therefore plausible that INO80 also mediates the exit from G_0. Future gene expression analysis in cells transitioning from G_0 to growth would address this interesting question.

Autophagy factors have been found to promote entry into quiescence and yeast strains deleted for *Atg* proteins accumulated in telophase (An et al., 2014). Analysing cell cycle progression of *ino80Δ* mutants following starvation would reveal if *Ino80* mutants have a similar defect.

What mechanism may be causing the increased cell death in the absence of *Ino80*?

Autophagy deficient cells are unable to achieve protein translation in starvation due to deficiencies in the availability of amino acids (Onodera and Ohsumi, 2005). Cell death of autophagy deficient mutants in nitrogen starvation is associated acidification of the growth media. Prolonged growth leads to metabolites being secreted from cells and autophagy mutants are sensitive to the resulting low pH, in part due to their inability to upregulate enzymes of the respiratory pathway (Suzuki et al., 2011). Ultimately accumulation of reactive oxygen species (ROS) lead compromised respiratory function and cell death. Our subsequent work suggests *ino80Δ* shares similarities with *Atg* mutants. The viability of autophagy mutants is restored by buffering of the starvation medium, indicating that the failure to respond to starvation is the dominant cause of cell death. It would be interesting to test whether a similar approach would rescue *ino80Δ* loss of viability as this would strongly link sensitivity of *ino80*Δ to nitrogen starvation defective autophagy response. In addition, the build-up of ROS is closely linked with

cell death and so measuring changes in cellular ROS levels would further describe the phenotype and cause of cell death we have observed.

5.4. INO80 activity promotes cell growth in the presence of rapamycin

Recent work by the Morrison lab had identified metabolic genes as targets of INO80 mediated transcriptional regulation , specifically identifying a similarity between the transcriptome of mTOR inhibited cells and *ino80Δ* (Beckwith et al., 2018). The authors of the study concluded that INO80 activity promoted active mTOR signalling in nutrient rich conditions, and therefore *ino80Δ* resembled starved cells. To support the finding that *ino80Δ* transcriptome resembled TORC1 inhibition, the authors tested whether *ino80Δ* phenotypically resembled starved cells. To do this, *ino80Δ* was grown on rapamycin containing medium to inhibit the TOR complex (Zaragoza et al., 1998), and compared to growth of a wild-type strain. In line with their previous finding, the severely reduced growth of WT budding yeast was rescued by the loss of Ino80 and the authors argued that this was due to *ino80Δ* being 'primed' by already being in an TORC1 inhibited-like state (Beckwith et al., 2018)

Surprisingly, and contrary to the published findings, we found that loss of *Ino80* led to reduced growth in media containing rapamycin and resembled autophagy deficient strains when cultured in starvation conditions.

In line with our observations in SD-N, we found that *ino80Δ* grew worse in rapamycin. A compromised growth in rapamycin was observed regardless of whether we measured the acute response (0-48 hours after treatment), or a long-term response (growth on solid media plate for over 48 hours). This suggests that the loss of *ino80Δ* led cells to become more sensitive to rapamycin.

We conducted the same experiment in various budding yeast genetic backgrounds, including the S288C background used in the study by Beckwith et al (2018). In all cases, we observed the same sensitivity to rapamycin in *Ino80* deleted mutants.

Therefore, we conclude that the difference cannot be explained by yeast genetic background, suggesting that INO80 activity promotes survival and growth in both TOR-inhibited conditions of starvation and rapamycin.

Directly measuring cell viability using Phloxine B may be an additional experiment to carry out moving forward as it is likely to agree with these previous results and support this conclusion.

What can explain the different results obtained in our study and the published work of Beckwith et al (2018)?

The discrepancy may be caused by the specific differences between our own *ino80Δ* strain and the *ino80Δ* described by the authors. Deletion of the *INO80* gene is lethal in certain yeast genetic backgrounds while tolerated by others (Poli et al., 2017b). It is possible that the biological adaptations to the loss of Ino80 differ slightly between different *ino80Δ* cells, even of the same genetic background. Even though we tried three different strains, the uniqueness of each strain may induce differences. It would be reasonable to request use of the Morrison lab *ino80Δ* strain to repeat the experiment using their own yeast. A direct comparison of both strains would conclusively reveal any differences.

Importantly, the authors did not demonstrate that their effect was reversed when *INO80* was supplied ectopically and therefore it is possible that effect they observe is due to an exogenous mutation.

Our own findings are strongly supported by their reproducibility across different conditions. We see the same effect being caused by different TORC1 inhibiting conditions (rapamycin and SD-N), in different *ino80Δ* genetic background-based yeast, and using mutants of different Ino80 subunits. This make us confident in our conclusion that loss of INO80 activity does not lead cells to be adapted to TORC1 inhibited conditions and instead leads to sensitivity to TORC1 inhibition.

5.5. INO80 subunits show genetic interaction with autophagy components

Autophagy is a central pathway in the response to nutrient starvation as it is a critical method by which eukaryotic cells are able to sustain protein synthesis and survive starvation.

Our results have demonstrated that INO80 activity protects cells from nitrogen starvation and the loss of INO80 resembles the growth defect observed in autophagy-deficient yeast when exposed to nitrogen deplete conditions. We found that when mutations in the autophagy pathways were combined with INO80 complex mutants, the resulting phenotype resembled a synthetic lethal effect in nitrogen starvation. This implies that the INO80 and autophagy

pathways are likely to function in complement to each other during the response to starvation, leading to their combined loss producing a synthetic lethal effect.

This approach however suffers from being semi-quantitative and therefore difficult to conclude with certainty whether the observed effect was additive or synthetic. Phloxine B produced a quantitative measurement of viability which showed that, compared to the single mutants, the two mutations led to an epistatic effect in starvation. This implied that both INO80 and autophagy functioned in the same pathway since their combined loss did not lead to a significant difference in viability relative to the viability of individual mutant strains.

As discussed above, an explanation for the difference in the results may be due to two different pathways governing susceptibility to Phloxine B staining in SD-N and the ability of budding yeast to recover on rich media plates after starvation.

The epistasis of INO80 and autophagy mutants strongly suggests that both proteins promote viability in nitrogen starvation through the same pathway. These results further support our results showing that loss of *Ino80* led to a phenotype resembling autophagy deficient yeast. Importantly in both strategies, spot test and Phloxine B measurement, the effect of combining the mutations was not additive, suggesting that these pathways are not independent of each other.

5.6. Ubiquitin clearance following nitrogen starvation is mediated by INO80

Metabolic stresses such as starvation leads to a dependence on timely turnover of proteins by the autophagy, and to a lesser extent, ubiquitin proteome system (UPS). Ubiquitin is a shared signalling molecule in both of these pathways (Dargemont and Ossareh-Nazari, 2012; Khaminets et al., 2016; Lu et al., 2014; Marshall et al., 2019). The turnover of proteins in starvation conditions both serves to replenish reduced amino acid pools, allowing for essential protein production, and clearing mis-folded protein aggregates conjugated to ubiquitin.

Our results demonstrate that INO80 activity is required to prevent the accumulation ubiquitinated conjugates following starvation. Previous work had found that INO80 activity was required to promote the clearance of ubiquitinated RNAPII machinery (Lafon et al., 2015), however our work strongly suggest that INO80 regulation of the cell ubiquitome is far more widespread.

We found that many of the differentially ubiquitinated proteins are membrane bound proteins and are associated with various organelles. Unlike higher eukaryotes, ubiquitin-mediated cargo recognition of organelles has not been described in yeast, although many components of the autophagy pathway are well conserved between lower and higher eukaryotes. Proteomic analysis of the experiments in collaboration with the lab of Petra Beli, identified many of these ubiquitinated species as originating in protein aggregates. Finally immunoblotting experiments confirmed these to be accumulating in the absence of INO80.

The turnover of ubiquitinated protein aggregates in starvation conditions is mediated in budding yeast by the ubiquitin-binding Cue5 protein and the Rsp5 ubiquitin ligase (Lu et al., 2014). The finding that this pathway is compromised in the absence of INO80 potentially suggests that INO80 is part of the Cue5-atuophagy clearance of protein aggregates. Transcriptomic data of gene expression in *ino80Δ* does not show significant changes to *CUE5* and *RSP5* genes, suggesting that INO80 does not regulate the transcription of these proteins.

Protein aggregates and misfolded proteins are dangerous to cells as they can lead to unintended toxic reactions that compromise cell activity (Dobson, 2003). Protein aggregation is the basis of many human neurodegenerative disorders, such as Huntington's, and the clearance of aggregates by autophagy is a critical process for health (Choi et al., 2013). The accumulation of protein aggregates in the absence of Ino80 is likely contributing to the growth and viability defects we observe.

This finding is the first time that INO80 activity has been linked to the degradation of protein aggregates and if it is found to be conserved in humans, may implicate INO80 activity in protecting against neurodegenerative diseases. One potential approach to further investigate this possibility would be to use existing data sets from patients of such conditions to investigate for links with the INO80 complex. For instance, if there is a correlation between patients with these conditions and those with SNPs and other mutations in INO80 subunits.

5.7. INO80 promotes selective autophagy of the ER

The loss of viability decreased growth, and defective clearance of ubiquitinated aggregates following metabolic stress in the absence of INO80 closely resembles phenotypes observed in autophagy-deficient yeast cells. Intriguingly, we found that bulk autophagy was not dependent on the presence of INO80, as delivery of autophagosomes to the vacuole and efficient degradation of GFP-Atg8 was observed in *ino80Δ* cells.

During the immunoblotting experiments it was repeatedly observed that in protein samples from *ino80Δ,* the GFP band was fainter than that of WT. This potentially implies different rates of bulk autophagy in the absence of *Ino80*. A possible strategy to investigate this further would be using the quantitative Pho8Δ60 assay, an enzymatic assay which allows the accurate measurement of autophagic flux (Noda and Klionsky, 2008). Atg8 activity is not limited to non-selective pathways of autophagy.

The selective targeting of cellular compartments and organelles to the autophagic pathway is a fundamental pathway both in normal and stress conditions (Farré and Subramani, 2016; Gatica et al., 2018). Our subsequent finding of defective selective degradation of organelles, which is also an Atg8-dependant process, may explain the difference in GFP-Atg8 degradation rates between WT and *ino80Δ*.

The selective autophagy of the ER plays an important role in the regulation of the size and homeostasis of the ER. The ER does not have a fixed volume and dynamically responds to changes in the protein and lipid biosynthetic demand, as well as other changes in the cellular environment (Schäfer et al., 2020). Starvation induces ER-phagy to regulate the organelle and the selective degradation of parts of the ER clears faulty proteins and lipids. Overall this process reduces the ER stress caused to the cell by unfolded protein accumulation (Loi et al., 2018).

Following nitrogen starvation, we found that the induction of ER-phagy was dependent on the presence of INO80, for the first time demonstrating an ATP-dependent chromatin remodelling complex to be a regulator of reticulophagy. Intriguingly, defective ER function can lead to the accumulation of unfolded proteins which could potentially contribute to protein aggregates, the accumulation of which is also a phenotype of INO80. However little evidence connecting ER stress and the unfolded protein response with protein aggregation exists, and so it is not possible to conclude the two phenotypes we observe in the *ino80Δ* are directly linked. Studies in higher eukaryotes have found that the failure to clear misfolded proteins within the ER can lead to some aggregation within the ER itself, termed “ER storage disease”, although the ER-associated degradation (ERAD) pathway is primarily responsible for this process (Li and Sun, 2021).

We propose that INO80 activity promotes ER-phagy in response to starvation and the absence of this pathway likely contributes to the growth defect of *ino80Δ* cell in starvation conditions. The growth defect is likely caused by the increased levels of ER stress. ER stress can be measured by monitoring the induction of components of the budding yeast unfolded protein

response (UPR) by immunoblotting or quantitative OCR of reverse transcribed (RT) RNA (Oslowski and Urano, 2011). Alternatively, the small molecule Thioflavin T (ThT) binds selectively to protein aggregates and has fluorescent properties making it a useful tool for investigating ER stress (Beriault and Werstuck, 2013). These strategies could be used to confirm that *ino80Δ* cell suffer increased ER stress.

The non-selective nature of bulk autophagy means that it is possible for non-receptor mediated autophagic degradation of the ER to occur in nitrogen starvation. To rule out the possibility that we are observing a bulk autophagy mediated effect, the drug tunicamycin can be used to specifically induce only ER-phagy. Tunicamycin directly inhibits N-linked glycosylation and leading to ER stress and does not induce other autophagy pathways (Mizuno et al., 2020).

ER-phagy in budding yeast is primarily regulated through *ATG39* and *ATG40* genes. Rpd3-Pho23 histone deacetylase complex negatively regulates *ATG40*. TORC1 inhibition counteracts this silencing, thereby activating *ATG40* expression (Cui et al., 2019). *ATG39* is instead regulated by the Mig1 and Mig2 which repress the gene in the presence of TORC1 signalling (Mizuno et al., 2020). Additionally both genes are upregulated by Msn2 and Msn4 following nitrogen starvation and ER stress (Mizuno and Irie, 2021). Interestingly, the RNA levels of these two genes were found to be completely unaffected by *INO80* deletion in our RNA-seq data, suggesting INO80 activity does not regulate their expression. However previous research has found that over-expression of *ATG39* and *ATG40* did not induce ER-phagy (Mochida et al., 2015), and it is therefore likely that expression levels alone do not directly correlate with activity of this protein. Post-translational modification of autophagy receptors is common in yeast and it is likely that both Atg39 and Atg40 require phosphorylation to activate them, as this is common in other selective autophagy receptors (Kanki et al., 2013; Mochida et al., 2014, p. 25; Tanaka et al., 2014). INO80 might be indirectly regulating the activity of Atg39 and Atg40 through controlling the expression of their associated kinase. Since a specific kinase regulating Atg39/Atg40 has not be identified, measuring the phosphorylation state of these two proteins in the presence and absence of INO80 activity would investigate this possibility. Phosphorylation of the two proteins would be expected to not be observed irrespective of metabolic state of the cell in *ino80Δ* cells if the process was indeed dependent on INO80 activity.

5.8. COS genes promote the selective autophagy of mitochondria

Saccharomyces cerevisiae can carry out metabolism both in anaerobic and aerobic conditions, favouring to respire anaerobically by the process of fermentation. In non-optimal growth conditions such as in the presence of non-fermentable carbon sources, for example lactose and glycerol, budding yeast switch to aerobic respiration. Budding yeast mitochondria subsequently accumulate damage, partially through the creation of radical oxygen species (ROS) as a by-product of aerobic respiration and as a result require turnover of damaged mitochondria to prevent further stress to the cell (Deffieu et al., 2009; Karavaeva et al., 2017; Okamoto et al., 2009). The selective autophagic degradation of mitochondria by mitophagy is the primary mechanism for this process (Kurihara et al., 2012).

By measuring mitophagy in the presence and absence of INO80, we showed that the presence of the complex is required to achieve the turnover of mitochondria under conditions of selective mitophagy. This strongly implies that INO80 activity promotes mitophagy. We used protein measurements of Idh1-GFP and free GFP to identify the defective mitophagy, but other methods for measuring mitophagy are available. Microscopic analysis in future work would help confirm that in WT cells the accumulation of GFP occurs within the vacuole, a process only achievable through mitophagy.

Another circumstance in which mitophagy is critical is during the switch from growth in a non-fermentable to a fermentable carbon source such as from lactose to glucose. Following this switch there is a substantial activation of mitophagy to reduce the number of mitochondria within the cell, as the organelle is no longer required in high amounts (Eiyama and Okamoto, 2017). INO80's regulation of mitophagy should be further explored by performing an immunoblotting experiment with WT and *ino80Δ* against Idh1-GFP, but with the conditions reversed, so that the cells are initially cultured in lactose or glycerol containing medium and subsequently moved to glucose containing medium. Demonstrating a role for INO80 in mitophagy induced by different approaches would strongly suggest that INO80 is a core regulator of the pathway. This would also rule out the possibility that INO80 mediates mitophagy only in specific conditions, for example during ROS accumulation.

How does INO80 activity promote the selective autophagy of mitochondria?

We identified that the *COS* gene family is strongly repressed in the absence of INO80. By measuring mitophagy in the yeast strain partially deleted for every *COS* gene, we found mitophagy to also be compromised, similar to INO80. This finding provides a correlation between the regulation of *COS* expression and INO80 regulation of mitophagy but does not

conclusively prove that the loss of mitophagy in *ino80Δ* is due to lack of COS activity. To support a model where INO80 regulated mitophagy by promoting the expression of the *COS* genes, the genes should be supplied ectopically to the autophagy deficient *ino80Δ.* If the model is correct, this would be expected to rescue the cell's ability to perform mitophagy.

Our finding that the *cosΔ* strain lacks mitophagy implies that Cos activity promotes mitophagy, however the mechanism through which this may take place is unclear.

The *COS* genes encode membrane integrated tetraspanin proteins which are highly ubiquitinated. The Cos factors are known to function within the endosomal sorting via multi-vesicular body (MVB) pathway (MacDonald et al., 2015). The (endosomal sorting complex required for transport) ESCRT pathway controls endosomal sorting of proteins, including the degradation of membrane-integral proteins of the outer membrane following nutrient stress (Raiborg and Stenmark, 2009).

Work on Cos5 found that it is localised to the outer cell membrane and functions to promote protein sorting to the vacuole via endosomal pathway. Importantly this process was found to be dependent on the ubiquitinated state of Cos5 (MacDonald et al., 2015).

Selective autophagy machinery in budding yeast has not been found to interact with ubiquitin other than through Cue5 in aggrephagy as described previously (Lu et al., 2014, p. 5). It is therefore unclear how ubiquitination would direct mitophagy. One possibility is that the ubiquitin acts indirectly and does not itself signal for autophagic turnover. Instead, the ubiquitinated Cos proteins may recruit ESCRT machinery which in turn promotes mitophagy. Mitochondrial fission is an essential step in mitophagy prior to their sequestration into autophagosomes (Abeliovich et al., 2013; Mao et al., 2013). ESCRT complexes are evolved to mediate vesicle budding from lipid membranes, and have been found to mediate the abscission of lipid membranes during cell division (Guizetti et al., 2011). It is therefore possible that a similar mechanism may be required during mitochondrial fission.

Autophagy and endosomal sorting via the MVB pathway may be more linked than previously assumed. Both pathways converge on the vacuole or lysosome and MVBs resemble autophagosomes in function (Piper and Katzmann, 2007). Work in higher eukaryotes has already demonstrated such a link between ESCRT machinery and the autophagy pathway (Raiborg and Stenmark, 2009). For instance, the autophagic clearance of protein aggregates associated with neurodegenerative disease was found to require MVB, and ESCRT mutants were found to compromise the autophagy pathway in such cells (Filimonenko et al., 2007; Lee

et al., 2007; Rusten et al., 2007). In ESCRT mutants, autophagosomes were found to accumulate, potentially suggesting a failure to fuse with the lysosome and deliver their cargo for proteolysis. Testing for the accumulation of protein aggregates in the absence of Cos proteins, for example by measuring for the accumulation of ubiquitinated conjugates by immunoblotting in the *cosΔ* mutant, would reveal whether compromised MVB sorting in yeast similarly leads to defective aggrephagy. Although not in the scope of this thesis, future work on ESCRT mutants could determine the connection between aggregate turnover by autophagy and MVB sorting in budding yeast.

Recent work has further linked the ESCRT pathway and selective autophagy, demonstrating that the selective autophagy of the ER (macro- and micro-ER-phagy) are both dependent on functioning ESCRT machinery (Schäfer et al., 2020). This agrees with results we generated which suggested that ER-phagy was compromised in *cosΔ* mutants. Although we found the loss of ER-phagy function to not be complete as observed for mitophagy, the *cosΔ* strain is not completely deleted for every gene of the *COS* family. The partially deleted genes can be seen to be expressed by RNA-seq, and their expression may be leading to the incomplete ER-phagy defect we find.

Protein turnover by the MVB pathway has been shown to be an important early response to starvation and required for increasing amino acid availability immediately following starvation (Müller et al., 2015). The loss of MVB function was found to lead reduced amino acid levels early during the starvation response and reduced de novo synthesis of vacuolar hydrolases, ultimately leading to reduced lytic activity in the vacuole (Müller et al., 2015). Despite this, we still observed autophagic delivery of GFP-Atg8 to the vacuole and the accumulation of free GFP comparable to WT when the *cosΔ* strain was tested. The use of a quantitative method such as the Pho80delta6 assay would reveal more subtle difference that may be caused by the loss of Cos activity.

If INO80 functions to promote the endosomal sorting of proteins and through this process promotes autophagy, it would be important to confirm that *ino80Δ* is defective for MVB sorting. This could be done by measuring the localisation of a known MVB target fused to a fluorescent protein, such as Mup1-GFP, before and after starvation and growth arrest (MacDonald et al., 2015).

The role of Cos proteins in regulating mitophagy may by completely, or in-part, independent from their role in MVB sorting. Endosomal sorting is a pathway nearly exclusively targeting

plasma membrane protein and the Cos proteins, particularly Cos5, are reported to promote this process by providing a ubiquitin signal in trans to cargo destined for sorting to the vacuole.

However, evidence suggests that the over 10 Cos proteins expressed by *S. cerevisiae,* may function in differing pathways and are likely to be localised to a variety of membranes. The existence of several *COS* pseudo-genes implies that non-useful duplications of this sequence have been selected against. This suggests that the remaining, functional, *COS* genes play discrete albeit similar roles. Secondly, while some Cos proteins share a high similarity (Cos5 and Cos7 share a 94% protein identity at the amino acid level), many do not; Cos5 and Cos8 share 76% protein sequence identity while Cos5 and Cos12 only share 40% amnio acid identity. Recent advances in protein structure modelling using neural networks, such as the AlphaFold 2 (Jumper et al., 2021), demonstrates this point as even the highly similar Cos5 and Cos1 proteins have visible structural differences. Together this is suggestive of functional diversity in Cos proteins. One example of this can be seen by studying open source high-throughput data sets such as the GFP fusion screens which aim to identify protein cellular localisation by microscopy (Huh et al., 2003; Yofe et al., 2016). While many Cos proteins predominantly localise exclusively to the vacuole – Cos1, Cos4, Cos5 – or to both the vacuole and the outer cell membrane – Cos5, Cos6 – others localise to the nuclear membrane, for example Cos8 and Cos10. Finally, protein localisation can be predicted using high-throughput assays which measure genetic networks through experiments such as synthetic genetic array (SGA) screens (Costanzo et al., 2016). The measurement of what proteins and pathways are most affected by the loss of specific genes can provide information on the "network" of the gene and bias in the representation of certain cellular compartments within such networks is indicative of a connection between the protein in question and a given cellular compartment. By using online tools to carry out such an analysis we found that Cos1, Cos2, Cos3, Cos5, Cos6 and Cos9 are predominantly associated with the vacuole and endosomal system. However, it also suggests that Cos4, Cos8 and Cos10 are associated with the nuclear envelope, while Cos7 is associated with the mitochondria and Cos10 is additionally found to be associated with the ER. This presents an interesting future direction of study, and Cos7 should be further investigated for a role in mitochondrial regulation including mitophagy.

Taken together, these data suggest that different Cos proteins may reside in the membranes of different organelles and perform somewhat distinct functions. If a molecular link exists between Cos function and mitophagy, Cos proteins would be likely to physically interact with autophagy machinery such as Atg8. Additionally, interactions with other mitochondrial

membrane proteins would be expected. To test this, a fusion of Cos7 to a biochemical tag just as HA or FLAG could be generated and used to co-purify the Cos protein along with interacting partners, which could be screened by mass spectrometry, before and after the induction of mitophagy.

5.9. Transcriptome of *ino80Δ* resembled nitrogen starved cells

The activity of many chromatin remodelling complexes is well established to be closely linked with the maintenance of proper transcriptional dynamics. The INO80 complex can bind around 80% of all budding yeast gene promoters (Yen et al., 2013) and is thought to influence transcription predominantly through the establishment of appropriate nucleosome spacing and composition at the nucleosome free region (NFR) (Krietenstein et al., 2016; Poli et al., 2017b). Loss of INO80 leads to the mis-regulation of around 20% of the budding yeast genome and the resulting changes are roughly equally split between up and down regulated expression, demonstrating that INO80 activity is not limited to only activation or repression of transcription (Attikum et al., 2004).

It is certain that INO80 activity plays a fundamental role in chromatin organisation with broad effects on the organisation of many if not most gene promoters. However, evidence of a direct role for the INO80 complex in controlling specific biological pathways has so far been relatively inconclusive.

INO80 recruitment to various stress responsive genes was found to rapidly respond to hyperosmotic and heat stress and the loss of Ino80 subunits *arp4Δ* and *arp8Δ* leading to hyper-induced stress gene expression (Klopf et al., 2009). However the recruitment of INO80 to osmotic stress response genes was later demonstrated to be irrespective of the genes themselves and was mediated by their increased transcription rate (Klopf et al., 2017). This argues against a model where INO80 acts as a transcriptional regulator of specific pathways.

More recently, transcriptomic analysis of *ino80Δ* in normal growth, suggested an overabundance of metabolic genes being de-regulated. Glycolysis associated genes were repressed and oxidative phosphorylation genes were upregulated in various mutants of INO80 subunits (Yao et al., 2016). In 2018, Beckwith and colleagues proposed that INO80 was a direct mediator of active TORC1 signalling due to the similarity in the transcriptome of rapamycin treated WT yeast and *ino80Δ,* suggesting that the mutant resembled TORC1 inhibition both transcriptionally and functionally (Beckwith et al., 2018).

Our own transcriptomic analysis allowed us to confirm the observation that the loss of Ino80 led to transcriptional changes that resemble those observed following mTOR inhibition, and our work is the first to demonstrate this in nitrogen starvation. Indeed, the similarity between the transcriptional changes taking place following nitrogen starvation and the gene expression changes following loss of Ino80, does suggest that the chromatin remodelling activity of the complex plays a part in facilitating these pathways in conditions where TORC1 signalling is active. However, without any direct mechanistic link between TORC1 signalling and INO80, it is impossible to conclude if this observed link is direct effect - or an indirect result of unrelated INO80 function. For example, the maintenance of genome stability during pro-growth conditions may target INO80 to some of the most highly expressed genes, which are almost by definition are TORC1-mediated genes.

Our own results do not agree with the authors conclusion that loss of Ino80 leads to a 'starved-like state'. Our data demonstrates that unlike WT, *ino80Δ* is sensitive to TORC1 inhibited conditions such as nitrogen starvation and rapamycin. We were unable to replicate the rescue of WT growth defect the authors observed when growing *ino80Δ* in rapamycin. Instead, we found the opposite result, observing WT cells to grow better than *ino80Δ* in the presence of rapamycin. This agrees with a model where INO80 function is not essential for TORC1 mediated cell state. Instead, our results suggest INO80 plays a significant role during the TORC1 inhibited state.

We found that most of the nitrogen starvation-induced transcriptional program is unaffected by the loss of *Ino80*, suggesting that INO80 is not a major mediator of the TORC1-inhibited transcriptional state. Instead, we identified several specific examples of highly mis-regulated genes in *ino80Δ*. Among these the most differentially expressed was nearly the entire *COS* gene family, which were strongly repressed in the absence of INO80. We found that *COS* genes were dependent on a functional INO80 complex both before and after nutrient starvation, but their differential expression was greater following starvation. While the transcriptomic data showed *COS* genes had a greater dependence on INO80 for expression following starvation, our data clearly showed that INO80 activity regulates the genes in nutrient rich conditions also. The fact that INO80 impacts the transcription of these genes both in non-starved and starved conditions implies that the complex may function independently of metabolic stress.

S. cerevisiae grown in nutrient limited conditions designed to replicate growth in the wild organise their metabolism into cyclic oscillations of oxygen consumption. This is called the

yeast metabolic cycle (YMC) and the expression of around half of all budding yeast genes is correlated with the YMC (Tu and McKnight, 2007). The low oxygen phase of the YMC strongly resembles a TORC1-inhibited cell and accordingly *COS* genes expression is induced during this phase of the cycle (Tu et al., 2005). A possible explanation for dependence of *COS* gene expression on INO80 in non-starved conditions is that INO80 activity is specifically required during the low oxygen phase of the YMC. This conclusion is supported by other studies which have implicated the INO80 complex as a regulator of gene expression during the YMC (Gowans et al., 2018b).

5.10. INO80 regulates transcriptional pathways in response to nitrogen starvation

Under conditions of severe nutrient stress, *S. cerevisiae* can switch to a developmental program whereby a diploid cell undergoes sporulation. This produces haploid daughters that are stress-resistant and can remain dormant for long periods of time. The process of sporulation is initiated by two consecutive chromosome segregations through meiosis. The initiation and progression of this pathway is controlled by a series of transcriptional regulators which control early, middle and late parts of sporulation (van Werven and Amon, 2011).

In nitrogen starvation conditions, we found that loss of INO80 led to the de-repression of many meiosis and sporulation associated genes relative to WT. Indeed, the majority of the most significantly enriched genes in *ino80Δ* following nitrogen starvation are associated with meiosis, sporulation, and generally fall under reproductive processes. This suggested that INO80 activity repressed reproductive processes during nitrogen starvation. This conclusion was supported by finding that Ime1, a master regulator of early sporulation genes, and Ndt80, a regulator of middle sporulation genes, were both de-repressed in the absence of *Ino80*.

An interesting observation we made was that both *IME1* and *NDT80* were located adjacent or overlapping non-coding RNA (ncRNA) sequences. The INO80 complex has a well-documented role in repressing ncRNA which is associated with its role in promoting genome stability (Poli et al., 2017b). Loss of *Ino80* leads to the de-repression of many ncRNAs which may lead to indirectly activating other proximal promoters.

The sporulation pathway is associated with TORC1 inhibition however nitrogen starvation is not sufficient to activate this pathway alone. Glucose supresses *IME1* expression (Matsuura et al., 1997; Smith et al., 1998)**,** and it would not be expected to be expressed in our conditions since our nitrogen starvation media contains dextrose. Defective glucose sensing by the *ino80Δ*

strain may be another explanation for the activation of *IME1* and *NDT80* genes, although at present we do not have any evidence of this.

Importantly, different yeast genetic background differ in their ability to undergo sporulation and the W303 and SK1 backgrounds are the best established models for sporulation (Dirick et al., 1998). Since the LS20 yeast is not derived from these genetic backgrounds, drawing conclusions from this result needs to be avoided. However, our data is suggestive of a role for INO80 in the regulation of the sporulation process, and work to investigate this further in an appropriate yeast strain would be able to confirm or refute this finding.

5.11. INO80 activity at COS genes counteracts Sir-mediated heterochromatin silencing

We showed that the loss of INO80 led to *COS* gene silencing and that nitrogen starvation in the absence of Ino80 led to further inhibition of their expression. To study the molecular mechanism of this process we focussed on the local chromatin context of *COS* genes.

The location of all *COS* genes at sub-telomeric heterochromatin meant that these are in a predominantly repressive chromatin environment. Sub-telomeric and heterochromatin silencing in budding yeast is mediated by the SIR complex and is well established to respond to various signals, including metabolic regulation (Lin et al., 2000, p. 2; Ringel et al., 2013; Wang et al., 2016).

Sir-dependent silencing is mediated by the activity of Sir2, an NAD^+-dependant histone deacetylase (Gartenberg and Smith, 2016). Interestingly, the abundance of NAD^+ is closely linked to the metabolic state of the cell. In starved conditions, reduced metabolism leads to a decrease in NADH levels and an increase of NAD^+, leading to increased Sir2 activity in starved conditions (Lin et al., 2002). Despite this, starvation has not been found to lead to significantly increased telomeric gene silencing, highlighting the important role of mechanisms counteracting NAD^+-dependent silencing (Kaeberlein et al., 2005; Riesen and Morgan, 2009; Ringel et al., 2013). Multiple species of yeast have been shown to harbour many stress response genes at telomeric regions, implicating chromosome ends as stress response hubs (Ai et al., 2002; De Las Peñas et al., 2015; Jethmalani et al., 2021). As expression of these genes is required under stress conditions, it raises the question of how is Sir2-mediated silencing being counteracted.

We found that the loss of INO80 led to significantly lower expression of the Sir2-regulated telomeric *COS* genes suggesting that chromatin remodelling by INO80 antagonizes Sir2-dependent silencing.

By measuring the transcription of these genes following starvation, in a strain harbouring deletion for both Sir and INO80 subunits, we were able to show that loss of Sir proteins led to rescue of expression in the absence of INO80 activity. The de-repression of these genes was found regardless of whether INO80 was present or absent. This implies that the reduced levels of *COS* gene expression in *ino80Δ* is directly linked to the activity of the SIR complex and suggests that INO80 functions to counteract this activity.

This strongly implies that in the absence of INO80 activity, Sir activity creates a suppressive environment for *COS* gene expression. While our analysis in nitrogen starvation conditions only focussed on two genes *COS1* and *COS8* in our RT-qPCR, based on published RNA-seq results for *atg5Δsir3Δ* (Xue et al., 2015), we predict that a similar pattern would be expected if more *COS* genes were assayed. Since we found that nitrogen starvation leads to a strong growth defect following 5 and 10 days of growth for *ino80Δ* and *arp5Δ* respectively, collecting and measuring RNA levels for *COS* gene expression at a later point, such as 5 days, would demonstrate whether COS levels remain low throughout this time. Providing *COS* genes exogenously to nitrogen starved *ino80Δ* or *arp5Δ* should have a positive effect on their growth and this experiment should be carried out to demonstrate conclusively that *COS* gene expression is associated with their improved survival.

Having demonstrated that loss of Sir mediated silencing rescue *COS* gene RNA levels in an INO80 mutant strain, we were also able to show that this correlates with a rescue of growth defect found in *arp5Δ* and *arp8Δ*. While it would be significant to confirm the same rescue in the *ino80Δ*, we struggled to generate the double mutant *ino80Δsir2Δ*, potentially because the combination is lethal to the already sick *ino80Δ*. Instead, we inhibited Sir2 activity using NAM, a potent Sir2 inhibitor, and found to rescue growth of *ino80Δ* following growth in nitrogen starvation conditions. This further supports our conclusion that the sensitivity of *Ino80* mutants to starvation is mediated by Sir2-mediated gene repression. Although not possible to conclude from our data alone, we propose that this is mediated by Sir-dependent regulation of the *COS* genes.

It is possible that the rescue of *ino80Δ* by NAM is not limited to the de-repression of the *COS* genes and therefore, a genome wide approach such as RNA-sequencing would likely produce

differentially expressed genes which may be contributing to the phenotype of *ino80Δ*. However, INO80 has never been reported to regulate to telomeric gene activity broadly and our own data suggests that its role in *COS* mRNA expression is specific to this gene family. What is the mechanism that leads to the loss of Sir activity rescuing *ino80Δ*?

Correlating with the increased levels of *COS* gene expression, we found that *arp5Δsir3Δ* double mutant also rescued the turnover of ubiquitinated proteins and aggregates following starvation. The failure to clear ubiquitinated protein conjugates and aggregates is therefore likely to be at least partially due to Sir-dependent silencing of *COS* gene expression. This is supported by the observation that partial *COS* gene deletions compromised selective autophagic degradation of ER and mitochondria proteins. If failure to express Cos proteins is responsible for the accumulation we see in *ino80Δ* and *arp5Δ* then the *cosΔ* strain would be expected to also show an accumulation of ubiquitinated conjugates and aggregates.

Critically, mitophagy and ER-phagy should be assayed in the double mutants *arp5Δsir3Δ* or *arp8Δsir2Δ* and it would also be expected to be rescue if our hypothesis is correct. Additionally, measuring Aggrephagy, mitophagy and ER-phagy in the *ino80Δ* strain supplemented with NAM would also be expected to rescue the defects.

Our results demonstrate that a novel genetic pathway controlling *COS* gene expression is critical to survival in starvation conditions. The data demonstrates the importance of correctly regulating chromatin silencing following starvation and highlights the INO80 complex as a critical regulator of this process.

5.12. SIR recruitment at *COS* genes is unaffected by INO80 but responds to nitrogen starvation

Telomeric silencing is thought to be predominantly controlled by the establishment of epigenetically euchromatic and heterochromatic regions and the controlling of the spread of SIR complex, predominantly the function of H4K16ac (Kimura et al., 2002). INO80 has been implicated in further maintaining heterochromatin-euchromatin boundaries although this study found INO80 preventing transcription of telomeric heterochromatin through inhibiting Dot1-mediated H3K79 tri-methylation (me3) (Xue et al., 2015). Set1-catalysed H3K4me3 was also found to repress SIR complex invasion into euchromatic chromatin by inhibiting Sir3 spreading (Santos-Rosa et al., 2004).

We hypothesised that the inhibition of Sir spreading to *COS* genes and promoters was the simplest model to explain INO80's ability to counteract Sir-dependent silencing. We found a significant enrichment of INO80 at these genes, and this enrichment remained constant before and after nitrogen starvation. The increased dependence of *COS* expression on INO80 following starvation makes it likely that INO80 activity is required more in starvation conditions. For this reason, the lack of change in recruitment was surprising and it suggests that a mechanism other than recruitment leads to an increased dependence on INO80 function. Post-translational modification (PTM) of the INO80 complex may alter the activity or interaction of the complex thereby accounting for such a change. Multiple residues of INO80 subunits can be modified, and a high-throughput study measuring rapamycin-induced phosphorylation found that the Ino80 protein was phosphorylated at 3 positions in its C-terminal tail, while Arp8 and Ies2 both gained a phosphorylation mark (Iesmantavicius et al., 2014). It is likely that mTOR inhibition directly signals to the complex and point-mutagenesis of these phosphorylated residues should be used to investigate the role of these PTMs. For example, to study the mechanism underlying INO80 function at the *COS* genes, and to determine whether INO80 activity is mediated by mTOR induced phosphorylation, point-mutants would be expected to resemble *ino80Δ* mutation in phenotype.

We were unable to find conclusive evidence that INO80 activity disrupts the binding of Sir proteins at the *COS* promoters following nitrogen starvation. We hypothesised that loss of Ino80 would lead to significantly increased Sir3 levels at the promoters of *COS* genes and the genes themselves, thus accounting for the decreased expression. In line with the de-repression of *COS* expression following TORC1 inhibition, nitrogen starvation leads to a significant decrease in Sir3 recruitment at the *COS* promoter. However, when Sir3 recruitment was assayed in a strain lacking *Ino80*, we found no significant difference between the nitrogen starved samples. The high variability of the ChIP results from the *ino80Δ* samples meant we saw no significant difference between non-starved and starved samples either. Several variables may explain this; first, the heterochromatic nature of sub-telomeres means the chromatin is more compacted and resistant to shearing by sonication, therefore less DNA fragments are ultimately pulled down during the experiment. Further optimisation of the sonication protocol may yield better results. Repeating the experiment but targeting Sir2 would allow for further confidence in any conclusions from the Sir3 data. A physical interaction between INO80 and Sir proteins may be expected in a model where INO80 physically disrupts their binding at COS promoters. Performing protein co-immunoprecipitation to measure

physical interactions between the chromatin remodeller and Sir proteins before and after nitrogen starvation would help better understand the mechanism controlling sub-telomeric regulation.

Additionally, the histone modification H4K16 acetylation is indicative of both Sir2 levels and since H4K16 hypoacetylation recruits Sir3 and other Sir complex subunits, it is also indicative of the presence of the Sir complex in general. Any disruption of Sir-dependant silencing by INO80 would be expected to be reflected in increased levels of H4K16 acetylation, and accordingly, the loss of INO80 would be expected to lead to decreased levels of H4K16 acetylation.

It is possible that any mechanism of INO80 counteracting Sir-dependent silencing at telomeric genes is not restricted to the *COS* genes alone. High-throughput sequencing of ChIP for Sir3, Sir2 and histone acetylation following nitrogen starvation and importantly in an *ino80Δ* background, would generate an important data set which would be able to address the significance of our finding across all silent chromatin.

Recently it was discovered that Sir2 is itself a target of autophagic degradation through a yet poorly understood mechanism. Following treatment with rapamycin, Sir2 was found to be degraded over the in an autophagy-dependent manner during the first hour and a half following mTOR inhibition (Zhang et al., 2021). An intriguing possibility is that defective autophagy in the *ino80Δ* background leads to reduced Sir2 degradation and therefore increased telomere silencing. However, the lack of a significant increase is Sir3 recruitment at *COS* genes in *ino80Δ* suggest this is unlikely. It would be interesting to disrupt autophagic degradation of Sir2, for example by treating cells with Phenylmethanesulfonyl-fluoride (PMSF), and inhibitor of lysosomal proteases, or by deleting the Atg2 or Atg12 proteins which were found to be essential for Sir2 degradation. In such conditions, *COS* RNA levels would be expected to resemble those seen in the *ino80Δ* background if this was the mechanism behind their repression.

Overall, our data supports a model where INO80 activity at *COS* genes promotes their expression however we do not find strong evidence that this is the result of controlling SIR occupancy at the genes.

5.13. Histone acetylation of COS promoters, and lysine acetylation across the cell require INO80 activity

Histone acetylation leads to decompaction of chromatin and increases the accessibility of underlying DNA to transcriptional machinery. As a result, the acetylation of gene promoters, in particular at H3K9 and H3K14, is strongly associated with transcriptional activation (Agalioti et al., 2002; Eberharter et al., 2005).

The acetylation of histone H3 lysine 9 (H3K9ac) as well as H4K16ac, are the main targets for Sir2 de-acetylation activity (Bosch-Presegué and Vaquero, 2015; Xu et al., 2007).

In line with starvation-induced transcriptional activation of the *COS* genes, we identified the H3K9ac modification becoming significantly enriched at *COS* promoters following nitrogen starvation. This suggests the previously described decrease of SIR complex at *COS* promoters facilitates the increased promoter acetylation.

Interestingly, the increase in H3K9ac was found to be dependent on INO80, as the *ino80Δ* strain showed significantly lower acetylation levels at the sub-telomeric promoters compared to WT. This difference was most evident following 2 hours of nitrogen starvation highlighting that INO80 function is particularly important in these conditions.

Our results indicate that INO80 induces the expression of these sub-telomeric genes following nitrogen starvation by facilitating promoter acetylation. How does INO80 lead to higher acetylation?

The possibility that recruitment of Sir proteins is disrupted in the presence of INO80 is refuted by our observation that SIR recruitment is not increased in *ino80Δ* cells. Alternatively, INO80 may promote deposition of the acetylation mark at the H3 lysine 9 through acting on mediators of histone acetylation. The failure to recruit the histone acetyltransferases (HAT) of H3K9, or a reduced capacity of the cell to carry out site-specific acetylation in the absence of *Ino80* might explain the reduced levels of H3K9ac in *ino80Δ* cells.

We did not find evidence of reduced histone acetylation at non-telomeric genes, suggesting *ino80Δ* did not lead to a global defect in chromatin acetylation. Instead, an investigation of the recruitment of H3K9 HATs to the *COS* promoter in *Ino80* deleted cells would help elucidate the mechanism controlling the expression of *COS* genes.

Strikingly, we found that INO80 is required for the recruitment of the nuclear acetyl-CoA synthetase Acs2 to *COS* promoters. We found that following nitrogen starvation, Acs2

recruitment to *COS* promoters and intergenic unique telomere sequence was strongly dependent on INO80.

Recently, Acs2 was shown to regulate telomere silencing and cell senescence by direct recruitment to budding yeast telomeres (Chen et al., 2021). The availability of acetyl-CoA is critical for histone acetylation, among other processes, as it provides the acetyl group for acetylation reactions by HATs. Synthetases such as Acs2 convert acetate, a key intermediary metabolite, into acetyl-CoA, thus facilitating the regulation of nuclear processes such as histone acetylation, chromatin structure and ultimately gene expression.

It is likely that reduction of Acs2 recruitment in *ino80Δ* leads to the lower histone acetylation levels we observe. Acs2 functions as part of a complex, SESAME (serine-responsive SAM-containing metabolic enzyme complex), which is recruited by in part by Set1 mediated H3K4me, and functions to phosphorylate histone H3T11 (H3pT11). At sub-telomeres H3pT11 promotes SIR complex recruitment and gene silencing, however SESAME recruitment to heterochromatin is independent of H3K4 methylation (Zhang et al., 2021).

Sub-telomeres recruitment of SESAME leads to concomitant increases to H4K16 acetylation mediated by its interaction with the SAS acetyltransferase complex. The complex bound Acs2 converts local acetate into acetyl-CoA which both increases acetylation by the SAS complex, and antagonizes Sir2 spreading (Chen et al., 2021). Both promoting silencing by inducing H3pT11, and chromatin activation through increasing H4K16ac; the SESAME complex is an important factor in establishing the boundary between euchromatin and heterochromatin. It is not known whether Acs2 can function independently of the SESAME complex. Our work demonstrates that INO80 recruits Acs2 to heterochromatin and suggests that INO80 may be a regulator of the SESAME complex. H3pT11 is mediated by the Pyk1 subunit of SESAME and both Pyk1 and H3pT11 enrichment should be investigated in the absence of *Ino80*.

The mechanism by whichh InO80 increases Acs2 occupancy at *COS* genes is an intriguing question. Physical interaction between Acs2 and Ino80 can be assessed by co-immunoprecipitation assay and should be carried out in starvation conditions. The previously published temperature sensitive, *acs2-ts* mutant has been found to repress *COS8* mRNA expression (Chen et al., 2021; Eisenberg et al., 2014; Takahashi et al., 2006b). It would be interesting to explore whether all other *COS* genes are similarly repressed in this mutant and whether *acs2-ts* resembles *ino80Δ* in starvation conditions.

Finally, over-expressing Acs2 or increasing nuclear acetyl-CoA levels would be expected to rescue some or all *ino80Δ* phenotypes as this would increase acetylation of heterochromatin. This would confirm that ino80Δ phenotype is mediated by INO80's role in recruiting Acs2 and histone acetylation.

Our results suggest that INO80 activity controls *COS* expression in starvation conditions by regulating Acs2 recruitment, and potentially recruitment of the SESAME complex. As SESAME is a regulator of heterochromatin boundaries, INO80's previously reported role in enforcing heterochromatin boundaries may be linked to its ability to recruit Acs2.

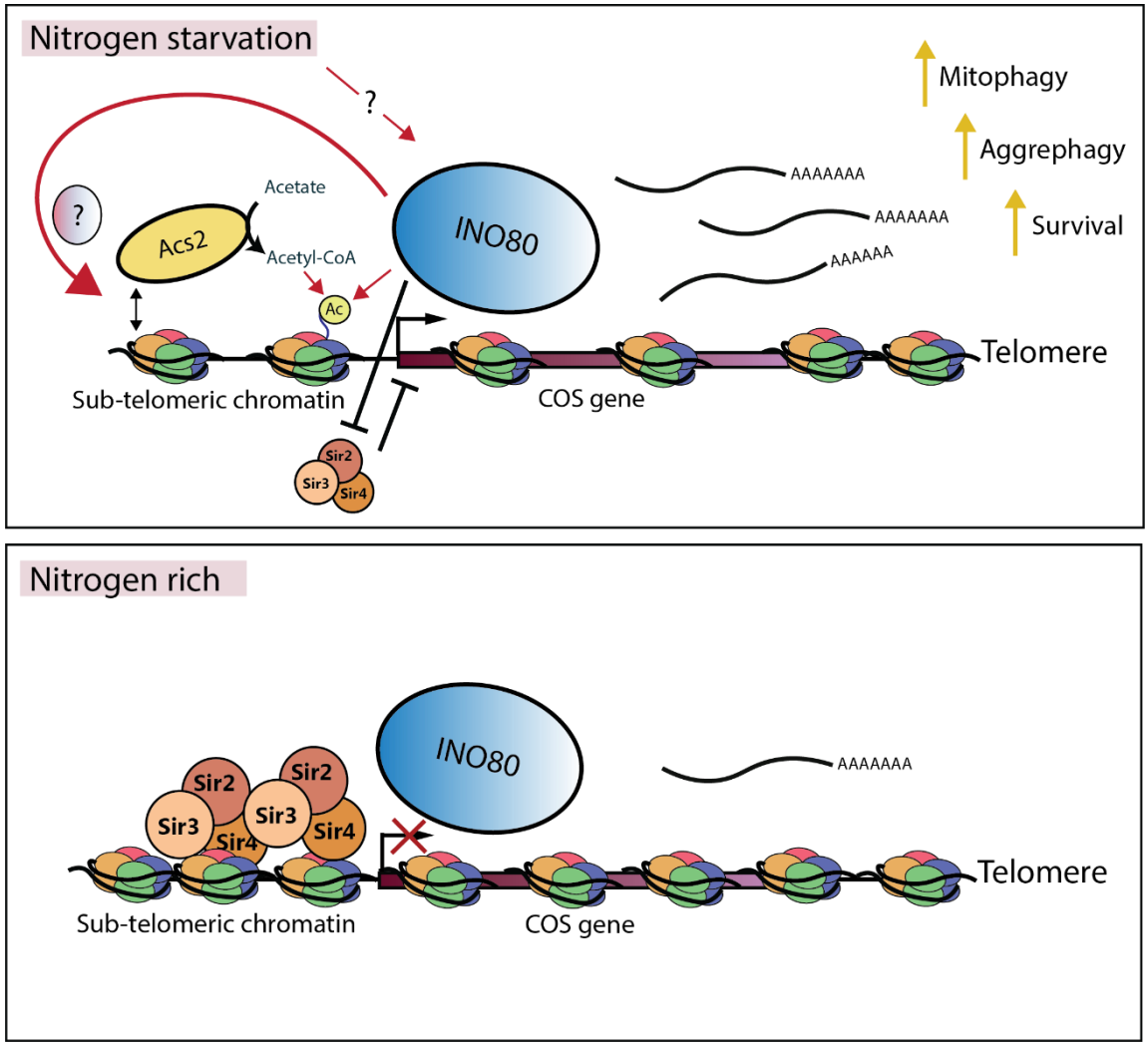

Figure 5.1. Proposed model of INO80 activity at *COS* gene promoters. Following nutrient depletion and the onset of nitrogen starvation, the activity of INO80 located at the subtelomeric promoters of *COS* genes leads to the activation of Cos transcription. INO80 counteracts the repressive activity of SIR complex proteins by decreasing SIR enrichment at *COS* promoters. (Continued overleaf)

Concomitantly, INO80 promotes the acetylation of *COS* promoter-proximal histones, in particular at the H3K9 residue, by promoting the recruitment of Acs2. Whether INO80 directly recruits Acs2 or the recruitment is mediated by an additional factor (signified by "?") is not yet known. Acs2 activity promotes histone acetylation by increasing the available pool of acetyl-CoA at sub-telomeric chromatin. Together this results in an open chromatin state which promotes the expression of *COS* gene mRNA, leading to the production of Cos proteins. The production of Cos proteins leads to increased budding yeast survival in starvation conditions by promoting selective autophagy of mitochondria and turnover of protein aggregates. How the metabolic state of the cell is signalled to INO80 is not clear.

In non-starved, nitrogen rich conditions, INO80 does not counteract the repressive activity of SIR complex on *COS* genes, and SIR proteins accumulate at the promoters of *COS* genes. Sir2 deacetylase activity counteracts H3K9 acetylation, and the resulting chromatin state is more compact and inhibitory to transcription. This leads to markedly reduced *COS* expression in non-starved conditions.

5.14. Conclusion and future work

The onset of metabolic stress requires organisms to respond rapidly and correctly to ensure survival. Despite this, the epigenetic regulation of stress response and particularly selective autophagy remains poorly understood.

Here we have shown that the ATP dependent chromatin remodelling complex INO80 promotes the selective autophagy of ubiquitinated protein aggregates, ER and the mitochondria. We demonstrate that the complex activity is required for survival in response to nitrogen starvation and propose this is likely through its regulation of selective autophagy. INO80 promotes ubiquitin turnover and survival following starvation through counter-acting Sir-dependent silencing, coinciding with increased acetylation and Acs2 recruitment. Finally, this epigenetic regulation derepresses *COS* genes following nitrogen starvation which we find to be novel regulators of mitophagy.

Our study expands the understanding of budding yeast stress response, highlighting INO80's role in regulating telomere silencing and the novel function of the *COS* genes during nitrogen starvation. Future work studying the regulation of INO80 by the TOR pathway should investigate the effects of complex phosphorylation and ubiquitination following starvation to understand how this pathway is controlled. The Cos proteins remain poorly understood and their newly identified role in mitophagy as well as their probable localisation to multiple membrane bound organelles makes their cellular function likely broader then currently known. Our work singles out the *COS* gene family as important targets of study. Understanding the mechanistic role of ubiquitinated Cos proteins in mitophagy will increase understanding of protein sorting in budding yeast and how endosomal sorting co-operates with autophagy.

The role of acetyl-CoA generation in telomere silencing has only recently been discovered and our finding that INO80 recruits Acs2 opens interesting new directions for study. Establishing the mechanism through which INO80 recruits Acs2 would expand our understanding of both INO80 and telomere silencing.

Our study presents exciting new functions for the INO80 complex which is strongly conserved throughout evolution and defects of it are known to contribute to human disease and cancer.

Appropriate nutrient stress response and regulation of selective autophagy are widely implicated in human disease (Choi et al., 2013; Schneider and Cuervo, 2014) and mis-regulation of these pathways are hallmarks of cancer (Anderson and Macleod, 2019).

Epigenetic control of these pathways is an emerging field and still poorly understood. Thus, the work presented here furthers the understanding of epigenetic control of budding yeast nutrient stress response and offers avenues of further investigation of epigenetic pathways controlling stress response in higher eukaryotes.

Better understanding the vital complex and exploring its role in connecting metabolic state with epigenetic regulation would greatly expand our understanding of these critical conditions.

Our study leads to many interesting research questions requiring further investigation.

In conclusion, we propose that starvation conditions increase the need for strict control of heterochromatin-euchromatin boundaries, in part to ensure *COS* expression. Through its recruitment of Acs2, INO80 promotes this process and thus promotes clearance of ubiquitinated proteins, mitophagy and enables survival in starvation conditions.

References

Abeliovich, H., Zarei, M., Rigbolt, K.T.G., Youle, R.J., Dengjel, J., 2013. Involvement of mitochondrial dynamics in the segregation of mitochondrial matrix proteins during stationary phase mitophagy. Nat Commun 4, 1–11. https://doi.org/10.1038/ncomms3789

Agalioti, T., Chen, G., Thanos, D., 2002. Deciphering the Transcriptional Histone Acetylation Code for a Human Gene. Cell 111, 381–392. https://doi.org/10.1016/S0092-8674(02)01077-2

Ai, W., Bertram, P.G., Tsang, C.K., Chan, T.-F., Zheng, X.F.S., 2002. Regulation of Subtelomeric Silencing during Stress Response. Molecular Cell 10, 1295–1305. https://doi.org/10.1016/S1097-2765(02)00695-0

Alberts, B., Johnson, A., Lewis, J., Raff, M., Roberts, K., Walter, P., 2002. Fractionation of Cells. Molecular Biology of the Cell. 4th edition.

An, Z., Tassa, A., Thomas, C., Zhong, R., Xiao, G., Fotedar, R., Tu, B.P., Klionsky, D.J., Levine, B., 2014. Autophagy is required for G1/G0 quiescence in response to nitrogen starvation in Saccharomyces cerevisiae. Autophagy 10, 1702–1711. https://doi.org/10.4161/auto.32122

Anderson, C.M., Macleod, K.F., 2019. Autophagy and cancer cell metabolism. Int Rev Cell Mol Biol 347, 145–190. https://doi.org/10.1016/bs.ircmb.2019.06.002

Aranguren, M.E., Bechhofer, S., Lord, P., Sattler, U., Stevens, R., 2007. Understanding and using the meaning of statements in a bio-ontology: recasting the Gene Ontology in OWL. BMC Bioinformatics 8, 57. https://doi.org/10.1186/1471-2105-8-57

Attikum, H. van, Fritsch, O., Hohn, B., Gasser, S.M., 2004. Recruitment of the INO80 Complex by H2A Phosphorylation Links ATP-Dependent Chromatin Remodeling with DNA Double-Strand Break Repair. Cell 119, 777–788. https://doi.org/10.1016/j.cell.2004.11.033

Babst, M., Odorizzi, G., 2013. The balance of protein expression and degradation: an ESCRTs point of view. Current Opinion in Cell Biology, Cell organelles 25, 489–494. https://doi.org/10.1016/j.ceb.2013.05.003

Beck, T., Hall, M.N., 1999. The TOR signalling pathway controls nuclear localization of nutrient-regulated transcription factors. Nature 402, 689–692. https://doi.org/10.1038/45287

Beckwith, S.L., Schwartz, E.K., Garc, P.E., 2018. The INO80 chromatin remodeler sustains metabolic stability by promoting TOR signaling and regulating histone acetylation. Plos Genetics 28.

Bekers, K.M., Heijnen, J.J., van Gulik, W.M., 2015. Determination of the in vivo NAD:NADH ratio in Saccharomyces cerevisiae under anaerobic conditions, using alcohol dehydrogenase as sensor reaction. Yeast 32, 541–557. https://doi.org/10.1002/yea.3078

Belenky, P., Racette, F.G., Bogan, K.L., McClure, J.M., Smith, J.S., Brenner, C., 2007. Nicotinamide Riboside Promotes Sir2 Silencing and Extends Lifespan via Nrk and Urh1/Pnp1/Meu1 Pathways to NAD+. Cell 129, 473–484. https://doi.org/10.1016/j.cell.2007.03.024

Beriault, D.R., Werstuck, G.H., 2013. Detection and quantification of endoplasmic reticulum stress in living cells using the fluorescent compound, Thioflavin T. Biochimica et Biophysica Acta (BBA) - Molecular Cell Research 1833, 2293–2301. https://doi.org/10.1016/j.bbamcr.2013.05.020

Bieganowski, P., Brenner, C., 2004. Discoveries of Nicotinamide Riboside as a Nutrient and Conserved NRK Genes Establish a Preiss-Handler Independent Route to NAD+ in

Fungi and Humans. Cell 117, 495–502. https://doi.org/10.1016/S0092-8674(04)00416-7

Bonnet, J., Wang, C.-Y., Baptista, T., Vincent, S.D., Hsiao, W.-C., Stierle, M., Kao, C.-F., Tora, L., Devys, D., 2014. The SAGA coactivator complex acts on the whole transcribed genome and is required for RNA polymerase II transcription. Genes Dev 28, 1999–2012. https://doi.org/10.1101/gad.250225.114

Bosch-Presegué, L., Vaquero, A., 2015. Sirtuin-dependent epigenetic regulation in the maintenance of genome integrity. The FEBS Journal 282, 1745–1767. https://doi.org/10.1111/febs.13053

Carmen, A.A., Milne, L., Grunstein, M., 2002. Acetylation of the Yeast Histone H4 N Terminus Regulates Its Binding to Heterochromatin Protein SIR3*. Journal of Biological Chemistry 277, 4778–4781. https://doi.org/10.1074/jbc.M110532200

Chen, R.-H., Chen, Y.-H., Huang, T.-Y., 2019. Ubiquitin-mediated regulation of autophagy. Journal of Biomedical Science 26, 80. https://doi.org/10.1186/s12929-019-0569-y

Chen, W., Yu, X., Wu, Y., Tang, J., Yu, Q., Lv, X., Zha, Z., Hu, B., Li, X., Chen, J., Ma, L., Workman, J.L., Li, S., 2021. The SESAME complex regulates cell senescence through the generation of acetyl-CoA. Nat Metab 3, 983–1000. https://doi.org/10.1038/s42255-021-00412-9

Choi, A.M.K., Ryter, S.W., Levine, B., 2013. Autophagy in Human Health and Disease. N Engl J Med 368, 651–662. https://doi.org/10.1056/NEJMra1205406

Chu, S., Herskowitz, I., 1998. Gametogenesis in Yeast Is Regulated by a Transcriptional Cascade Dependent on Ndt80. Molecular Cell 1, 685–696. https://doi.org/10.1016/S1097-2765(00)80068-4

Costanzo, M., VanderSluis, B., Koch, E.N., Baryshnikova, A., Pons, C., Tan, G., Wang, W., Usaj, M., Hanchard, J., Lee, S.D., Pelechano, V., Styles, E.B., Billmann, M., Leeuwen, J. van, Dyk, N. van, Lin, Z.-Y., Kuzmin, E., Nelson, J., Piotrowski, J.S., Srikumar, T., Bahr, S., Chen, Y., Deshpande, R., Kurat, C.F., Li, S.C., Li, Z., Usaj, M.M., Okada, H., Pascoe, N., Luis, B.-J.S., Sharifpoor, S., Shuteriqi, E., Simpkins, S.W., Snider, J., Suresh, H.G., Tan, Y., Zhu, H., Malod-Dognin, N., Janjic, V., Przulj, N., Troyanskaya, O.G., Stagljar, I., Xia, T., Ohya, Y., Gingras, A.-C., Raught, B., Boutros, M., Steinmetz, L.M., Moore, C.L., Rosebrock, A.P., Caudy, A.A., Myers, C.L., Andrews, B., Boone, C., 2016. A global genetic interaction network maps a wiring diagram of cellular function. Science 353, aaf1420. https://doi.org/10.1126/science.aaf1420

Cui, Y., Parashar, S., Zahoor, M., Needham, P.G., Mari, M., Zhu, M., Chen, S., Ho, H.-C., Reggiori, F., Farhan, H., Brodsky, J.L., Ferro-Novick, S., 2019. A COPII subunit acts with an autophagy receptor to target endoplasmic reticulum for degradation. Science 365, 53–60. https://doi.org/10.1126/science.aau9263

Dargemont, C., Ossareh-Nazari, B., 2012. Cdc48/p97, a key actor in the interplay between autophagy and ubiquitin/proteasome catabolic pathways. Biochimica et Biophysica Acta (BBA) - Molecular Cell Research 1823, 138–144. https://doi.org/10.1016/j.bbamcr.2011.07.011

De Las Peñas, A., Juárez-Cepeda, J., López-Fuentes, E., Briones-Martín-del-Campo, M., Gutiérrez-Escobedo, G., Castaño, I., 2015. Local and regional chromatin silencing in Candida glabrata: consequences for adhesion and the response to stress. FEMS Yeast Research 15, fov056. https://doi.org/10.1093/femsyr/fov056

Deffieu, M., Bhatia-Kiššová, I., Salin, B., Galinier, A., Manon, S., Camougrand, N., 2009. Glutathione Participates in the Regulation of Mitophagy in Yeast *. Journal of Biological Chemistry 284, 14828–14837. https://doi.org/10.1074/jbc.M109.005181

Despons, L., Wirth, B., Louis, V.L., Potier, S., Souciet, J.-L., 2006. An evolutionary scenario for one of the largest yeast gene families. Trends in Genetics 22, 10–15. https://doi.org/10.1016/j.tig.2005.10.001

Dikic, I., 2017. Proteasomal and Autophagic Degradation Systems. Annual Review of Biochemistry 86, 193–224. https://doi.org/10.1146/annurev-biochem-061516-044908

Dion, V., Shimada, K., Gasser, S.M., 2010. Actin-related proteins in the nucleus: life beyond chromatin remodelers. Current Opinion in Cell Biology, Nucleus and gene expression 22, 383–391. https://doi.org/10.1016/j.ceb.2010.02.006

Dirick, L., Goetsch, L., Ammerer, G., Byers, B., 1998. Regulation of Meiotic S Phase by Ime2 and a Clb5,6-Associated Kinase in Saccharomyces cerevisiae. Science 281, 1854–1857. https://doi.org/10.1126/science.281.5384.1854

Dobson, C.M., 2003. Protein folding and misfolding. Nature 426, 884–890. https://doi.org/10.1038/nature02261

Ebbert, R., Birkmann, A., Schüller, H.-J., 1999. The product of the SNF2/SWI2 paralogue INO80 of Saccharomyces cerevisiae required for efficient expression of various yeast structural genes is part of a high-molecular-weight protein complex. Molecular Microbiology 32, 741–751. https://doi.org/10.1046/j.1365-2958.1999.01390.x

Eberharter, A., Ferreira, R., Becker, P., 2005. Dynamic chromatin: concerted nucleosome remodelling and acetylation 386, 745–751. https://doi.org/10.1515/BC.2005.087

Eisenberg, T., Schroeder, S., Andryushkova, A., Pendl, T., Küttner, V., Bhukel, A., Mariño, G., Pietrocola, F., Harger, A., Zimmermann, A., Moustafa, T., Sprenger, A., Jany, E., Büttner, S., Carmona-Gutierrez, D., Ruckenstuhl, C., Ring, J., Reichelt, W., Schimmel, K., Leeb, T., Moser, C., Schatz, S., Kamolz, L.-P., Magnes, C., Sinner, F., Sedej, S., Fröhlich, K.-U., Juhasz, G., Pieber, T.R., Dengjel, J., Sigrist, S.J., Kroemer, G., Madeo, F., 2014. Nucleocytosolic Depletion of the Energy Metabolite Acetyl-Coenzyme A Stimulates Autophagy and Prolongs Lifespan. Cell Metabolism 19, 431–444. https://doi.org/10.1016/j.cmet.2014.02.010

Eiyama, A., Okamoto, K., 2017. Assays for Mitophagy in Yeast, in: Mokranjac, D., Perocchi, F. (Eds.), Mitochondria: Practical Protocols, Methods in Molecular Biology. Springer, New York, NY, pp. 337–347. https://doi.org/10.1007/978-1-4939-6824-4_20

Eustermann, S., Schall, K., Kostrewa, D., Lakomek, K., Strauss, M., Moldt, M., Hopfner, K.-P., 2018a. Structural basis for ATP-dependent chromatin remodelling by the INO80 complex. Nature 556, 386–390. https://doi.org/10.1038/s41586-018-0029-y

Eustermann, S., Schall, K., Kostrewa, D., Lakomek, K., Strauss, M., Moldt, M., Hopfner, K.-P., 2018b. Structural basis for ATP-dependent chromatin remodelling by the INO80 complex. Nature 556, 386–390. https://doi.org/10.1038/s41586-018-0029-y

Farré, J.-C., Subramani, S., 2016. Mechanistic insights into selective autophagy pathways: lessons from yeast. Nature Reviews Molecular Cell Biology 17, 537–552. https://doi.org/10.1038/nrm.2016.74

Feldman, J.L., Dittenhafer-Reed, K.E., Denu, J.M., 2012. Sirtuin Catalysis and Regulation *. Journal of Biological Chemistry 287, 42419–42427. https://doi.org/10.1074/jbc.R112.378877

Filimonenko, M., Stuffers, S., Raiborg, C., Yamamoto, A., Malerød, L., Fisher, E.M.C., Isaacs, A., Brech, A., Stenmark, H., Simonsen, A., 2007. Functional multivesicular bodies are required for autophagic clearance of protein aggregates associated with neurodegenerative disease. J Cell Biol 179, 485–500. https://doi.org/10.1083/jcb.200702115

Flick, J.S., Johnston, M., 1990. Two systems of glucose repression of the GAL1 promoter in Saccharomyces cerevisiae. Mol Cell Biol 10, 4757–4769.

Gartenberg, M.R., Smith, J.S., 2016. The Nuts and Bolts of Transcriptionally Silent Chromatin in Saccharomyces cerevisiae. Genetics 203, 1563–1599. https://doi.org/10.1534/genetics.112.145243

Gatica, D., Lahiri, V., Klionsky, D.J., 2018. Cargo recognition and degradation by selective autophagy. Nature Cell Biology 20, 233–242. https://doi.org/10.1038/s41556-018-0037-z

Goeman, J.J., Mansmann, U., 2008. Multiple testing on the directed acyclic graph of gene ontology. Bioinformatics 24, 537–544. https://doi.org/10.1093/bioinformatics/btm628

Gowans, G.J., Schep, A.N., Wong, K.M., King, D.A., Greenleaf, W.J., Morrison, A.J., 2018a. INO80 Chromatin Remodeling Coordinates Metabolic Homeostasis with Cell Division. Cell Reports 22, 611–623. https://doi.org/10.1016/j.celrep.2017.12.079

Gowans, G.J., Schep, A.N., Wong, K.M., King, D.A., Greenleaf, W.J., Morrison, A.J., 2018b. INO80 Chromatin Remodeling Coordinates Metabolic Homeostasis with Cell Division. Cell Reports 22, 611–623. https://doi.org/10.1016/j.celrep.2017.12.079

Gray, J.V., Petsko, G.A., Johnston, G.C., Ringe, D., Singer, R.A., Werner-Washburne, M., 2004. “Sleeping Beauty”: Quiescence in Saccharomyces cerevisiae. Microbiology and Molecular Biology Reviews 68, 187–206. https://doi.org/10.1128/MMBR.68.2.187-206.2004

Gross, A.S., Graef, M., 2020. Mechanisms of Autophagy in Metabolic Stress Response. Journal of Molecular Biology, Molecular Mechanisms of Selective Autophagy 432, 28–52. https://doi.org/10.1016/j.jmb.2019.09.005

Guizetti, J., Schermelleh, L., Mäntler, J., Maar, S., Poser, I., Leonhardt, H., Müller-Reichert, T., Gerlich, D.W., 2011. Cortical Constriction During Abscission Involves Helices of ESCRT-III–Dependent Filaments. Science 331, 1616–1620. https://doi.org/10.1126/science.1201847

Hatakeyama, R., De Virgilio, C., 2019. TORC1 specifically inhibits microautophagy through ESCRT-0. Curr Genet. https://doi.org/10.1007/s00294-019-00982-y

Hecht, A., Laroche, T., Strahl-Bolsinger, S., Gasser, S.M., Grunstein, M., 1995. Histone H3 and H4 N-termini interact with SIR3 and SIR4 proteins: A molecular model for the formation of heterochromatin in yeast. Cell 80, 583–592. https://doi.org/10.1016/0092-8674(95)90512-X

Hecht, A., Strahl-Bolsinger, S., Grunstein, M., 1996. Spreading of transcriptional represser SIR3 from telomeric heterochromatin. Nature 383, 92–96. https://doi.org/10.1038/383092a0

Henne, W.M., Buchkovich, N.J., Emr, S.D., 2011. The ESCRT Pathway. Developmental Cell 21, 77–91. https://doi.org/10.1016/j.devcel.2011.05.015

Huh, W.-K., Falvo, J.V., Gerke, L.C., Carroll, A.S., Howson, R.W., Weissman, J.S., O’Shea, E.K., 2003. Global analysis of protein localization in budding yeast. Nature 425, 686–691. https://doi.org/10.1038/nature02026

Iesmantavicius, V., Weinert, B.T., Choudhary, C., 2014. Convergence of ubiquitylation and phosphorylation signaling in rapamycin-treated yeast cells. Mol. Cell Proteomics 13, 1979–1992. https://doi.org/10.1074/mcp.O113.035683

Imai, S., Armstrong, C.M., Kaeberlein, M., Guarente, L., 2000. Transcriptional silencing and longevity protein Sir2 is an NAD-dependent histone deacetylase. Nature 403, 795–800. https://doi.org/10.1038/35001622

Jethmalani, Y., Tran, K., Negesse, M.Y., Sun, W., Ramos, M., Jaiswal, D., Jezek, M., Amos, S., Garcia, E.J., Park, D., Green, E.M., 2021. Set4 regulates stress response genes and coordinates histone deacetylases within yeast subtelomeres. Life Science Alliance 4. https://doi.org/10.26508/lsa.202101126

Jónsson, Z.O., Jha, S., Wohlschlegel, J.A., Dutta, A., 2004. Rvb1p/Rvb2p Recruit Arp5p and Assemble a Functional Ino80 Chromatin Remodeling Complex. Molecular Cell 16, 465–477. https://doi.org/10.1016/j.molcel.2004.09.033

Jumper, J., Evans, R., Pritzel, A., Green, T., Figurnov, M., Ronneberger, O., Tunyasuvunakool, K., Bates, R., Žídek, A., Potapenko, A., Bridgland, A., Meyer, C., Kohl, S.A.A., Ballard, A.J., Cowie, A., Romera-Paredes, B., Nikolov, S., Jain, R., Adler, J., Back, T., Petersen, S., Reiman, D., Clancy, E., Zielinski, M., Steinegger, M., Pacholska, M., Berghammer, T., Bodenstein, S., Silver, D., Vinyals, O., Senior, A.W., Kavukcuoglu, K., Kohli, P., Hassabis, D., 2021. Highly accurate protein structure prediction with AlphaFold. Nature 596, 583–589. https://doi.org/10.1038/s41586-021-03819-2

Kaeberlein, M., R. Wilson Powers, I.I.I., Steffen, K.K., Westman, E.A., Hu, D., Dang, N., Kerr, E.O., Kirkland, K.T., Fields, S., Kennedy, B.K., 2005. Regulation of Yeast Replicative Life Span by TOR and Sch9 in Response to Nutrients. Science. https://doi.org/10.1126/science.1115535

Kanki, T., Kurihara, Y., Jin, X., Goda, T., Ono, Y., Aihara, M., Hirota, Y., Saigusa, T., Aoki, Y., Uchiumi, T., Kang, D., 2013. Casein kinase 2 is essential for mitophagy. EMBO reports 14, 788–794. https://doi.org/10.1038/embor.2013.114

Karavaeva, I.E., Golyshev, S.A., Smirnova, E.A., Sokolov, S.S., Severin, F.F., Knorre, D.A., 2017. Mitochondrial depolarization in yeast zygotes inhibits clonal expansion of selfish mtDNA. J Cell Sci 130, 1274–1284. https://doi.org/10.1242/jcs.197269

Kassir, Y., Granot, D., Simchen, G., 1988. IME1, a positive regulator gene of meiosis in S. cerevisiae. Cell 52, 853–862. https://doi.org/10.1016/0092-8674(88)90427-8

Kataura, T., Sedlackova, L., Otten, E.G., Kumari, R., Shapira, D., Scialo, F., Stefanatos, R., Ishikawa, K., Kelly, G., Seranova, E., Sun, C., Maetzel, D., Kenneth, N., Trushin, S., Zhang, T., Trushina, E., Bascom, C.C., Tasseff, R., Isfort, R.J., Oblong, J.E., Miwa, S., Lazarou, M., Jaenisch, R., Imoto, M., Saiki, S., Papamichos-Chronakis, M., Manjithaya, R., Maddocks, O.D.K., Sanz, A., Sarkar, S., Korolchuk, V.I., 2022. Autophagy promotes cell survival by maintaining NAD levels. Developmental Cell 57, 2584-2598.e11. https://doi.org/10.1016/j.devcel.2022.10.008

Kato, M., Lin, S.-J., 2014. Regulation of NAD+ metabolism, signaling and compartmentalization in the yeast Saccharomyces cerevisiae. DNA Repair (Amst) 0, 49–58. https://doi.org/10.1016/j.dnarep.2014.07.009

Keogh, M.-C., Mennella, T.A., Sawa, C., Berthelet, S., Krogan, N.J., Wolek, A., Podolny, V., Carpenter, L.R., Greenblatt, J.F., Baetz, K., Buratowski, S., 2006. The Saccharomyces cerevisiae histone H2A variant Htz1 is acetylated by NuA4. Genes Dev 20, 660–665. https://doi.org/10.1101/gad.1388106

Khaminets, A., Behl, C., Dikic, I., 2016. Ubiquitin-Dependent And Independent Signals In Selective Autophagy. Trends in Cell Biology 26, 6–16. https://doi.org/10.1016/j.tcb.2015.08.010

Kim, J., Guan, K.-L., 2019. mTOR as a central hub of nutrient signalling and cell growth. Nature Cell Biology 21, 63. https://doi.org/10.1038/s41556-018-0205-1

Kimura, A., Umehara, T., Horikoshi, M., 2002. Chromosomal gradient of histone acetylation established by Sas2p and Sir2p functions as a shield against gene silencing. Nat Genet 32, 370–377. https://doi.org/10.1038/ng993

Klopf, E., Paskova, L., Solé, C., Mas, G., Petryshyn, A., Posas, F., Wintersberger, U., Ammerer, G., Schüller, C., 2009. Cooperation between the INO80 Complex and Histone Chaperones Determines Adaptation of Stress Gene Transcription in the Yeast Saccharomyces cerevisiae. Molecular and Cellular Biology 29, 4994–5007. https://doi.org/10.1128/MCB.01858-08

Klopf, E., Schmidt, H.A., Clauder-Münster, S., Steinmetz, L.M., Schüller, C., 2017. INO80 represses osmostress induced gene expression by resetting promoter proximal nucleosomes. Nucleic Acids Res. 45, 3752–3766. https://doi.org/10.1093/nar/gkw1292

Klosinska, M.M., Crutchfield, C.A., Bradley, P.H., Rabinowitz, J.D., Broach, J.R., 2011. Yeast cells can access distinct quiescent states. Genes Dev. 25, 336–349. https://doi.org/10.1101/gad.2011311

Knoll, K.R., Eustermann, S., Niebauer, V., Oberbeckmann, E., Stoehr, G., Schall, K., Tosi, A., Schwarz, M., Buchfellner, A., Korber, P., Hopfner, K.-P., 2018. The nuclear actin-containing Arp8 module is a linker DNA sensor driving INO80 chromatin remodeling. Nat Struct Mol Biol 25, 823–832. https://doi.org/10.1038/s41594-018-0115-8

Krietenstein, N., Wal, M., Watanabe, S., Park, B., Peterson, C.L., Pugh, B.F., Korber, P., 2016. Genomic Nucleosome Organization Reconstituted with Pure Proteins. Cell 167, 709-721.e12. https://doi.org/10.1016/j.cell.2016.09.045

Kueng, S., Oppikofer, M., Gasser, S.M., 2013. SIR Proteins and the Assembly of Silent Chromatin in Budding Yeast. Annual Review of Genetics 47, 275–306. https://doi.org/10.1146/annurev-genet-021313-173730

Kurihara, Y., Kanki, T., Aoki, Y., Hirota, Y., Saigusa, T., Uchiumi, T., Kang, D., 2012. Mitophagy Plays an Essential Role in Reducing Mitochondrial Production of Reactive Oxygen Species and Mutation of Mitochondrial DNA by Maintaining Mitochondrial Quantity and Quality in Yeast*. Journal of Biological Chemistry 287, 3265–3272. https://doi.org/10.1074/jbc.M111.280156

Lafon, A., Taranum, S., Pietrocola, F., Dingli, F., Loew, D., Brahma, S., Bartholomew, B., Papamichos-Chronakis, M., 2015. INO80 Chromatin Remodeler Facilitates Release of RNA Polymerase II from Chromatin for Ubiquitin-Mediated Proteasomal Degradation. Molecular Cell 60, 784–796. https://doi.org/10.1016/j.molcel.2015.10.028

Landry, J., Slama, J.T., Sternglanz, R., 2000. Role of NAD+ in the Deacetylase Activity of the SIR2-like Proteins. Biochemical and Biophysical Research Communications 278, 685–690. https://doi.org/10.1006/bbrc.2000.3854

Lee, J.-A., Beigneux, A., Ahmad, S.T., Young, S.G., Gao, F.-B., 2007. ESCRT-III Dysfunction Causes Autophagosome Accumulation and Neurodegeneration. Current Biology 17, 1561–1567. https://doi.org/10.1016/j.cub.2007.07.029

Lee, S., Gaspar, M.L., Aregullin, M.A., Jesch, S.A., Henry, S.A., 2013. Activation of protein kinase C-mitogen-activated protein kinase signaling in response to inositol starvation triggers Sir2p-dependent telomeric silencing in yeast. J Biol Chem 288, 27861–27871. https://doi.org/10.1074/jbc.M113.493072

Li, H., Sun, S., 2021. Protein Aggregation in the ER: Calm behind the Storm. Cells 10, 3337. https://doi.org/10.3390/cells10123337

Li, X., Egervari, G., Wang, Y., Berger, S.L., Lu, Z., 2018. Regulation of chromatin and gene expression by metabolic enzymes and metabolites. Nat Rev Mol Cell Biol 19, 563–578. https://doi.org/10.1038/s41580-018-0029-7

Li, X., Yu, W., Qian, X., Xia, Y., Zheng, Y., Lee, J.-H., Li, W., Lyu, J., Rao, G., Zhang, X., Qian, C.-N., Rozen, S.G., Jiang, T., Lu, Z., 2017. Nucleus-Translocated ACSS2 Promotes Gene Transcription for Lysosomal Biogenesis and Autophagy. Molecular Cell 66, 684-697.e9. https://doi.org/10.1016/j.molcel.2017.04.026

Lin, S.-J., Defossez, P.-A., Guarente, L., 2000. Requirement of NAD and SIR2 for Life-Span Extension by Calorie Restriction in Saccharomyces cerevisiae. Science 289, 2126–2128. https://doi.org/10.1126/science.289.5487.2126

Lin, S.-J., Kaeberlein, M., Andalis, A.A., Sturtz, L.A., Defossez, P.-A., Culotta, V.C., Fink, G.R., Guarente, L., 2002. Calorie restriction extends Saccharomyces cerevisiae lifespan by increasing respiration. Nature 418, 344–348. https://doi.org/10.1038/nature00829

Loi, M., Fregno, I., Guerra, C., Molinari, M., 2018. Eat it right: ER-phagy and recovER-phagy. Biochemical Society Transactions 46, 699–706. https://doi.org/10.1042/BST20170354

Longtine, M.S., Mckenzie III, A., Demarini, D.J., Shah, N.G., Wach, A., Brachat, A., Philippsen, P., Pringle, J.R., 1998. Additional modules for versatile and economical PCR-based gene deletion and modification in Saccharomyces cerevisiae. Yeast 14, 953–961. https://doi.org/10.1002/(SICI)1097-0061(199807)14:10<953::AID-YEA293>3.0.CO;2-U

Lu, K., Psakhye, I., Jentsch, S., 2014. Autophagic Clearance of PolyQ Proteins Mediated by Ubiquitin-Atg8 Adaptors of the Conserved CUET Protein Family. Cell 158, 549–563. https://doi.org/10.1016/j.cell.2014.05.048

Luzzi, S., Szachnowski, U., Greener, S., Schumacher, K., Fulton, S., Gautier, C., Han, K.H., Darke, J., Piccinno, R., Lafon, A., Pugh, B.F., Devys, D., Tora, L., Morillon, A., Papamichos-Chronakis, M., 2021. Chromatin remodelling by INO80 at promoter proximal pause sites promotes premature termination of mRNA synthesis. https://doi.org/10.1101/2020.03.02.973685

MacDonald, C., Payne, J.A., Aboian, M., Smith, W., Katzmann, D.J., Piper, R.C., 2015. A Family of Tetraspans Organizes Cargo for Sorting into Multivesicular Bodies. Developmental Cell 33, 328–342. https://doi.org/10.1016/j.devcel.2015.03.007

Mao, K., Wang, K., Liu, X., Klionsky, D.J., 2013. The Scaffold Protein Atg11 Recruits Fission Machinery to Drive Selective Mitochondria Degradation by Autophagy. Developmental Cell 26, 9–18. https://doi.org/10.1016/j.devcel.2013.05.024

Marshall, R.S., Hua, Z., Mali, S., McLoughlin, F., Vierstra, R.D., 2019. ATG8-Binding UIM Proteins Define a New Class of Autophagy Adaptors and Receptors. Cell 0. https://doi.org/10.1016/j.cell.2019.02.009

Matsuura, A., Tsukada, M., Wada, Y., Ohsumi, Y., 1997. Apg1p, a novel protein kinase required for the autophagic process in Saccharomyces cerevisiae. Gene 192, 245–250. https://doi.org/10.1016/S0378-1119(97)00084-X

Miles, S., Bradley, G.T., Breeden, L.L., 2021. The budding yeast transition to quiescence. Yeast 38, 30–38. https://doi.org/10.1002/yea.3546

Mizuguchi, G., Shen, X., Landry, J., Wu, W.-H., Sen, S., Wu, C., 2004. ATP-Driven Exchange of Histone H2AZ Variant Catalyzed by SWR1 Chromatin Remodeling Complex. Science 303, 343–348. https://doi.org/10.1126/science.1090701

Mizuno, T., Irie, K., 2021. Msn2/4 transcription factors positively regulate expression of Atg39 ER-phagy receptor. Sci Rep 11, 11919. https://doi.org/10.1038/s41598-021-91480-0

Mizuno, T., Muroi, K., Irie, K., 2020. Snf1 AMPK positively regulates ER-phagy via expression control of Atg39 autophagy receptor in yeast ER stress response. PLOS Genetics 16, e1009053. https://doi.org/10.1371/journal.pgen.1009053

Mochida, K., Ohsumi, Y., Nakatogawa, H., 2014. Hrr25 phosphorylates the autophagic receptor Atg34 to promote vacuolar transport of α-mannosidase under nitrogen starvation conditions. FEBS Letters 588, 3862–3869. https://doi.org/10.1016/j.febslet.2014.09.032

Mochida, K., Oikawa, Y., Kimura, Y., Kirisako, H., Hirano, H., Ohsumi, Y., Nakatogawa, H., 2015. Receptor-mediated selective autophagy degrades the endoplasmic reticulum and the nucleus. Nature 522, 359–362. https://doi.org/10.1038/nature14506

Morrison, A.J., 2020. Chromatin-remodeling links metabolic signaling to gene expression. Molecular Metabolism, You Are What You Eat 38, 100973. https://doi.org/10.1016/j.molmet.2020.100973

Müller, M., Schmidt, O., Angelova, M., Faserl, K., Weys, S., Kremser, L., Pfaffenwimmer, T., Dalik, T., Kraft, C., Trajanoski, Z., Lindner, H., Teis, D., 2015. The coordinated action

of the MVB pathway and autophagy ensures cell survival during starvation. eLife 4. https://doi.org/10.7554/eLife.07736
Nair, U., Thumm, M., Klionsky, D.J., Krick, R., 2011. GFP-Atg8 protease protection as a tool to monitor autophagosome biogenesis. Autophagy 7, 1546–1550. https://doi.org/10.4161/auto.7.12.18424
Noda, T., Klionsky, D.J., 2008. Chapter 3 The Quantitative Pho8Δ60 Assay of Nonspecific Autophagy, in: Methods in Enzymology, Autophagy: Lower Eukaryotes and Non-Mammalian Systems, Part A. Academic Press, pp. 33–42. https://doi.org/10.1016/S0076-6879(08)03203-5
Okamoto, K., Kondo-Okamoto, N., Ohsumi, Y., 2009. Mitochondria-Anchored Receptor Atg32 Mediates Degradation of Mitochondria via Selective Autophagy. Developmental Cell 17, 87–97. https://doi.org/10.1016/j.devcel.2009.06.013
Onishi, M., Liou, G.-G., Buchberger, J.R., Walz, T., Moazed, D., 2007. Role of the conserved Sir3-BAH domain in nucleosome binding and silent chromatin assembly. Mol Cell 28, 1015–1028. https://doi.org/10.1016/j.molcel.2007.12.004
Onodera, J., Ohsumi, Y., 2005. Autophagy Is Required for Maintenance of Amino Acid Levels and Protein Synthesis under Nitrogen Starvation. J. Biol. Chem. 280, 31582–31586. https://doi.org/10.1074/jbc.M506736200
Oppikofer, M., Kueng, S., Martino, F., Soeroes, S., Hancock, S.M., Chin, J.W., Fischle, W., Gasser, S.M., 2011. A dual role of H4K16 acetylation in the establishment of yeast silent chromatin. The EMBO Journal 30, 2610–2621. https://doi.org/10.1038/emboj.2011.170
Orlandi, I., Pellegrino Coppola, D., Strippoli, M., Ronzulli, R., Vai, M., 2017. Nicotinamide supplementation phenocopies SIR2 inactivation by modulating carbon metabolism and respiration during yeast chronological aging. Mechanisms of Ageing and Development, SI:Yeast life and death 161, 277–287. https://doi.org/10.1016/j.mad.2016.06.006
Oslowski, C.M., Urano, F., 2011. Chapter Four - Measuring ER Stress and the Unfolded Protein Response Using Mammalian Tissue Culture System, in: Conn, P.M. (Ed.), Methods in Enzymology, The Unfolded Protein Response and Cellular Stress, Part B. Academic Press, pp. 71–92. https://doi.org/10.1016/B978-0-12-385114-7.00004-0
Pakos-Zebrucka, K., Koryga, I., Mnich, K., Ljujic, M., Samali, A., Gorman, A.M., 2016. The integrated stress response. EMBO reports 17, 1374–1395. https://doi.org/10.15252/embr.201642195
Papamichos-Chronakis, M., Peterson, C.L., 2008a. The Ino80 chromatin-remodeling enzyme regulates replisome function and stability. Nature Structural & Molecular Biology 15, 338–345. https://doi.org/10.1038/nsmb.1413
Papamichos-Chronakis, M., Peterson, C.L., 2008b. The Ino80 chromatin-remodeling enzyme regulates replisome function and stability. Nature Structural & Molecular Biology 15, 338–345. https://doi.org/10.1038/nsmb.1413
Papamichos-Chronakis, M., Watanabe, S., Rando, O.J., Peterson, C.L., 2011a. Global Regulation of H2A.Z Localization by the INO80 Chromatin-Remodeling Enzyme Is Essential for Genome Integrity. Cell 144, 200–213. https://doi.org/10.1016/j.cell.2010.12.021
Papamichos-Chronakis, M., Watanabe, S., Rando, O.J., Peterson, C.L., 2011b. Global Regulation of H2A.Z Localization by the INO80 Chromatin-Remodeling Enzyme Is Essential for Genome Integrity. Cell 144, 200–213. https://doi.org/10.1016/j.cell.2010.12.021
Parsons, X.H., Garcia, S.N., Pillus, L., Kadonaga, J.T., 2003. Histone deacetylation by Sir2 generates a transcriptionally repressed nucleoprotein complex. Proceedings of the

National Academy of Sciences 100, 1609–1614. https://doi.org/10.1073/pnas.0434064100
Piper, R.C., Katzmann, D.J., 2007. Biogenesis and Function of Multivesicular Bodies. Annual Review of Cell and Developmental Biology 23, 519–547. https://doi.org/10.1146/annurev.cellbio.23.090506.123319
Pokholok, D.K., Harbison, C.T., Levine, S., Cole, M., Hannett, N.M., Lee, T.I., Bell, G.W., Walker, K., Rolfe, P.A., Herbolsheimer, E., Zeitlinger, J., Lewitter, F., Gifford, D.K., Young, R.A., 2005. Genome-wide Map of Nucleosome Acetylation and Methylation in Yeast. Cell 122, 517–527. https://doi.org/10.1016/j.cell.2005.06.026
Poli, J., Gasser, S.M., Papamichos-Chronakis, M., 2017a. The INO80 remodeller in transcription, replication and repair. Philosophical Transactions of the Royal Society B: Biological Sciences 372, 20160290. https://doi.org/10.1098/rstb.2016.0290
Poli, J., Gasser, S.M., Papamichos-Chronakis, M., 2017b. The INO80 remodeller in transcription, replication and repair. Philosophical Transactions of the Royal Society B: Biological Sciences 372, 20160290. https://doi.org/10.1098/rstb.2016.0290
Radman-Livaja, M., Ruben, G., Weiner, A., Friedman, N., Kamakaka, R., Rando, O.J., 2011. Dynamics of Sir3 spreading in budding yeast: secondary recruitment sites and euchromatic localization. The EMBO Journal 30, 1012–1026. https://doi.org/10.1038/emboj.2011.30
Raiborg, C., Stenmark, H., 2009. The ESCRT machinery in endosomal sorting of ubiquitylated membrane proteins. Nature 458, 445–452. https://doi.org/10.1038/nature07961
Riesen, M., Morgan, A., 2009. Calorie restriction reduces rDNA recombination independently of rDNA silencing. Aging Cell 8, 624–632. https://doi.org/10.1111/j.1474-9726.2009.00514.x
Ringel, A.E., Ryznar, R., Picariello, H., Huang, K., Lazarus, A.G., Holmes, S.G., 2013. Yeast Tdh3 (Glyceraldehyde 3-Phosphate Dehydrogenase) Is a Sir2-Interacting Factor That Regulates Transcriptional Silencing and rDNA Recombination. PLOS Genetics 9, e1003871. https://doi.org/10.1371/journal.pgen.1003871
Ross, C.A., Poirier, M.A., 2004. Protein aggregation and neurodegenerative disease. Nat Med 10, S10–S17. https://doi.org/10.1038/nm1066
Rusten, T.E., Filimonenko, M., Rodahl, L.M., Stenmark, H., Simonsen, A., 2008. ESCRTing autophagic clearance of aggregating proteins. Autophagy 4, 233–236. https://doi.org/10.4161/auto.5396
Rusten, T.E., Vaccari, T., Lindmo, K., Rodahl, L.M.W., Nezis, I.P., Sem-Jacobsen, C., Wendler, F., Vincent, J.-P., Brech, A., Bilder, D., Stenmark, H., 2007. ESCRTs and Fab1 Regulate Distinct Steps of Autophagy. Current Biology 17, 1817–1825. https://doi.org/10.1016/j.cub.2007.09.032
Saksena, S., Emr, S.D., 2009. ESCRTs and human disease. Biochemical Society Transactions 37, 167–172. https://doi.org/10.1042/BST0370167
Sandell, L.L., Zakian, V.A., 1993. Loss of a yeast telomere: arrest, recovery, and chromosome loss. Cell 75, 729–739. https://doi.org/10.1016/0092-8674(93)90493-a
Santos-Rosa, H., Bannister, A.J., Dehe, P.M., Géli, V., Kouzarides, T., 2004. Methylation of H3 Lysine 4 at Euchromatin Promotes Sir3p Association with Heterochromatin *. Journal of Biological Chemistry 279, 47506–47512. https://doi.org/10.1074/jbc.M407949200
Schäfer, J.A., Schessner, J.P., Bircham, P.W., Tsuji, T., Funaya, C., Pajonk, O., Schaeff, K., Ruffini, G., Papagiannidis, D., Knop, M., Fujimoto, T., Schuck, S., 2020. ESCRT machinery mediates selective microautophagy of endoplasmic reticulum in yeast. The EMBO Journal 39, e102586. https://doi.org/10.15252/embj.2019102586

Schiestl, R.H., Gietz, R.D., 1989. High efficiency transformation of intact yeast cells using single stranded nucleic acids as a carrier. Curr Genet 16, 339–346. https://doi.org/10.1007/BF00340712
Schneider, J.L., Cuervo, A.M., 2014. Autophagy and human disease: emerging themes. Curr Opin Genet Dev 0, 16–23. https://doi.org/10.1016/j.gde.2014.04.003
Schuck, S., Gallagher, C.M., Walter, P., 2014. ER-phagy mediates selective degradation of endoplasmic reticulum independently of the core autophagy machinery. Journal of Cell Science 127, 4078–4088. https://doi.org/10.1242/jcs.154716
Shen, X., Ranallo, R., Choi, E., Wu, C., 2003a. Involvement of Actin-Related Proteins in ATP-Dependent Chromatin Remodeling. Molecular Cell 12, 147–155. https://doi.org/10.1016/S1097-2765(03)00264-8
Shen, X., Ranallo, R., Choi, E., Wu, C., 2003b. Involvement of Actin-Related Proteins in ATP-Dependent Chromatin Remodeling. Molecular Cell 12, 147–155. https://doi.org/10.1016/S1097-2765(03)00264-8
Shintani, T., Mizushima, N., Ogawa, Y., Matsuura, A., Noda, T., Ohsumi, Y., 1999. Apg10p, a novel protein-conjugating enzyme essential for autophagy in yeast. The EMBO Journal 18, 5234–5241. https://doi.org/10.1093/emboj/18.19.5234
Smith, A., Ward, M.P., Garrett, S., 1998. Yeast PKA represses Msn2p/Msn4p-dependent gene expression to regulate growth, stress response and glycogen accumulation. The EMBO Journal 17, 3556–3564. https://doi.org/10.1093/emboj/17.13.3556
Spode, I., Maiwald, D., Hollenberg, C.P., Suckow, M., 2002. ATF/CREB Sites Present in Sub-telomeric Regions of Saccharomyces cerevisiae Chromosomes are Part of Promoters and Act as UAS/URS of Highly Conserved COS Genes. Journal of Molecular Biology 319, 407–420. https://doi.org/10.1016/S0022-2836(02)00322-4
Stolz, A., Ernst, A., Dikic, I., 2014. Cargo recognition and trafficking in selective autophagy. Nat Cell Biol 16, 495–501. https://doi.org/10.1038/ncb2979
Suzuki, S.W., Onodera, J., Ohsumi, Y., 2011. Starvation Induced Cell Death in Autophagy-Defective Yeast Mutants Is Caused by Mitochondria Dysfunction. PLOS ONE 6, e17412. https://doi.org/10.1371/journal.pone.0017412
Swygert, S., Senapati, S., Bolukbasi, M., Wolfe, S., Lindsay, S., Peterson, C.L., 2018. SIR proteins create compact heterochromatin fibers. PNAS. https://doi.org/10.1101/346296
Takahashi, H., McCaffery, J.M., Irizarry, R.A., Boeke, J.D., 2006a. Nucleocytosolic Acetyl-Coenzyme A Synthetase Is Required for Histone Acetylation and Global Transcription. Molecular Cell 23, 207–217. https://doi.org/10.1016/j.molcel.2006.05.040
Takahashi, H., McCaffery, J.M., Irizarry, R.A., Boeke, J.D., 2006b. Nucleocytosolic acetyl-coenzyme a synthetase is required for histone acetylation and global transcription. Mol Cell 23, 207–217. https://doi.org/10.1016/j.molcel.2006.05.040
Tanaka, C., Tan, L.-J., Mochida, K., Kirisako, H., Koizumi, M., Asai, E., Sakoh-Nakatogawa, M., Ohsumi, Y., Nakatogawa, H., 2014. Hrr25 triggers selective autophagy–related pathways by phosphorylating receptor proteins. Journal of Cell Biology 207, 91–105. https://doi.org/10.1083/jcb.201402128
Tanny, J.C., Dowd, G.J., Huang, J., Hilz, H., Moazed, D., 1999. An Enzymatic Activity in the Yeast Sir2 Protein that Is Essential for Gene Silencing. Cell 99, 735–745. https://doi.org/10.1016/S0092-8674(00)81671-2
Thurtle, D.M., Rine, J., 2014. The molecular topography of silenced chromatin in Saccharomyces cerevisiae. Genes Dev. 28, 245–258. https://doi.org/10.1101/gad.230532.113
Tong, A.H.Y., Evangelista, M., Parsons, A.B., Xu, H., Bader, G.D., Pagé, N., Robinson, M., Raghibizadeh, S., Hogue, C.W.V., Bussey, H., Andrews, B., Tyers, M., Boone, C.,

2001. Systematic Genetic Analysis with Ordered Arrays of Yeast Deletion Mutants. Science 294, 2364–2368. https://doi.org/10.1126/science.1065810

Tosi, A., Haas, C., Herzog, F., Gilmozzi, A., Berninghausen, O., Ungewickell, C., Gerhold, C.B., Lakomek, K., Aebersold, R., Beckmann, R., Hopfner, K.-P., 2013. Structure and Subunit Topology of the INO80 Chromatin Remodeler and Its Nucleosome Complex. Cell 154, 1207–1219. https://doi.org/10.1016/j.cell.2013.08.016

Tsukada, M., Ohsumi, Y., 1993. Isolation and characterization of autophagy-defective mutants of Saccharomyces cerevisiae. FEBS Letters 333, 169–174. https://doi.org/10.1016/0014-5793(93)80398-E

Tu, B.P., Kudlicki, A., Rowicka, M., McKnight, S.L., 2005. Logic of the Yeast Metabolic Cycle: Temporal Compartmentalization of Cellular Processes. Science 310, 1152–1158. https://doi.org/10.1126/science.1120499

Tu, B.P., McKnight, S.L., 2007. The Yeast Metabolic Cycle: Insights into the Life of a Eukaryotic Cell. Cold Spring Harb Symp Quant Biol 72, 339–343. https://doi.org/10.1101/sqb.2007.72.019

van Werven, F.J., Amon, A., 2011. Regulation of entry into gametogenesis. Phil. Trans. R. Soc. B 366, 3521–3531. https://doi.org/10.1098/rstb.2011.0081

Viswanathan, M., Muthukumar, G., Cong, Y.-S., Lenard, J., 1994. Seripauperins of Saccharomyces cerevisiae: a new multigene family encoding serine-poor relatives of serine-rich proteins. Gene 148, 149–153. https://doi.org/10.1016/0378-1119(94)90249-6

Wang, J., Jia, S.T., Jia, S., 2016. New Insights into the Regulation of Heterochromatin. Trends in Genetics 32, 284–294. https://doi.org/10.1016/j.tig.2016.02.005

Watanabe, S., Tan, D., Lakshminarasimhan, M., Washburn, M.P., Erica Hong, E.-J., Walz, T., Peterson, C.L., 2015. Structural analyses of the chromatin remodelling enzymes INO80-C and SWR-C. Nat Commun 6, 7108. https://doi.org/10.1038/ncomms8108

Weiner, A., Hsieh, T.-H.S., Appleboim, A., Chen, H.V., Rahat, A., Amit, I., Rando, O.J., Friedman, N., 2015. High-Resolution Chromatin Dynamics during a Yeast Stress Response. Molecular Cell 58, 371–386. https://doi.org/10.1016/j.molcel.2015.02.002

Wissink, E.M., Vihervaara, A., Tippens, N.D., Lis, J.T., 2019. Nascent RNA analyses: tracking transcription and its regulation. Nat Rev Genet 20, 705–723. https://doi.org/10.1038/s41576-019-0159-6

Wullschleger, S., Loewith, R., Hall, M.N., 2006. TOR Signaling in Growth and Metabolism. Cell 124, 471–484. https://doi.org/10.1016/j.cell.2006.01.016

Xu, F., Zhang, Q., Zhang, K., Xie, W., Grunstein, M., 2007. Sir2 Deacetylates Histone H3 Lysine 56 to Regulate Telomeric Heterochromatin Structure in Yeast. Molecular Cell 27, 890–900. https://doi.org/10.1016/j.molcel.2007.07.021

Xue, Y., Van, C., Pradhan, S.K., Su, T., Gehrke, J., Kuryan, B.G., Kitada, T., Vashisht, A., Tran, N., Wohlschlegel, J., Peterson, C.L., Kurdistani, S.K., Carey, M.F., 2015. The Ino80 complex prevents invasion of euchromatin into silent chromatin. Genes Dev. 29, 350–355. https://doi.org/10.1101/gad.256255.114

Yang, M., Luo, S., Wang, X., Li, C., Yang, J., Zhu, X., Xiao, L., Sun, L., 2021. ER-Phagy: A New Regulator of ER Homeostasis. Frontiers in Cell and Developmental Biology 9.

Yao, W., King, D.A., Beckwith, S.L., Gowans, G.J., Yen, K., Zhou, C., Morrison, A.J., 2016. The INO80 Complex Requires the Arp5-Ies6 Subcomplex for Chromatin Remodeling and Metabolic Regulation. Molecular and Cellular Biology 36, 979–991. https://doi.org/10.1128/MCB.00801-15

Yen, K., Vinayachandran, V., Pugh, B.F., 2013. SWR-C and INO80 Chromatin Remodelers Recognize Nucleosome-free Regions Near +1 Nucleosomes. Cell 154, 1246–1256. https://doi.org/10.1016/j.cell.2013.08.043

Yofe, I., Weill, U., Meurer, M., Chuartzman, S., Zalckvar, E., Goldman, O., Ben-Dor, S., Schütze, C., Wiedemann, N., Knop, M., Khmelinskii, A., Schuldiner, M., 2016. One library to make them all: streamlining the creation of yeast libraries via a SWAp-Tag strategy. Nat Methods 13, 371–378. https://doi.org/10.1038/nmeth.3795

Zal, T., Anna Zal, M., Lotz, C., Goergen, C.J., Gascoigne, N.R.J., 2006. Spectral Shift of Fluorescent Dye FM4-64 Reveals Distinct Microenvironment of Nuclear Envelope in Living Cells. Traffic 7, 1607–1613. https://doi.org/10.1111/j.1600-0854.2006.00498.x

Zaragoza, D., Ghavidel, A., Heitman, J., Schultz, M.C., 1998. Rapamycin Induces the G0 Program of Transcriptional Repression in Yeast by Interfering with the TOR Signaling Pathway. Molecular and Cellular Biology 18, 4463–4470. https://doi.org/10.1128/MCB.18.8.4463

Zeiner, G.M., Cleary, M.D., Fouts, A.E., Meiring, C.D., Mocarski, E.S., Boothroyd, J.C., 2008. RNA analysis by biosynthetic tagging using 4-thiouracil and uracil phosphoribosyltransferase. Methods Mol Biol 419, 135–146. https://doi.org/10.1007/978-1-59745-033-1_9

Zhang, S., Yu, X., Zhang, Y., Xue, X., Yu, Q., Zha, Z., Gogol, M., Workman, J.L., Li, S., 2021. Metabolic regulation of telomere silencing by SESAME complex-catalyzed H3T11 phosphorylation. Nat Commun 12, 594. https://doi.org/10.1038/s41467-020-20711-1